The transition between thin-to-thick-skinned styles of deformation in the Western Pyrenean Belt

Eloi Carola i Molas

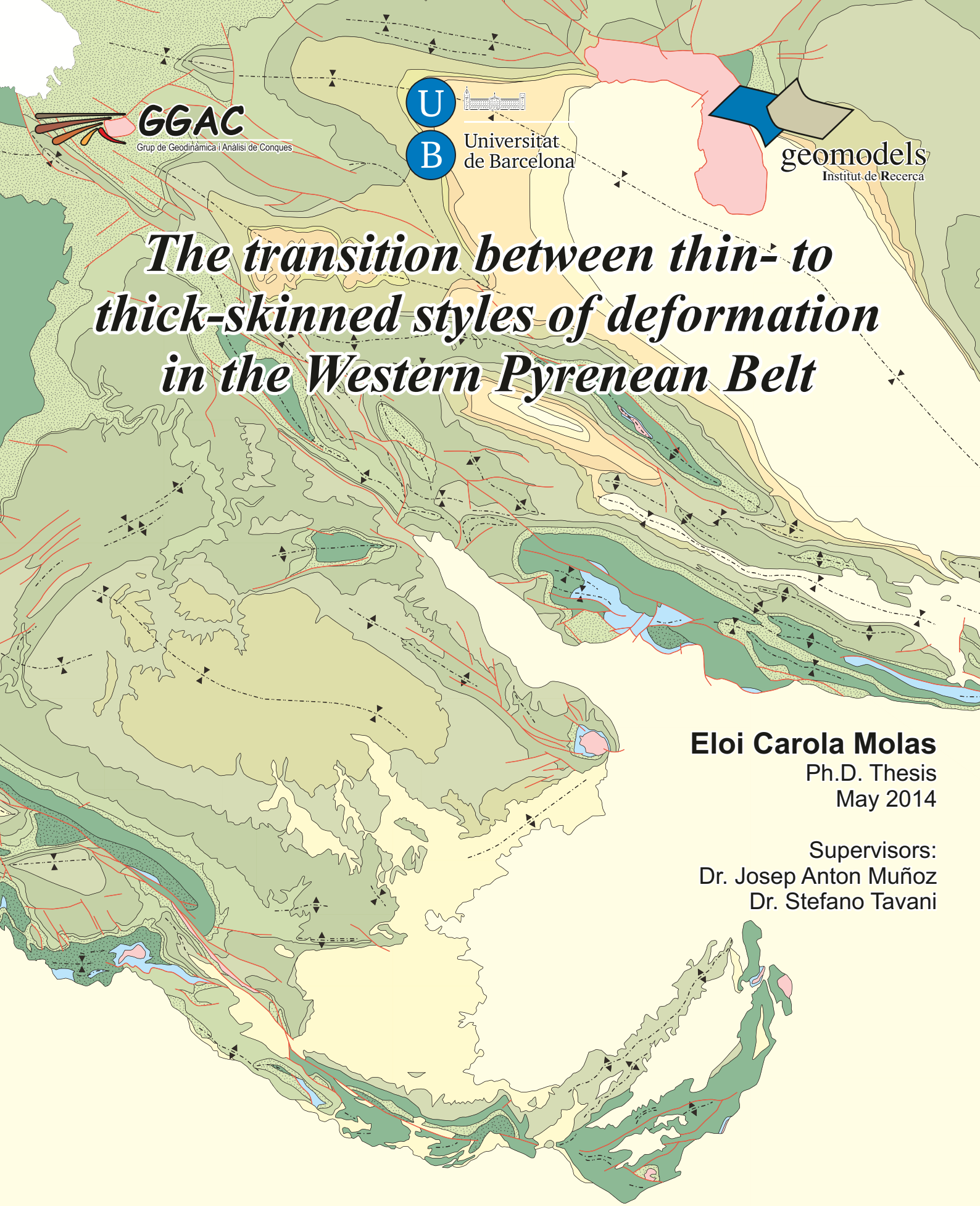

The transition between thin- to thick-skinned styles of deformation in the Western Pyrenean Belt

Eloi Carola Molas

Ph.D. Thesis
May 2014

Supervisors:
Dr. Josep Anton Muñoz
Dr. Stefano Tavani

Institut de Recerca Geomodels
Grup de Recerca Consolidat de Geodinàmica i Anàlisi de Conques
Departament de Geodinàmica i Geofísica
Universitat de Barcelona

Institut de Recerca Geomodels
Universitat de Barcelona
Grup de Recerca Consolidat de Geodinàmica i Anàlisi de Conques
Departament de Geodinàmica i Geofísica

The transition between thin- to thick-skinned styles of deformation in the Western Pyrenean Belt

Memòria presentada per **Eloi Carola i Molas** per optar al grau de Doctor en Geologia. Aquesta memòria s'ha realitzat dins el Programa de Doctorat de Ciències de la Terra i sota la direcció del Dr. **Josep Anton Muñoz de la Fuente** i del Dr. **Stefano Tavani**.

Eloi Carola Molas

Barcelona, Maig de 2014

Dr. Josep Anton Muñoz de la Fuente

Dr. Stefano Tavani

La investigació presentada en aquest volum s'ha realitzat gràcies al suport del "Grup de Geodinàmica i Anàlisi de Conques" de la Universitat de Barcelona el qual forma part dels grups consolidats de la Generalitat de Catalunya amb referència 2009SGR-1198 i del "Institut de Recerca GEOMODELS" amb finançament per part de la Generalitat de Catalunya, Instituto Geológico y Minero de España i altres empreses privades.
A més a més aquesta tesi ha estat econòmicament suportada gràcies a una beca predoctoral de formació de personal investigador i un contracte de formació en pràctiques gratament concedides per la Fundación Ciudad de la Energía.
Els treballs d'investigació s'enmarquen dins dels projectes: "Construcción de un modelo geológico tridimensional de potenciales ubicaciones de una planta piloto de almacenamiento geológico de CO_2" (FBG305049), "Caracterización geológica del complejo de almacenamiento de la Planta Piloto y estructuras análogas en superficie y subsuelo (Campo de Ayoluengo)" (FBG305657) i "Inversión positiva de estructuras tectónicas salina" INTECTOSAL (CGL2010-21968-C02- 01).
També volem agrair a SMT, Midland Valley, Schlumberger i Paradigm per facilitar llicències acadèmiques dels respectius softwares utilitzats durant el transcurs dels treballs realitzats. Finalment, al laboratori de Paleomagnetisme de Barcelona (CCiTUB - ICTJA CSIC) on es van dur a terme els anàlisis.

A tots els qui estimo.

Agraïments

Ja sé que estàs començant a llegir la tesi i et semblarà que és el principi però, desafortunadament per a mi, és el final d'una etapa. Una etapa molt bonica de la meva vida i en part també de molta altra gent que m'ha acompanyat per aquest camí, a vegades una mica més negre del que m'esperava tot s'ha de dir.

Primer de tot vull agrair als dos directors, l'Anton i l'Stefano per la tutela d'aquesta tesi. No simplement aquesta ha estat la tasca que heu realitzat, inconscientment heu inculcat uns valors i unes normes tant personals com científiques que m'han ajudat a madurar i ser crític. No només això, per escoltant-me en els moments d'ofuscació, per fer-me veure el bon camí quan per mi sol no era capaç de trobar-lo i donar-me consells perquè jo acabés trobant la solució. A l'Anton l'hi estic molt agraït per tota "la feina que no es veu". Buscar finançament, projectes i contactes no ha de ser gens fàcil ni agraït i tot i així ho continues fent perquè molts tinguem la sort de poder realitzar la tesi. També he d'agrair-te per enviar-me a Tucson, sí al desert, quan la meva idea era anar a un lloc on s'estigués més fresc. Reconec que em vas enganxar amb la guàrdia baixa perquè no sabia on era però tot i així l'experiència em va encantar i ho repetiria amb els ulls tancats! Són molts els bons moments que recordo d'aquesta etapa especialment les xerrades per skype durant les respectives estades, als matins quan tot el departament encara està en calma i no hi han interrupcions o quan et feia alguna pregunta i... dos copets a l'espatlla i enfilaves cap al despatx. Reconec que em desconcertaven però que alhora m'ajudaven a pensar per mi mateix! A l'Stefano per els bons moments a les campanyes de camp i les converses per skype intentant discutir coses indiscutibles en aquestes condicions. També per trobar un moment sempre que l'he necessitat ja sigui per revisar qualsevol text o per preguntar coses encara que ni compartís la interpretació ni entengués el perquè de la pregunta. I finalment, per tenir sempre un bon insult en qualsevol llengua apunt.

Seguidament a l'Eduard, per burxar-me amb les discussions tant científiques com no i per aconsellar-me tant amb els CMYK com amb altres aspectes més personals. Tot i que oficialment mai tens temps, sempre has trobat un moment per parlar i escoltar-me i ho aprecio moltíssim!

També vull agrair a tota la gent de la Universitat. Primer de tot als de la sala 224, l'Anna, la Xènia, la Lena, l'Eloi, el David i la planteta, ha estat molt divertit compartir aquest temps amb vosaltres. Especialment l'Anna, la qual ha patit bastant aquesta tesi. També donar les gràcies a tots els que han passat i que estan a la sala 226/227, al principi havia començat a posar noms, però quan ja en portava més de 23 m'he adonat que és molt fàcil que em descuidi algú! Així que us dono gràcies per tot el que heu fet per mi durant el temps que hem compartit. Especial menció a l'Oscar Gratacós, entre moltes altres coses per mantenir les llicències operatives a l'Ainsa tot i que l'ordinador estava quasi mort i per mantenir el plòter sempre a punt. A l'Oriol pel material científic d'estraperlo i per ensenyar-me a modelitzar tot i que no hagi quedat reflectit en aquest volum. I a la Bet per introduir-me a l'obscur món del paleomagnetisme. Al grup dels esmorzars al bar, tot i que amb el pas del temps s'ha anat reduint considerablement, m'ho he passat molt bé fent un descans cada matí i xerrar de

moltes coses. Finalment, als que no estan a cap de les dues sales anteriors, als Ovillistes, als geofísics i als petròlegs! M'hauria agradat passar més temps amb tots vosaltres, però sou molts i molt escampats per diferents departaments i institucions...

A tot el personal d'administració, el Joan Ramon, l'Aida, la Mª José, l'Ana i especialment a la Teresa! Sense vosaltres tota la tesi no hauria anat tant fluida ja que la burocràcia m'hauria col·lapsat o si més no, l'hauria enrederit força. Així que moltes gràcies.

Tot i que no heu passat per la facultat de Geologia, a la Marta per les "colacoles" al bar Universitat, al Starbucks o simplement passejant per Camprodon i Barcelona tot parlant de com arreglar el món. I l'Eva que juntament amb la Marta des de petits hem format un grup bastant indivisible! Gràcies per cedir-me el llit de matrimoni durant el meu primer any a Barcelona ☺.

I would like to thank all the people that shared my experience during my stay, specially Peter G. DeCelles for hosting me at the University of Arizona. I have really nice memories and at the same time I miss the time I spent in Tucson a lot. Your field trip was amazing, Arizona's landscapes are some of the best that I have ever seen. Doing geology in these places is awesome. Pete and Barbara that opened their house to me, I really appreciate it and I am sorry I couldn't come more often. The rest of UofA grad students for the great time spent in Manlove house and in the field. Finally I want to thank you Pete C.L., no I didn't forgot you, the Starbucks breaks, all the jokes and funny things, the hikes and cooking sessions made the stay more pleasant and enjoyable.

A la familia Cantarero-Abad por todo lo que han hecho durante el periodo en que me alojaron en su casa y por todas las veces que hemos hecho de paparras ya sea por pereza, por morro o simplemente porque nos invitaban y nos considerábamos paparras igualmente.

Gràcies de tot cor a la família, als que ens han acompanyat i als que encara ens acompanyen, per tots els bons moments que passem junts. En especial als meus pares, en Siscu i la Rita per haver-me donat l'educació que jo he desitjat sense dubtar en cap moment de les meves aptituds. Quan molts altres no ho tenien del tot clar, i es veien amb autoritat per jutjar, vosaltres vàreu creure en les possibilitats d'en "lustucrú" i vàreu deixar que jo escollís i tracés la meva línia! Als meus germans, en Bernat i la Núria, que tot i que arrufeu el nas i em dieu que calli quan dic més de tres paraules seguides de geologia sabeu que no és avorrida (almenys per mi). Finalment, a l'avi Esteve que tot i que no ho has pogut veure, sé que hauries estat orgullós de mi en aquest moment.

Ja per acabar, vull donar les gràcies a la Irene una altra patidora d'aquesta tesi. Gràcies per aguantar-me als matins quan l'hiperactivitat em remou i per comprendre'm a la nit quan les forces em manquen. Per estar al meu costat recolzant-me tant en les decisions fàcils com en les difícils, per compartir viatges i experiències i en general per estimar-me tant.

Moltes gràcies a tots de veritat!

Index

Index of figures

Resum extens en català

Preface

Chapter 1

Chapter 2

Chapter 3

Chapter 4

Chapter 5

Resum

Aquesta tesi doctoral descriu la cinemàtica dels Pirineus Basco-Cantàbrics, més concretament de la Plataforma Burgalesa, mitjançant la integració de i) geologia de superfície; ii) interpretació de línies sísmiques i pous; i iii) estudis paleomagnètics de rotacions d'eix vertical. La integració d'aquest conjunt de dades permet comprendre la relació entre la Plataforma Burgalesa i les conques d'avantpaís de l'Ebre i del Duero durant la orogènia Pirenaica.

La principal contribució de la tesi és la de presentar un model estructural, el qual honora totes les restriccions imposades per l'estratigrafia, la preconfiguració de l'àrea prèvia a la deformació contractiva i les dades tant superficials com profundes. Aquest model permet comprendre com és la transició entre la deformació pel·licular present a l'est de la zona d'estudi i la deformació no pel·licular present a l'oest.

La interpretació conjunta tant de pous com de seccions sísmiques permet comprendre l'estructuració esdevinguda durant el període extensiu així com també el resultat del període orogènic posterior. La distribució dels depocentres va estar condicionada per l'extensió que va tenir lloc durant el Cretaci Inferior degut a l'obertura de l'Atlàntic nord i del Golf de Biscaia. A més a més durant aquest estadi de deformació, la mobilització de la sal degut a l'extensió va generar unes zones on es van acumular grans quantitats de sal d'edat triàsica tal com mostren els pous o l'abundància de diapirs en superfície accentuant els depocentres ja generats inicialment. Durant aquest estadi és quan es desenvolupen les geometries sedimentàries en *onlap* observades en els sediments sin-extensius les quals, presenten una direcció de migració cap al sud amb una traça paral·lela a la traça que presenta la falla d'Ubierna. El model que permet explicar tals geometries és un model extensiu compost el qual es caracteritza pel desenvolupament de plecs forçats en extensió i transport cap al nord de la cobertora juntament amb migració de sal cap al marge sud de la conca. L'extensió produïda a nivell de basament no es transmetria directament a la cobertora sinó que es veuria desacoblada degut al nivell de desenganxament entre les dues unitats. Aquest fet provoca que la cobertora estigui plegada sobre el graó de basament mentre que la sal està sotmesa a mobilització. Aquest fet genera geometries en *onlap* entre els materials pre-extensius i els sin-extensius. A més a més durant aquest mateix estadi extensiu, té lloc el desenvolupament d'estructures contractives a la zona de Huidobro on s'acaba produint la repetició de part de la successió mesozoica.

L'estadi post-extensiu està caracteritzat per l'erosió de part dels sediments dipositats i deformats prèviament. Aquest procés genera una truncació erosional afectant bàsicament als sediments sin-extensius d'edat cretaci inferior. Els primers estadis de deformació deguts a la orogènia Pirenaica van resultar en el desenvolupament de l'estructura de San Pedro, en la qual els encavalcaments estan dirigits cap al nord-est i on el basament hi està involucrat, la qual està fossilitzada actualment sota els sediments de la conca d'avantpaís del Duero. Cap al nord, la Plataforma Burgalesa, caracteritzada per encavalcaments arrelats a les sals triàsiques, va ésser transportada cap al sud fins al punt en el qual l'alt de San Pedro va actuar com a contrafort forçant a la Plataforma Burgalesa a modificar la trajectòria i cinemàtica del encavalcaments. Aquest procés va resultar en l'extrusió de la Plataforma Burgalesa cap al sud-est encavalcant la conca d'avantpaís de l'Ebre. La part més occidental de la zona d'estudi està caracteritzada per encavalcaments dirigits cap al sud els quals involucren el basament. Aquesta deformació no es limita tan sols a la Plataforma Burgalesa sinó que també és present sota els sediments Cenozoic

de la conca d'avantpaís del Duero on aquests encavalcaments deformen tant el basament com les successions mesozoiques i cenozoiques.

El treball combinat entre geologia de superfície i les dades aportades pels pous d'exploració han permès reinterpretar l'estructura de Zamanzas situada al nord de la Plataforma Burgalesa. Anteriorment, aquesta àrea havia estat interpretada com a un conjunt de falles extensives dirigides cap al nord-est. Amb aquesta tesi s'ha posat de manifest la dificultat d'encaixar les dades amb la interpretació proposada anteriorment per aquesta estructura. Gràcies a les relacions geomètriques entre els diferents blocs limitats per les falles aportades pel treball de camp i les dades dels pous d'exploració, aquesta estructura s'ha reinterpretat com un *popup* generat durant la Orogènia Pirenaica.

Els estudis paleomagnètics focalitzats a determinar possibles rotacions d'eix vertical allarg dels Pirineus, duts a terme per a diferents grups d'investigació durant els últims anys, posa de manifest que la densificació que algunes zones presenten no es dóna a la zona de la Plataforma Burgalesa i als seus voltants on hi ha una mancança d'estacions. Així doncs un altre dels objectius d'aquesta tesi és esmenar aquest buit i aportar noves dades de rotacions d'eix vertical per a la zona esmentada anteriorment. L'estudi dut a terme durant el transcurs de la tesi permet aportar dades de vint-i-sis estacions repartides per la zona d'estudi i que permeten caracteritzar el patró de rotacions d'eix vertical.

Les dades obtingudes mitjançant l'estudi de paleomagnetisme focalitzat a caracteritzar les rotacions d'eix vertical durant el Cenozoic revelen que i) la magnetització dels materials Cenozoic és anterior a la deformació i que ii) la Plataforma Burgalesa i les zones adjacents han sofert rotacions tant horàries com antihoràries. A la terminació occidental de l'encavalcament frontal dels Pirineus Bascos es poden dividir dos sectors en funció de la rotació que la zona ha experimentat essent aquests el sinclinal de Miranda a l'est i el sinclinal de Villarcayo a l'oest. A la part central del sector del sinclinal de Miranda, les estacions no presenten rotació mentre que el patró de rotacions a la terminació oest d'aquest sector, està definit per rotacions horàries d'uns vint graus. Al sector del sinclinal de Villarcayo, el patró de rotacions està caracteritzat per rotacions antihoràries amb quinze graus de mitjana. Les estacions situades a la Plataforma Burgalesa es poden separar en tres àrees en les quals les rotacions presenten diferents direccions de rotació. A la terminació oriental de la zona d'estudi, les rotacions obtingudes per els sediments Cenozoics demostren una rotació de vint graus antihoràris de mitjana. A la part

central els valors de rotació són menyspreables podent assumir que no ha experimentat rotació. La terminació occidental de la zona d'estudi les rotacions obtingudes són horàries amb una mitjana de vint-i-cinc graus. Aquest patró de rotacions és coherent amb el model d'un arc secundari o progressiu en el qual rotacions horàries i antihoràries es donen als dos extrems de l'arc i no rotació a la part central d'aquest.

Els models evolutius proposats anteriorment per a la Plataforma Burgalesa han estat basats o en geologia de superfície o mitjançant sísmiques d'exploració que almenys encaixaven amb algunes de les restriccions imposades. Degut al fet que cap model englobava totes les observacions abans descrites, un nou model s'ha proposat per a l'evolució de la Plataforma Burgalesa. Aquest model està caracteritzat per presentar deformació no pel·licular al sector oest mentre que quan el nivell de desenganxament augmenta de potència els encavalcaments es desenganxen i deformen la cobertora presentant un estil estructural pel·licular. Els resultats d'aquesta tesi demostren que la pre-configuració tant de la conca extensiva pròpiament dita com la del seu voltant, tenen una forta implicació en el desenvolupament i estructuració de la Plataforma Burgalesa durant la Orogènia Pirenaica. Finalment durant l'estructuració d'aquesta part dels Pirineus, rotacions horàries i antihoràries han tingut lloc en els diferents sectors mostrejats tal i com han posat de manifest els estudis paleomagnètics realitzats durant aquesta tesi.

Abstract

This PhD Thesis describes the kinematics of the Basque-Cantabrian Pyrenees, more specifically of the Burgalesa Platform, by means of the integration of i) surface geology; ii) seismic and well data interpretation; and iii) vertical axis rotation paleomagnetic studies. The integration of all the data allow to understand the relationship between the Burgalesa Platform and the Ebro and Duero foreland basins during the Pyrenean Orogeny.

The principal contribution of the Thesis is to present a new structural model, that fits with all the constraints imposed by the stratigraphy, the pre-configuration of the area prior to the contractive deformation and both deep and surface data. This model allows to understand how is the transition between the thin-skinned tectonics present at the east of the study area and the thick-skinned tectonics present at the west.

The combined interpretation of wells and seismic sections allow to partially comprehend the structure of the area during the extensional event as well as the result of the Pyrenean Orogeny occurred later. The distribution of the Lower Cretaceous depocenters was conditioned by the extension that took place during the Late Jurassic-Early Cretaceous due to the opening of the North Atlantic and the Bay of Biscay. Moreover, during this stage of deformation, salt mobilisation triggered by extension generated areas where the Triassic salt layer was thickened as demonstrated by the well data and the abundance of outcropping diapirs. This process accentuated the development of the depocenters. The extensional event also generated the onlap sedimentary geometries observable in the syn-rift sediments with a direction of migration pointing towards the south with a distribution almost parallel to the Ubierna Fault. The extensional model that allow to fit the constraints is a combined model with the development of cover forced folding and northwards translation of the cover and salt migration at the southern boundary. The extension produced in the basement was not transmitted to the cover because the latter was decoupled by the Triassic salt layer. The syn-rift successions onlapping both, the pre-rift and syn-rift were generated in this period. In addition, during the extensional event, contractional structures were developed such as the north-directed thrust in the Huidobro area in which part of the Mesozoic succession is duplicated.

The post-extensional stage is characterised by the erosion of part of the previously deposited and deformed successions. This process generated the erosional truncation thus basically affecting the Lower Cretaceous syn-extensional sediments. The early stages of the Pyrenean Orogeny resulted in the development of the San Pedro Structure, in which the thrusts are directed towards the northeast and in where the basement is involved, that was later fossilised by the Duero foreland sediments. To the north, the Burgalesa Platform, characterised by south-directed thrusts rooted into the Triassic salts, was southwards displaced until the San Pedro started to act as a backstop forcing the Burgalesa Platform to change the trajectory and kinematics. This resulted in the lateral extrusion towards the southeast of the Burgalesa Platform overriding the Ebro Foreland Basin. The westernmost part of the Burgalesa Platform is characterised by south-directed and basement-involved thrusts. This deformation is not restricted to the Burgalesa Platform itself, it is also present below the Cenozoic sediments of the Duero Foreland Basin in where the basement, the Mesozoic and the Cenozoic succession appears deformed.

The combined work between surface geology and well data has allowed to reinterpret the Zamanzas structure located at the northern boundary of the Burgalesa Platform. Previously, this structure had been interpreted as a set of northeast-directed extensional faults. This Thesis pointed out the difficulties of applying all the constraints with this previous interpretation. The surface geometric relationships between the different blocks limited by the faults and the deep data provided by the well allowed to reinterpret the Zamanzas structure as a popup generated during the Pyrenean Orogeny.

The paleomagnetic studies focussed on determine the possible vertical axis rotations along the Pyrenees, carried out by different research groups in the lasts years, denotes a lack of sites in the Burgalesa Platform and vicinities. For that reason, another objective of this Thesis is to provide new vertical axis paleomagnetic sites for the study area. The study carried out is made up of twenty-six new sites widely distributed and that allow to characterise the vertical axis rotation pattern.

The obtained paleomagnetic data focussed on vertical axis rotation occurred during the Cenozoic reveals that i) the magnetisation of the Cenozoic sediments was prior to deformation and that ii) clockwise and counter clockwise rotation occurred in the Burgalesa Platform and adjacent areas. At the western tip of the Basque Pyrenees Frontal Thrust two domains can be divided depending on the rotation that characterised the domains being the Miranda Syncline towards the east and the Villarcayo Syncline towards the west. In the central part of the Miranda Syncline, the sites do not present significant rotation whereas, the rotation at the western part are defined by clockwise rotations of about twenty degrees. At the Villarcayo Syncline, the rotation pattern is characterised by counter clockwise rotations of about fifteen degrees. The paleomagnetic sites within the Burgalesa Platform can be grouped into three sectors thus presenting different rotations. At the eastern part of the study area, the reported rotations for the Cenozoic sediments are about twenty degrees counter clockwise. At the central part the rotations are not significant thus denoting that the area did not rotated. The western part of the study area, the rotations are about twenty-five degrees clockwise. This pattern is in agreement with a secondary or progressive arch model in which clockwise and counter clockwise rotations characterise the tips of the thrust thus pointing towards the interior of the arch and no rotation at the central parts of it.

The evolution models previously proposed for the Burgalesa Platform were based either from surface geology or from geophysical data thus fitting some of the constraints. Because any model integrated all the observations and available data, a new model explaining the Burgalesa Platform evolution has been proposed. This model is characterised by presenting thick-skinned deformation at the western sector whereas, thin-skinned at the eastern one where the Triassic salt layer thickens. At this point, the thrusts detached the cover from the basement. The results of this Thesis demonstrate that the pre-configuration of the former extensional basin and its vicinities have a strong implication in the development and evolution of the Burgalesa Platform during the Pyrenean Orogeny. Finally, during this evolution, clockwise and counter clockwise rotations occurred in the different sectors as shown by the paleomagnetic studies carried out during this Thesis.

Resum extens en català

Motivacions i objectius de la tesi

Durant el desenvolupament d'un sistema orogènic, la deformació causada a la litosfera pot estar caracteritzada per dos estils. Per una banda, la tectònica de tipus *thick-skinned* on les falles creuen tota l'escorça superior aixecant i desplaçant el sòcol i la cobertora solidàriament. Aquest estil estructural està típicament associat a les parts internes dels orògens com per exemple els Alps o la Cordillera Oriental dels Andes (Pfiffner and Hitz, 1997; Carrera and Muñoz, 2013). Per l'altra banda, la tectònica de tipus *thin-skinned* està caracteritzada per encavalcaments de baix angle que estan arrelats a un nivell mecànicament dúctil tot definint rampes i replans en el sentit ascendent dels encavalcaments. Aquest estil estructural està típicament associat a les parts externes dels orògens on els encavalcaments desplacen la cobertora per sobre la conca d'avantpaís. Exemples d'aquests estil es poden trobar a les parts externes de les Foothills de Canadà, a les Rocky Mountains o als Zagros entre altres (Bally *et*

al., 1966; Stockmal *et al.*, 2001; Blanc *et al.*, 2003). Tot i que els dos tipus de deformació esmentats anteriorment poden estar presents a través dels orògens, des de les parts internes caracteritzades per tectònica *thick-skinned* cap a les parts externes predominades per tectònica *thin-skinned*, els dos estils de deformació poden estar presents allarg de l'orogen tal i com s'ha posat de manifest als Andes o als Pirineus entre altres (Kley *et al.*, 1999; Muñoz, 2002). A més a més de les variacions espacials, variacions temporals en l'estil de deformació també s'han de tenir presents (Hill *et al.*, 2002; 2008; Mazzoli *et al.*, 2008).

L'orogen Pirenaic (Fig. R.1), caracteritzat per presentar una alineació Oest-Est amb doble vergència, és el resultat de la història de deformació multifàsica la qual involucra els dos estils de deformació. L'estadi extensiu relacionat amb la obertura de l'Atlàntic Nord i el Golf de Biscaia durant el Juràssic terminal-Cretaci Inferior va desenvolupar conques intracontinentals al marge passiu, el subseqüent aprimament cortical va resultar en l'exhumació de mantell i acreció d'escorça oceànica al sector oest de la dorsal del Golf de Biscaia. Aquest fet va permetre la deposició de més de 10 km de sediments sin-extensius cobrint la successió ben estratificada Juràssica així com també l'escorça continental aprimada (e.g. Le Pichon & Sibuet, 1971; García de Cortázar & Pujalte, 1982; Pujalte, 1982; Mathieu, 1986; Ziegler, 1987; Bois *et al.*, 1997; Pedreira *et al.*, 2007; Ruiz, 2007; Ferrer *et al.*, 2008; Jammes *et al.*, 2009, Roca *et al.*, 2011). L'arquitectura pre-contractiva del sistema de rift Pirenaic va determinar les variacions tant a través com allarg de l'orogen desenvolupat durant la convergència entre les plaques Eurasiàtica i Ibèrica. Aquest estadi va tenir lloc des del Cretaci Superior fins al Cenozoic produint la subducció d'Ibèria cap al nord amb la subseqüent inversió de les conques mesozoiques (e.g. Le Pichon & Sibuet, 1971; Muñoz, 1992, 2002; Alonso *et al.*, 1996; Vergés & García-Senz, 2001).

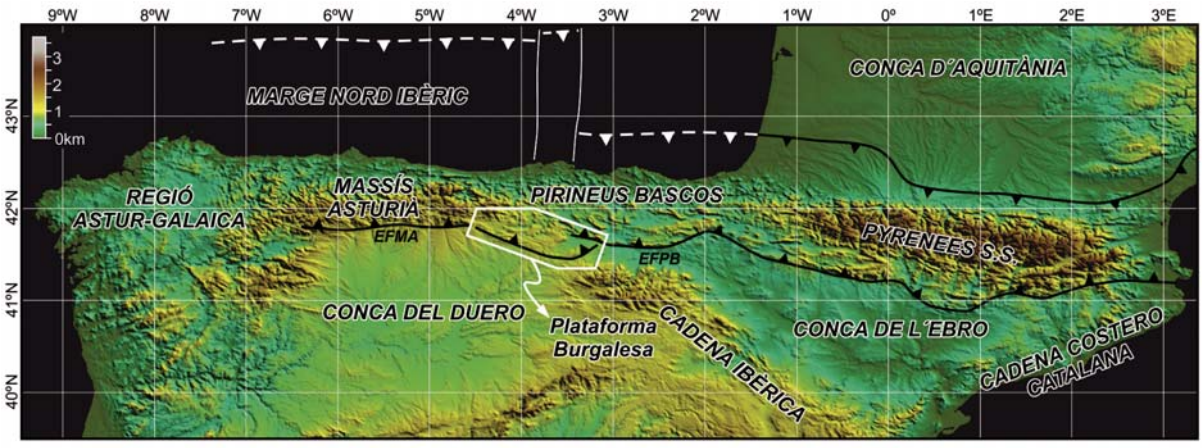

Fig. R.1: Mapa d'elevacions del límit nord d'Ibèria amb la localització de les majors unitats estructurals. EFMA i EFPB correspon a Encavalcament Frontal del Massís Asturià i Encavalcament Frontal dels Pirineus Bascos, respectivament.

Els Pirineus Bascos estan constituïts per la inversió d'una d'aquestes conques juràssiques a cretàcica superior (Fig. R.1). L'estructura frontal situada al sud (encavalcament de Sierra de Cantabria), desenganxat a les evaporites del Triàsic Superior, té una alineació O-E la qual defineix un arc on els seus extrems est i oest es corben adquirint una orientació NE-SO i NO-SE respectivament. Cap a l'est, el bloc inferior de l'encavalcament correspon a la conca d'avantpaís de l'Ebre. Per contra, a l'oest una altra unitat estructural ocupa una posició intermèdia entre la conca d'avantpaís i l'encavalcament frontal. Aquesta unitat, coneguda com Plataforma Burgalesa, també presenta una geometria en arc còncava cap al nord, tot i que asimètrica i més pronunciada que la descrita anteriorment. Aquest va ésser desenvolupat durant l'Oligocè i Miocè Inferior i va invertir la conca extensiva juràssica terminal i cretàcica inferior. Més cap a l'oest i amb continuïtat amb la Plataforma Burgalesa, el Massís Asturià, constituït per roques paleozoiques, va ser aixecat i transportat cap al sud per un sistema d'encavalcaments arrelats al basament i on l'encavalcament frontal aflora amb una orientació oest-est. La significació estructural de la Plataforma Burgalesa i la transició entre els dos estils de deformació (*Thick-skinned vs. Thin-skinned*) presents en aquestes àrees no és del tot coneguda avui dia.

Per aquest motiu, els objectius principals de la tesi estan centrats en:

1) Caracterització de la transició cap a l'est entre l'estil *thick-skin* present al Massís Asturià a l'estil *thin-skin* de la part est a la zona de la Plataforma Burgalesa i Pirineus Bascos.

2) Determinar les principals característiques geomètriques del sistema extensional del Juràssic Terminal i Cretaci Inferior i obtenir un guany en la comprensió del paper que han tingut les evaporites del Triàsic Superior durant l'estadi extensiu.

3) Comprendre i dilucidar les relacions tectono-estratigràfiques observades en les línies sísmiques disponibles a la Plataforma Burgalesa.

4) Constrènyer l'evolució cenozoica de la Plataforma Burgalesa mitjançant estudis paleomagnètics focalitzats en rotacions d'eix vertical.

Metodologia i dades d'estudi

Durant el transcurs de la Tesi s'han emprat quatre metodologies diferents i dades que han permès extreure les interpretacions i els resultats obtinguts les quals es detallen a continuació. La sísmica ha estat interpretada mitjançant els programaris *The Kingdom Suite*® i *Petrel*® on totes les sísmiques van carregar-s'hi. Del total de línies utilitzades, 28 no estaven en format digital i per tant van ser digitalitzades emprant les eines descrites a la memòria. Totes les línies van passar per un control de qualitat previ a la seva interpretació a fi de reduir errors durant aquesta darrera tasca. La malla de línies sísmiques interpretada cobreix tota la Plataforma Burgalesa així com també les àrees veïnes. Les dades provinents dels pous d'exploració també van passar per un control de qualitat i van esser utilitzats en conjunció amb les línies sísmiques per tal de poder interpretar els horitzons més rellevants. El treball de camp va consistir bàsicament en refinar les cartografies existents així com també per a la obtenció de dades de superfície per tal de poder construir els talls regionals realitzats durant aquesta tesi. L'estudi paleomagnètic dut a terme ha consistit en el mostreig i anàlisi de 62 estacions repartides tant a la Plataforma Burgalesa com als Pirineus Bascs (Fig. R.2). Per a cada estació es van prendre i analitzar una mitjana de deu mostres les quals han permès obtenir la direcció característica mitjana de 26 estacions. A més a més, es va realitzar l'estudi d'IRM per tal de conèixer la mineralogia magnètica de les mostres així com tests del plec per tal de conèixer el moment de la magnetització de les diferents unitats mostrejades.

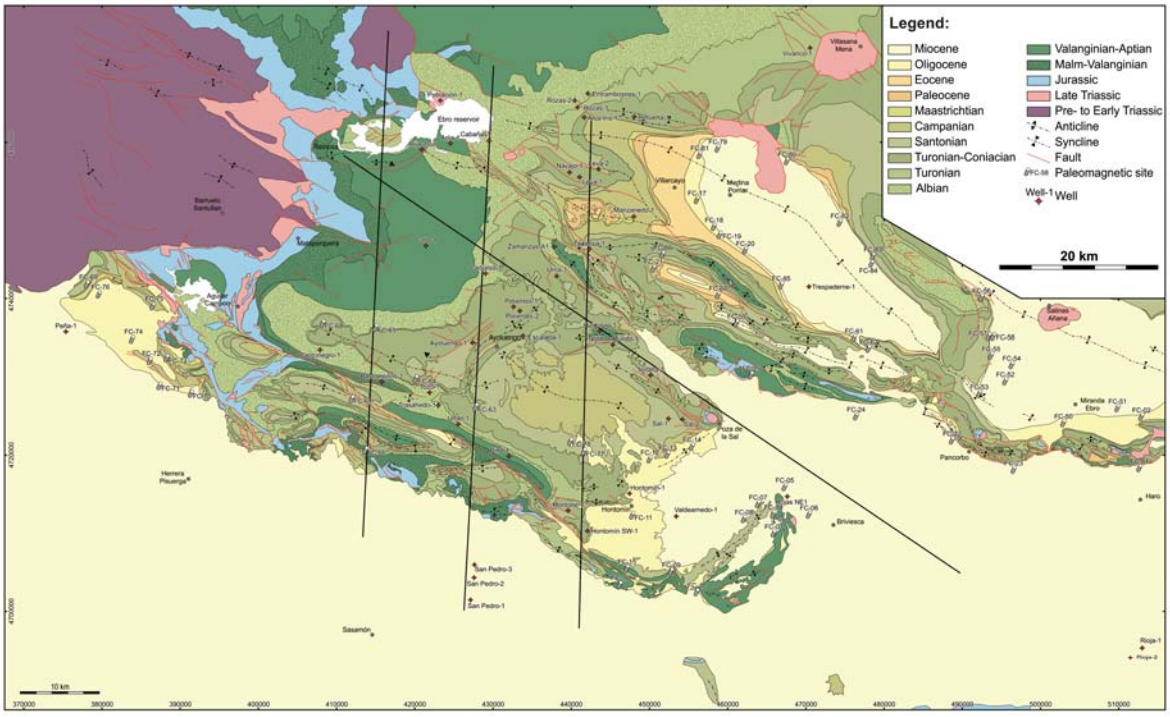

Fig. R.2: Mapa de la Plataforma Burgalesa i àrees veïnes amb la posició de les estacions de paleomagnetisme així com també dels talls.

Publicacions derivades de la Tesi

Aquesta tesi ha estat presentada com a compendi d'articles publicats o acceptats per a la seva publicació en revistes o llibres internacionals indexats. Concretament, està constituïda per tres publicacions detallades a continuació les quals han derivat dels resultats obtinguts durant el període de recerca.

- Carola, E., Tavani, S., Ferrer, O., Granado, P., Quintà, A., Butillé, M., Muñoz, J.A. (2013). Along-strike extrusion at the transition between thin- and thick-skinned domains in the Pyrenean Orogen (northern Spain). In: *Thick-Skin-Dominated Orogens: From Initial Inversion to Full Accretion* edited by Nemčok, M., Mora, A.R. and Cosgrove, J.W. Geological Society of London Special Publications **377**. 119-140. DOI: 10.1144/SP377.3

- Tavani, S., Carola, E., Granado, P., Quintà, A., Muñoz, J.A. (2013). Transpressive inversion of a Mesozoic extensional forced fold system with an intermediate décollement level in the Basque-Cantabrian Basin (Spain). *Tectonics* **32**. DOI: 10.1002/tect.20019.

- Carola, E., Muñoz, J.A., Roca, E. (submitted). The transition from basement-involved thick-skinned to detachment thin-skinned tectonics in the Basque-Pyrenees: The Burgalesa Platform and vicinities. *International Journal of Earth Science.*

Resultats i conclusions

Relacions geomètriques i sedimentaries del sistema extensional.

La integració de la geologia de superfície amb les interpretacions de les dades de subsòl (i.e. línies sísmiques i pous d'exploració) ha permès determinar les principals característiques geomètriques i cinemàtiques de la conca extensiva desenvolupada durant el Juràssic Terminal-Cretaci Inferior.

Els estadis inicials de l'extensió a la Plataforma Burgalesa van estar caracteritzats per plecs d'acomodació a la cobertora per sobre un graó al sòcol. El desenganxament del basament respecte de la cobertora es va produir al continuar l'extensió moment en el qual aquesta darrera va traslladar-se cap al nord. La interpretació sísmica ha mostrat que durant el Cretaci Inferior,

un encavalcament dirigit cap al nord es va desenvolupar acomodant l'extensió produïda al marge de la conca (Fig. R.3). Els onlaps observats al marge sud demostren que la cobertora es va desplaçament cap al nord almenys 10 km i que una quantitat similar d'escurçament va ésser acomodada per l'estructura compressiva. Aquests onlaps es van desenvolupar degut al moviment de la cobertora sobre el graó de basament, motiu per el qual tenen una direcció de migració cap al sud. La truncació erosional observada en els sediments sin-extensius sumat al fet que el Cretaci Superior no presenta deformació a la transició entre replà i rampa al *backlimb* d'aquesta estructura permet afirmar que el desenvolupament d'aquest encavalcament va ser durant l'etapa extensiva. Aquest fet ajuda a comprendre les diferencies de relleu estructural entre els nivells profunds i els superficials així com també que la quantitat d'escurçament que es pot observar al Juràssic sigui diferent a la quantitat d'escurçament que presenten les unitats del Cretaci Superior.

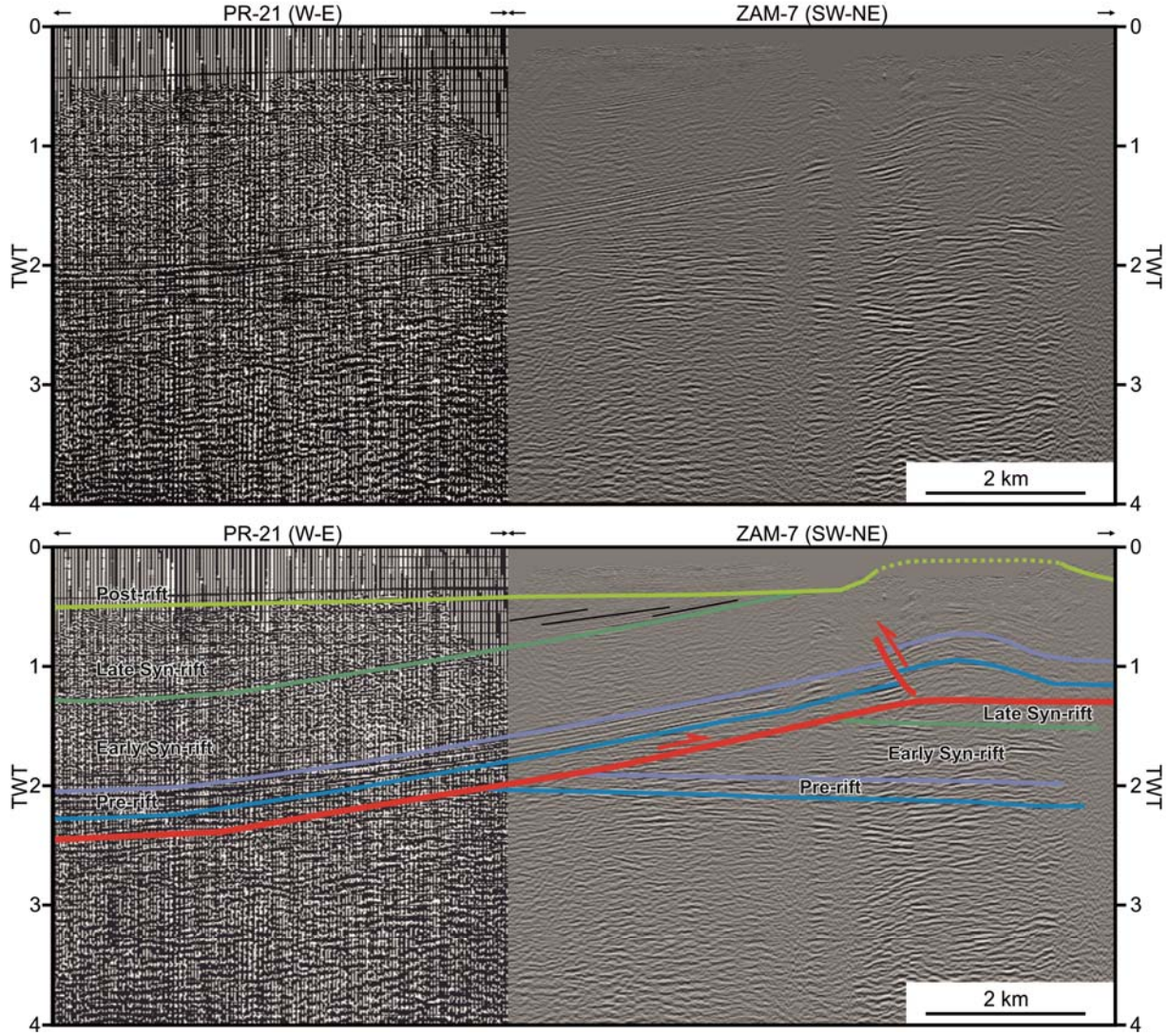

Fig. R.3: Línia sísmica on es posa de manifest l'encavalcament dirigit cap al nord, el qual es va desenvolupar durant l'extensió que va afectar la zona durant el Cretaci Inferior.

El patró de distribució del nivell evaporític del Triàsic Superior al final del període extensiu a la Plataforma Burgalesa va estar caracteritzat per dues orientacions preferents (Fig. R.4). La principal, amb una orientació ONO-ESE, està relacionada amb les falles extensives principals i es troba localitzada als marges sud i nord de la zona d'estudi. La segona, amb una orientació NE-SO, està controlada per les estructures transversals de segon ordre que es van desenvolupar a la zona d'estudi.

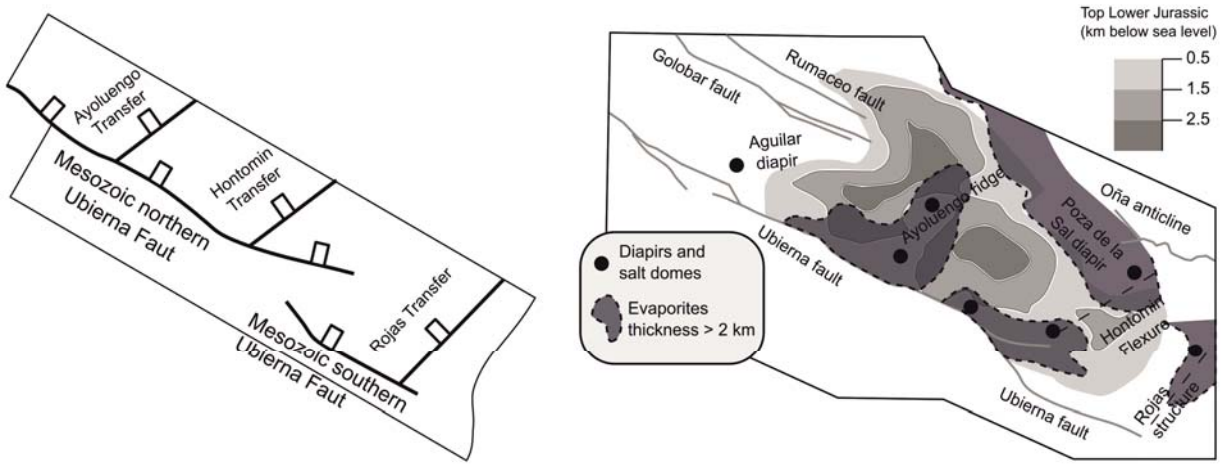

Fig. R.4: Situació de les principals falles que caracteritzaven el sistema extensiu així com també el patró de distribució del nivell salí del Triàsic Superior.

La posició d'aquestes acumulacions de sal, especialment la ONO-ESE localitzada al nord, va condicionar el desenvolupament de l'estructura compressiva degut a l'efecte de contrafort que va produir l'acumulació de sal així com també la potència de sediments sin-extensius del Cretaci Inferior dipositats al bloc superior d'aquesta estructura. Així doncs, el model extensiu proposat per a la Plataforma Burgalesa està compost per falles de basament que provoquen plecs d'acomodació a la cobertora que al mateix temps és desplaçada almenys 10 km cap al nord, lloc on es desenvolupa una estructura compressiva que acomoda part del desplaçament extensiu produït al marge sud. Aquest desplaçament cap al nord de la cobertora queda palès en el desenvolupament de les geometries d'onlap observades al marge sud (Fig. R.5).

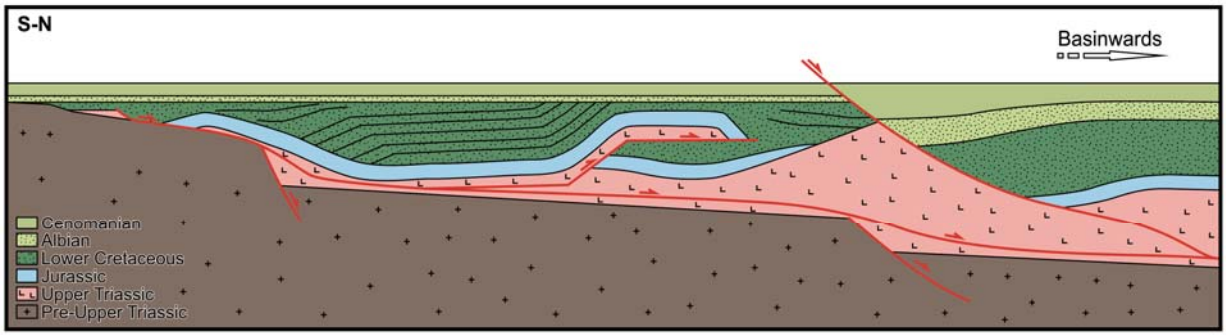

Fig. R.5: Representació esquemàtica del sistema extensiu amb la cobertora mesozoica desenganxada al nivell salí i desplaçada cap al nord on es desenvolupa l'estructura compressiva.

Estudi paleomagnètic de rotacions d'eix vertical a la zona d'estudi.

L'estudi paleomagnètic dut a terme a la Plataforma Burgalesa i als seus voltants ha revelat que la mineralogia magnètica de les calcàries i les argiles grises del Cretaci Superior i del Miocè és el grup de la (titano)magnetita (Fig. R.6A i B). Per contra, les sorres fines i les argiles vermelles del Cretaci Inferior i de l'Oligocè-Miocè estan caracteritzades pel grup de l'hematites (Fig. R.6C i D)

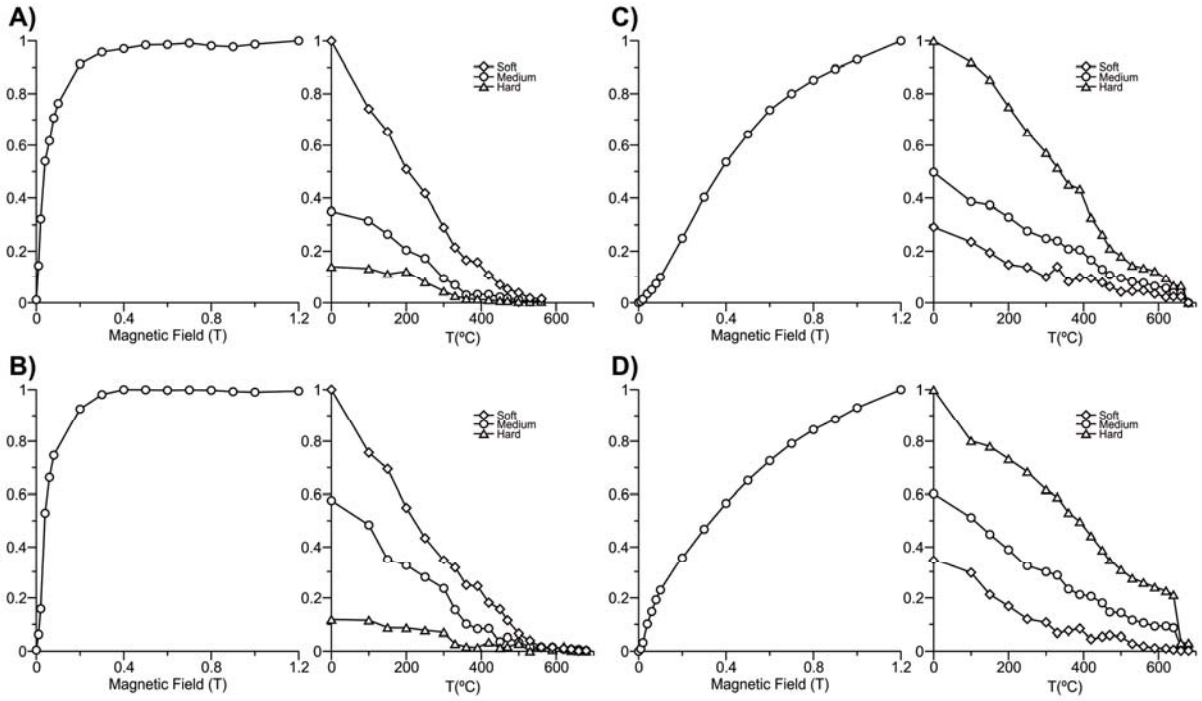

Fig. R.6: Gràfiques d'adquisició de IRM i anàlisis normalitzats de desmagnetització en els tres eixos de: A) Argiles grises del Miocè; B) Lutites negres del Cretaci Superior: C) Argiles vermelles del Miocè Inferior; i D) Argiles vermelles de l'Oligocè. A i B corresponen al grup de la (titano)magnetita mentre que C i D corresponen al grup de l'hematites.

El test del plec, realitzat a la conca d'avantpaís de l'Ebre just al sud de l'encavalcament frontal als materials Cenozoics (Fig. R.7), ha resultat positiu mostrant que la magnetització va ser adquirida amb anterioritat a la deformació de l'àrea (Fig. R.8).

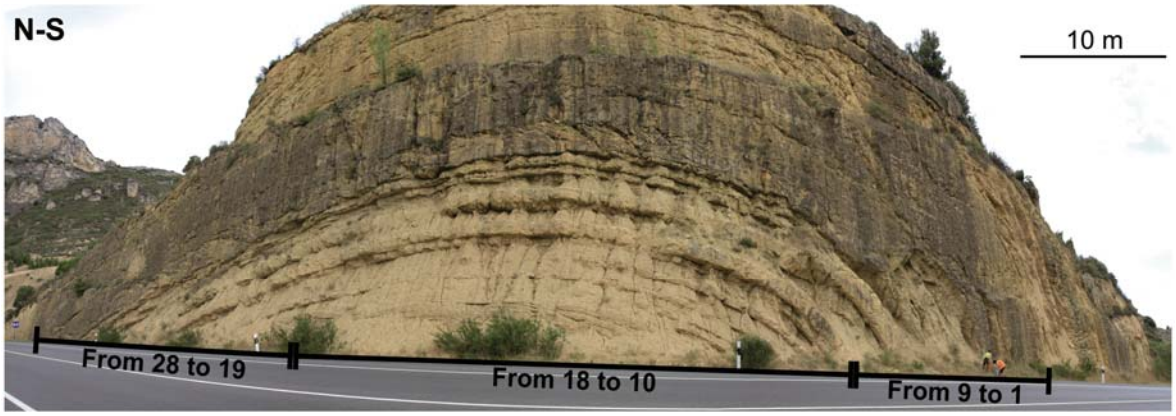

Fig. R.7: Estació FC-01 on es va realitzar el test del plec, el qual va resultar positiu.

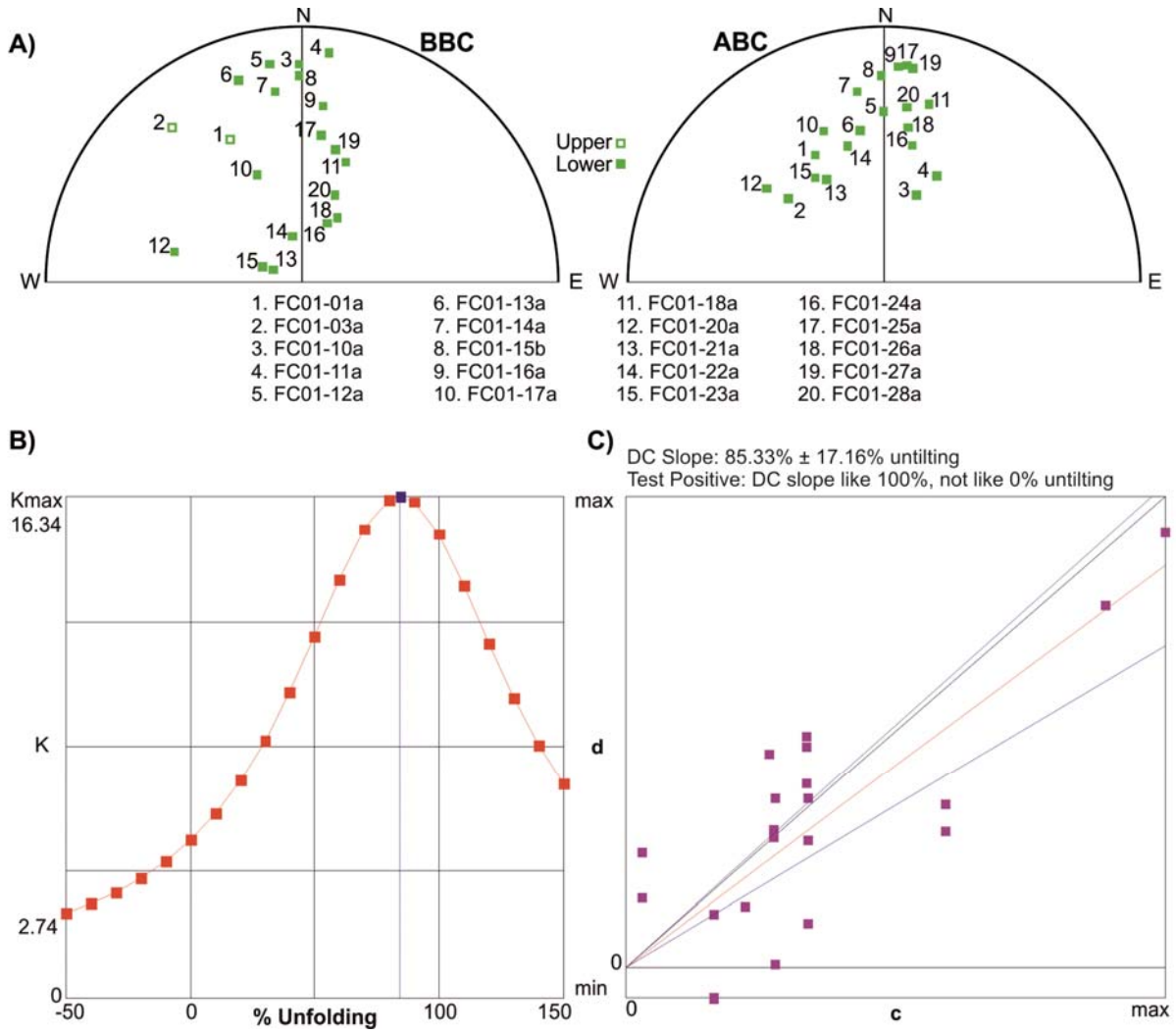

Fig. R.8: Resultats del test del plec local realitzat a l'estació FC-01. A) Projecció estereogràfica de les direccions abans (BBC) i després (ABC) de la correcció tectònica. B) Test del plec de McFadden. C) Test de direcció-correcció segons Enkin.

Aquest fet permet aplicar el mètode paleomagnètic focalitzat a rotacions d'eix vertical que hagin tingut lloc durant el Cenozoic a la zona dels Pirineus Bascos.

L'estudi està compost per 62 estacions de mostreig de les quals les mostres analitzades van permeten calcular la direcció característica mitjana de 26 estacions amb un valor de α_{95} inferior a 20 (Fig. R.9). Els resultats obtinguts mostren que al sector est de la Plataforma Burgalesa la rotació és anti-horària d'uns 20º mentre que al sector oest la rotació és de 25º però en aquest cas horària. Aquest patró de rotacions d'eix vertical està completament d'acord amb el model teòric d'un arc que ha estat comprimit posteriorment. Aquest model teòric no prediu rotacions al centre de l'arc mentre que espera rotacions horàries i anti-horàries, les quals es tanquen apuntant cap a l'interior de l'arc, al extrems d'aquest.

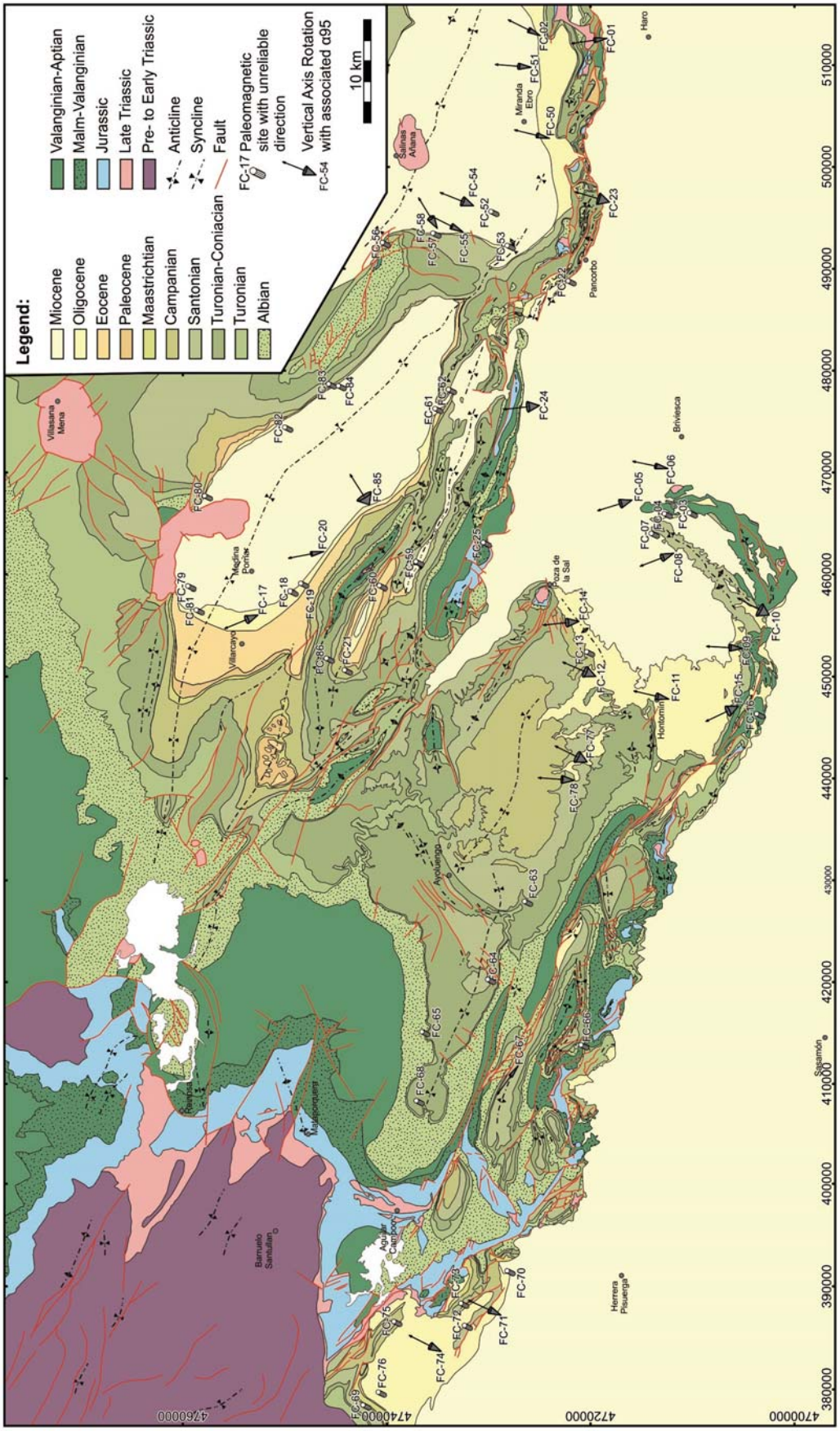

Fig. R.9: Mapa geològic de la zona on s'ha realitzat l'estudi paleomagnètic amb la posició de 1) estacions amb el vector paleomagnètic i el seu α_{95} associat i 2) estacions mostrejades les quals no s'ha pogut calcular el vector paleomagnètic.

Transició *thick-skin* a *thin-skin* i evolució durant el Cenozoic.

Els resultats obtinguts durant aquesta tesi han demostrat que la geometria de la conca extensiva i la obliqüitat entre la orientació de les falles i la direcció de compressió van condicionar la inversió de la Plataforma Burgalesa i la subseqüent incorporació a l'orogen Pirenaic durant el Cenozoic.

Un nou model evolutiu que explica la història de deformació de la zona ha estat presentat. Aquest model és una combinació dels estils de deformació *thick-skinned* i *thin-skinned* durant la inversió obliqua, la qual va estar condicionada per el nivell evaporític del Triàsic Superior. El domini *thick-skinned*, situat a l'oest, està caracteritzat per encavalcaments que involucren basament amb una orientació ONO-ESE a O-E al sector del Massís Asturià i la conca d'avantpaís del Duero. Per contra, el domini *thin-skinned* s'estén cap a l'est del *cutoff* de basament on el nivell evaporític del Triàsic Superior desacobla la successió mesozoica de la Plataforma Burgalesa i dels Pirineus Bascos (Fig. R.10).

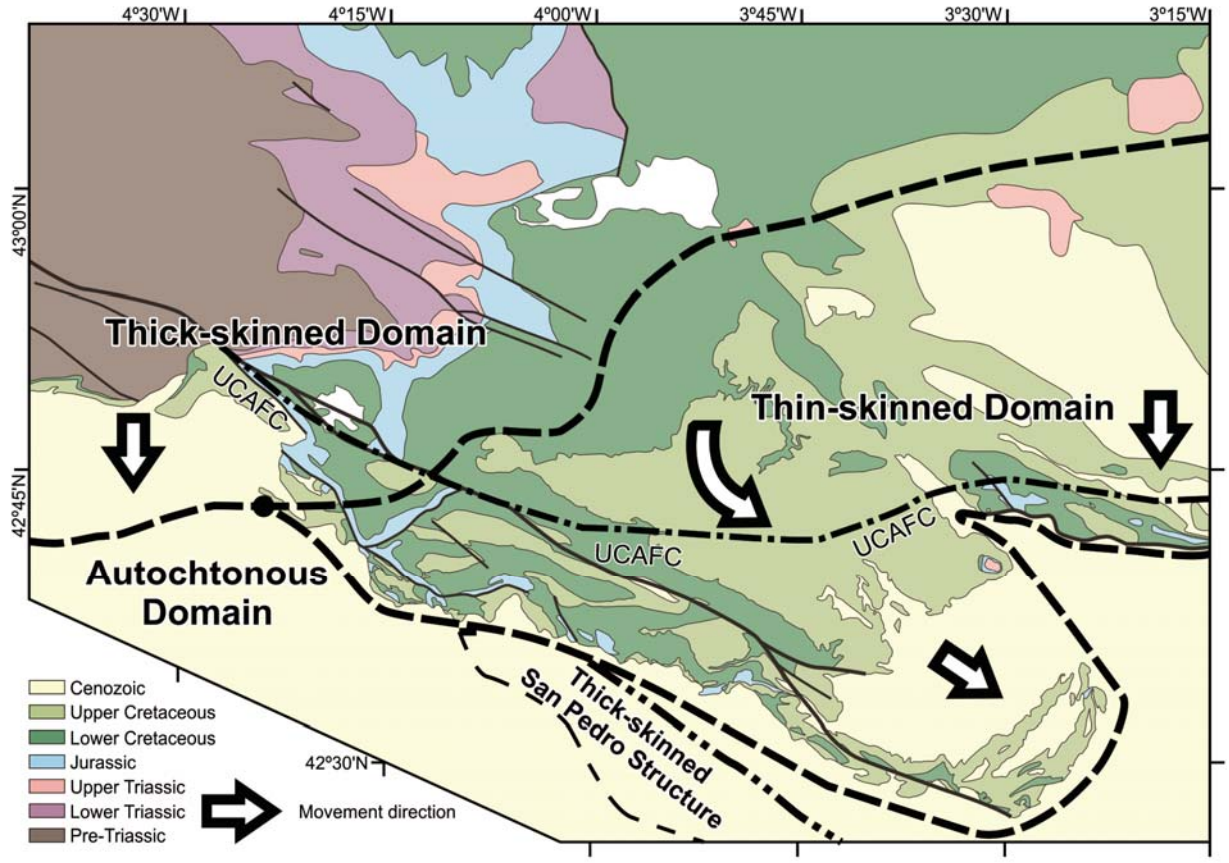

Fig. R.10: Mapa de la zona de la Plataforma Burgalesa amb la distribució dels estils estructurals definits en el model evolutiu presentat en aquesta tesi.

El domini *thick-skinned* (i.e. Massís Asturià i Conca d'Avantpaís del Duero), caracteritzat per encavalcaments d'alt angle els quals deformen el sòcol i la cobertora (Fig. R.11), està restringit no tan sols en l'espai sinó també en el temps.

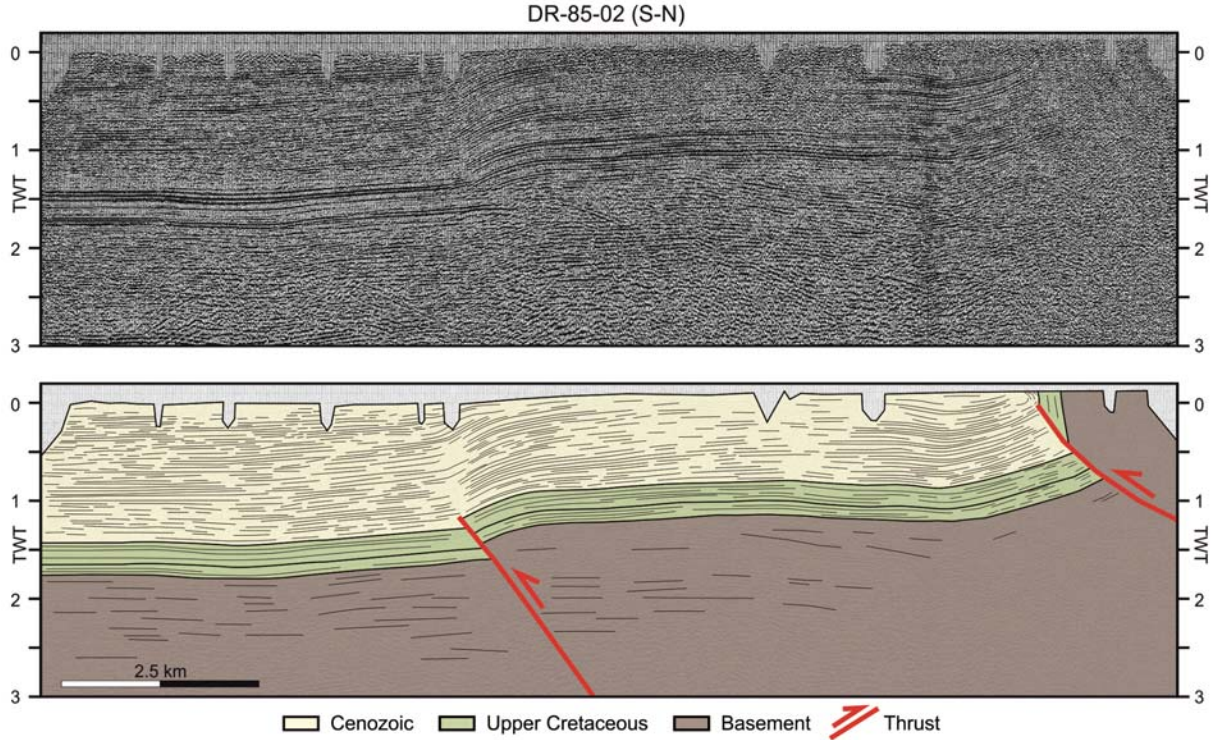

Fig. R.11: Línia sísmica situada a la conca d'avantpaís del Duero on els encavalcaments, d'alt angle, afecten tota la successió.

L'engruiximent progressiu de la potència del Triàsic Superior va permetre el desacoblament de les estructures i transferir la deformació de basament del Massís Asturià cap a la cobertora de la Plataforma Burgalesa (Fig. R.12).

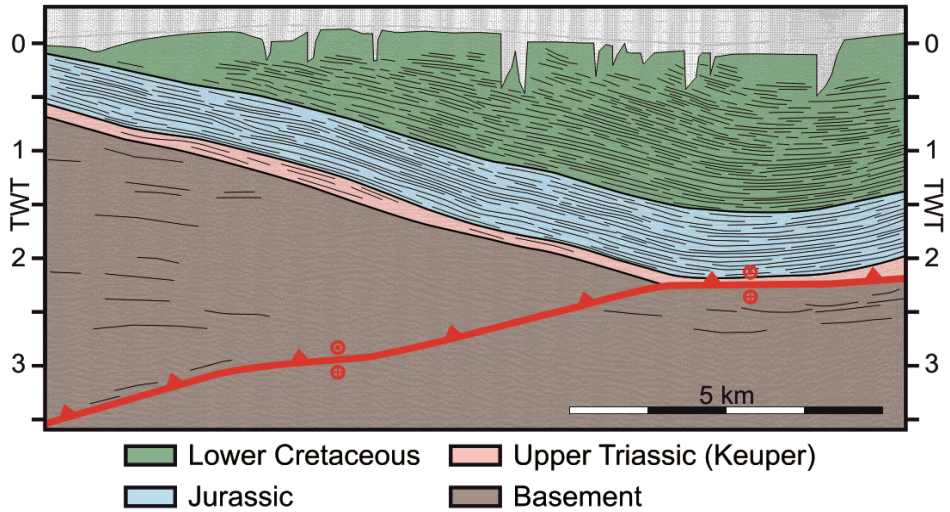

Fig. R.12: Línia sísmica del sector de Golobar on la deformació causada al basament és transferida al nivell de desenganxament salí desacoblant les estructures de basament i cobertora.

A més a més, la progressió en el temps de la deformació, cap al sud i involucrant nivells estructurals més profunds, va produir la reactivació i inversió d'estructures de basament heretades dirigides cap al sud, les quals estan situades al sud així com també sota la Plataforma Burgalesa. Aquest fet va resultar en un increment del relleu estructural i la immersió cap a l'est de les estructures presents a la terminació oriental del Massís Asturià i sector occidental de la Plataforma Burgalesa (Fig. R.12).

Al domini *thin-skinned*, l'estudi combinat entre la geologia de superfície i les dades proporcionades pels pous d'exploració ha permès reinterpretar l'estructura de Zamanzas. Anteriorment, aquesta estructura havia estat considerada com a un parell de falles extensives dirigides cap al nord-est afectant el Cretaci Inferior així com també el Superior. Amb aquest estudi s'ha demostrat que totes les restriccions s'ajusten millor re-interpretant aquesta estructura com un *pop-up* enlloc de falles extensives. Amb aquesta interpretació, els blocs situats al sud-oest i al nord-est constituirien els blocs inferiors del *pop-up* mentre que el bloc entre els dos anteriors correspondria el bloc superior d'aquesta estructura (Fig. R.13).

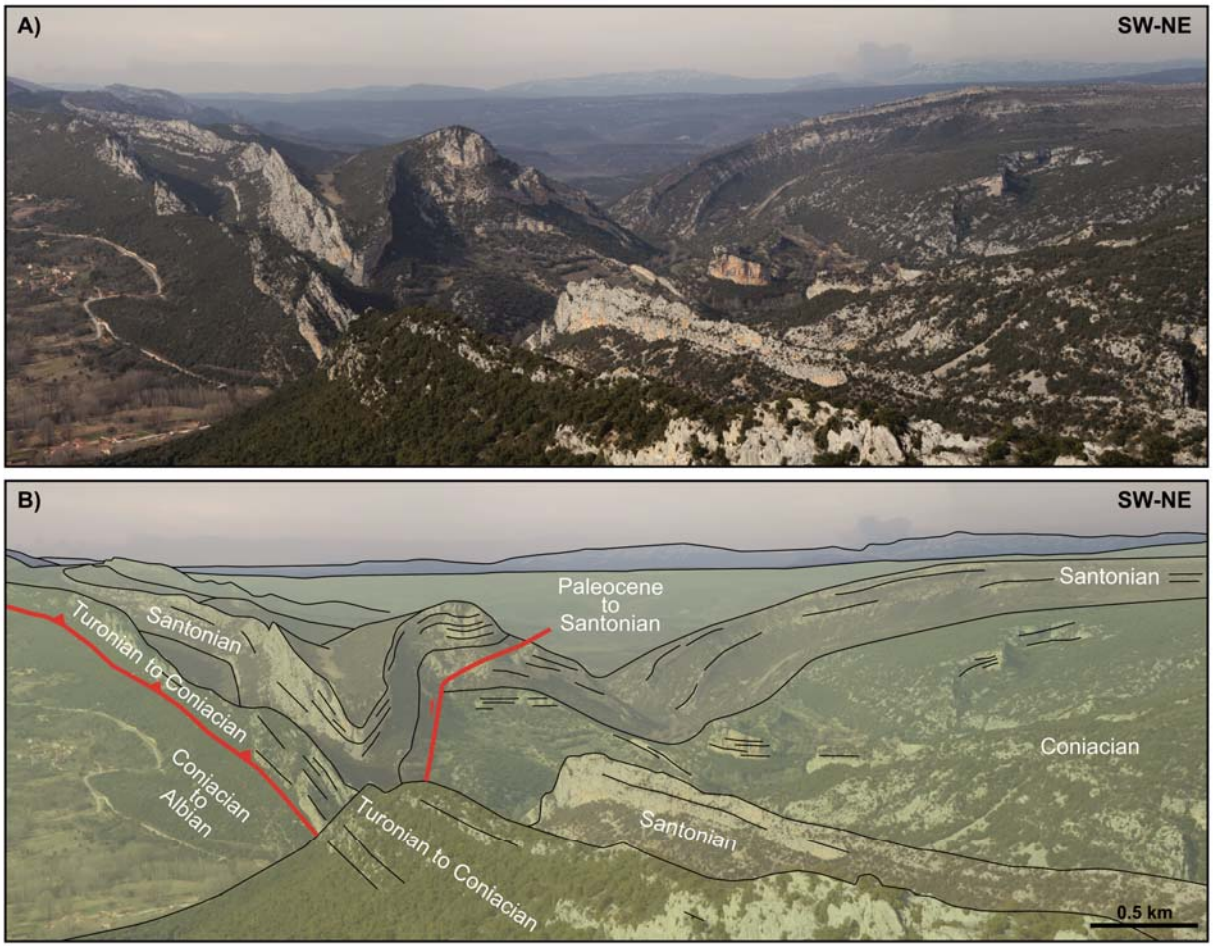

Fig. R.13: Fotointerpretació de l'estructura de Zamanzas com a *pop-up* on els blocs situats al sud i al nord corresponen als blocs inferiors d'aquesta estructura mentre que el bloc central correspon al bloc superior del *pop-up.*

Més cap al sud-est, la interpretació sísmica de la zona de la Bureba, situada entre l'estructura de Rojas al sud i l'encavalcament frontal dels Pirineus Bascos al nord, ha demostrat la continuïtat de l'estratigrafia sísmica de les facies atribuïdes al Cenozoic de la conca d'avantpaís del Duero i de l'Ebre (Fig. R.14). Així doncs, es demostra que l'estructura de Rojas no pot ser connectada amb l'encavalcament frontal dels Pirineus Bascos per mitjà d'una estructura lateral amb una orientació SO-NE. A més a més, reafirma el desenganxament i encavalcament de la Plataforma Burgalesa sobre la conca d'avantpaís de l'Ebre. Més cap a l'est, no s'aprecia deformació a l'avantpaís. Per contra, cap al sud la Plataforma Burgalesa encavalca l'estructura de San Pedro, la qual està caracteritzada per encavalcaments amb una orientació NO-SE i una direcció de transport cap al nord-est els quals afecten el sòcol. Aquesta estructura s'ha associat a la deformació causada durant l'Oligocè pel desenvolupament de la Cadena Ibèrica la qual està situada al sud dels Pirineus. Totes aquestes observacions permeten a més a més associar la deformació produïda al sector oest a la deformació causada per el desenvolupament dels Pirineus en els darrers estadis durant el Miocè mentre que la deformació de San Pedro va desenvolupar-se amb anterioritat i està associada a la Cadena Ibèrica.

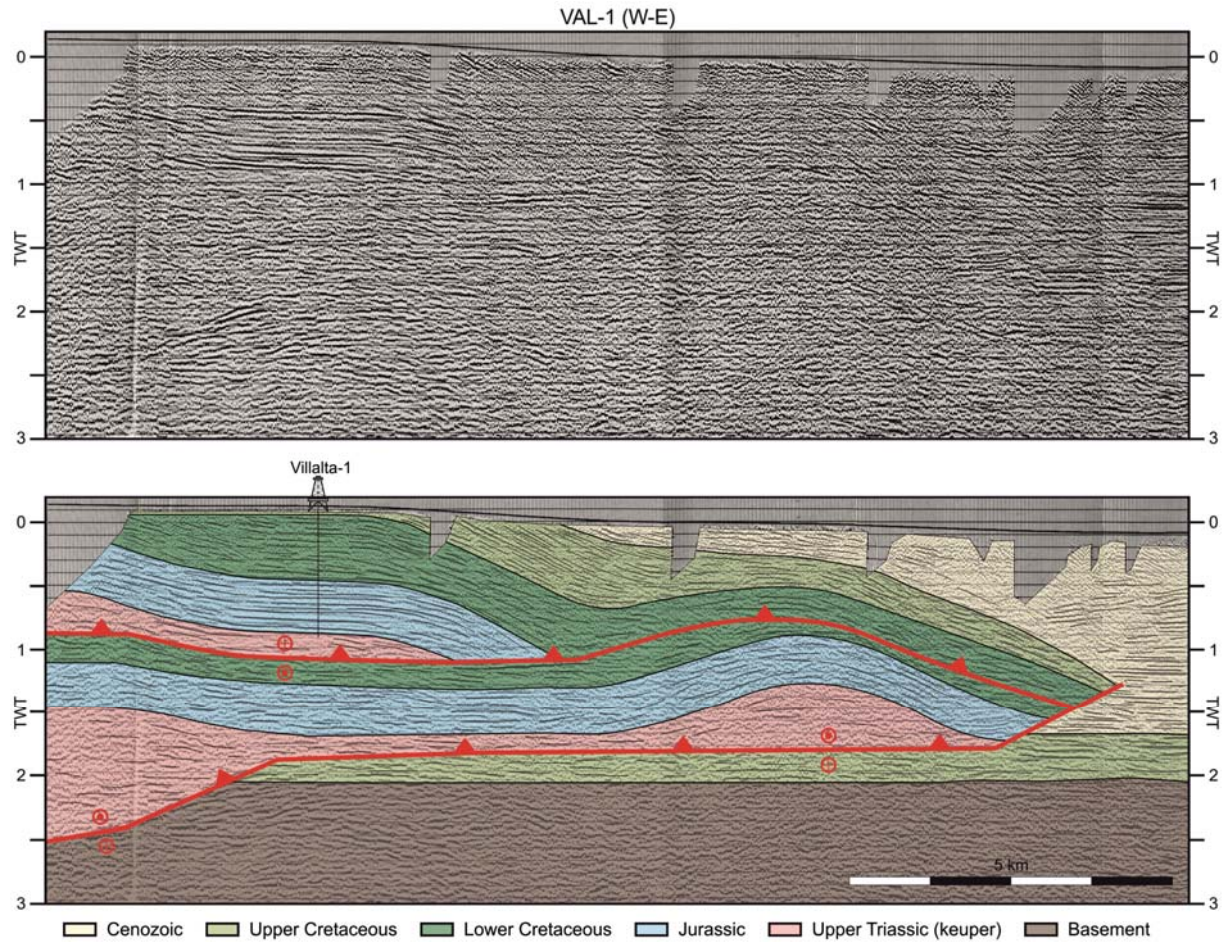

Fig. R.14: Línia sísmica on s'observa la successió mesozoica de la Plataforma Burgalesa encavalcant sobre la conca d'avantpaís i com cap a l'est, les facies sísmiques de la conca de l'Ebre no presenten deformació.

Finalment, la zona central dels Pirineus Bascos, situada més a l'est de la Plataforma Burgalesa, està caracteritzada per la inversió de la conca extensiva tal i com mostra el fet que la cobertora mesozoica es troba desenganxada a nivell del triàsic salí. Aquesta unitat estructural està encavalcant la conca d'avantpaís de l'Ebre amb un desplaçament cap al sud d'uns 20 km mínims tal i com es posa de manifest en la línia sísmica que creua aquesta àrea (Fig. R.15).

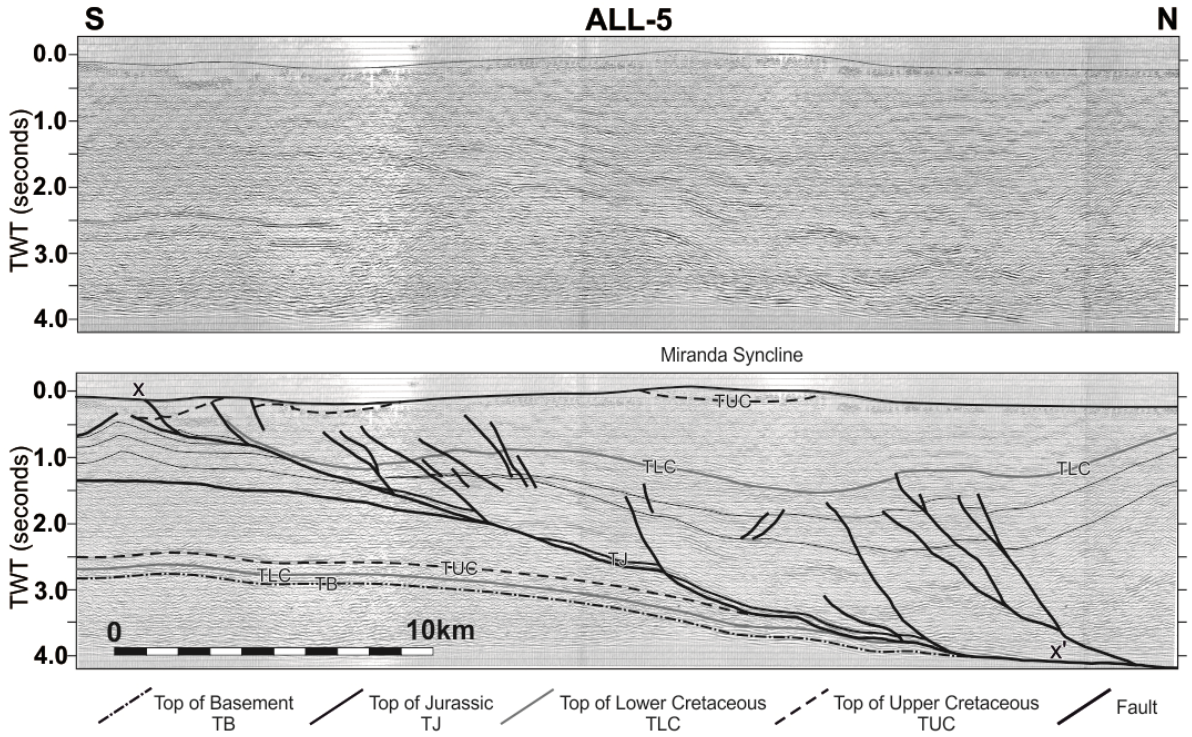

Fig. R.15: Línia sísmica que creua l'encavalcament frontal dels Pirineus Bascos i on s'observa el desenganxament de la successió mesozoica dels Pirineus sobre la conca d'avantpaís de l'Ebre.

La situació confinada de la Plataforma Burgalesa entre el Massís Asturià a l'oest i la prolongació nord-oest de la deformació associada a la Cadena Ibèrica (i.e. estructura de San Pedro) condicionà l'evolució cenozoica de l'àrea d'estudi. Durant els estadis inicials de la deformació cenozoica, el desplaçament cap al sud de la Plataforma Burgalesa, invertint la conca extensiva, i el desplaçament cap al nord-est de l'estructura de San Pedro van ser les principals àrees actives permetent el desenvolupament de la conca d'avantpaís entre aquests dos dominis. Al continuar la deformació, aquestes dues unitats estructurals varen anar reduint l'espai deixant un corredor entre les dues fins al punt en el qual la Plataforma Burgalesa encavalca l'alt de San Pedro. La interferència de contrafort que aquesta darrera estructura produeix, força la reactivació en direcció de la falla d'Ubierna i, com a conseqüència, l'extrusió lateral de part de la Plataforma Burgalesa, amb més de 15 km de desplaçament, cap al sud-est encavalcant la conca d'avantpaís de l'Ebre. Durant els darrers estadis de deformació es va produir, la reactivació de la falla de Golobar per tal de mantenir l'angle crític de l'orogen i la

inversió obliqua de les estructures de basament sota la Plataforma Burgalesa al sector oest com a conseqüència de la progressió de la deformació (Fig. R.16).

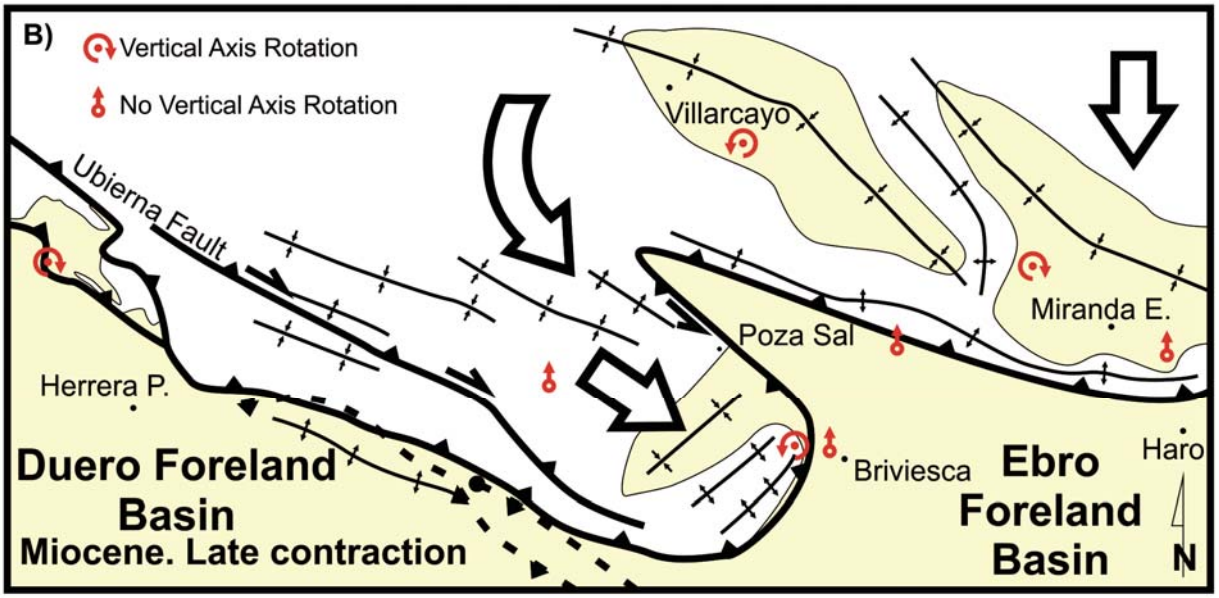

Fig. R.16: Evolució dels darrers estadis de deformació durant els quals va tenir lloc 1) la reactivació de la falla d'Ubierna; 2) l'extrusió lateral de la Plataforma Burgalesa; 3) el desenvolupament d'estructures de basament al sector oest; i 4) les rotacions d'eix vertical.

Preface

Motivations and objectives of the thesis

During the development of an orogenic system, two possible styles of deformation characterise the deformation of the lithosphere. On one hand, thick-skinned tectonics in which the faults cut across the entire upper crust uplifting and displacing the basement and the cover without decoupling. This style of deformation is typically associated with the inner parts of the orogens such as the Alps or the Cordillera Oriental in the Andes (Pfiffner and Hitz, 1997; Carrera and Muñoz, 2013). On the other hand, thin-skinned tectonics characterised by low angle thrusts detached into mechanically weak horizons and defining ramps and flats as the thrusts climb up-section. This style is typically associated to the external parts of the orogens being the cover displaced over the foreland basin by the thrust system. Examples of thin-skinned tectonics can be found at the external Foothills of the Canadian Rocky Mountains and the Zagros, among others (Bally *et al.*, 1966; Stockmal *et al.*, 2001; Blanc *et al.*, 2003). Although the two types of deformation pointed above can be present across the orogens, from

the internal parts characterised by thick-skinned tectonics to the external parts where thin-skinned style may dominate, both styles of deformation may also coexist along-strike of the fold and thrust belts such as in the Andes and in the Pyrenees, to name a few (Kley *et al.*, 1999; Muñoz, 2002).

In addition to the across and along-strike variations of the structural style, temporal variations have to be taken into account. Among others, two good examples of temporal variations of the style of deformation are the Papua New Guinea and the Apennines fold and thrust belts. The early stages of development of the Papua New Guinea orogen were characterised by the thick-skinned inversion of inherited extensional faults involving the basement. During this stage the development of anticlines in where hydrocarbons where accumulated took place. Later, the style of deformation changed and the anticlines were detached, decapitated and south-westward displaced above the basement (Hill *et al.*, 2002; 2008). In the Apennines, the early stages of rift inversion were determined by the reactivation of the faults and then northward displaced over a detachment located in the Triassic. Later, inherited basement faults were reactivated deforming the detached succession and producing extension in the allochtonous thin-skinned overburden (Mazzoli *et al.*, 2008).

The doubly-vergent roughly W-E striking Pyrenean Orogen resulted from a multiphase deformational history involving thick- and thin-skinned styles of deformation. An extensional event related to the opening of the North Atlantic and the Bay of Biscay during Late Jurassic-Early Cretaceous resulted into the development of intracontinental basins at the passive margins, subsequent further crustal thinning and mantle exhumation and the spreading of oceanic crust at the western part the Bay of Biscay ridge. This allowed the local deposition of more than 10 km of syn-rift sediments overlying the well-layered Jurassic succession and the stretched and thinned continental crust (e.g. Le Pichon & Sibuet, 1971; García de Cortázar & Pujalte, 1982; Pujalte, 1982; Mathieu, 1986; Ziegler, 1987; Bois *et al.*, 1997; Pedreira *et al.*, 2007; Ruiz, 2007; Ferrer *et al.*, 2008; Jammes *et al.*, 2009, Roca *et al.*, 2011). The pre-contractive articulated architecture of the Pyrenean rift system determined the across and along-strike variations of the fold and thrust belt developed during the convergence between the Eurasian and the Iberian plates. This stage took place from Late Cretaceous to Cenozoic producing the subduction of the Iberia towards the north with the subsequent inversion of the Mesozoic basins (e.g. Le Pichon & Sibuet, 1971; Muñoz, 1992, 2002; Alonso *et al.*, 1996; Vergés & García-Senz, 2001).

The Basque Pyrenees involves a large and thick inverted Jurassic to Upper Cretaceous basin (Fig. P.1). Its southern frontal structure (Sierra de Cantabria Frontal Thrust), detached at Upper Triassic evaporites, is a roughly E-W trending major thrust which defines a broad thrust salient with the eastern and western edges trending NE-SW and NW-SE respectively. To the east, the footwall of this Basque-Cantabrian thrust front corresponds to the Ebro foreland basin. However, to the west another structural unit occupies an intermediate position between the foreland and the main Basque-Cantabrian thrust front. This unit, known as Burgalesa Platform, also shows a thrust salient concave to the north, although asymmetric and more pronounced than the previously described one. It developed during the Oligocene and Early Miocene times and inverted an Upper Jurassic-Lower Cretaceous extensional basin. More to the west and in continuity with the Burgalesa Platform, the Cantabrian Mountains, constituted by Paleozoic rocks, were uplifted and southward displaced by a thrust system rooted into the crust and emerging along a roughly W-E trending thrust front (Cantabrian Mountains Frontal Thrust). The structural significance of the Burgalesa Platform and the transition between the two styles of deformation (thick-skin and thin-skin) present in these areas is not well known up to date.

During the last decades the construction of cross-sections and 3D models, based on geometrical models, and constrained with the integration of surface and subsurface data allowed to reconstruct the evolution and kinematic of structures (Medwedeff, 1992; Yamamoto, 1993; de Kemp, 1998, 2000; Maerten et al., 2001; Lemon and Jones, 2003; Fernández *et al.*, 2004; Bistacchi *et al.*, 2008; Carrera *et al.*, 2009, Mencos *et al.*, 2011, among others). More recently, the integration of paleomagnetic vertical axis rotations data provided new constraints for cross-sections construction or orogenic scale interpretations (Schwartz and Van der Voo, 1984; Allerton, 1998; Pueyo *et al.*, 2002; Weil *et al.*, 2010; Muñoz *et al.*, 2013).

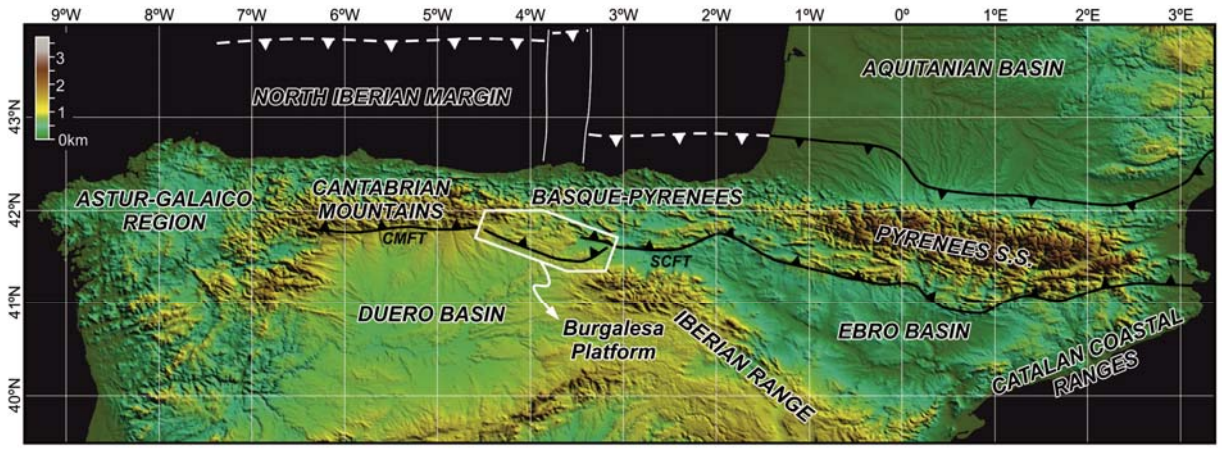

Fig. P.1: Map of the northern Iberia with the location of the main structural units of the Pyrenees. CMFT and SCFT corresponds to Cantabrian Mountains Frontal Thrust and Sierra de Cantabria Frontal Thrust, respectively.

Within the Pyrenees, several well studied areas with paleomagnetic sites (Fig. P.2A) allowed to obtain solid interpretations by integrating all these data (Bates, 1989; Dinarès *et al.*, 1992; Pueyo *et al.*, 2002; 2003; Oliva-Urcia and Pueyo, 2007; Soto *et al.*, 2011; Muñoz *et al.*, 2013, among others). Although the amount of sites for the Pyrenees *s.s.*, the scarcity of paleomagnetic sites reported for the Burgalesa Platform (Fig. P.2B) does not allow to constraint the possible vertical axis rotations occurred during the Cenozoic evolution. The studies carried out in the Burgalesa Platform were either focussed on the Mesozoic successions or northwards in the Cabuérniga area (Stauffer & Tarling, 1971; Vandenberg, 1980; Schott, 1985; Schott & Peres, 1987; Soto *et al.*, 2007a; Soto *et al.*, 2008; Almar *et al.*, 2008; Soto *et al.*, 2011).

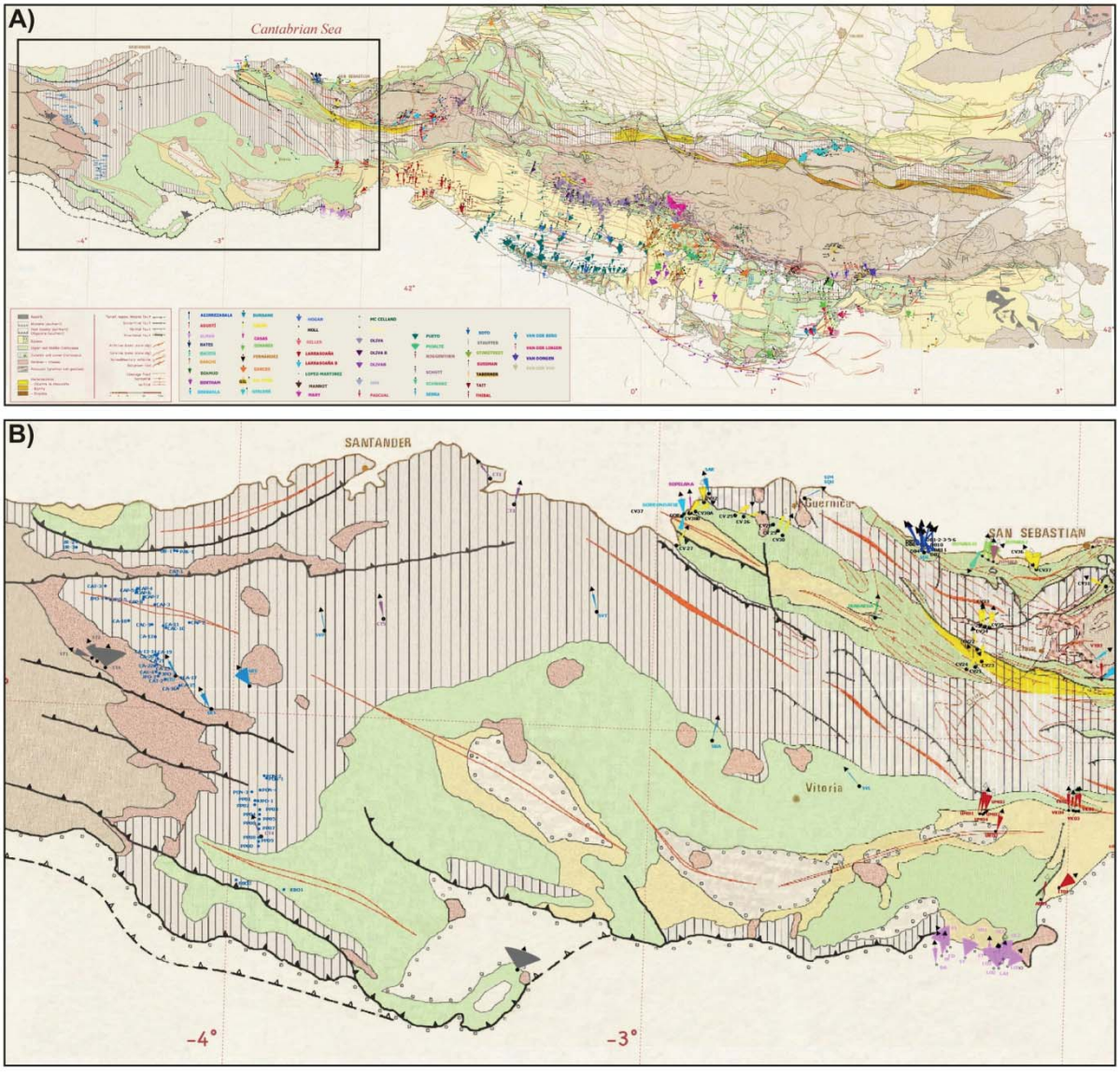

Fig. P.2: A) Geological map of the Pyrenees with the location of the paleomagnetic sites reported for other authors. B) Detail of the previous map with the paleomagnetic sites of the Burgalesa Platform and also for the Basque Pyrenees. Modified from Pueyo *et al.* (2006).

Finally, CO_2 Capture and Storage (CCS) is being actively implemented by many countries as one of the key options to reduce atmospheric CO_2 emissions. Storage of CO_2 in the subsurface currently involves three types of geological reservoirs (IPCC, 2005): Abandoned coal seams, depleted hydrocarbon reservoirs, and saline aquifers. Spain is characterised by the paucity of the first two types of reservoirs and, consequently, the possibility of CO_2 storage relies on saline aquifers. The Ciudad de la Energía Foundation was developing a CCS experimental project in the Burgalesa Platform (the Hontomín CO_2 storage site), where methodologies and technologies for CO_2 storage and subsequent monitoring will be developed and tested (Pérez-Estaún *et al.*, 2009). Several pre-injection studies have been carried out, with the aim of fully define the structure and baseline framework of the Hontomín site (Elío *et al.*, 2012; Ogaya *et al.*, 2013; Quintà, 2013; Alcalde *et al.*, 2013). In order of better understand the development and evolution of the Hontomín structure, a better understanding of the Burgalesa Platform is needed.

For this purpose, the principal objectives of the thesis are focused to:

1) Characterise the transition from the thick-skinned tectonic style of the Cantabrian Mountains eastwards into the thin-skinned structures of the eastern part of the studied area.

2) Determine the main geometric features of the Late Jurassic-Early Cretaceous extensional system and gain insight into the understanding of the role played by the Triassic evaporites during the rifting event.

3) Understand and elucidate the tectono-sedimentary relationships observable in the seismic lines available in the Burgalesa Platform.

4) Constrain the Cenozoic evolution of the Burgalesa Platform by means of paleomagnetic vertical axis rotations studies.

Thesis organisation

This thesis has been structured as a compendium of different scientific papers published or accepted for its publication in peer-review international journals and special volumes. More specifically, it is made up of three articles with the following references:

- Carola, E., Tavani, S., Ferrer, O., Granado, P., Quintà, A., Butillé, M., Muñoz, J.A. (2013). Along-strike extrusion at the transition between thin- and thick-skinned domains in the Pyrenean Orogen (northern Spain). In: *Thick-Skin-Dominated Orogens: From Initial Inversion to Full Accretion* edited by Nemčok, M., Mora, A.R. and Cosgrove, J.W. Geological Society of London Special Publications **377**, 119-140. DOI: 10.1144/SP377.3

- Tavani, S., Carola, E., Granado, P., Quintà, A., Muñoz, J.A. (2013). Transpressive inversion of a Mesozoic extensional forced fold system with an intermediate décollement level in the Basque-Cantabrian Basin (Spain). *Tectonics* **32**. DOI: 10.1002/tect.20019.

- Carola, E., Muñoz, J.A., Roca, E. (submitted). The transition from basement-involved thick-skinned to detachment thin-skinned tectonics in the Basque-Pyrenees: The Burgalesa Platform and vicinities. *International Journal of Earth Science.*

Most of the work and the results that have been obtained during this period of research are summarised in this scientific papers and they give an overview of the western termination of the Basque Pyrenees. Additionally, the 4th chapter encloses the paleomagnetic study focussed on determining vertical axis rotations occurred in the study area. The 5th chapter concerns the discussion of the results obtained during the accomplishment of this thesis and the final chapter encloses the conclusions. Within the annexes are enclosed the publication of the "Photograph of the month" published in 2012 in the Journal of Structural Geology volume 42 by Stefano Tavani and Eloi Carola and also the description of the paleomagnetic sites.

Geological setting

The aim of this part of the Thesis is to give an overview of the evolution of the Pyrenees and to describe the main structural domains and also the stratigraphic and seismostratigraphic record of the studied area. It is not the scope of this section to discuss about the structural domains or the significance of each sedimentary unit. Rather than that, we think necessary to include it because of the short descriptions enclosed in the different scientific papers.

P1.1 Regional framework

The E-W Himalayan-Alpine orogenic system that extends from eastern Asia to western Europe is the largest contractional deformed area during Mesozoic and Cenozoic times (Fig. P.3). The Pyrenean orogen is the westernmost mountain belt of this orogenic system and

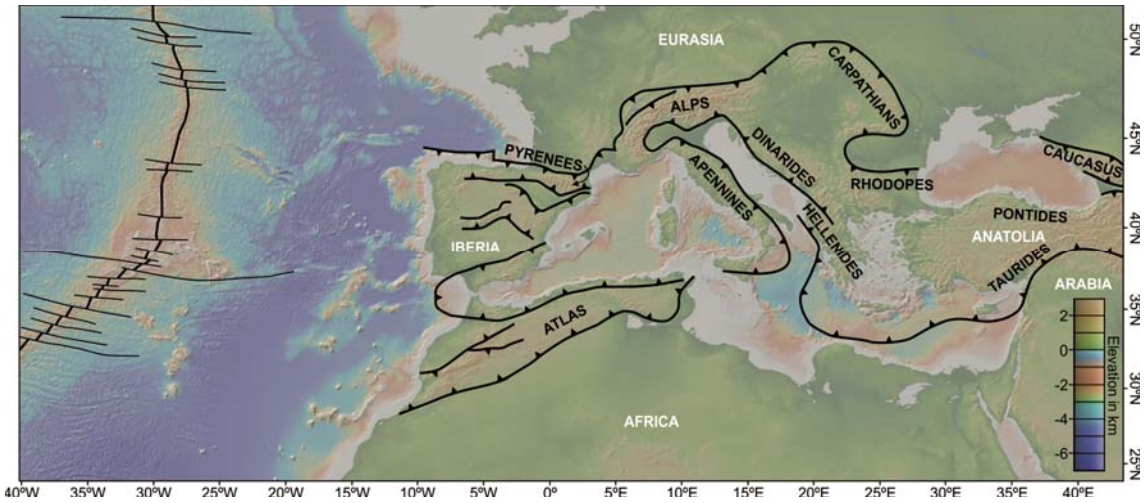

Fig. P.3: Principal mountain belts of the western portion of the Himalayan-Alpine orogenic system labelled in black and main tectonic plates labelled in white (elevation map from GeoMapApp).

extends from the Mediterranean Sea to the North Atlantic Ocean with a roughly E-W orientation. The Pyrenees resulted from the inversion of previously developed Mesozoic basins during the convergence between Iberian plate and Eurasian plates (Late Cretaceous to middle Miocene) (i.e. Le Pichon & Sibuet, 1971; Srivastava *et al.*, 1990; Álvarez-Marrón *et al.*, 1996; Muñoz, 1992, 2002; Vergés & García-Senz, 2001; Vergés *et al.*, 2002; Rosenbaum *et al.*, 2002).

The development of Mesozoic basins during the Upper Jurassic-Lower Cretaceous was associated with the opening of the Western Tethys, the North Atlantic and the Bay of Biscay (Olivet *et al.*, 1984; Savotin *et al.*, 1986; Srivastava *et al.*, 1990; Roest & Srivastava, 1991, among others). Two possible extreme models have been purposed in order to explain the kinematics during the rifting and subsequent convergence event that resulted in the present day configuration of the orogen (Fig. P.4).

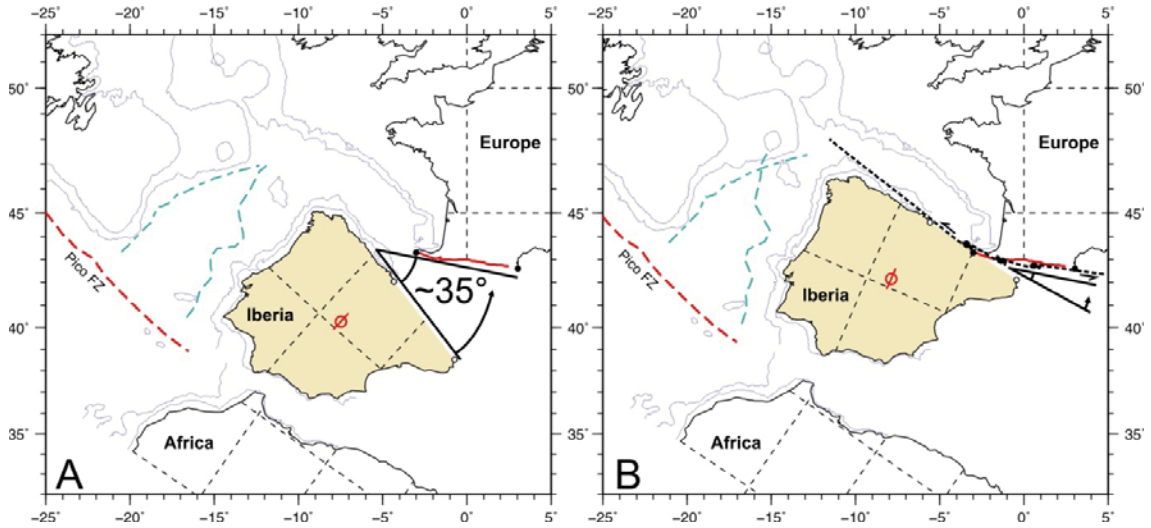

Fig. P.4: Two extreme models purposed for the evolution of Iberia. A) Scissor-type model and B) Left-lateral strike-slip model (Modified from Vissers & Meijer, 2012).

The first model, purposes a scissor-type opening of the Bay of Biscay (Fig. P.4A) and implies a counter-clockwise rotation of about 35º of Iberia with respect to the stable Europe (Carey, 1958; Srivastava *et al.*, 1990, 2000; Rosenbaum *et al.*, 2002; Sibuet *et al.*, 2004; Vissers & Meijer, 2012, among others). The second model, defenses a strike-slip opening and left-lateral motion (Fig. P.4B) implying a small counter-clockwise rotation and was purposed by other authors (Le Pichon *et al.*, 1970; Le Pichon & Sibuet, 1971; Olivet *et al.*, 1984; Olivet, 1996; Jammes *et al.*, 2009, among others). Despite this ongoing debate, the articulated Pyrenean Rift was developed between the two plates. During this stage, the continental crust was strongly thinned in the eastern arm of the rift system, whereas in the western arm, the stretching was enough to produce mantle exhumation (e.g. Pedreira *et al.*, 2007; Ruiz, 2007; Ferrer *et al.*, 2008; Jammes *et al.*, 2009, Roca *et al.*, 2011). This different amount of stretching is explained by the fact that the rift system was segmented by NNE-SSW soft transfer zones and structural highs that individualised the area into several sedimentary basins (Roca *et al.*, 2011) (Fig. P.5).

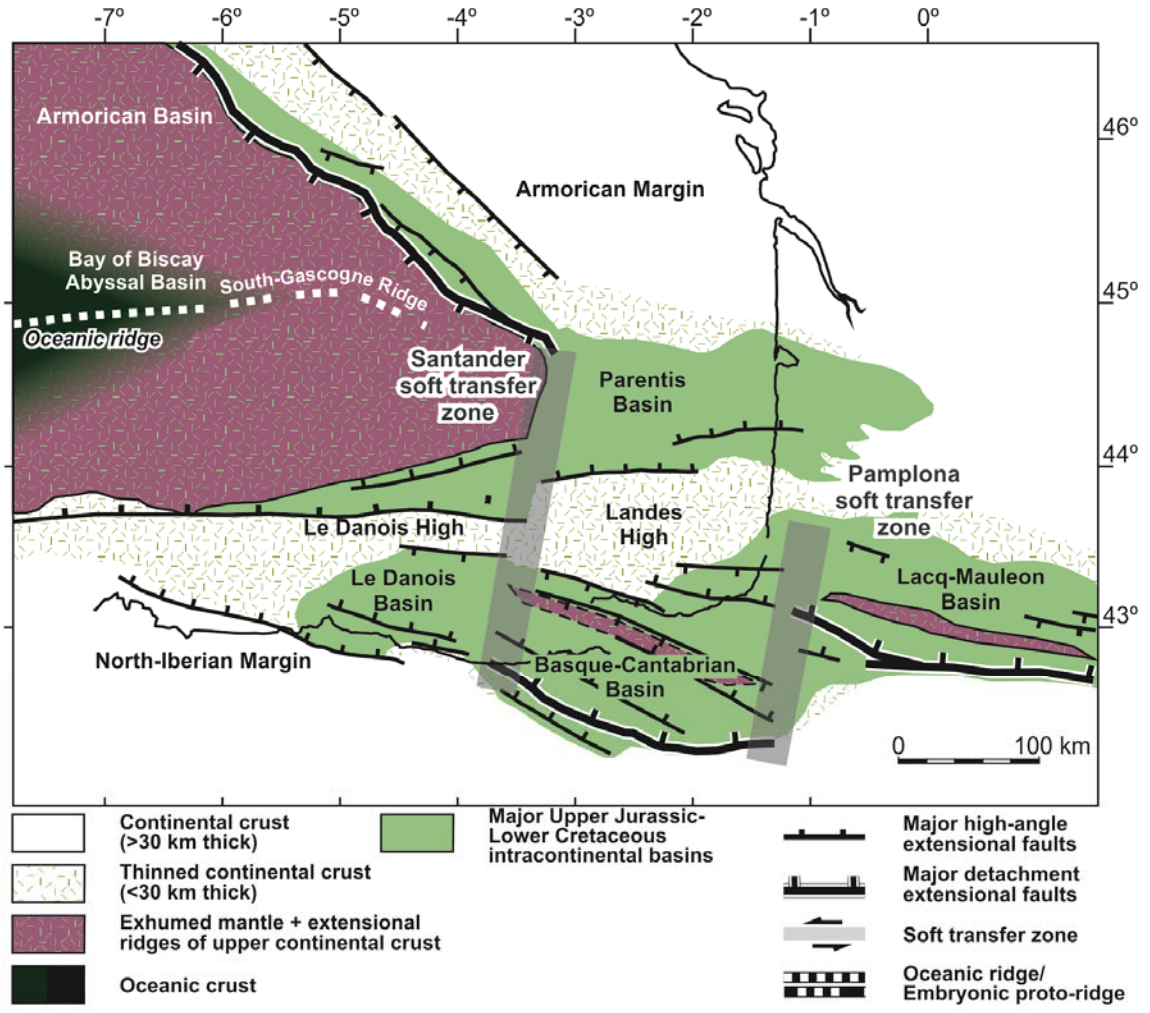

Fig. P.5: Palinspastic reconstruction of the extensional basins developed during the Upper Jurassic-Lower Cretaceous rifting stage. Soft transfer zones are highlighted by the wide grey bands (Roca *et al.*, 2011).

The development of the Pyrenean mountain belt started in the Late Santonian when the African plate started to drift towards the north. At the same time this plate motion, produced the movement of Iberia to the north and the initiation of the subduction of the Iberian plate underneath the Eurasian plate (Fig. P.6). As a result, the basins developed in the Pyrenean Rift where inverted and incorporated into the thrust belt. This pre-contractive configuration conditioned the inversion explaining the exposition of different structural levels along-strike of the orogen (Muñoz, 2002).

Typically the Pyrenees has been associated to the mountain belt that divides Spain and France and it is characterised by a double wedge of crustal rocks. The structures present in the southern wedge (i.e. Southern Pyrenees) are south-directed thrust sheets involving the cover and in the inner part of the belt a duplex of basement rocks. Contrary, at the northern wedge of the orogen (i.e. Northern Pyrenees), the thrust system is a stack of north-directed structures. Since the acquisition of the ECORS and ESCIN deep seismic profiles the along-strike subdivision of the Pyrenees has changed because of the recognition of the subduction between Iberia and Eurasia all along the northern border of Iberia (Choukroune *et al.*, 1989; Roure *et al.*, 1989; Choukroune *et al.*, 1990; Muñoz, 1992; Choukroune, 1992; Pulgar *et al.*, 1996; Álvarez-Marrón *et al.*, 1996; Bois *et al.*, 1997; Teixell, 1998; Pedreira *et al.*, 2003; Ferrer *et al.*, 2008 among others). Since then, the Pyrenees has been divided into four main realms that from east to west are: the Pyrenees *s.s.*, the Basque Pyrenees, the Cantabrian Mountains and the Astur-Galaico Region (Fig. P.6). The Pyrenees *s.s* and the Basque Pyrenees are divided by the inherited Early Cretaceous Pamplona soft transfer zone (Fig. P.5), reactivated during the Pyrenean Orogeny. The Basque Pyrenees and the Cantabrian Mountains are divided by a diffuse boundary that would correspond to the inherited Santander soft transfer zone where the Variscan basement rises up in the eastern boundary of the Cantabrian Mountains (Fig. P.5 and Fig. P.6).

Each realm present a different crustal configuration. The Pyrenees *s.s.* is characterised by the presence of a south-verging antiformal stack at the inner parts of the orogen. Towards the external parts, thrusts are detached at the Keuper facies determining a thin-skinned style of deformation where the thrust sheets ride over the Ebro foreland basin (Choukroune *et al.*, 1989; Muñoz, 1992, 2002 among others) (Fig. P.6 section 1). The Basque Pyrenees and the Cantabrian Mountains are characterised by an asymmetry between the southern and northern wedges (Fig. P.6 section 2).

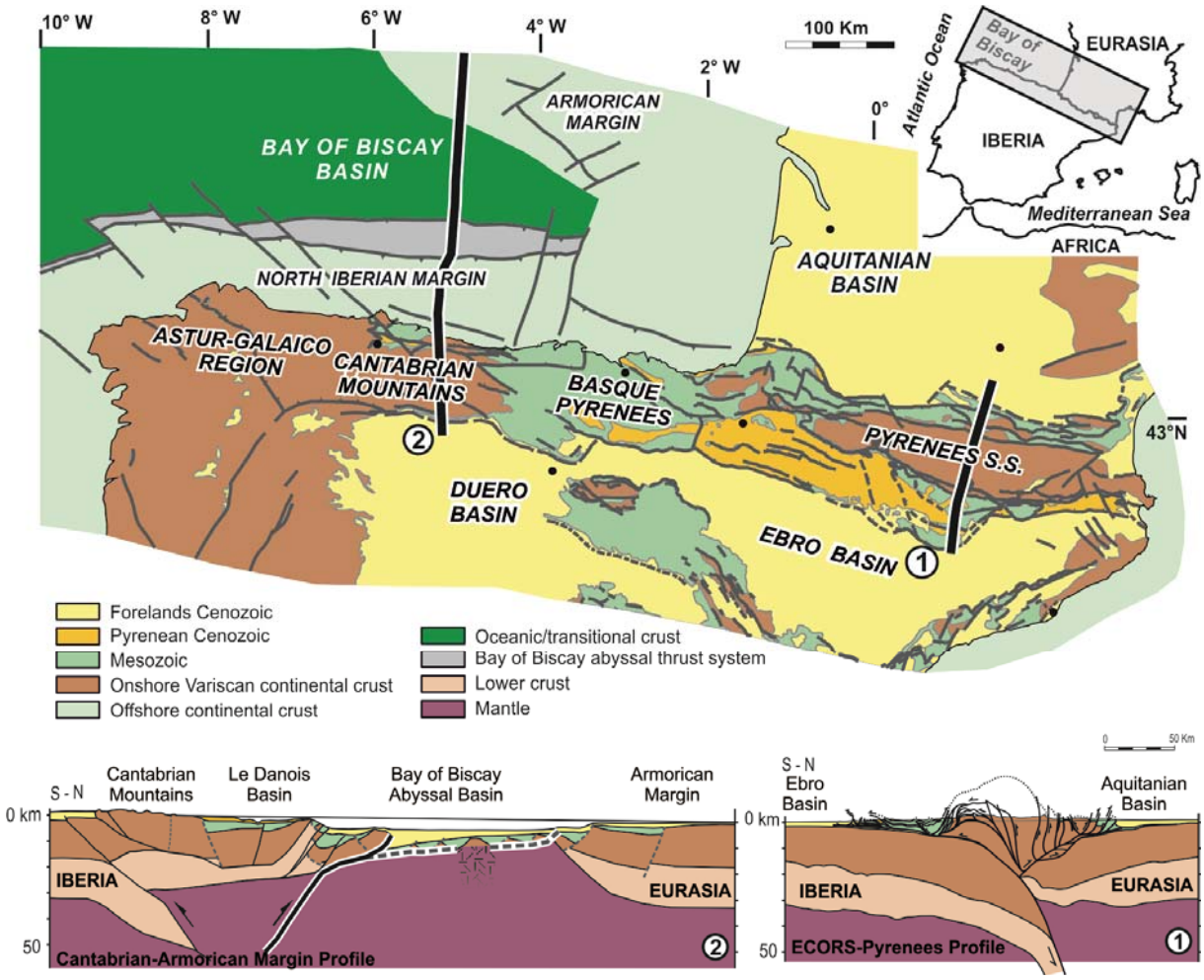

Fig. P.6: Main subdivisions of the Pyrenees and crustal-scale cross-sections across the orogen (Modified from Muñoz, 2002 and Roca *et al.*, 2011).

The southern limit of the Basque Pyrenees is by means of the E-W frontal structure (i.e. Sierra de Cantabria Frontal Thrust in Fig. P.7A) and its associated trailing syncline that are detached and southward displaced over the Ebro foreland basin with a thin-skinned style of deformation (e.g. Martínez-Torres, 1991). More to the west, a WNW-ESE salient is present and it divides the Ebro and Duero foreland basins located to the east and to the west respectively (i.e. Burgalesa Platform Domain in Fig. P.7A). Finally, the southern limit of the Cantabrian Mountains is characterised by an E-W deeply rooted thrust system (Cantabrian Mountains frontal thrust) involving the basement that displaces the Cantabrian Mountains towards the south over the Duero foreland basin with a thick-skinned style of deformation (Fig. P.7A) (e.g. Alonso *et al.*, 2009). The northern limit of the Basque Pyrenees and Cantabrian Mountains are characterised by several north-directed thrusts that involve the upper crust nowadays submerged in the Bay of Biscay (Sánchez, 1991; Pulgar *et al.*, 1996; Gallastegui, 2000; Muñoz, 2002; Pedreira *et al.*, 2003; Ruiz, 2007; Ferrer *et al.*, 2008) (Fig. P.6 section 2).

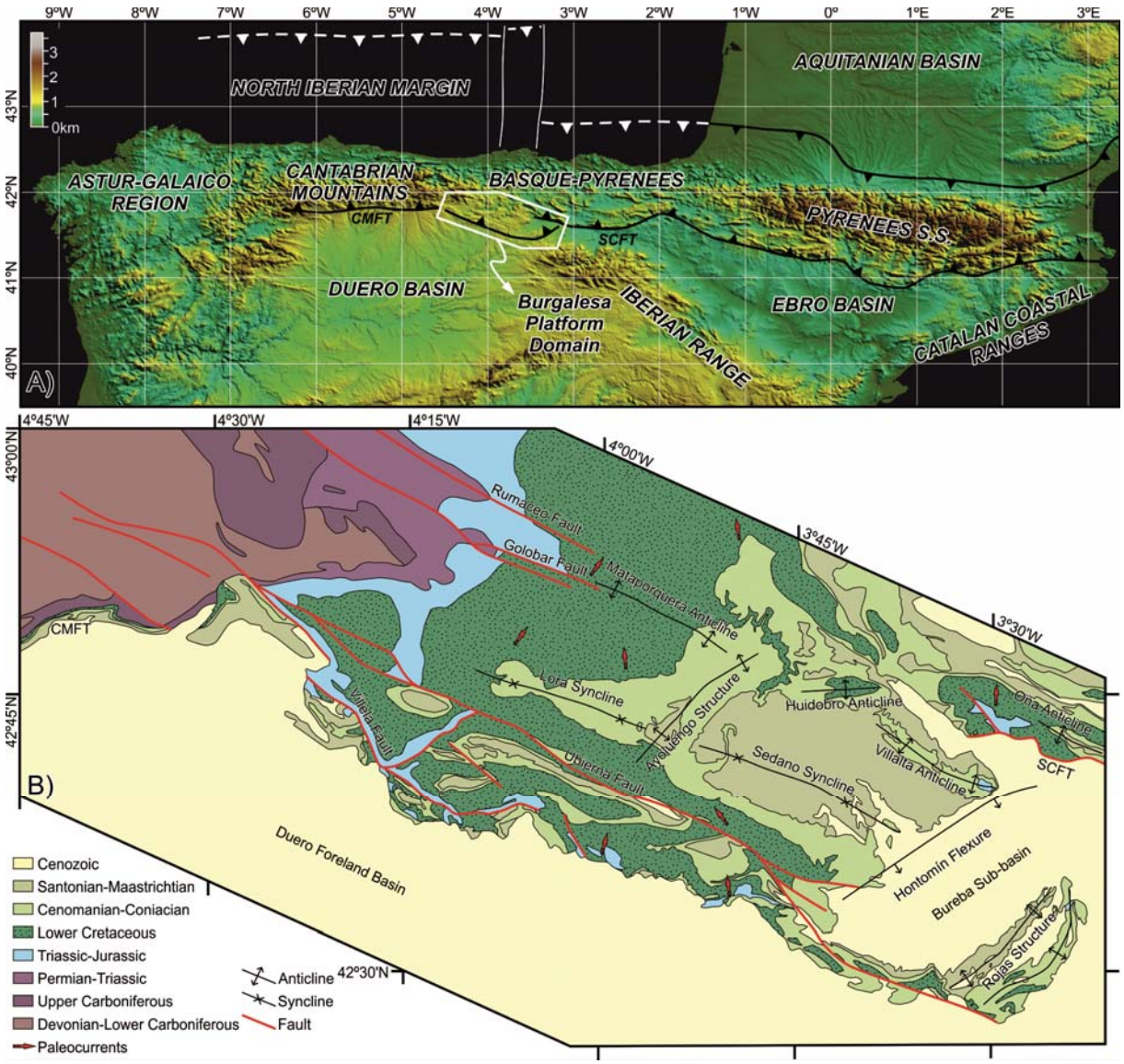

Fig. P.7: A) Location of the study area with the main geological realms. SCFT and CMFT correspond to Sierra de Cantabria Frontal Thrust and Cantabrian Mountains Frontal Thrust, respectively. B) Main geological structures of the study area (modified from Tavani *et al.*, 2011). Paleocurrents are from Pujalte, 1981 and 1982.

The study area of this thesis is located in the transition between the Basque Pyrenees and the Cantabrian Mountains. More in detail, at the south-western termination of the Basque Pyrenees, which is the so-called Burgalesa Platform Domain (Fig. P.7A). The extension of this domain is about 90 km long in the WNW-ESE direction and 40 km wide in the NE-SW direction. The Burgalesa Platform Domain is delimited towards the south by the WNW-ESE Ubierna Fault System and Folded Band and towards the north, by the roughly E-W Sierra de Cantabria Frontal Thrust that attains a NW-SE attitude at its western tip (Fig. P.7B). The main faults present in the study area are the WNW-ESE Rumaceo, Golobar, Ubierna and Villela faults from north to south. Most of these faults where active since the Triassic rifting event as

reported García-Mondéjar *et al.* (1986). Later, during the Upper Jurassic-Lower Cretaceous rifting event they were reactivated allowing the deposition of more than 2000 meters of sediment at their northern blocks (Pujalte *et al.*, 2004). Finally, during the convergence they were reactivated as transpressive (Tavani *et al.*, 2011), generating folds with three main directions (NE-SW, ENE-WSW and WNW-ESE). The NE-SW orientation is shared by the Rojas anticlines, the Hontomín flexure and the Ayoluengo anticline from south-east to north-west. The ENE-WSW fold direction is the one that presents the Huidobro Anticline. Finally, the WNW-ESE direction is present at the Lora and Sedano synclines and at the Mataporquera, Villalta and Oña anticlines. The latter one is located at the hangingwall of the Sierra de Cantabria Frontal Thrust whereas the others are located within the Burgalesa Platform Domain (Fig. P.7B).

P1.2 Stratigraphy

The multiphase deformational history of the Burgalesa Platform Domain is also reflected at the stratigraphic and seismostratigraphic record (Fig. P.8). In this manuscript, the term “basement” refers to the mechanical behaviour of the strata below the main detachment level (the salt layer of Keuper Facies that belongs to Triassic) and “cover” is associated to the strata above this level.

Within the studied area, materials from Permo-Triassic to Cenozoic times crop out. Because of the ESE regional plunge of this domain, the oldest rocks outcrop towards the western boundary whereas the younger rocks are exposed towards the east (Fig. P.7B). The stratigraphic record is divided by four regional unconformities related to major tectonic events occurred in this area (Fig. P.8). The first major unconformity divides the Carboniferous and the Permian. The second major unconformity divides the Permian and the Triassic succession. It is associated to the rifting stage during the Permo-Triassic that produced the breakup of Pangea. The third major unconformity divides the Jurassic and the Cretaceous. It is associated to the second rifting stage due to the opening of the Bay of Biscay. The last major unconformity divides the Upper Cretaceous and the Cenozoic succession and is associated with the convergence between Iberian and Eurasian plates. Below, a brief sedimentological description and the seismic facies characteristics of the different rocks subdivided into the different age and formations is given.

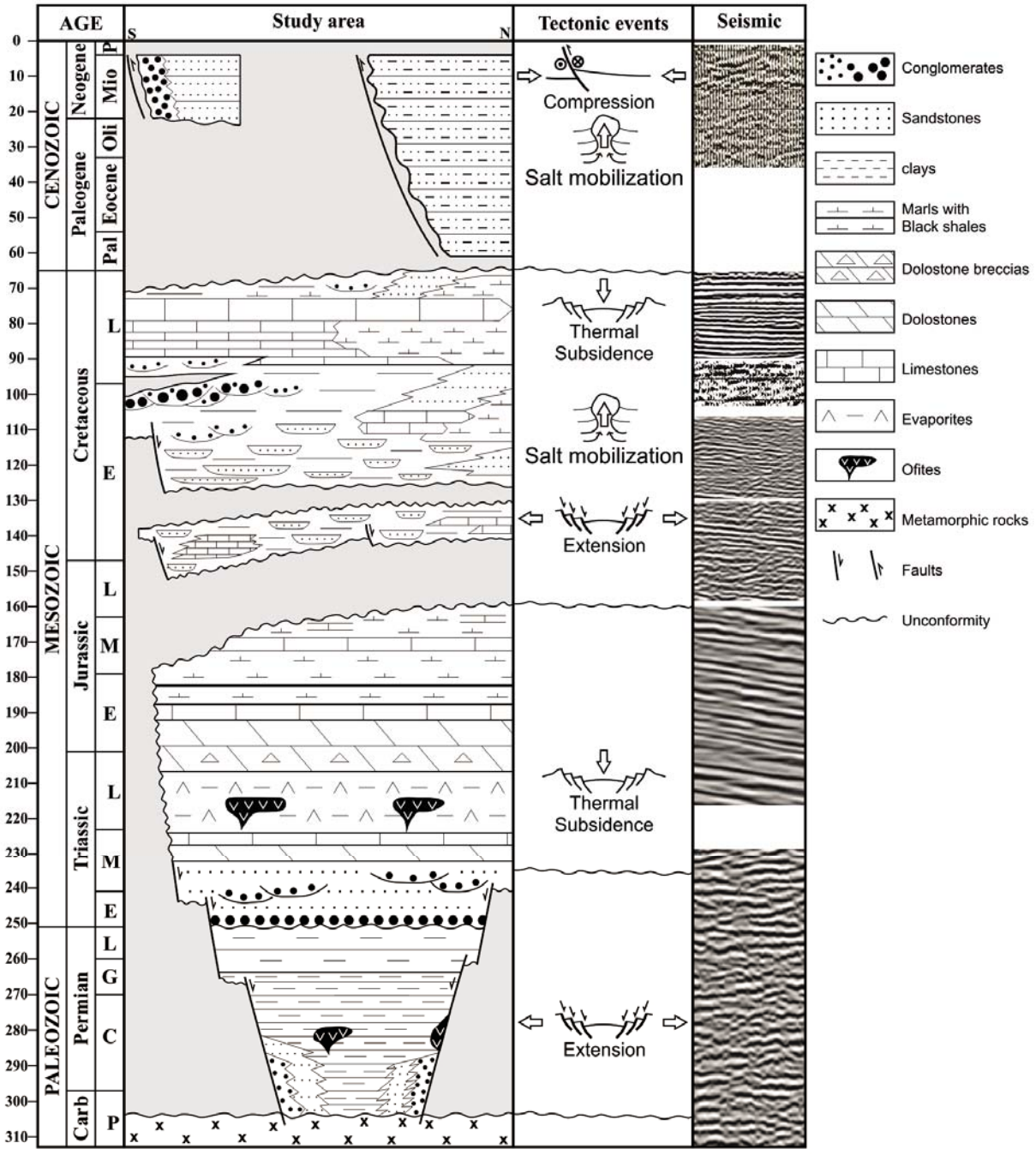

Fig. P.8: Stratigraphic column of the study area and the corresponding tectonic events. Examples of the seismic facies are also provided (Modified from Barnolas & Pujalte, 2004).

P1.2.1 Pre-Triassic

- The **pre-Triassic** succession outcrops only at the western boundary of the study area. It is composed by Ordovician quartzites, alternation of Devonian ferruginous sandstones and clays (Fig. P.9A) and by Carboniferous limestones. The Permian unconformably overlays the previously described succession and it is characterised by grey clays that passes to sandstones

Fig. P.9: A) Ordovician quartzites. B) Carboniferous limestones affected by intrusions. (Images courtesy of Stefano Tavani).

at top with paleocurrents pointing towards the north-west. All these units are affected by intrusive rocks (Fig. P.9 B). The seismic response of this succession is characterised by chaotic strong reflections without lateral continuity (Fig. P.8).

P1.2.2 Triassic

- The **Lower Triassic** rocks (Buntsandstein facies) described by García-Mondéjar *et al.* (1986) consist of siliciclastic red fluvial conglomerates, with clasts of centimetric size, sandstones and clays (Fig. P.10A and B). The thickness of this unit varies between 100 and 1000 meters depending on the structural position. This unit only crops out at the western sector of the study area and also in the northern sector. The formation that constitutes this facies association is the **Alto Campoo Formation** and has four different units. The basal unit of the succession is the more proximal facies and corresponds to conglomerates, with paleocurrents pointing towards the north-east (Fig. P.10A). They are formed by up to 50 cm long rounded cobbles of quartzites distributed in positive sequences. The intermediate unit associated to longitudinal bars is characterised by siliciclastic grey sandstones with interbedded conglomerates in which the pebbles do not exceed 10 cm in the long axis. The third unit is made up of red massive sandstones and clays associated to channels with cross-bed lamination and crevasse splay deposits with parallel lamination, respectively (Fig. P.10B). The last unit is only constituted by red clays with evaporitic levels. The seismic response of this unit is denoted by chaotic strong reflections without lateral continuity within transparent seismic areas

(Fig. P.8). Typically the top of this megasequence is a twin strong and semi-continuous reflector.

- The **Upper Triassic** (Keuper Facies) consists of red shales, grey limestones, salt and gypsum intruded by sub-volcanic rocks (Fig. P.10C and D). The thickenss of this unit is difficult to characterise due to the halokinetic processes related to the extensional event of the opening of the Bay of Biscay. For this reason, this unit is not formal defined into formation and the germanic facies term is used. The seismic facies are typically chaotic weak reflections at its base whereas the upper part of the succession is more sub-parallel and reflective (Fig. P.8).

The Keuper facies are the most important detachment level within the Pyrenees. In the study area, it outcrops at the western boundary, at the vicinities of the Ubierna Fault and in some diapiric areas (e.g. Aguilar (Serrano & Martínez del Olmo, 2004), Poza de la Sal (Fig. P.11) (Quintà *et al.*, 2012), Reinosa (Rat, 1988), among others).

Fig. P.10: A) Basal units of the Buntsandstein facies made up of conglomerates in positive sequences. B) Buntsandstein outcrop located to the north of the study area in the Pas structure. C) Keuper Facies with sub-volcanic intrusions outcropping in the Poza de la Sal area. D) Limestones within the Keuper succession.

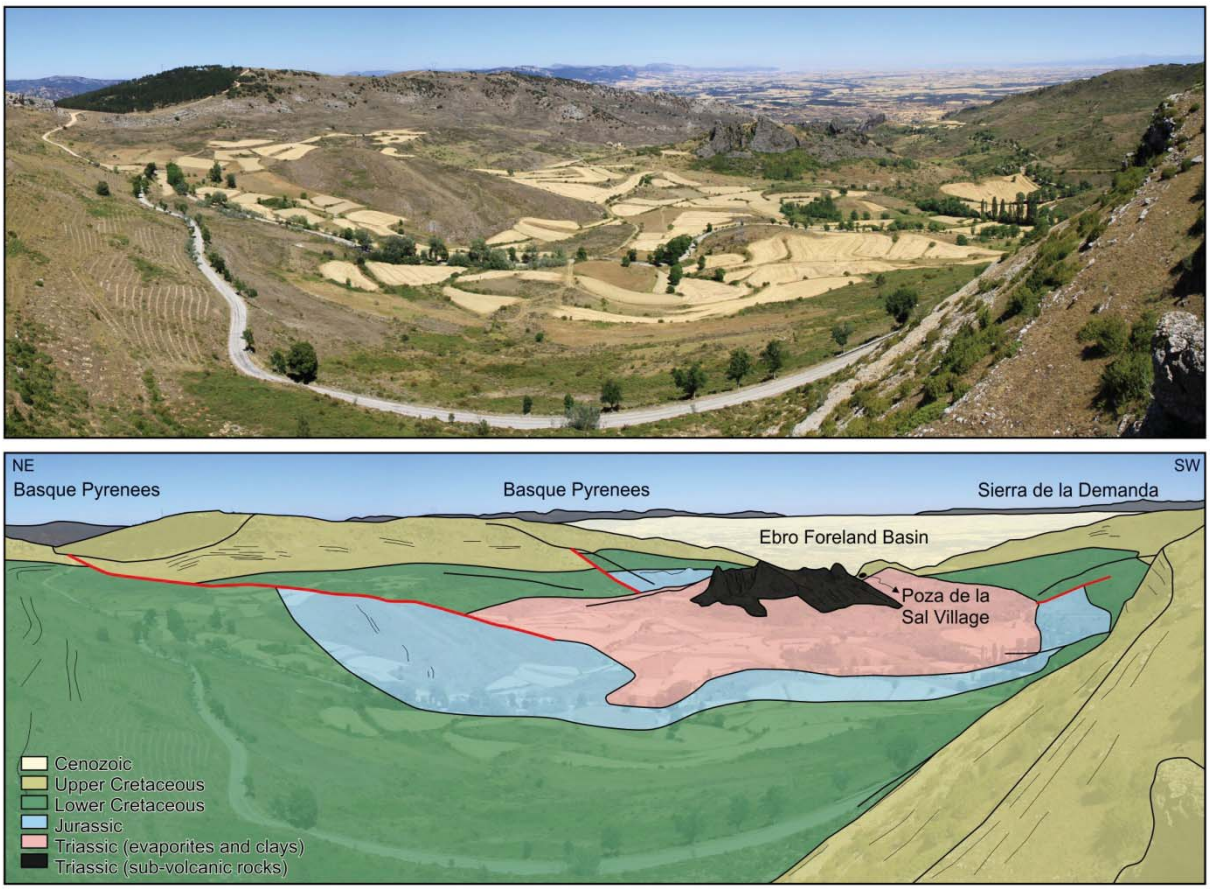

Fig. P.11: Panoramic view of Poza de la Sal Diapir with the sub-volcanic rocks outcropping at the core of the structure.

P1.2.3 Jurassic

The Jurassic succession is constituted by seven lithostratigraphic units that are informally grouped into two main depositional systems (e.g. Pujalte *et al.*, 1988; Robles *et al.*, 1989, 2004; Quesada *et al.*, 1991; 2005). The first depositional system is a shallow carbonate ramp constituted by evaporites, dolostones, limestones and siliciclastic rocks from older to younger. The second depositional system is an hemipelagic carbonate ramp made up of alternations of marly limestones and marls, shales and limestones (Fig. P.12). This is the easiest recognisable succession within the seismic stratigraphy. It is constituted by strong reflectors parallel to each other. The continuous and isopach reflectors of this succession are associated to the carbonatic rocks of the first depositional system. The upper portions of Jurassic succession are characterised by weaker reflectors but still continuous and isopach. This drop in reflectivity is due to the lithological change of the second depositional system in which marly rich intervals are predominant (Fig. P.8).

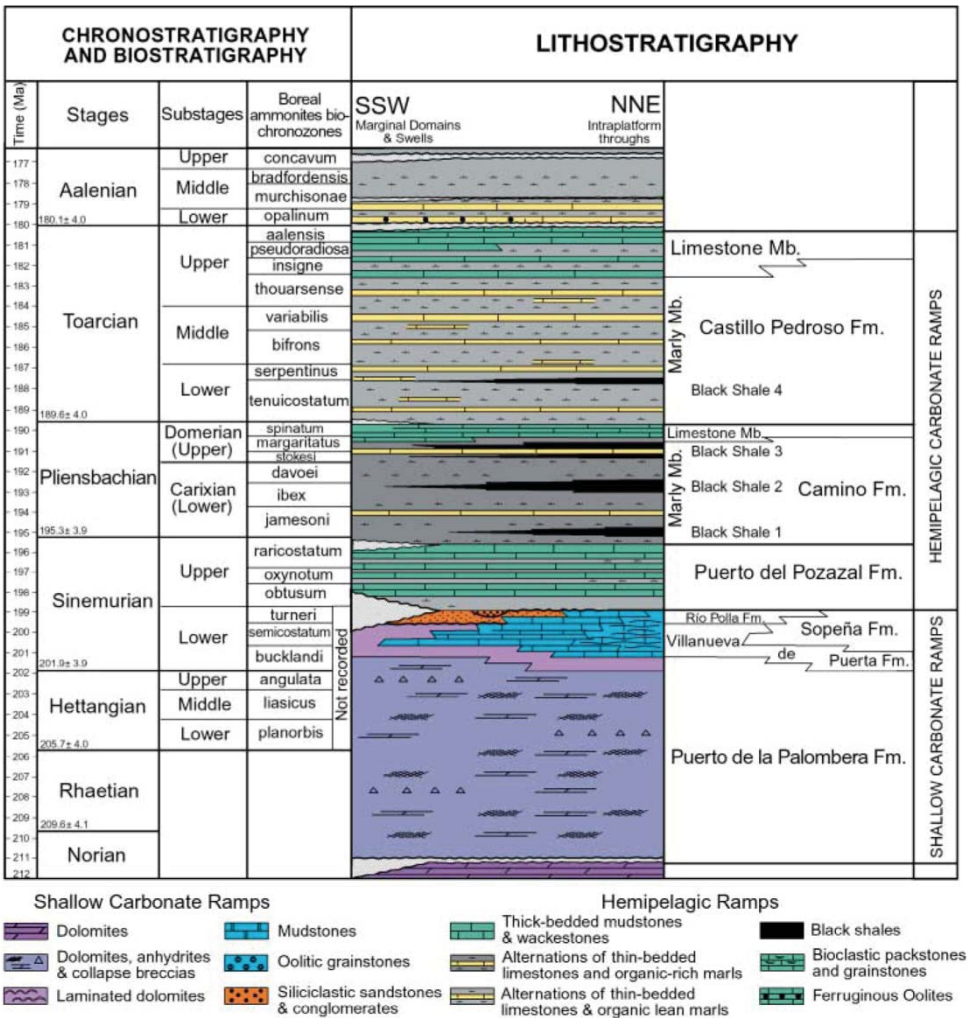

Fig. P.12: Summary of the Jurassic stratigraphic and biostratigraphic record (from Quesada *et al.*, 2005).

The first depositional system is characterised by four different formations.

- The **Puerto de la Palombera Formation** (Fig. P.13A) is constituted by dolostones that present dissolution casts at surface (Fig. P.13B) whereas, the wells testify evaporites at depth. The upper parts of this formation are characterised by the presence of stromatolites developed in supratidal flats and in hypersaline lagoonal sabkha environments during the Rhaetian and Hettangian.

- The **Villanueva de Puerta Formation** is mainly formed by limestones (Fig. P.13C). The presence of oolitic facies denotes the peritidal environment developed during the Lower Sinemurian. The upper portions of this formation represents a lateral change with the Sopeña Formation.

- The **Sopeña Formation** is also constituted by limestones with storm deposit levels (Fig. P.13D) developed in a subtidal environment during the Lower Sinemurian.

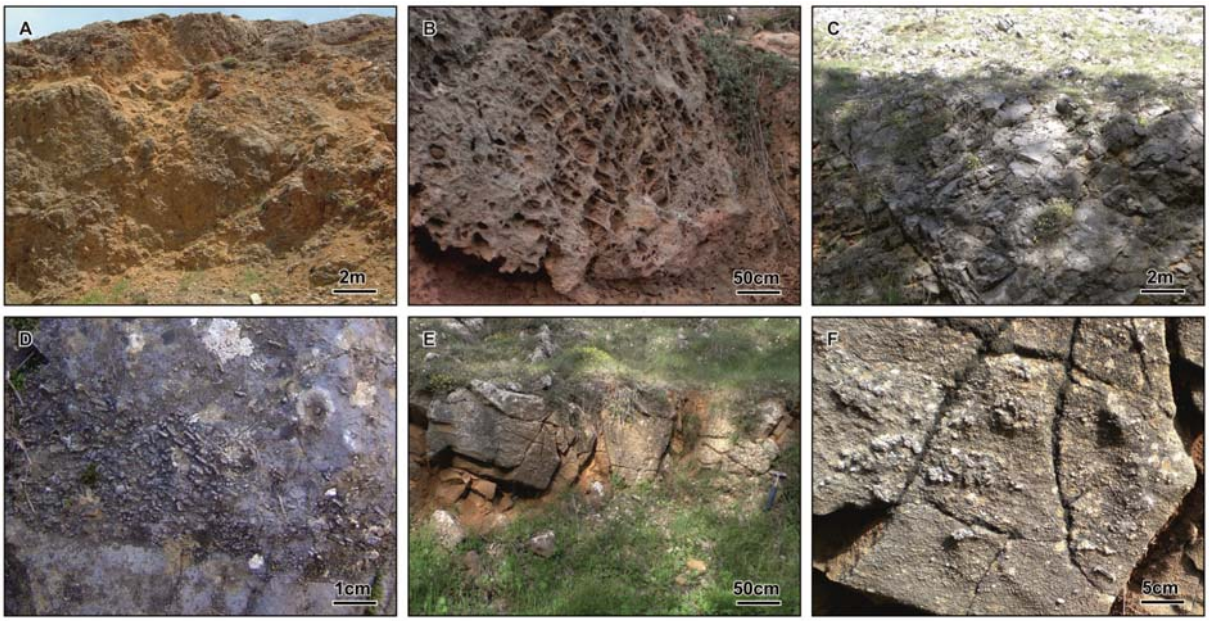

Fig. P.13: Photographs of the different formations enclosed in the first Jurassic depositional system. A) Outcrop of the Puerto de la Palombera Formation. B) Detail of the casts produced by the dissolution of evaporites. C) Limestones of the Sopeña Formation. D) Detail of a storm deposit level present in the Sopeña Formation. E) Siliciclastic Río Polla Formation. F) Detail of the Río Polla Formation.

- The siliciclastic unit of the **Río Polla Formation** is the last formation of this first depositional system attributed to the early Upper Sinemurian (Fig. P.13E and F). It is characterised by a prograding wedge of sandstones deposited in a fluvial to marine environment. This formation laterally disappears towards the northeast, being only present the marine limestones of the Sopeña Formation.

The second depositional system is characterised by a major transgressive event that produced the drowning of the previously developed platform and established the sedimentation of deep-water hemipelagic facies. In this system, three formations have been defined.

- The **Puerto del Pozazal Formation** is composed of marly limestones from the Upper Sinemurian (Fig. P.14A).

- The **Camino Formation** is made up of alternations of marls and thin limestones strata (Fig. P.14B) and contains several anoxic organic-rich intervals (Fig. P.14C). This formation is defined as Pliensbachian in age.

- The **Castillo Pedroso Formation** is the last pre-rift Jurassic formation. It is constituted by alternations of marls and metric limestones strata (Fig. P.14D) and contains sponges and zoophycus (Fig. P.14E). This formation is defined as Toarcian to Aalenian in age.

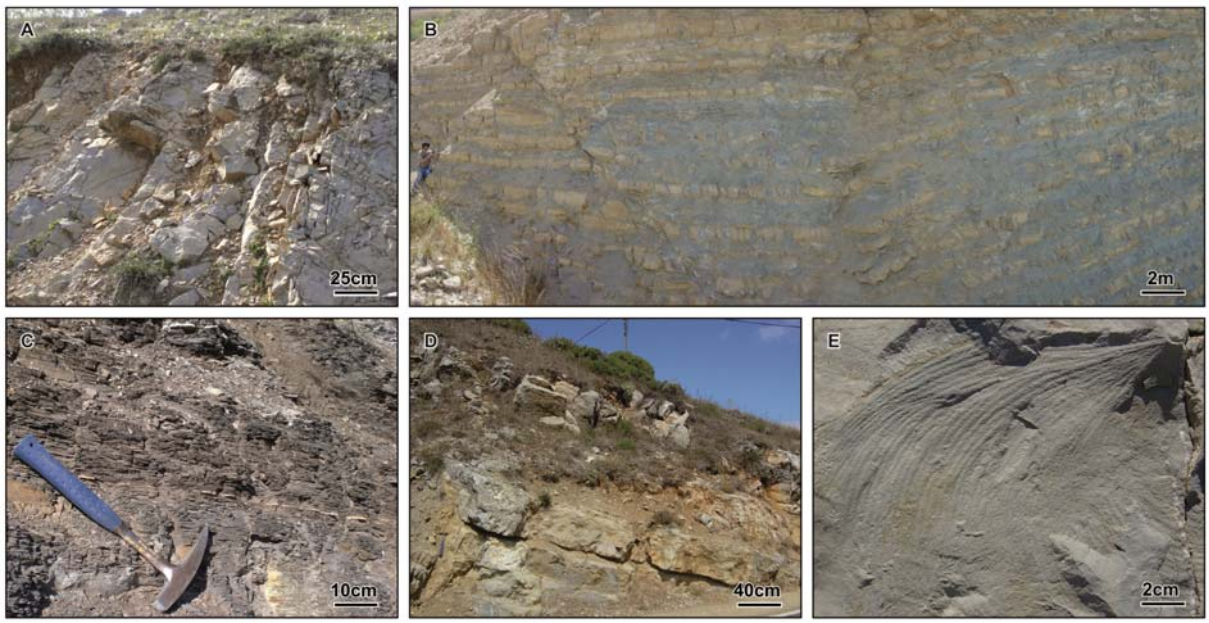

Fig. P.14: Photographs of the different formation enclosed in the second depositional system. A) Marly limestones of the Puerto del Pozazal Formation. B) Marls and limestones of the Camino Formation. C) Detail of the black shales present in the Camino Formation. D) Limestones of the Castillo Pedroso Formation. E) Zoophycus detail present in the Castillo Pedroso Formation.

P1.2.4 Cretaceous

The Upper Jurassic - Lower Cretaceous rocks (Kimmeridgian - Valanginian), traditionally known as Purbeck and Weald Facies, consist of several lithologies in the study area. Pujalte (1976) divided the Upper Jurassic - Lower Cretaceous rocks into seven formations grouped into two groups defining their relationship in space and time. The paleocurrents reported for the Upper Jurassic - Lower Cretaceous units show a direction pointing towards the north (Fig. P.7B) (Pujalte, 1981, 1982).

The first group is the Cabuérniga Group that unconformably overly the Jurassic. It is constituted by five formations (Fig. P.15A). The basal part of the group is defined by a lateral change from south-west to north-east of Aguilar Fm., Arcera Fm. and Saja Fm. Upwards, the Arcera Fm. laterally change to the Aroco Fm. and the Loma Somera Fm. The seismic response of the Cabuérniga Group is characterised by smaller reflectivity than the Jurassic seismic facies. In addition, the continuity of the reflectors and the parallelism between them is reduced too (Fig. P.8). Also, it is characteristic the presence of minor intraformational unconformities.

- The **Aguilar Fomation**, formally described by García de Cortazar and Pujalte (1982), is constituted by lacustrine limestones organised in metric packages (Fig.

P.15B). It contains gastropods, ostracodes and charophytes that allow to determine the Berriasian age of this formation (Platt and Pujalte, 1994).

- The **Arcera Formation** is characterised by a constant succession of alternating clays with dissacation cracks, silicic sandstones and siltstones (Fig. P.15C). The environment associated to this unit corresponds to fluvial channel and flood plains (García de Cortazar and Pujalte, 1982).

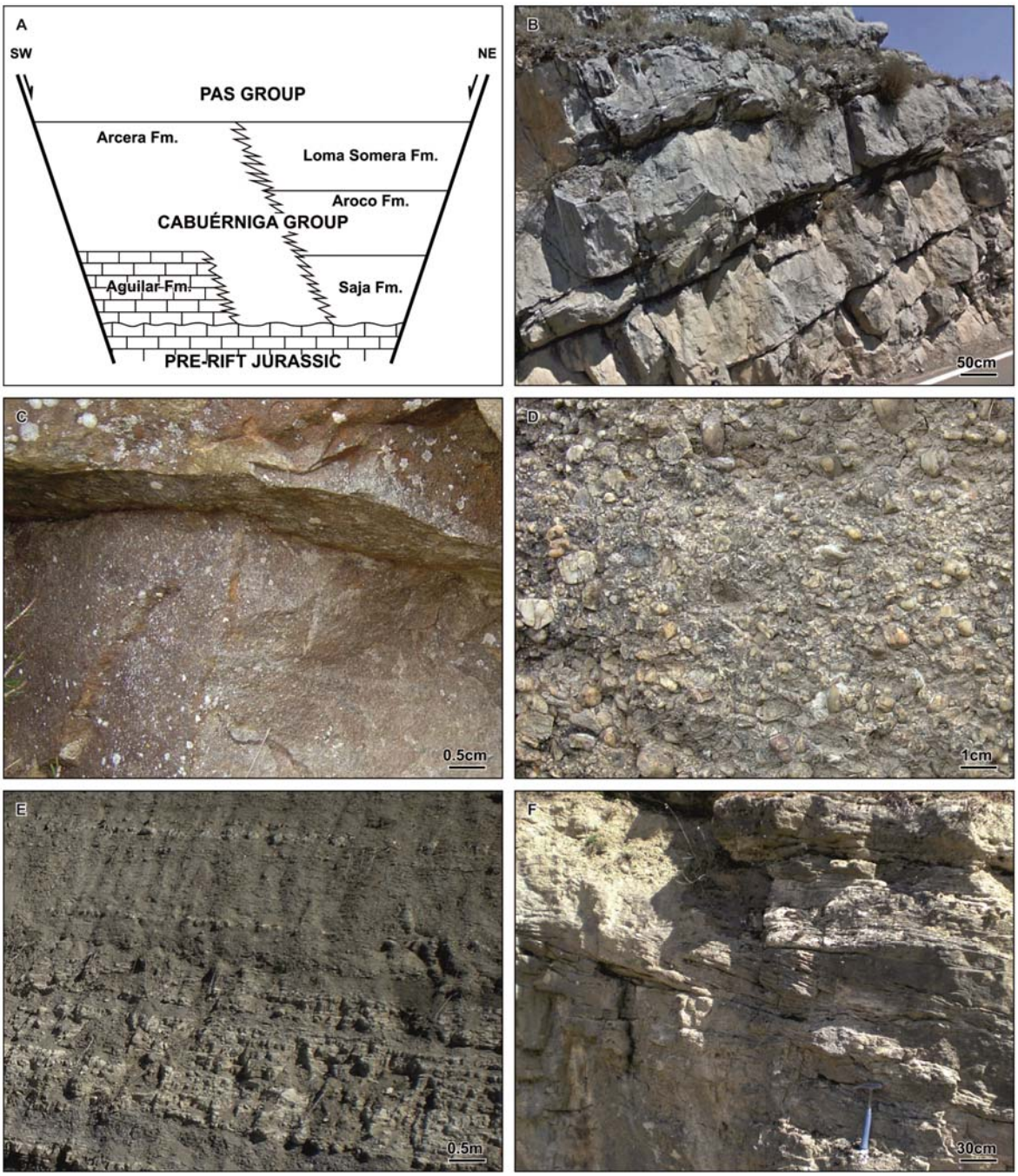

Fig. P.15: Synthesis of the Cabuérniga Group. A) Sketch of the different Cabuérniga Group Formations with the distribution in space and its lateral relationships. B) Thick limestone packages of the Aguilar Formation. C) Sandstones of the Arcera Formation. D) Micro-conglomerates of the Saja Formation. E) Grey clays with thin sandstone levels of the Aroco Formation. F) Detail of the cross-bed lamination present in the Loma Somera Formation.

- The **Saja Formation** is made up of siliciclastic conglomerates (Fig. P.15D) interbedded with thin marls organised in positive sequence. The cobbles of the conglomerates are well rounded. Pujalte (1982) interpreted the conglomerates as point bar deposits and the marly levels to crevasse splay deposits.

- The **Aroco Formation** (Fig. P.15E) is represented by a thick succession of dark grey clays with interbedded levels of sandstones up to 1 meter thick. This unit is associated to transitional fluvio-marine facies such as a lagoon environment (García de Cortazar and Pujalte, 1982).

- The **Loma Somera Formation** (Fig. P.15F) is characterised by a thick sandstone succession with crossbed lamination developed in a fully marine environment with sporadic influence of fluvial channels (García de Cortazar and Pujalte, 1982).

The second group is the Pas Group that in some areas unconformably overly the Cabuérniga Group and in some areas the Jurassic pre-rift units. This group is constituted by two formations, the Bárcena Mayor Fm. and the Vega de Pas Fm. The seismic characteristics of the Pas Group are the sub-parallelism between reflectors and the bigger reflectivity and continuity in comparison to the seismic facies of the first group (Fig. P.8). Additionally, this group has minor intraformational unconformities.

- The **Bárcena Mayor Formation** (Fig. P.16A) is characterised by thick packages of sandstones with plants (Fig. P.16B) and roots interpreted as channel facies of a fluvial environment (Pujalte, 1981).

- The **Vega de Pas Formation,** described by Pujalte (1981), is associated to a fluvial environment. The most important lithology are thick packages of reddish sandstones, interpreted as meander rivers organised in positive sequences with erosive bases, and flood plain deposits defined by red clays (Fig. P.16C).

The Lower Cretaceous - Upper Cretaceous (Aptian - Albian) limit is characterised by the presence of two siliciclastic units deposited in a fluvial environment, the Escucha Fm. and the Utrillas Fm. The latter one is very constant throughout the study area. The seismic facies of these two formations are characterised by reflective semi-continuous horizons (Fig. P.8). The Utrillas Formation is unconformable respect to the Escucha Formation as shown by offlap geometries, which denotes a period of erosion or non sedimentation.

Fig. P.16: A) Photograph of the Bárcena Mayor Formation. B) Detail of the wood fragments present in the Bárcena Mayor Fm. C) Vega de Pas Fm. with positive sequences of channel facies eroding the flood plain facies.

- The **Escucha Formation** is made up of reddish conglomerates and sandstones organised in thick positive sequences that represents braided river deposits (Fig. P.17A). Cobbles are rounded and mainly from few centimetres up to 10 cm (Fig. P.17B). The top of this succession is characterised by clays and sandstones.

Fig. P.17: A) Outcrop photograph of the Escucha Formation characterised by thick reddish conglomerate successions. B) Detail of the conglomeratic levels of the Escucha Fm. C) Outcrop photograph of the Utrillas Formation. D) Detail of the sedimentary lamination of the Utrillas Fm.

- The **Utrillas Formation** is made up of grey metric-thick beds of sandstones and clays with internal crossbedded lamination organised in positive sequences. They are associated to braided rivers but more distal than the Escucha Formation (Fig. P.17C and Fig. P.17D).

The Upper Cretaceous is represented by a carbonatic and marly succession (Fig. P.18A) that is divided into seven different formations defined by Floquet (1991). The seismic facies of the Upper Cretaceous is characterised by continuous and parallel reflectors. The carbonatic intervals are highly reflective opposite to the marly intercalations which shows a drop in reflectivity due to the rheological differences between both lithologies (Fig. P.8).

- The **Olleros de Pisuerga Formation** is mainly composed by marls and clays with thin sandstone levels (Fig. P.18C). The base of this formation shows some similarities with the Utrillas Formation.

- The **Villaescusa Formation** is divided into two different packages. The lower one is basically composed by marls and marly limestones with abundant fauna such as echinoderms and benthonic foraminifers. The upper package is characterised by stratified massive grey limestones (Fig. P.18C). Micropaleontological studies suggest a Cenomanian to Coniacian age for this formation (Ramírez del Pozo, 1971).

- The **Nidáguila Formation** is characterised by grey to ochre marls that are usually delimited by two more competent levels located above and below it (Fig. P.18B and C). The fauna association allowed Floquet (1991) to define this formation as a result of a drowning event and to attribute it a Coniacian age.

- The **Nocedo Formation** is a competent unit reflected by well observable scarps in the field (Fig. P.18B and C). It is constituted by thick greyish limestones, sometimes with cross-lamination, attributed to the Santonian (Floquet, 1991).

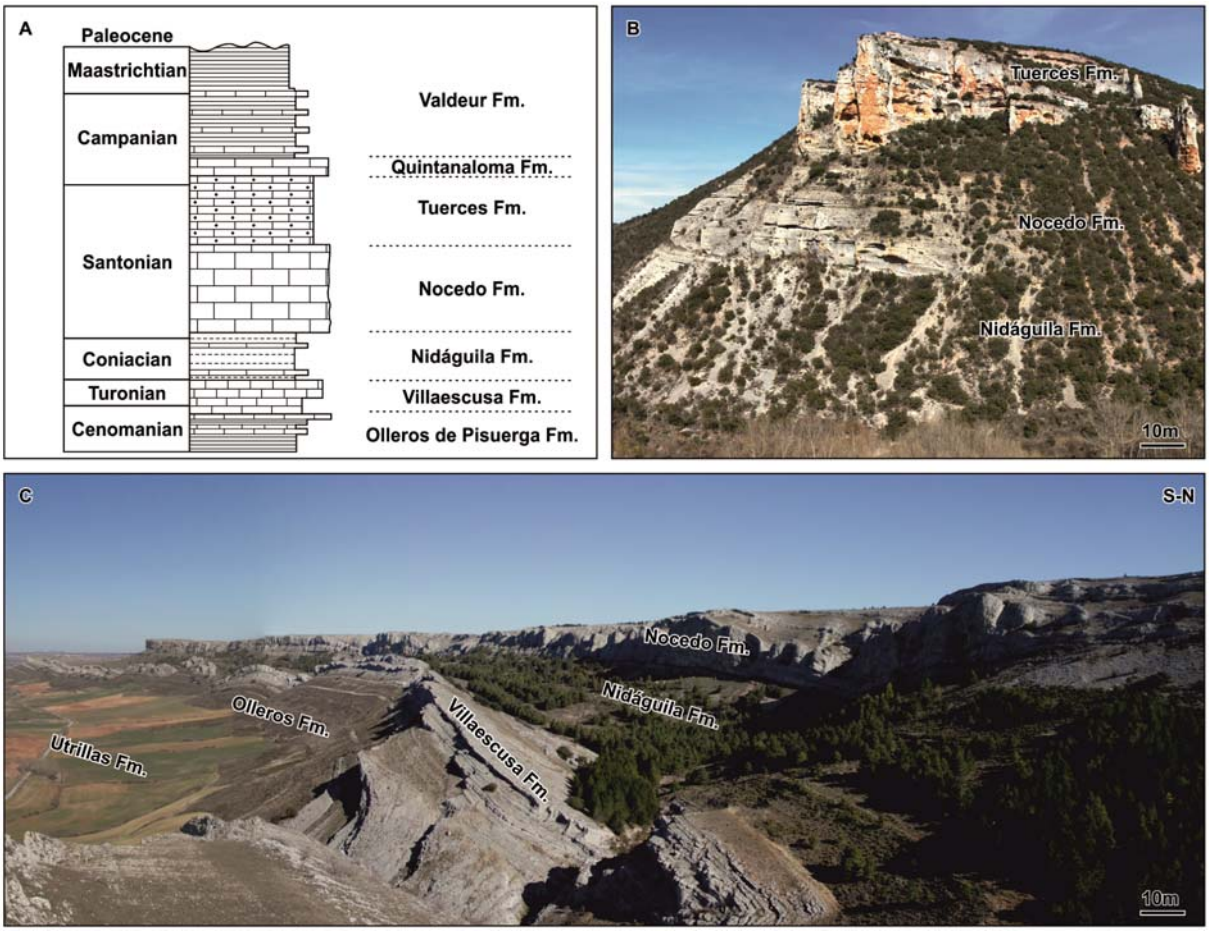

Fig. P.18: A) Synthesis of the lithology of Upper Cretaceous marine succession and the different associated formations. B) Outcrop of the Nidáguila, Nocedo and Tuerces Formations. C) Panoramic view of the stratigraphic sequence between Utrillas and Nocedo Fm.

- The **Tuerces Formation** is made up of ochre marly limestones with fragments of brachiopods and echinoderms in which the iron oxides attributes its characteristic colour. This formation is defined as Upper Santonian to Lower Campanian (Fig. P.18B).

- The **Quintanaloma Formation** is constituted by stratified limestones and dolostones with a grey colour attributed to the Campanian (Floquet, 1991).

- The **Valdeur Formation** is subdivided into a carbonatic interval and a marly rich-interval. The environment of this formation has been defined, using the fauna association, as littoral. Also, the fauna association has established a Maastrichtian age (García-Ramos *et al.*, 1982).

P1.2.5 Cenozoic

The Cenozoic rocks are restricted at the southern border areas of the Burgalesa Platform Domain (Fig. P.7B). This unit is constituted by two formations (i.e. Ojeda Formation and Cantoral Formation) both related to fluvial environments. The seismic facies are characterised by chaotic reflectors without both parallelism and lateral continuity (Fig. P.8).

- The **Ojeda Formation** is characterised by grey polymictic conglomerates with centimetric angular to sub-angular cobbles and interbedded red sandstones and clays (Fig. P.19A). Cobbles are from the Upper Cretaceous carbonatic succession and in some cases they can reach more than 40 cm in size. This formation is associated to a proximal fluvial environment. This formation is defined as Oligocene in age.

- The **Cantoral Formation** is characterised by proximal to intermediate fluvial facies being the reddish colour the most representative characteristic of this formation. The intermediate facies are defined by red clays with lenticular bodies of sandstones (Fig. P.19B). In contrast, the proximal facies are characterised by conglomerates, sandstones and clays unconformably overlying the Mesozoic succession (Fig. P.19C). This formation is defined as Miocene in age.

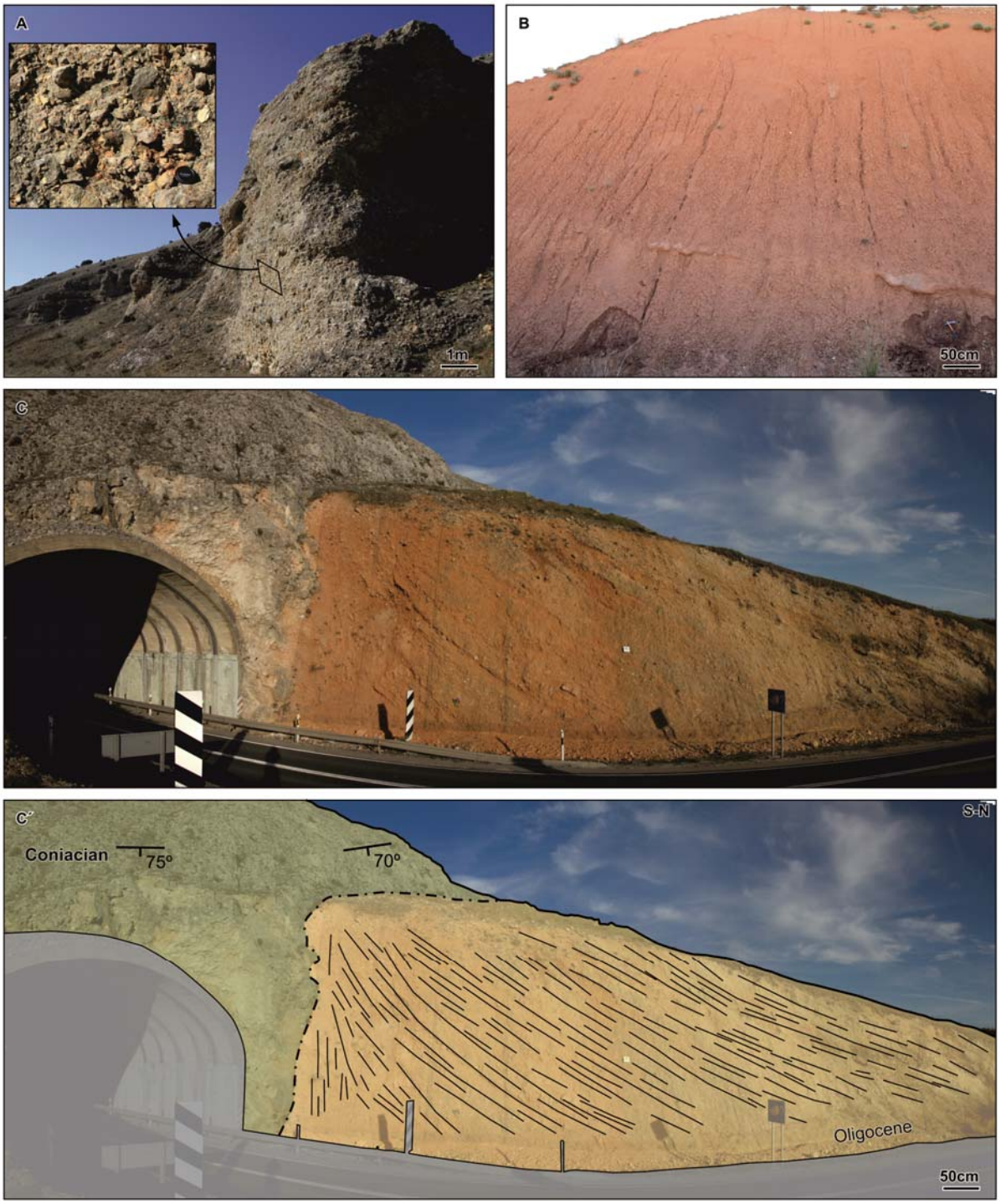

Fig. P.19: A) Thick conglomerate succession of the Ojeda Fm. deposited in the Duero Foreland Basin and detail of the cobbles present. B) Distal facies of the Cantoral Fm. with red clays and thin lenticular sandstones packages characteristic of the Bureba sub-basin. C) Oligocene conglomerates, sandstones and clays associated to proximal - intermediate fluvial facies of the Cantoral Fm. C') Linedrawing of C in which the conglomeratic succession with an angular unconformity onlaps the Coniacian.

Methodology

This section deals with different methodologies and procedures used to collect and then import the data into the specific software to finally perform the interpretations of this thesis. Additionally, the different dataset used and its provenance and errors are also described. The methodology is structured in four sub-sections according to the data used and it is divided as it follows:

- P2.1 Seismic data
- P2.2 Well data
- P2.3 Field work
- P2.4 Paleomagnetism

P2.1 Seismic data

The seismic network used to carry out this thesis was made up of digital and printed seismic sections respectively, gently provided by IGME (Spanish geological survey) and Repsol. Because of confidentiality agreements between both parties, in this thesis only the allowed seismic sections are going to be shown although all the data have been used. The seismic network was acquired during eleven different campaigns between the early 70's and 90's, when hydrocarbon exploration took place in the study area. As a resulting of this, the quality of the lines may vary depending on the process method they used and the filters they applied. From the total of the seismic sections, more than 28 lines only the scanned physical support and the trace file was available. In this case, the data was processed in order to obtain a SEG-Y. The methodology to transform from the physical support into SEG-Y files the seismic lines is scanned. The seismic line in .tiff format is cropped keeping the area in which the position of the shot-points and geophones are known. The last step is to associate the pixels of the .tiff image with the information from the trace file. This process was done with the application "image2segy", developed by the "Grup de Geologia Marina (ICM)" and "Institut de Ciències del Mar (CMIMA-CSIC)", which runs with MATLAB®, obtaining a SEG-Y file.

The different provenance of the data required to apply a quality control of all the seismic network in order to detect mistakes. The most common errors were in the datum, the coordinates of the shot-points, X and Y coordinates, the common depth points or the sampling interval. All the data was unified using the UTM projection, zone 30 and European Datum 50. In consequence all the wrong coordinates and mistakes detected were modified using the software Seisee®. Once all the data were corrected and introduced in the 3D seismic interpretation software, the vertical offset (misties) of the seismic sections in a same reflector between the different surveys were corrected checking the intersection lines. Using a reference network, the vertical shift was manually displaced until the reflectors mutually matched. With this process, the errors during the interpretation are reduced and a more solid interpretation is obtained. The last step of the processing workflow was to homogenise the amplitudes of the survey. This correction allows to change the appearance of the reflectors so that the different surveys present similar reflector facies facilitating the interpretation throughout the study area.

During the initial stages of this thesis, The Kingdom Suite® interpretation software was used. Later it was shifted to Petrel® because of its easiest way to interpret data in 3D, as it works either in time or depth data, and the more efficient way of producing models and maps, minimizing the time for exporting and importing all the interpretations into other softwares.

P2.2 Well data

The methodology followed in this thesis concerning the well data is similar to the one used for the seismic data. All the well data were obtained by oil companies from the 1940's to 1980's when most of the exploration work was done in the study area and up to the 2000's when a second stage of exploration took place. The well data have been used to complement the seismic information and surface data. The well information was provided by the IGME and Repsol. Following confidentiality agreements, most of the data will not be presented in this thesis although it has been used to obtain the interpretations. From all the wells the lithological log was used to constrain the different formations. In addition, from 18 wells the sonic, gamma ray, tension, spontaneous potential, thermal neutron, resistivity among other logs were available in a .las format.

An initial quality control was performed in order to detect errors and to homogenise all the data either in physical or digital support. Once all the units were changed and the formation names were replaced to a standard nomenclature, the coordinates of the wells were set to a fix coordinate system, using the UTM projection, zone 30 and European Datum 50. This homogenisation process minimises the possible positioning errors in the subsequent stages and usages of the data together with other sources. This process was carried out using Global Mapper® software.

The combination of the lithological and sonic logs allow the possibility to transform the different horizon depths from meters to time in order to allow the interpretation in time of the different horizons of interest within the seismic network. The sonic log is used to obtain the velocity of a determined formation at a specific depth. This log is in microseconds per feet (μs/FT), that is usually the unit in oil procedures, and has to be transformed to meters per second (m/s) that are the units in which the interpretation software works. Following the different steps shown beneath, the initial data is changed to fit the software requirements.

From microseconds per feet to feet per second:

$$\text{Initial data ID in } (\mu s/FT) \rightarrow \left(\frac{1}{ID(\mu s/FT)}\right) \text{ x } 1{\cdot}10^{6} \rightarrow \text{Pseudo-data PD in } (FT/s)$$

From feet per second to meters per second:

$$\text{Pseudo-data PD in } (FT/s) \rightarrow \text{PD x } 0.3048 \rightarrow \text{Final data FD in } (m/s)$$

Moreover, in order to construct the cross-sections and to constrain the deep geometry and thickness of the different formations the well data was imported to Move® software where the cross-sections were done.

P2.3 Field work

Field work was mainly focused on the characterisation of the surface geology in order to refine the geological cartography and to obtain dip data. During the different field campaigns, 1:25.000 ortophotographs and 1:5.000 topographical cartography, provided by the "Junta de Castilla y León", were used. The 1:5.000 topographical cartography was obtained from the DEMs (Digital Elevation Models). Moreover, a GPS unit with ±5 meters error was used to position the data gathered in the field.

All the dip data were imported into a 3D software (Microstation®) in order to make a 3D geological cartography using the DEM with the ortophotographs pasted on it. After that, the traces of the geological map, the dip data, the seismic lines and the wells data were imported into Move® software that allowed the construction of three N-S and an NW-SE regional cross-sections covering the study area. The surface dip data were not more distant than 500 meters from the trace of the cross-section and only the wells and seismic lines closer to the trace were projected.

P2.4 Paleomagnetism

The methodology for the paleomagnetic studies can be subdivided into two different stages. The first consists of the sampling procedure and the second of the analytical procedure.

The paleomagnetic study carried out in this thesis was made up of sixty-two different sampling sites in the vicinities of the Burgalesa Platform Domain and also in the frontal structure of the Basque Pyrenees. A site is defined as the place of outcropping target materials from the sedimentary record of a determined age (Fig. P.20A). The main target units of this study were the Cenozoic. For that reason, from the total sampled sites, forty-three were drilled from Oligocene to Miocene red to grey clays, eighteen in the Upper Cretaceous limestones and one in the Lower Cretaceous siliciclastic rocks. Sampling sites were chosen away from power lines to reduce the error during the sample orientation and to reduce secondary IRM (Isothermal Remanent Magnetism). A mean of ten samples were taken for each site in order to minimise the error and also to average the geomagnetic field secular variation. Samples were collected from fresh unweathered outcrops in order to minimise the oxidation of magnetite. A sample is defined as an oriented core of rock from the site of sampling and were obtained with a portable driller (Fig. P.20B). An electrical powered driller was used in the sites where the materials were soft whereas a fuel powered driller was used in the sites with hard rocks. Both drillers were cooled with water in order to refrigerate the drill bit. Once the core was gathered, it was *in situ* oriented with a compass equipped with an inclinometer. After the field work, samples were sectioned into three specimens of $10cm^3$ (Fig. P.20C). From these specimens, one was measured to obtain the geomagnetic field vector and the others were stored for additional tests.

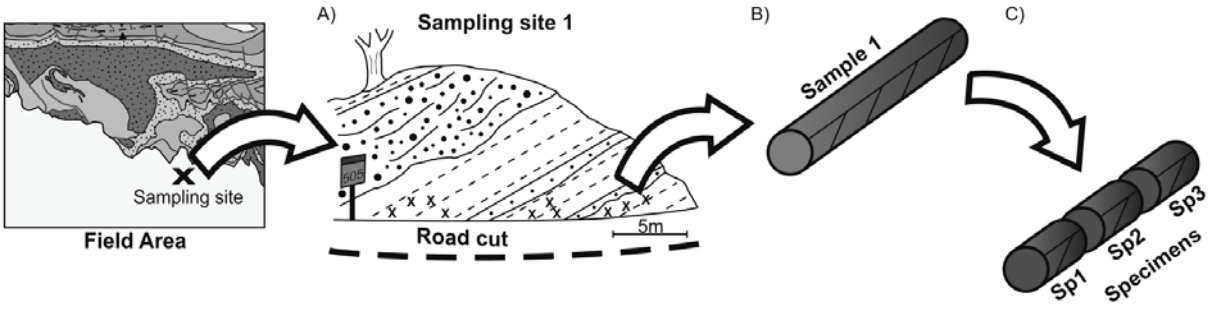

Fig. P.20: Definition of site (A), sample (B) and specimen (C) for the paleomagnetic study.

Samples were processed and analysed in the Paleomagnetic Laboratory of Barcelona (CCiTUB-CSIC) located in the "Institut de Ciències de la Terra Jaume Almera". The palaeomagnetic analysis consisted of a stepwise thermal demagnetisation and subsequent

measurement of the natural remanent magnetisation (NRM) at intervals ranging between 50ºC and 10ºC depending on the lithology. Thermal demagnetisation was conducted up to about 510ºC for most of the limestones and grey clays and up to 680ºC for the rest of the reddish clays using a MMTD-80 (Magnetic Measurements) and TSD1 (Schonstedt) thermal demagnetiser. Remanent magnetisation was measured using the superconducting rock magnetometer SRM755R (2G Enterprises) that has a noise level of $<10^{-7}$ $A \cdot m^{-1}$ for a 10 cm^3 volume of rock. Magnetic susceptibility was also measured after each demagnetisation step using the magnetic susceptibility bridge KLY-2 (Kappabridge). In addition, coercivity and three-axis IRM analysis where performed using an impulse magnetiser IM10-30 (ASC Scientific) and then demagnetised using the same procedure and apparatus previously described.

Chapter 1

Thin-skinned and thick-skinned style of deformation, surrounding the study area, resulted from the inversion of the Lower Cretaceous extensional basin

This chapter contains the first scientific article that forms part for this thesis, in it we describe the style of deformation that characterises the different sectors of the study area and surroundings that resulted from the reactivation of inherited extensional faults during the Pyrenean Orogeny. The present article has been published in the Geological Society of London Special Publications number 377 and it is cited as follows:

Carola, E., Tavani, S., Ferrer, O., Granado, P., Quintà, A., Butillé, M., Muñoz, J.A. 2012. Along-strike extrusion at the transition between thin- and thick-skinned domains in the Pyrenean Orogen (northern Spain). in: *Thick-Skin-Dominated Orogens: From initial inversion to full accretion*, edited by: Nemčok, M., Mora, A. and Cosgrove, J.W. Geological Society of London Special Publications. v.377. DOI:10.1144/SP377.3.

Resum

En aquest capítol es presenta el primer article que s'inclou en aquesta Tesi i en el qual es descriuen els estils de deformació que caracteritza els diferents sectors de la zona d'estudi i els seus voltants. Els dos estils de deformació presents van resultar de la reactivació i inversió, durant la orogènia pirenaica, de les estructures extensives heretades de l'etapa extensiva del Juràssic terminal Cretaci inicial.

Al sector vergent al sud de la part occidental de l'orogen Pirenaic, la conca mesozoica i part del marge continental adjacent van ésser deformats durant el període de col·lisió Pirenaic. La obliqüitat entre les direccions extensives i compressives així com també la presencia d'una zona de transferència mesozoica va implicar que els dos dominis fossin exposats allarg de l'edifici muntanyenc en una posició estructural equivalent. Aquestes dues àrees no estan únicament caracteritzades per l'extensa reactivació dels sistemes de falles heretats sinó que a més a més, els diferents estils de deformació estan relacionats amb la presència o absència del nivell de desenganxament evaporític del Triàsic Superior.

Cap a l'est, a la conca mesozoica, hi ha present un encavalcament dirigit cap al sud amb un angle baix i amb un desplaçament important que desenganxa sobre el Triàsic evaporític. Cap a l'oest, al marge continental, les falles de tipus inverses i dextrògires arrelades a molta profunditat i amb un estil estructural de pell gruixuda esdevenen els elements principals. La presència d'una component direccional va produir l'extrusió cap al sud-est del sector localitzat a l'est del marge continental, que a la seva vegada va produir una component d'escurçament cap al límit est del bloc extruït.

L'àrea de transició entre l'estil de deformació de pell pel·licular i de pell gruixuda, la transició entre la inversió a favor del cabussament a una de tipus transpresiva i l'àrea que acomoda l'extrusió estan localitzades allarg d'una banda orientada nord-sud representant l'extensió cap al sud de la zona de transferència mesozoica.

Abstract

In this chapter it is presented the first article enclosed in the present Thesis in which the main deformational styles that characterise the different sectors of the study area and surroundings are described. The two styles of deformation present resulted from the reactivation and inversion, during the Alpine Orogeny, of inherited extensional structures developed during the rifting stage that took place during the Upper Jurassic - Lower Cretaceous.

In the south-verging portion of the Western Pyrenean Orogen, a Mesozoic basin and part of the adjacent continental margin were deformed during the Pyrenean collisional stage. The slight obliquity between extensional and compressional trends and the presence of a Mesozoic transfer zone implied that both extensional domains were exposed along-strike of the belt in the same structural position. These two areas are not only characterised by the widespread reactivation of inherited fault systems but also by different styles of deformation related to the presence or absence of an evaporitic detachment level.

To the east, in the Mesozoic basin, a large-displacement south-directed low-dipping thrust detached above Triassic evaporites is present. To the west, in the Mesozoic continental margin, thick-skinned and deeply-rooted right-lateral and reverse faults become first order elements. The presence of a strike-slip component produced the eastward extrusion of the eastern portion of the Mesozoic continental margin, which imposed an along-strike shortening at the edge of the extruded block.

The transitional area from thin- to thick-skinned style of deformation, from a dip-slip to a transpressive framework, and the area accommodating the extrusion are located along a N-S oriented band representing the southern extension of a Mesozoic transfer zone.

Along-strike extrusion at the transition between thin- and thick-skinned domains in the Pyrenean Orogen (northern Spain)

E. CAROLA[1,2]*, S. TAVANI[1,3], O. FERRER[1], P. GRANADO[1], A. QUINTÀ[1], M. BUTILLÉ[1] & J. A. MUÑOZ[1]

[1]*Department de Geodinàmica i Geofísica, Institut de Recerca Geomodels, Facultat de Geologia, Universitat de Barcelona, Martí i Franquès s/n, 08028 Barcelona, Spain*

[2]*Fundación Ciudad de la Energía (CIUDEN), C/II Avenida de Compostilla 2, 24404 Ponferrada, Spain*

[3]*Dipartimento di Scienze della Terra, Università Federico II, Via Mezzocannone, 8 I-80134 Napoli, Italy*

**Corresponding author (e-mail: e.carola@ub.edu)*

Abstract: In the south-verging portion of the western Pyrenean Orogen, a Mesozoic basin and part of the adjacent continental margin were deformed during the Pyrenean collisional stage. The slight obliquity between extensional and compressional trends, and the presence of a Mesozoic Transfer Zone, implied that both extensional domains were exposed along-strike of the belt in the same structural position. These two areas are not only characterized by the widespread reactivation of inherited fault systems but also by different styles of deformation related to the presence or absence of an evaporitic detachment level. To the east, in the Mesozoic basin, a large-displacement south-directed low-dipping thrust detached above Triassic evaporites is present. To the west, in the Mesozoic continental margin, thick-skinned and deeply rooted right-lateral and reverse faults become first-order elements. The presence of a strike-slip component produced the eastwards extrusion of the eastern portion of the Mesozoic continental margin, which imposed an along-strike shortening at the edge of the extruded block. The transitional area from thin- to thick-skinned style of deformation, from a dip-slip to a transpressive framework, and the area accommodating the extrusion are located along a north–south-orientated band representing the southern extension of a Mesozoic Transfer Zone.

The presence of structural inheritances (e.g. Butler *et al.* 2006) plays an important role in controlling the style of deformation during the positive inversion of formerly extensional structures (e.g. Lamplugh 1920; Harding 1985; Ziegler 1987; Cooper & Williams 1989; Buchanan & Buchanan 1995; McClay 1995; Nielsen & Hansen 2000; Turner & Williams 2004; Amilibia *et al.* 2005, 2008). Structural inheritances include different parameters, such as rheological properties (e.g. Dewey & Bird 1970; Sandiford 1999; Ranalli 2000), inherited fault systems (e.g. Coward 1994; Holdsworth 2004; Tavani *et al.* 2011*a*), and anisotropies and competence contrasts (e.g. Marshak 2004; Pfiffner 2006). Fluid pressure, frictional properties of the fault zone and acting stress field can determine the reactivation of inherited faults during basin inversion (e.g. Sibson 1985, 1995). Typically, the axis of maximum horizontal stress during inversion is orientated obliquely with respect to the pre-existing extensional fault systems, which determines the partitioning between dip-slip, transpressive and strike-slip kinematics (e.g. Williams *et al.* 2005; Quintana *et al.* 2006), and the release of the geometrical relationship between major fold axes orientation and regional stress field (Tavani *et al.* 2011*a*). Such a situation can be further complicated by the presence of inherited anisotropies in deeper crustal levels (e.g. Sandiford 1999; Van Wees & Beekman 2000) and in upper portions of inverted basins. In particular, the presence of weak layers within the sedimentary pile either with frictional (e.g. Davis *et al.* 1983; Dahlen 1984) or viscous rheology (Davis & Engelder 1985) can favour the onset of a thin-skinned style of deformation, commonly with synchronous (but decoupled) deformation of both cover and basement (e.g. Mouthereau *et al.* 2007). In these cases, the spatial distribution of weak units is another key factor in controlling the style of deformation (e.g. Bahroudi & Koyi 2003; Storti *et al.* 2007).

Consequently, it is not easy to understand the contractional structural framework in areas where significant inheritances exist. The aim of this work

From: Nemčok, M., Mora, A. & Cosgrove, J. W. (eds) 2013. *Thick-Skin-Dominated Orogens: From Initial Inversion to Full Accretion*. Geological Society, London, Special Publications, **377**, 119–140.
First published online March 8, 2013, updated version March 14, 2013, http://dx.doi.org/10.1144/SP377.3

is to elucidate the relationships between structural inheritances and style of deformation in the western Pyrenean Orogen (Fig. 1), where inherited extensional architectures were widely reactivated during the Pyrenean compressional stage. The Mesozoic Pyrenean rift associated with the opening of the North Atlantic Ocean and the Bay of Biscay has been characterized by an articulated system of basins segmented by orthogonal transfer zones (Fig. 2) (e.g. Vergés & García-Senz 2001; Roca *et al.* 2011). In these basins, up to 10 km of syn-rift sediments were deposited on a well-layered pre-rift package that includes Triassic evaporites and Jurassic limestones (García de Cortázar & Pujalte 1982; Pujalte 1982; Mathieu 1986; Bois *et al.* 1997). This sedimentary succession overlies both a thinned and stretched continental crust and an exhumed continental mantle (e.g. Pedreira *et al.* 2007; Ruiz 2007; Ferrer *et al.* 2008; Jammes *et al.* 2009; Roca *et al.* 2011). As a result, these Mesozoic basins represent thin and well-layered continental blocks. By contrast, in the continental margin, a reduced and much thinner Mesozoic succession (up to a few hundred metres of post-rift Upper Cretaceous sediments) was directly deposited on top of Palaeozoic rocks consisting of the upper portion of an old and thick continental crust (Lanaja 1987; Gómez *et al.* 2002). Palaeozoic–Mesozoic fault systems

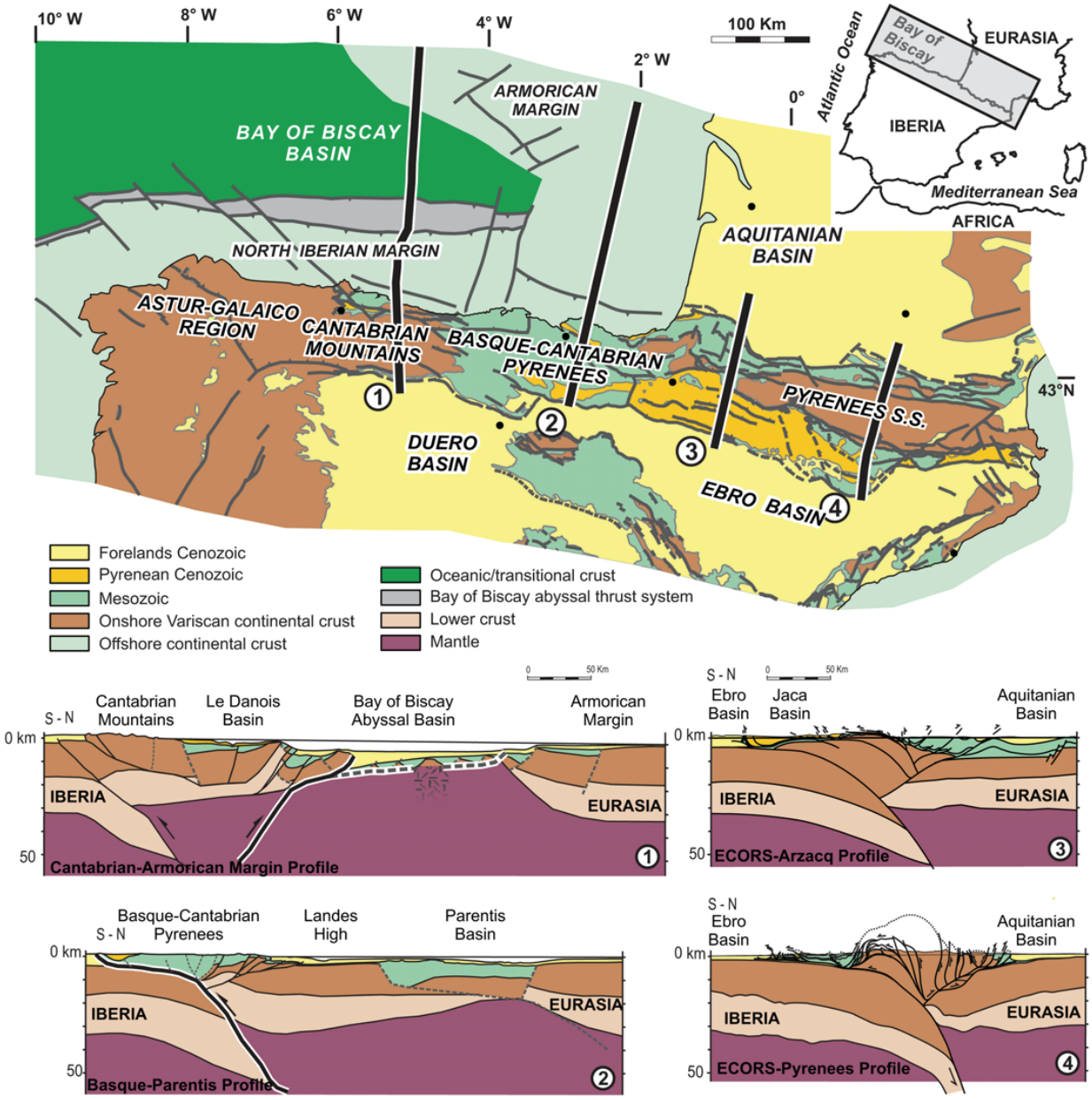

Fig. 1. Structural map of the Pyrenees with crustal sections depicting the main structural changes along the thrust and fold belt. 1, ECORS–Pyrenees; 2, ECORS–Arzaq; 3, Basque–Parentis; 4, Cantabrian–Armorican Margin (modified from Muñoz 2002 and Roca *et al.* 2011).

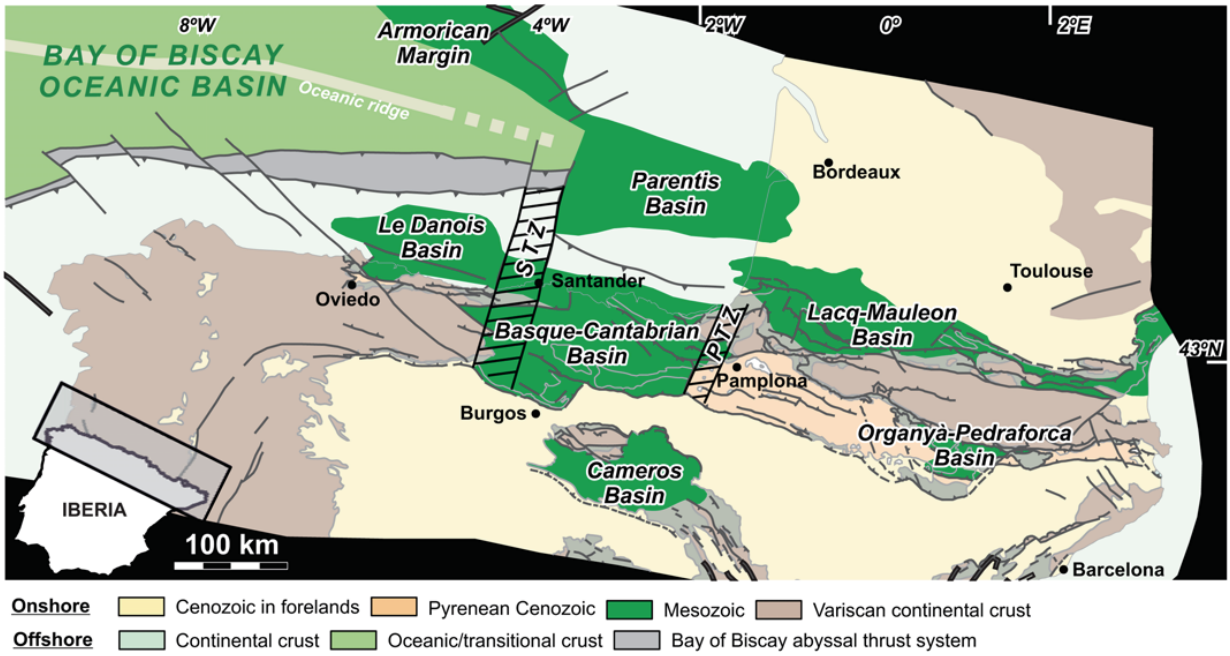

Fig. 2. Location of the main Mesozoic basins; STF and PTZ corresponds to the Santander Transfer Zone and the Pamplona Transfer Zone, respectively (modified from Ferrer *et al*. 2005).

(Muñoz 1992; Larrasoaña *et al.* 2003), as well as crustal-scale inherited rheological heterogeneities (Beaumont *et al.* 2000), played a major role in the evolution of the Pyrenean Orogen.

This is particularly evident in the Basque–Cantabrian Pyrenees at the western edge of the Pyrenean Orogen. In fact, a bulk parallelism, which exists between extensional and compressional trends in the central and eastern sectors of the Pyrenean Orogen (i.e. the Pyrenees *sensu strictu*), determines an *a priori* relationship between extensional and compressional across-strike deformation domains. By contrast, extensional and compressional trends are slightly oblique in the western Pyrenean Orogen, and different Mesozoic domains are exposed along the strike of the belt because of the presence of the Santander crustal-scale Mesozoic Transfer Fault (Roca *et al.* 2011) (Fig. 2).

A reinterpretation of the south-verging contractional structure of the Alpine domains of the western Pyrenean Orogen (i.e. the Basque–Cantabrian and Asturian areas) was carried out by seismic cross-sections and structural data. The Basque Pyrenees are constituted by a thick Mesozoic sedimentary pile, which is detached from Triassic evaporites. This pile overrides the Mesozoic continental margin along the large-displacement Sierra de Cantabria Thrust (Fig. 3). In this area, the style of deformation is fully thin-skinned and the amount of south-directed displacement associated with the frontal thrust exceeds 15 km (Martínez-Torres 1993). The depth and thickness of Triassic evaporites and the displacement associated with thin-skinned structures decrease westward. In this area, right-lateral strike-slip faults reactivating inherited extensional systems are significant (e.g. Boillot & Malod 1988; Hernaiz 1994). Further west, where Palaeozoic rocks are exposed in the Cantabrian Mountains (Heredia *et al.* 1990; Lepvrier & Martínez-García 1990; Pulgar *et al.* 1999), Pyrenean north–south shortening was accommodated by both low-displacement reverse and right-lateral deeply-rooted faults. The lateral juxtaposition of south-directed dip-slip movements and right-lateral transpressive movements along WNW–ESE- to NW–SE-orientated faults led to an eastwards extrusion of the basement and to the development of a structurally complex accommodation zone (Fig. 2).

Geological setting

The east–west-elongated Pyrenean doubly-vergent orogen that divides the Iberian and Eurasian plates constitutes the western branch of the Alpine–Himalayan orogenic system, and runs for about 1000 km from the Mediterranean Sea to the Atlantic Ocean (Fig. 1). It includes mountain ranges and areas with very different average elevations and offshore domains. The presence of such an articulated physiography suggests that the individualization of the first-order architecture of the orogen has been determined by geographical, rather than by geological, criteria. The study area represents an important internal boundary of the orogen in terms of the style of deformation. In line with recent work on the

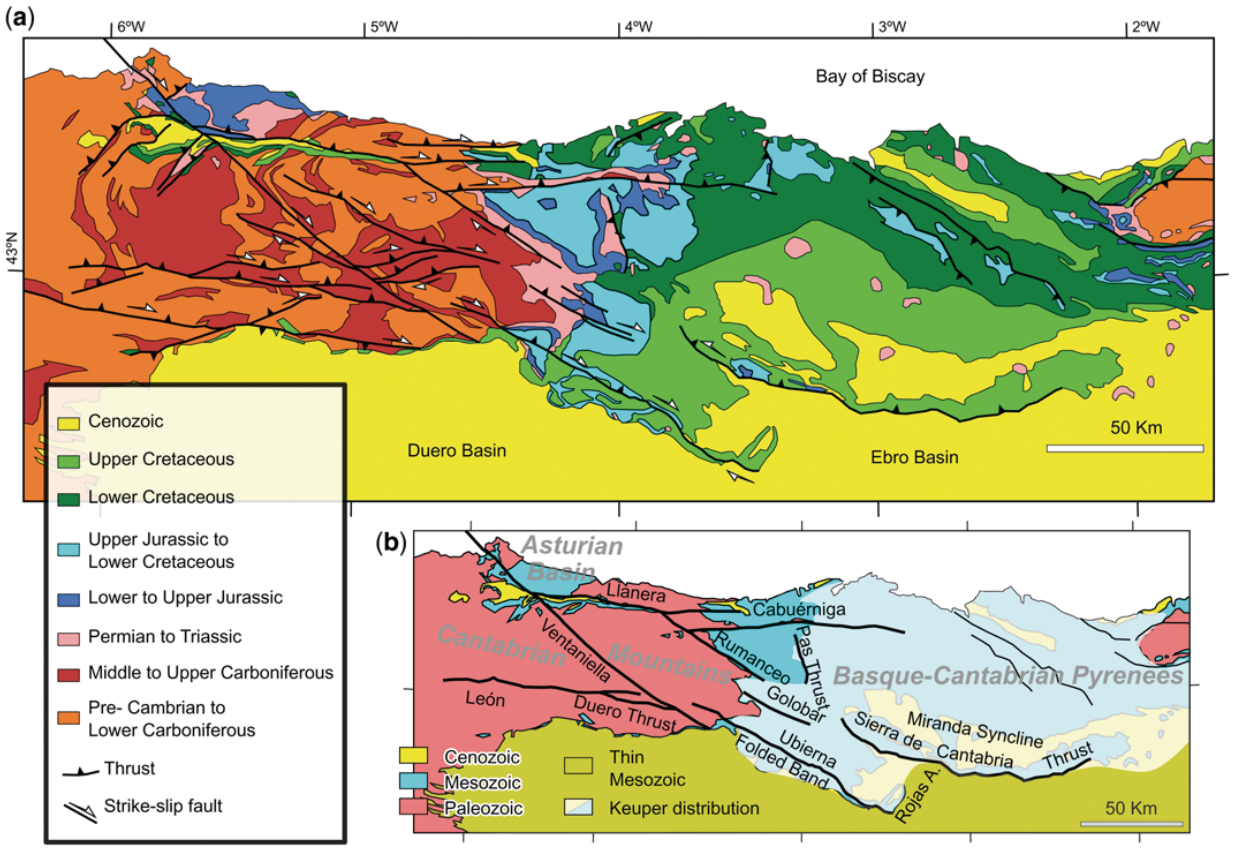

Fig. 3. (**a**) Geological map of the western Pyrenean Orogen. (**b**) Simplified map with distribution of the Keuper facies and the thinned Mesozoic sequence.

Pyrenean Orogen (Muñoz 2002; Martín-González & Heredia 2011*a*, *b*; Roca *et al.* 2011; among others), we adopt a consistent geological nomenclature; that is, the orogen is termed the Pyrenean Orogen given that the term Pyrenees is restricted to its central and eastern portion.

The Pyrenean Orogen resulted from the convergence between the Iberian and Eurasian plates during the Late Cretaceous–Cenozoic (Le Pichon & Sibuet 1971; Muñoz 1992, 2002) and, especially, from the subduction of the Iberian Plate below the Eurasian Plate, as has been unequivocally recognized in all of the deep seismic profiles crossing the orogen (Choukroune & ECORS Team 1989; Roure *et al.* 1989; Choukroune *et al.* 1990; Choukroune 1992; Muñoz 1992; Álvarez-Marrón *et al.* 1996; Pulgar *et al.* 1996; Bois *et al.* 1997; Teixell 1998; Pedreira *et al.* 2003; Ferrer *et al.* 2008). To the east, the orogen involved a previously thinned continental lithosphere; whereas, to the west, the Bay of Biscay passive continental margin and the oceanic–transitional crust were deformed during convergence (Gallastegui 2000; Gallastegui *et al.* 2002; Thinon *et al.* 2003; Jammes *et al.* 2009, among others). Because of this pre-contractive articulated architecture, the Pyrenean Orogen displays different characteristics along its strike (Muñoz 2002; Roca *et al.* 2011).

To the east, the Pyrenees *sensu strictu* form a continental collisional orogen with limited subduction of the continental Iberian lower crust and lithospheric mantle underneath the Eurasian Plate (Muñoz 1992; Beaumont *et al.* 2000). A south-verging antiformal stack is present in the central portion of this domain (section 1 of Fig. 1). Thrusts progressively climb up towards the more external sectors, and the structural style in the Ebro and Aquitanian foreland basins is totally thin-skinned (e.g. Choukroune & ECORS Team 1989) (sections 1 and 2 of Fig. 1). To the west, the Pyrenean Orogen includes a deformed crustal wedge of continental rocks above the north-directed subduction of the Iberian continental lithosphere (Pulgar *et al.* 1996; Gallastegui 2000; Pedreira *et al.* 2003; Ruiz, 2007; Ferrer *et al.* 2008) (sections 3 and 4 of Fig. 1). Mesozoic extensional basins have been deformed in this sector of the Pyrenees (Fig. 3), giving rise to the Basque–Cantabrian Pyrenees. The role played by the south-verging portion of the belt in accommodating the orogenic shortening is much more significant in the Basque Pyrenees than in the Astur–Galaico region of the westernmost Pyrenean

Orogen (Martín-González & Heredia 2011*a*, *b*), indicating that an internal boundary of the orogen is located in the Cantabrian Mountains.

The Basque–Cantabrian Pyrenees resulted from the deformation of the WNW–ESE-elongated Basque–Cantabrian Basin, where more than 10 km of Mesozoic sediments were deposited during the extensional stage, leading to the opening of the Bay of Biscay (García-Mondéjar 1987; Cámara 1997; Cuevas *et al.* 1999; Castañares & Robles 2004; Floquet 2004; García-Mondéjar *et al.* 2004). The basin is bounded to the east by the Mesozoic Pamplona Transfer Zone (Fig. 2), which was reactivated during the Pyrenean compression and marks the limit between the Basque Pyrenees and Pyrenees *sensu strictu* (Muñoz 2002). In this area, the leading edge of deformation corresponds to the Sierra de Cantabria Thrust and to its related anticline (Fig. 3). To the west, the mountain front is constituted by the Folded Band, to the south of the WNW–ESE-striking Ubierna–Ventaniella right-lateral transpressive fault system (Fig. 3). The trace of the Sierra de Cantabria Thrust and its related anticline in its westernmost part progressively rotates, attaining an almost NW–SE strike. This portion of the orogen is characterized by a set of WNW–ESE-striking anticlines and synclines running parallel to the main extensional faults (the Ventaniella, Ubierna, Golobar and Rumaceo faults). The structural trend changes to the north as evidenced by the Cabuérniga and Pas faults, amongst others (Fig. 3). The east–west-striking Cabuérniga Fault (Fig. 3) is the most important structure in the area. It is an Early Cretaceous south-dipping extensional fault that underwent inversion during the Pyrenean compression (e.g. García-Mondéjar *et al.* 1986). The north–south-trending and eastward-directed Pas Thrust (Fig. 3) runs perpendicular to the Cabuérniga Fault and represents the northwestward continuation of the Sierra de Cantabria Thrust. In this area, all the contractional elements resulted from the Pyrenean reactivation of Upper Jurassic–Lower Cretaceous elements, although many of these WNW–ESE faults were previously developed during a Permo-Triassic extensional event (García-Mondéjar *et al.* 1986; Rat 1988; Espina *et al.* 2004) or even earlier during the Late Stephanian (Lepvrier & Martínez-García 1990; Pulgar *et al.* 1999; Alonso *et al.* 2009).

This multiphase deformational history of the study area involved a complex stratigraphic architecture, characterized by thickness variations and frequent unconformities. Triassic syn-rift sediments are made up of conglomerates and sandstones belonging to the Buntsandstein facies, whereas the Triassic post-rift sediments consist of dolostones and carbonates assigned to the Muschelkalk facies, and evaporites and clays of the Keuper facies (García-Mondéjar *et al.* 1986). These units are well exposed in the Basque–Cantabrian Pyrenees (Espina 1997). Moreover, a number of wells have been drilled through Triassic sediments in the eastern Duero Basin and in the Basque–Cantabrian Pyrenees (Lanaja 1987). However, Triassic sediment distribution is not homogeneous and the Keuper evaporites are absent in the westernmost part of these basins (Lanaja 1987; Espina 1997) (Fig 3b). Upper Triassic–Middle Jurassic post-rift units are constituted of carbonate ramp sediments with evaporites, whereas the overlying Middle Jurassic is characterized by progressively deeper marine facies made up of marls and black shales (Quesada *et al.* 1993; Aurell *et al.* 2003). The second and main rifting stage occurred during the Upper Jurassic–Lower Cretaceous. Rifting-related sedimentation was characterized by siliciclastic fluvial sandstones organized in positive sequences that are almost 4 km in thickness (Pujalte *et al.* 1996, 2004). Late Cretaceous post-rift sediments are composed of limestones and marls unconformably overlying Palaeozoic–Lower Cretaceous rocks. The Cenozoic syn-compressional sediments include mostly conglomerates and sandstones, and are present along the boundary between the Duero Basin and the Basque–Cantabrian Pyrenees.

In the Cantabrian Mountains, Variscan and late Variscan structures are largely preserved (Fig. 3a). Major Pyrenean structures in this area resulted from the reactivation of inherited Palaeozoic and Mesozoic structures that controlled sedimentation during the latest Palaeozoic and Mesozoic rifting, respectively (De Sitter 1962; Julivert *et al.* 1971; Pérez-Estaún *et al.* 1988; Heredia *et al.* 1990; Pulgar *et al.* 1999). The most prominent fault systems strike east–west, NE–SW and NW–SE (Dallmeyer & Martínez-García 1990) (see Fig. 3), and are responsible for later reactivation during Pyrenean contraction in the Asturian sector (Alonso *et al.* 1996). The origin of these large-scale fault systems is a subject of controversy. A late Variscan origin has been suggested in order to accommodate problems of space during lithospheric buckling due to orocline development and related Variscan thrust sheet emplacement (Arthaud & Matte 1977; Pérez-Estaún *et al.* 1988, 1991; Gutiérrez-Alonso *et al.* 2008; Alonso *et al.* 2009). Late Stephanian transtension accompanied by sedimentation precluded the Permo-Triassic extensional event and led to the development of a series of small-scale basins (i.e. the Asturian Basin: Lepvrier & Martínez-García 1990).

The Variscan basement in the Cantabrian Mountains (Fig. 3a) mainly consists of Cambrian–Lower Carboniferous rocks and Middle–Late Carboniferous syn-orogenic deposits (Pérez-Estaún *et al.* 1991; Dallmeyer *et al.* 1997), which belong to the Cantabrian Zone in the inner part of the

Ibero-Armorican Arc of the Variscan Belt. Late Palaeozoic transtension to Mesozoic rifting is recorded by the development of the Asturian Basin, which has a considerably thinner sedimentary infill than its easterly located Basque–Cantabrian counterpart (Lepvrier & Martínez-García 1990; García-Ramos & Gutiérrez-Claverol 1995; Gutiérrez-Claverol & Torres-Alonso 1995; Menéndez-Casares *et al.* 2004). In general, the Mesozoic infill of the Asturian Basin is constituted by sedimentary facies similar to those in the Basque Pyrenees. The most important difference is that the Asturian Upper Triassic Keuper facies lacks well-developed evaporites (Gutiérrez-Claverol & Torres-Alonso 1995; Barrón *et al.* 2006).

Data

The Sierra de Cantabria Frontal Thrust

The mountain front in the Basque–Cantabrian Pyrenees is constituted by the bow-shaped Sierra de Cantabria Thrust (Fig. 3b). This structure is concave towards the hinterland and strikes from NW–SE to NE–SW with a primary east–west trend. The associated hangingwall anticline is cored by Jurassic–Upper Cretaceous sediments (with Triassic rocks that are locally exposed), whereas Cenozoic sediments crop out to the south in its footwall, and to the north in the Miranda Syncline. A north–south-orientated seismic cross-section located across the central portion of the thrust constrains the deep geometry of this structure (Fig. 4). Hangingwall and footwall ramp geometries are well imaged, indicating the presence of a staircase fault trajectory. In this seismic line only an upper footwall ramp is imaged as the lower ramp is located to the north, where seismic cross-sections are not available. The upper footwall ramp of the thrust dips less than 20° toward the north, where the footwall consists of flat-lying Cenozoic and thin Cretaceous sediments that overlie basement rocks (Fig. 4b). The hangingwall is constituted by a thick Mesozoic sequence with an almost flat-lying geometry in a large sector of the seismic line. The hangingwall is affected by folds, the Miranda Syncline being the main one. In the southern portion of the hangingwall, Lower Cretaceous syn-rift units overlie Jurassic pre-rift limestones and marls, where the contact is both tectonic and stratigraphic. To the north, the sediments of the Lower Cretaceous syn-rift increase in thickness. The hangingwall of the Sierra de Cantabria Thrust includes largely north-dipping extensional faults. Many of these faults provide evidence of tectonic inversion related to the Pyrenean compressional stage (Fig. 4). In conclusion, the first-order architecture of hangingwall and the footwall indicates an inverted normal fault system, with a minimum displacement of about 25 km where the upper footwall ramp is imaged (horizontal distance X–X′ in Fig. 4b). However, this value is probably underestimated because of the impossibility of determining the position of the lower ramp (i.e. the inverted normal fault) in the footwall.

The trace of the Sierra de Cantabria Thrust progressively rotates towards the west, approximately attaining a WNW–ESE orientation in the Cantabrian area. The amount of displacement is reduced, and Cenozoic sediments that fill the leading syncline progressively disappear (Fig. 4). Meso- and macrostructures in this area provide additional evidence of the positive inversion of an Upper Jurassic–Lower Cretaceous extensional system (Fig. 5a). Miocene growth strata host rotated conjugated reverse faults giving rise to a roughly north–south-orientated shortening direction (Tavani *et al.* 2011*b*). In the same structure, WNW–ESE-striking left-lateral transpressive faults are present (Fig. 5b) and, together with north–south-striking thrusts and NE–SW-striking right-lateral faults, are associated with a post-folding (i.e. late compressive) east–west-shortening. Further NW, the Sierra de Cantabria Thrust disappears and a set of NW–SE-striking synclines and anticlines provide the link between the WNW–ESE-striking and south-directed Sierra de Cantabria Thrust and the NNW–SSE-striking and ENE-directed Pas Thrust (Fig. 6). The associated Pas Anticline is cored by Permo-Triassic sediments, indicating the presence of a deeply-rooted thrust-fault. In the area of the Pas Anticline, a number of extensional faults run parallel to this fold (Fig. 7), suggesting that the structure resulted from the inversion of an inherited extensional structure.

The Ubierna Fault System

To the SW of the Sierra de Cantabria Thrust, the transpressive right-lateral Ubierna Fault System and the structural units of the Folded Band constitute the mountain front of the Cantabrian area, bounding to the north the Cenozoic Duero Basin (Fig. 3). This fault system is about 15 km wide and 120 km long, and is the southern boundary of the Mesozoic Basque–Cantabrian Basin (Rodríguez Cañas *et al.* 1994). To the north of this fault system, the accumulation of Mesozoic sediments exceeds 4 km (Pujalte 1979; Pujalte *et al.* 2004), whereas to the south, in the Duero Basin, the thickness of the Mesozoic fill does not attain 1 km (Lanaja 1987). To the east, the thickness of the Mesozoic sedimentary infill drastically diminishes across the NNE–SSW-striking Las Rojas Anticline (Fig. 3). This anticline is the contractional horsetail termination of the Ubierna Cenozoic transpressive

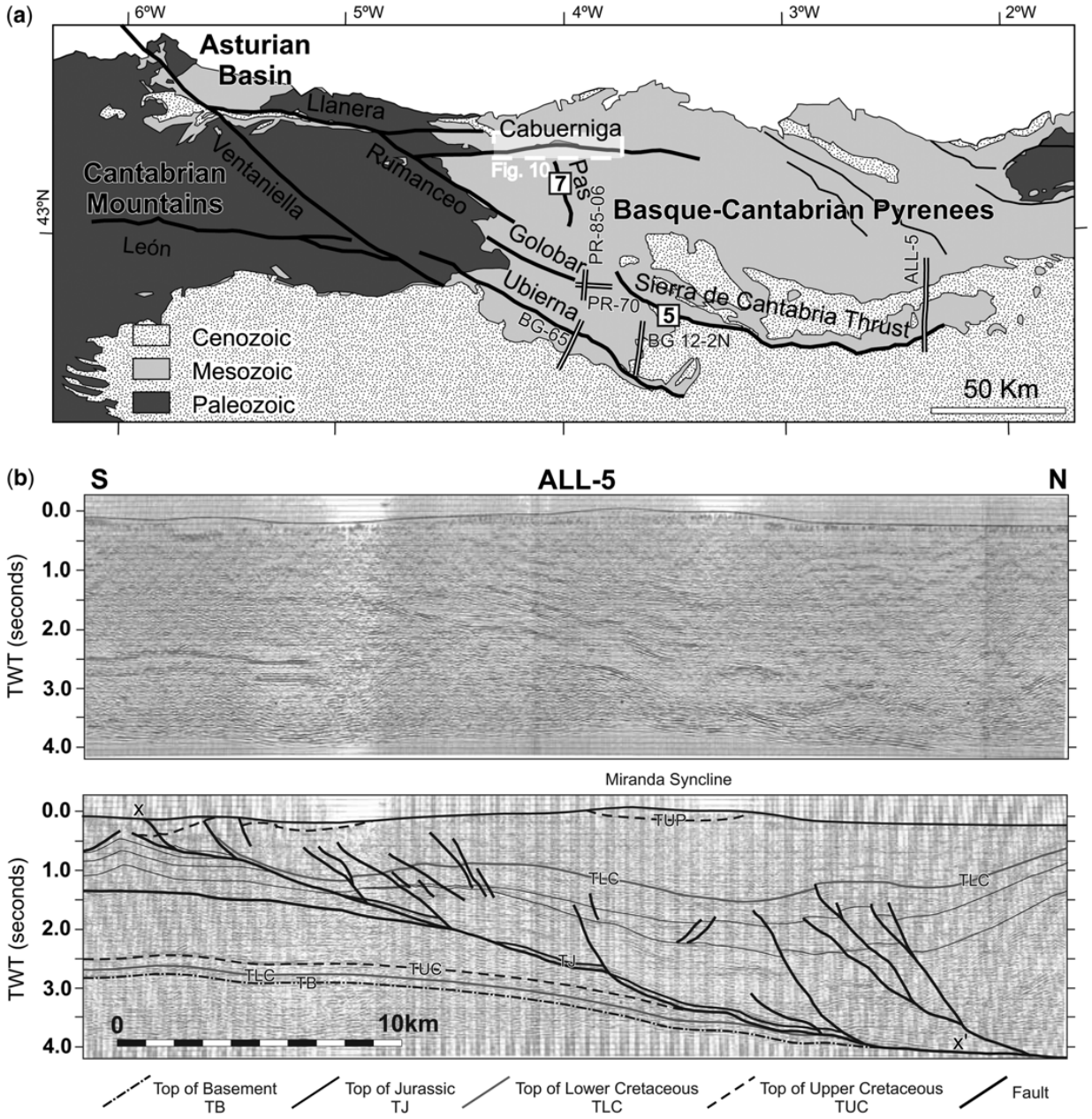

Fig. 4. (**a**) Location of seismic cross-sections of Figures 8 & 9. (**b**) Seismic cross-section across the Sierra de Cantabria Thrust; the X–X′ corresponds to the minimum displacement of the thrust.

right-lateral fault, and acted as a transfer fault between the Ubierna and Sierra the Cantabria faults during the Mesozoic rifting stage (Tavani & Muñoz 2012).

The presence of an Alpine reverse component along the Ubierna Fault System is constrained by about 3–4 km of Cenozoic uplift of its northern block (Malagón *et al.* 1994). The existence of a right-lateral strike-slip component along this fault system has also been recognized by Hernaiz (1994). However, some authors propose mainly dip-slip kinematics (e.g. Espina *et al.* 1996*a*, *b*), whereas other authors suggest 15 km of Cenozoic right-lateral displacement (Tavani *et al.* 2011*b*). This debate notwithstanding, the first-order Cenozoic framework of the area between the Ubierna, Sierra de Cantabria and Las Rojas faults is well constrained. The right-lateral movements along the Ubierna Fault System, the presence of left-lateral kinematics in the western sectors of the Sierra de Cantabria Thrust and the east-directed reverse displacement along the Las Rojas Fault indicate a SE- to ESE-directed relative extrusion of this sector, as recognized by Rodríguez Cañas *et al.* (1994). There is no agreement on the depth of the main Cenozoic faults in this area. Two end-member models have been advanced. Serrano *et al.* (1994) proposed a totally thin-skinned style of deformation, with

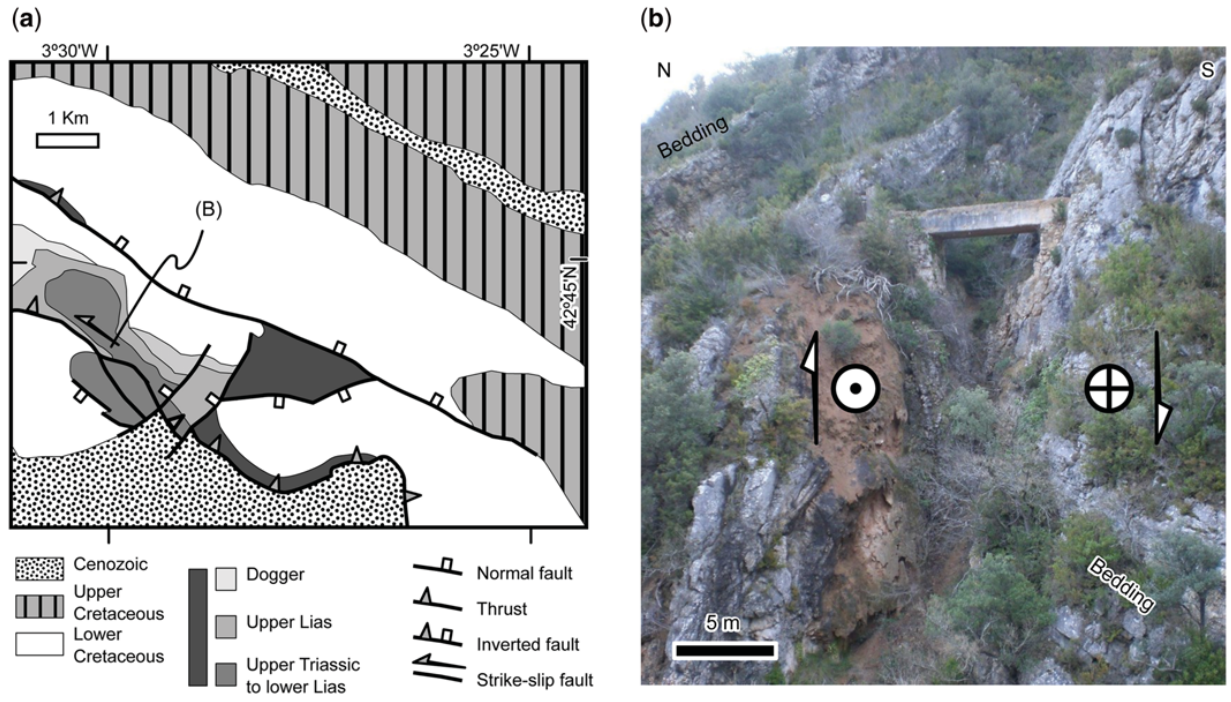

Fig. 5. (**a**) Geological map of the Oña Anticline located in the western sector of the Sierra de Cantabria thrust sheet. The NW–SE-striking and north-dipping faults located in the central portion of the map are recognized as older-on-younger and younger-on-older geometries. These geometries indicate the inversion of an extensional fault. To the south of this fault, Lower Cretaceous sediments unconformably overlie Lower and Middle Jurassic rocks, testifying to the existence of a Lower Cretaceous palaeorelief. (**b**) Detail of a left-lateral transpressive fault system located along the Sierra de Cantabria Frontal Thrust.

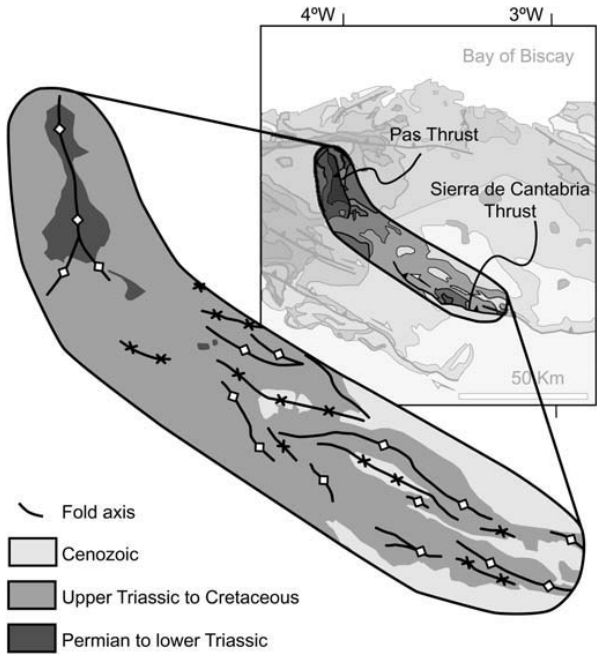

Fig. 6. Detail of the transitional area between the Sierra de Cantabria and the Pas thrusts, showing fold traces progressively rotating from a WNW–ESE to a NW–SE direction, and then attaining an almost NNE–SSW direction in the Pas Anticline.

the Mesozoic package detached and southwards-displaced above the Triassic evaporites. By contrast, Tavani *et al.* (2011*b*) suggested a thick-skinned framework, with steeply-dipping faults rooted in the lower crust.

The thick-skinned style is recognizable in the Ventaniella Fault, which in the Cantabrian Mountains displaces Palaeozoic rocks. However, the deep structure of the Ubierna Fault cannot be fully constrained by means of seismic surveying. In the eastern portion of the Ubierna Fault (Fig. 8a), the hangingwall is characterized by a north-dipping monocline of Upper Triassic–Middle Jurassic sediments. Upper Jurassic–Lower Cretaceous syn-rift sediments show onlap geometries and are also slightly tilted. To the north of the fault, the Upper Cretaceous sediments are almost flat-lying and unconformably overlie the syn-rift sediments. Pre-Keuper reflectors are subhorizontal and parallel to the overlying Triassic–Jurassic sequence in the northern portion of the seismic cross-section. However, Upper Triassic and basement reflectors delimit triangular bodies of Triassic evaporites close to the Ubierna Fault, providing evidence of a first-order role of this ductile unit during the Mesozoic extensional stage. The poor quality of the seismic line in its deeper portions prevents us from constraining the deep geometry of the extensional fault system.

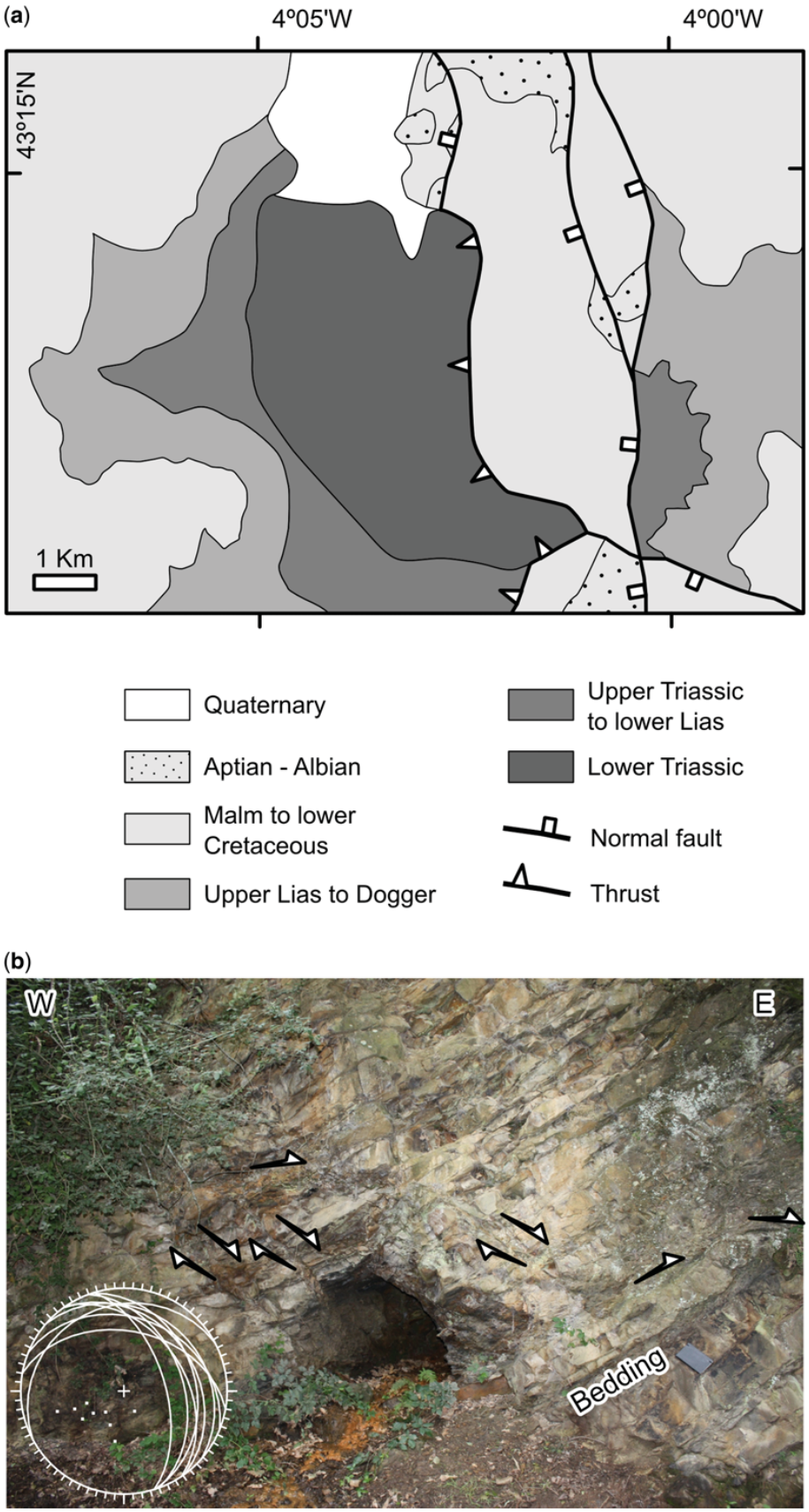

Fig. 7. (**a**) Simplified geological map of the southern portion of the Pas Anticline showing NNW–SSE-trending normal faults parallel to the anticline. (**b**) Detail of a tilted extensional system including NNW–SSE-striking and eastwards-dipping faults and layer-parallel steps. The tilting of these faults and, in particular, the layer-parallel steps indicates a pre-folding development.

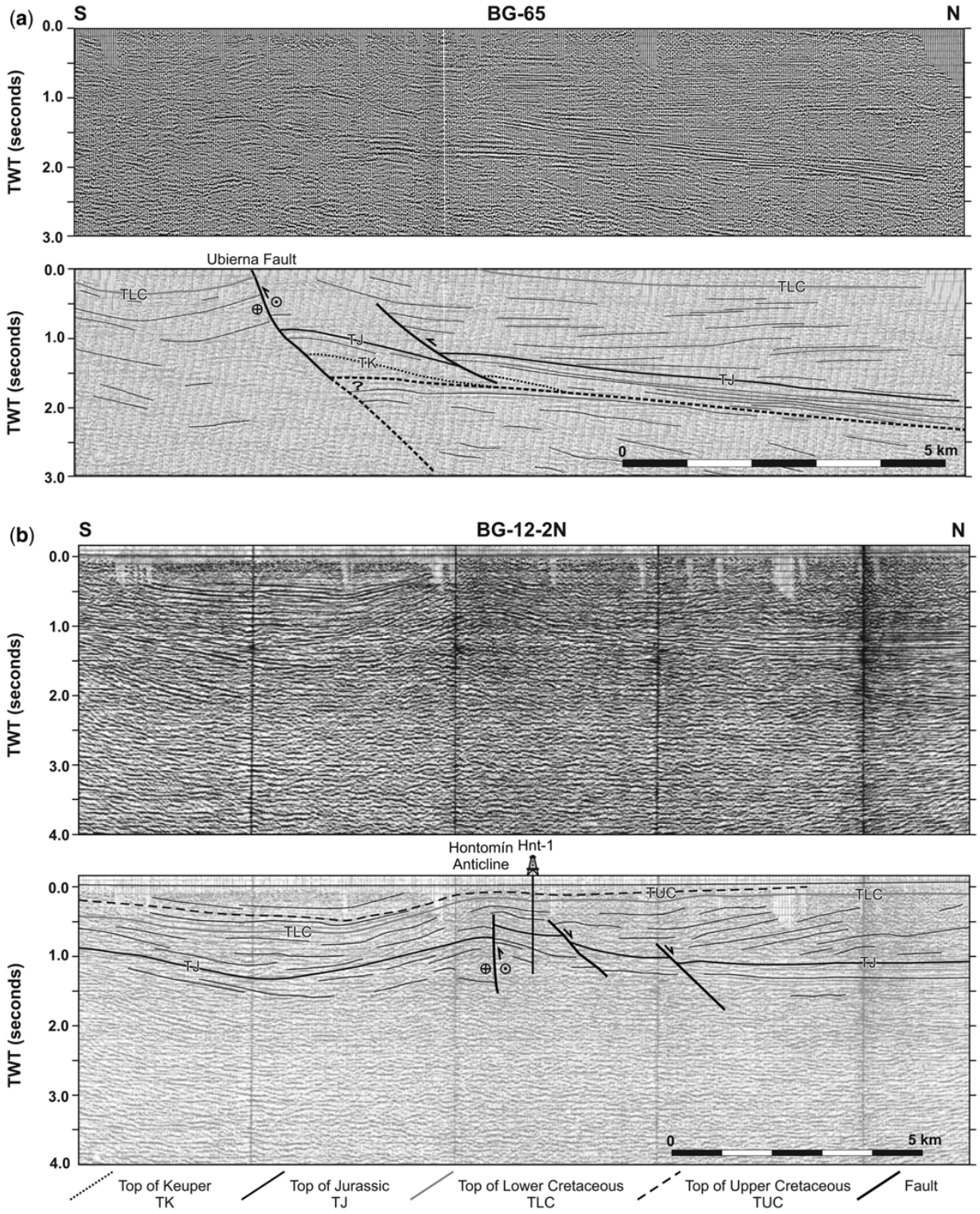

Fig. 8. (**a**) Seismic line across the Ubierna Fault. (**b**) Seismic line across the Hontomín Anticline located northwards of the Ubierna Fault.

To the south, in a small syncline immediately to the north of the Ubierna Fault (i.e. Hontomín Syncline), Cenozoic syn-folding sediments overlie Upper Cretaceous limestones and marls, which in turn overlie a reduced Upper Jurassic–Lower Cretaceous syn-rift package (Fig. 8b). The east–west-striking Cenozoic Hontomín Anticline separates this syncline from the northern portion of the section. The Upper Triassic–Middle Jurassic package dips towards the north and then progressively attains a subhorizontal attitude. To the north, the onlapping geometry of the Upper

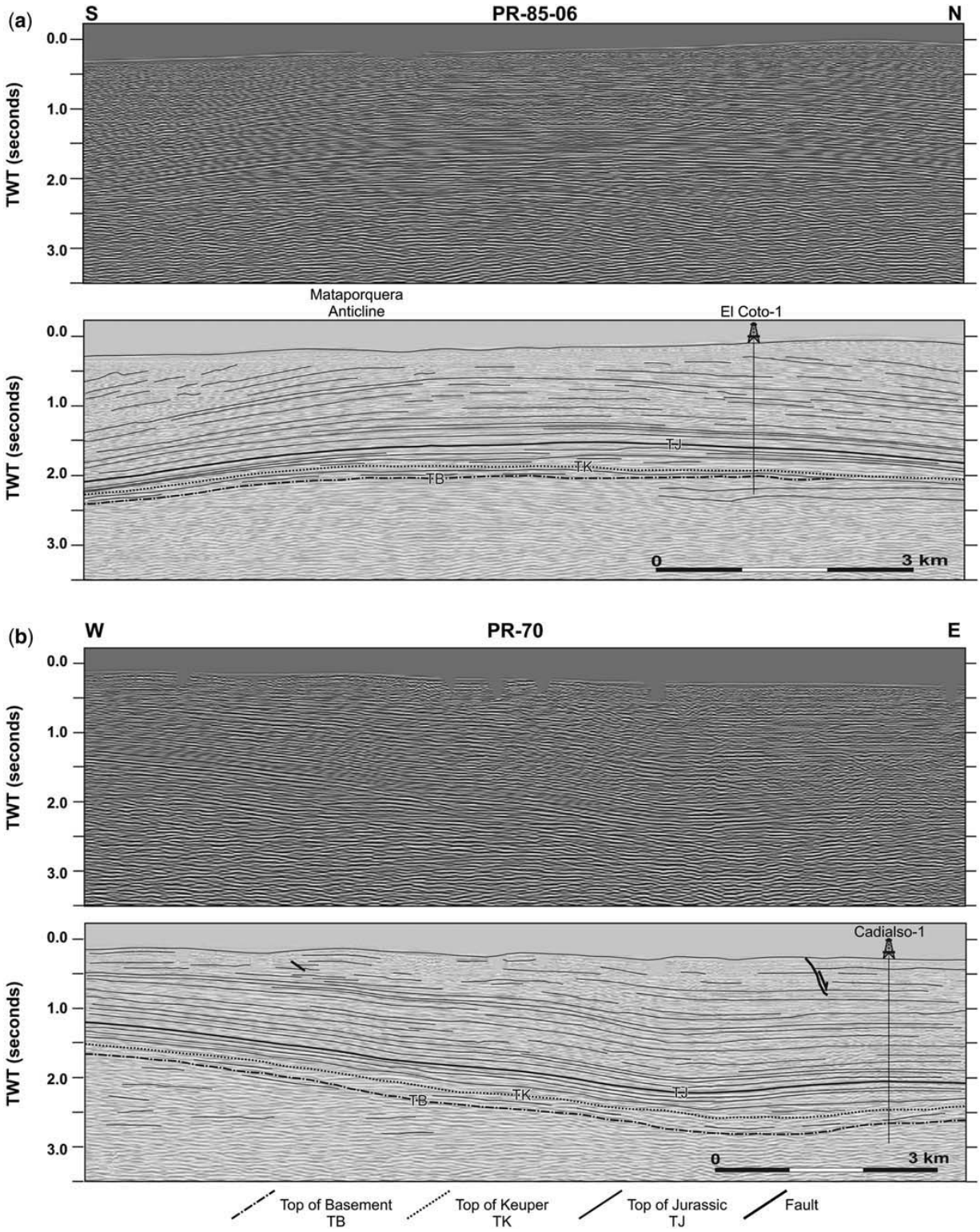

Fig. 9. (**a**) Seismic line striking perpendicular to the Golobar Fault. (**b**) Seismic line striking parallel to the Golobar Fault.

Jurassic–Lower Cretaceous sediments is well imaged. These units are folded in the central portion of the section where pre-rift sediments are subhorizontal. Almost flat-lying Upper Cretaceous sediments unconformably overlie the folded Lower Cretaceous sediments. The poor quality of the two seismic sections shown in Figure 8 does not allow us to constrain the basement geometry and the style of deformation. Two end-member interpretations are possible. In the thick-skinned hypothesis,

the features described above can be attributed to forced folding (e.g. Maurin & Niviere 2000) related to the extensional stage and to the subsequent inversion of the steeply-dipping faults. The alternative thin-skinned hypothesis demands the mobilization of significant volumes of salt during extension. Below the Triassic evaporites, the basement would only be slightly faulted and almost unaffected by contractive deformation.

The boundary between the Basque–Cantabrian Pyrenees and the Astur–Galaico Region

The Cantabrian area represents the transitional area between the Basque Pyrenees and the Cantabrian Belt, and it is characterized by a regional eastward plunge. WNW–ESE-striking faults – that is, the Ubierna, Ventaniella, Golobar and Rumaceo faults (Fig. 3) – were active during the Upper Jurassic–Lower Cretaceous rifting event, and were later reactivated during the contractive stage (Espina 1997). These faults progressively affect older rocks to the west (Fig. 3). As a result of this, the map view allows us to image their along-dip architecture. In particular, the trace of these faults continues through the contact between Palaeozoic and Mesozoic rocks without being displaced across Triassic evaporites, which indicates that the transition from thin- to thick-skinned tectonics occurs eastwards of this area. A seismic cross-section striking almost perpendicular to the axis of the Mataporquera Anticline, which to the west is cored by the Golobar Fault, shows that the former anticline has gentle limbs and is not associated with the Golobar Fault (Fig. 9a). The Golobar Fault is not observed in the Mesozoic sequence, indicating that it is located within the basement or is even absent. The thickness of the syn-rift package is almost constant across the anticline, and a slightly progressive thinning of 0.5 s in the Upper Jurassic–Lower Cretaceous package is imaged to the north. The same thinning of the syn-rift sequence occurs to the west, this difference being about 1 s, as shown in the seismic cross-section striking parallel to the fold axis (Fig. 9b). The westward thinning of the syn-rift sequence indicates that the eastwards regional plunge is at least partially rift-related. Thus, this area must be regarded as the western margin of the Basque–Cantabrian Mesozoic Basin. The Cenozoic deformational sequence in the surroundings of the Golobar and Rumaceo faults includes an early right-lateral transpressive reactivation of these faults followed by an east–west-orientated shortening stage. This led to the development of WNW–ESE-striking left-lateral faults and NE–SW-striking right-lateral mesofaults (Tavani *et al.* 2011*b*).

To the north of the Rumaceo Fault, the Cabuérniga Fault (Fig. 4) is a Palaeozoic element reactivated as an extensional fault during the Upper Jurassic–Lower Cretaceous rifting. In the northern block of the fault, Lower Cretaceous sediments were deposited over a thin Triassic–Jurassic prerift sequence or directly over the Permian–Lower Triassic Buntsandstein facies, whereas, to the south, the thickness of the Triassic–Jurassic and syn-rift sequences increases (Fig. 10a). The Pyrenean uplift of the northern block of the fault was accompanied by a right-lateral strike-slip component (Fig. 10b).

The Cantabrian Mountains

To the west, in the Cantabrian Mountains, the major structures are the late Variscan Ventaniella and León faults and the Cenozoic Duero Basin Frontal Thrust. The Ventaniella Fault strikes NW–SE and its trace crops out for more than 150 km from the Bay of Biscay to the Duero Basin. The Cenozoic displacement of this fault in the middle of its trace is about 4 km and Variscan markers are displaced in a right-lateral sense (García-Ramos *et al.* 1982; Heredia *et al.* 1990). The polyphasic deformation of this fault is recorded by mesostructures. Extensional assemblages reactivated as right-lateral elements are commonly found (Fig. 11a). In many locations, the Ventaniella Fault also shows Permian left-lateral kinematics with Permian dykes intruding into the fault-related assemblage (Fig. 11b) (Corretgé & Suárez 1991). In other outcrops, small Permian dykes orientated perpendicular to the fault trace are displaced by right-lateral mesofaults, which indicates that right-lateral movements post-dated the transtensive movement (Fig. 11c).

The boundary between the Cantabrian Mountains and the Duero Basin is marked by an east–west-striking and south-dipping monocline of Upper Cretaceous limestones unconformably overlying Palaeozoic rocks (Fig. 12). This structural panel represents the northern limb of the Duero Basin syncline, and extends for about 100 km from the Ubierna Fault System to the east and to the Galician area to the west. Cretaceous layers gently dip at both terminations and become almost vertical to overturned in its central portion, where the monocline is offset by the roughly east–west-striking and north-dipping frontal thrust. The cut-off of this thrust, which is constrained by seismic cross-sections (Gallastegui 2000), indicates a displacement of about 8 km in its central portion, progressively dying out westwards and eastwards.

Data collected from Palaeozoic rocks cropping out in the area between the León Fault and the Duero Frontal Thrust indicate an extensional event post-dated by right-lateral tectonics (Fig. 13).

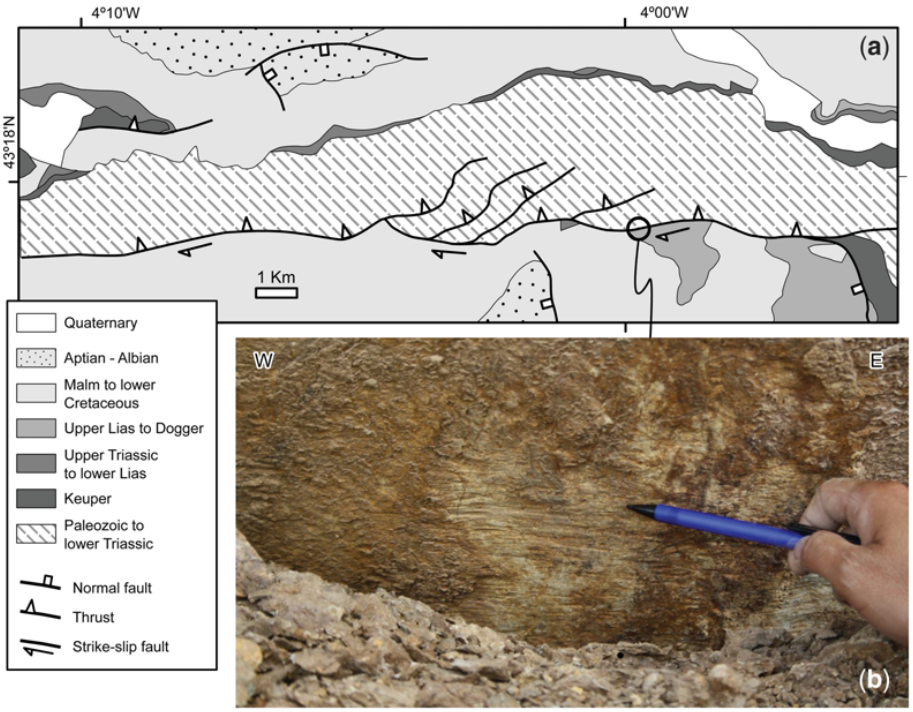

Fig. 10. (**a**) Geological map of the Cabuérniga Fault area. (**b**) Detail of strike-slip slickenlines along the Cabuérniga Fault (Palaeozoic limestones).

Right-lateral assemblages are commonly found, at different scales, both along major faults (including the León Fault) and in the surrounding areas (Heredia 1998). With the available data it was not possible to fully constrain the timing of this right-lateral tectonics. However, the reduced number of compressional mesostructures associated with dip-slip tectonics, in addition to the documented Cenozoic age of the right-lateral movements along the Ubierna Fault System, suggest an Alpine age.

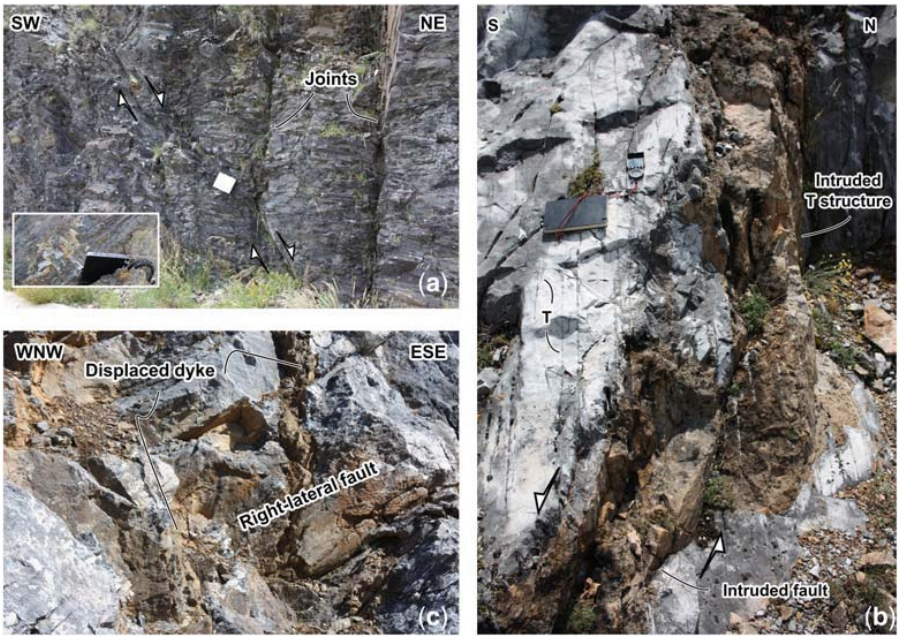

Fig. 11. (**a**) Normal faults and associated joints in Palaeozoic rocks near the Ventaniella Fault. (**b**) A Palaeozoic dyke intruding into a WNW–ESE-striking left-lateral fault and the associated east–west-striking T-structures close to the Ventaniella Fault. (**c**) WNW–ESE-striking right-lateral fault displacing a NNE–SSW-striking Palaeozoic dyke near the Ventaniella Fault.

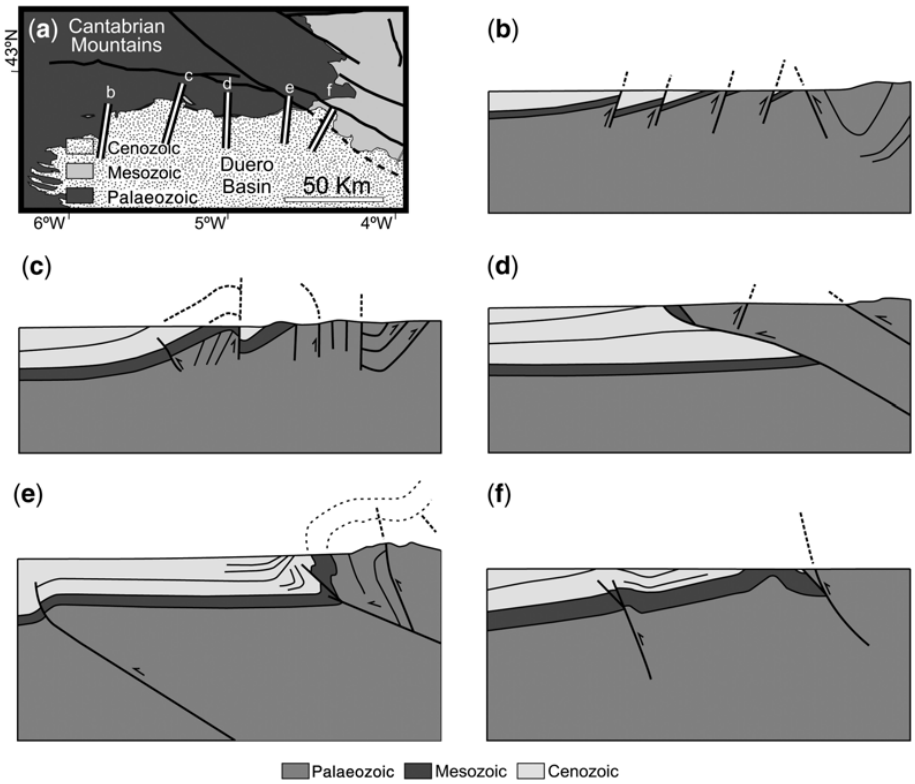

Fig. 12. Schematic cross-sections along the Duero Frontal Thrust (modified from Gallastegui 2000).

The tectonic framework was therefore transpressional in the southern portion of the Cantabrian Mountains.

Discussion

Our data indicate that the Alpine compressional stage was strongly influenced by the presence of inherited elements in the Pyrenean Orogen. Only a few structures can be considered fully Alpine in age, and most of the Cenozoic macrostructural pattern results from the reactivation of inherited Palaeozoic–Mesozoic faults (Alonso *et al.* 1996; Pulgar *et al.* 1999). A thick-skinned style of deformation characterizes the western portion of the study area in the belt (i.e. Cantabrian Mountains) and in the adjacent Duero Basin (Hernaiz & Solé 2000). Important high-angle faults with reverse and right-lateral kinematics are rooted in the middle–lower crust and accommodated a limited amount of north–south-orientated shortening. The amount of displacement along the Duero Frontal Thrust is usually less than 4–5 km, although it locally attains a minimum of 7–8 km. It is reasonable to assume that other major structures cumulatively accommodate only a few kilometres of displacement. Early interpretations of the tectonic framework of the area assume that the basement and the thin Mesozoic cover was detached along a north-dipping thrust joining a basal detachment at a depth of 15–20 km (e.g. Alonso *et al.* 1996). This thrust would accommodate more than 20 km of south-directed displacement (e.g. Alonso *et al.* 1996) and would offset the Ventaniella Fault in the order of 4–6 km. The recently recognized integrity of the latter fault down to 16 km (López-Fernández *et al.* 2004) is inconsistent with the existence of this low-angle south-directed thrust. However, an alternative solution to that proposed by Alonso *et al.* (1996) is a transpressive system along high-angle faults that accounts for the Alpine uplift of the area but limits the amount of shortening probably to less than 10–15 km. The deformation style in this area is slightly different from that in the eastern portion of the Pyrenean Orogen since the Duero Basin is basically a regional-scale synform only deformed by contractive and transpressive structures in its northern limb. Moreover, there is no evidence of an organized southwards migration of the compressive front through time. In other words, the Duero Basin acted as a sort of backstop and most of the deformation was accommodated in the north-verging portion of the Cantabrian Mountains.

The Ventaniella Fault, the Duero Frontal Thrust and the León Fault terminate in the SE portion of the Cantabrian Mountains. The transpressional right-lateral Ubierna Fault System commences towards the SE (Hernaiz *et al.* 1994; Tavani *et al.* 2011*b*).

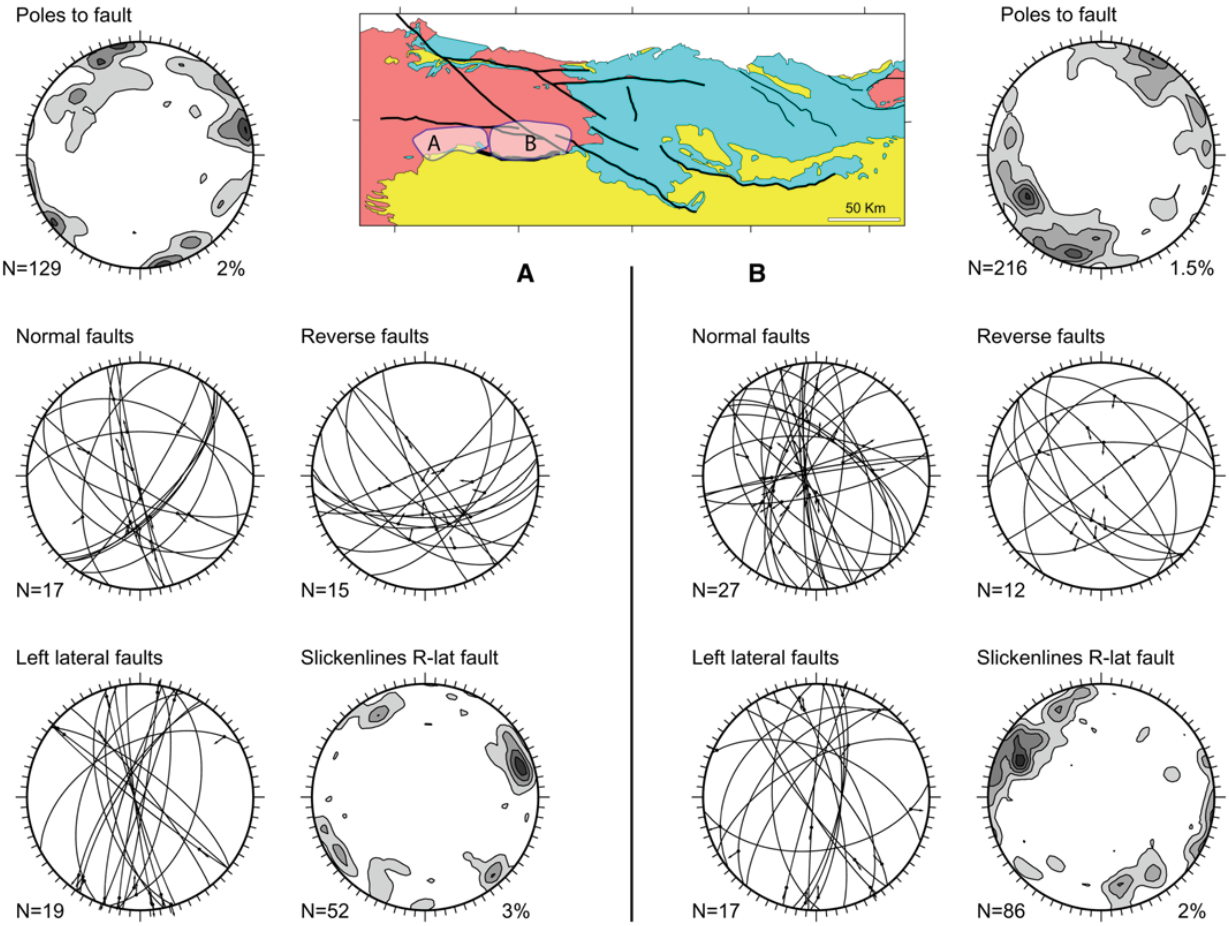

Fig. 13. Mesostructural data along the Duero Frontal Thrust and adjacent areas. The area is dominated by right-lateral tectonics along faults striking WNW–ESE, NE–SW and WSW–ENE. Reverse faults have slickenlines striking from north–south to NNW–SSE; that is, at about 45° from the WNW–ESE-striking right-lateral fault, indicating that they form part of the strike-slip assemblages. *N* corresponds to the amount of data gathered in the field.

Right-lateral movements along the WNW–ESE-striking Golobar and Rumaceo faults, and the east–west-striking Cabuérniga Fault, occurred to the north of this fault system. However, the right-lateral displacement of these faults cannot exceed a few kilometres. These movements predated an east–west shortening event that is recognizable in the area between the Golobar, Rumaceo and Pas faults and in the Oña Anticline. This event is evidenced by north–south-striking reverse faults, WNW–ESE-striking left-lateral faults and NE–SW-striking right-lateral faults. The contractive Alpine style of deformation of this area is totally thick-skinned in the western portions (i.e. the Pas, Cabuérniga, Rumaceo and Golobar faults) (e.g. Espina *et al.* 1996*b*), whereas it is uncertain in the easternmost portion of the Ubierna Fault System. Malagón *et al.* (1994) and Serrano *et al.* (1994) proposed a thin-skinned framework in which the Ubierna Fault would be a small structure within the hangingwall of a thrust sheet detached above Triassic evaporites with a large displacement above the Cenozoic sediments of the Duero Basin. However, Hernaiz & Solé (2000) argued that the thin- and thick-skinned styles of deformation coexisted during Alpine contraction. The tectonic style of this small portion of the study area cannot be constrained as the deeper portions of seismic cross-sections do not image the geometry of faults within the basement. Both thin- and thick-skinned style templates can be used to interpret the geometries imaged in the shallower portions.

Nevertheless, it is clear that the Ubierna Fault is a first-order structure of the area constituting the border of the Lower Cretaceous extensional basin together with the Folded Band. The right-lateral reactivation of the Ubierna Fault started at least during the Eocene (Tavani *et al.* 2011*b*) and was synchronous with the development of the Las Rojas structure, which is its contractional horse-tail termination. During the Miocene, the Sierra de Cantabria Frontal Thrust, in this part of the study area, was characterized by a left-lateral component. This fault, together with the Ubierna and Las Rojas structures, delimited an eastwards-extruded block, as previously recognized by Rodríguez

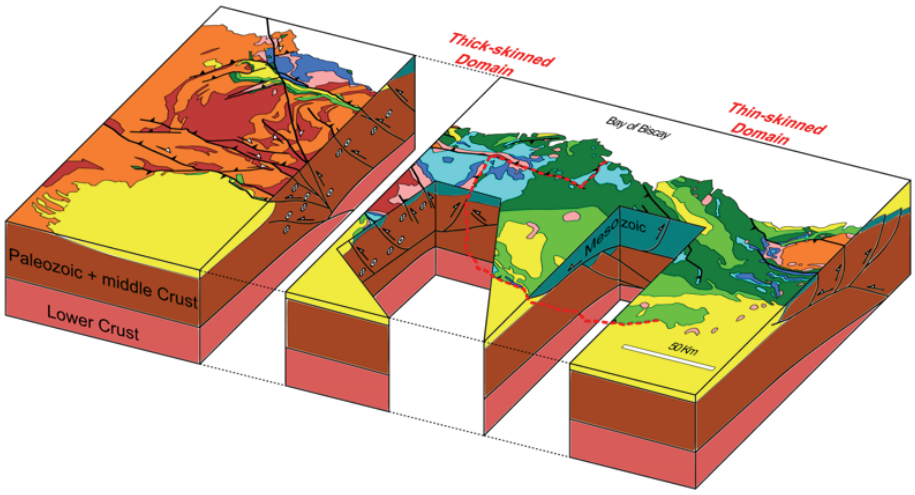

Fig. 14. Three-dimensional block diagram showing the crustal-scale architecture of the western Pyrenean Orogen. The dashed line corresponds to the limit between thin-skinned and thick-skinned styles of deformation.

Cañas *et al.* (1994) and Tavani *et al.* (2011*b*). This extruded area constitutes the eastern boundary of the transpressive system. More to the east, the Sierra de Cantabria Thrust is a thin-skinned structure that detached the Mesozoic sequences above Triassic evaporites onto the Cenozoic sediments of the Ebro Foreland Basin. Using geometrical constraints, Martínez-Torres (1993) computed about 15 km of south-directed displacement for this structure. In our interpretation, at least 25 km of south-directed displacement is assumed. The conglomerates deposited along the leading edge of the thrust indicate that the frontal structure was active at least since the Oligocene (Portero *et al.* 1979). In summary, the south-verging portion of the Pyrenean Orogen includes two distinct domains: the eastern and the western (Fig. 14). The eastern domain – that is, the Basque Pyrenees – is characterized by highly displaced and south-directed thin-skinned structures detached above the Triassic evaporites. The western domain – that is, the Cantabrian Mountains – is characterized by deeply-rooted transpressive faults. Alpine deformation implied transpressional right-lateral movements along west–east- to NW–SE-striking elements, which produced the eastwards extrusion of part of the Cantabrian area. The transitional area between thin- and thick-skinned tectonics and from a dip-slip to a strike-slip framework, and the region accommodating the lateral extrusion of the Cantabrian area, coincides with the southern prolongation of the Santander Mesozoic Transfer Zone (Figs 2 & 3). This transitional area is a first-order discontinuity in terms of the style of the deformation in the Pyrenean Orogen and the western limit of the Triassic evaporites.

The features described above indicate that structural inheritances (e.g. Marshak 2004; Butler *et al.* 2006), including the rheological properties of the crust (e.g. Harry *et al.* 1995), have played a central role in the evolution of the western Pyrenean Orogen. The part played by inherited fault systems is intuitive as the systems were almost entirely reactivated, forcing the Alpine compressional trends

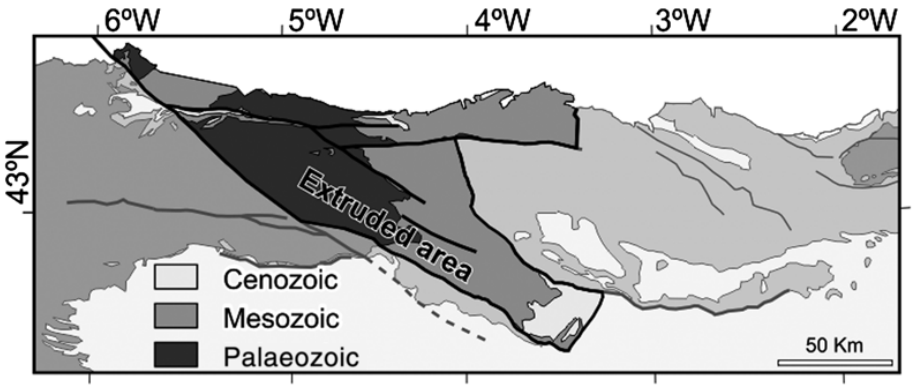

Fig. 15. Schematic geological map of the western Pyrenean Orogen, highlighting the extruded area.

onto the inherited systems. The presence of an efficient décollement level (i.e. Triassic evaporites) led to the development of the large-displacement south-directed Sierra de Cantabria Thrust. The Triassic evaporites favoured the southwards migration of the compressive front with respect to the surrounding areas where such a décollement level was absent. This behaviour is well known, and is widely recognized in the field and in analogue models (e.g. Davis & Engelder 1985; Bahroudi & Koyi 2003; Luján *et al.* 2003). The lack of this detachment level in the western portion of the study area also implied the along-strike transition to a thick-skinned style of deformation. A third aspect of structural inheritances is the transition from dip-slip to transpressional kinematics, which occurs along the boundary from the Mesozoic basin to the continental margin. Given that the orientation of inherited structures is fairly similar in the two domains and given that these are located in the same across-belt sector, it may be concluded that the transition from dip-slip to transpressional kinematics was also influenced by other factors. The Basque Pyrenees at the onset of contractive deformation was characterized by an Upper Jurassic–Cretaceous sedimentary package, Permo-Triassic sediments with a favourable detachment level (the Keuper facies) and by a thinned crust. In contrast, the Cantabrian Mountains domain was characterized by an older crust that was relatively unaffected by the Early Cretaceous extension, and by a lack of favourable detachment levels. These distributions result in different vertical strength profiles in these two sectors. This was probably a first-order factor controlling the structural style of deformation. The low-viscosity salt horizon of the Basque–Cantabrian multilayer was reactivated earlier leading to the development of a thin-skinned fold and thrust belt. This gave rise to the scraping of the post-evaporitic sequence and the coeval subduction of the underlying basement (at least in the frontal portion of the belt), which is a commonly observed scenario in the presence of weak décollement layers (e.g. Boyer & Elliot 1982; McClay 1992). Contextually, higher stress was required in the Cantabrian Mountains for fault reactivation as the faulted rock volume included the entire brittle crust. This area behaved as a sort of backstop, where deformation was mostly accomplished by strike-slip conjugated fault systems. The presence of east–west- to NW–SE-striking inherited elements forced the strike-slip system towards one of the expected conjugated array in a north–south-orientated shortening. The result is a fairly common behaviour, observed in many orogens worldwide, with continental lateral extrusion of lithospheric domains located beyond the contractive belts (e.g. Tapponnier *et al.* 1982; Ratschbacher *et al.* 1989, 1991; Lacombe *et al.* 2001; Sperner *et al.* 2002). In the study area, such a framework was characterized by smaller dimensions and, especially, by the extruded block that moved towards the central part of the belt rather than outwards (Fig. 15). Similar structures accommodating intrabelt shortening are less common and include, for example, the Olevano–Antrodoco Fault System of the Italian Apennines (Tavani & Cifelli 2010). This north–south-striking and westward-dipping Mesozoic extensional fault was reactivated during the NE–SW-orientated Cenozoic contraction, which determined the overthrusting of the Mesozoic Umbro–Marchean pelagic domain onto the Latium–Abruzzi carbonate platform domain. The overthrusting developed a complex transpressive pattern, including the rotation and reactivation of early orogenic thin-skinned thrusts (Tavani & Cifelli 2010). Similarly, the inward lateral extrusion documented in this work developed because of the existence of inherited Mesozoic faults. The western boundary of the Basque Pyrenees and, therefore, the boundary of Triassic evaporites and thinned continental crust mark the transition from dip-slip to strike-slip styles. In this regard, this boundary represents the limit of the extruded block. The presence of east–west-shortening related structures in this area is the result of the inwards lateral extrusion. This was accommodated by meso- and macroscale structures (including the Pas Thrust and associated anticline, and Las Rojas structures), which prevented the eastwards displacement of the east–west-orientated compression.

Conclusions

In conclusion, the western portion of the Pyrenean Orogen can be divided into two distinct domains: (1) an eastern domain that includes the Basque Pyrenees together with the Pyrenees *sensu stricto* and which is characterized by thin-skinned structures detached above a favourable décollement level (Triassic evaporites) with the development of a highly displaced and south-directed thrust; and (2) a western domain that is constituted by the western Pyrenean Orogen and which is characterized by deeply-rooted thick-skinned structures with the development of transpressive faults.

The distribution of Triassic evaporites, which is related to the Permo-Triassic rifting palaeogeographical context and to their subsequent migration, played a major role during the Cenozoic compression, controlling the development of thin-skinned v. thick-skinned structures.

During the contractional Alpine deformation, the right-lateral movement of the western domain towards the east along inherited west–east- to

NW–SE-striking elements produced the southeastwards extrusion of part of the Cantabrian area.

The transitional area between dip-slip and strike-slip, and thin-skinned and thick-skinned tectonics, and the area accommodating the lateral extrusion coincides with the western limit of the Triassic evaporites and also with the southern prolongation of the north–south-trending Santander Mesozoic Transfer Zone.

This work was carried within the framework of CIUDEN (FBG305657) and INTECTOSAL (CGL2010-21968-C02-01/BTE) projects and the 'Grup de Recerca de Geodinàmica i Anàlisi de Conques' (2009SGR-1198). Research by E. Carola is funded by a predoctoral grant from CIUDEN. We are grateful to IGME (Instituto Geológico y Minero de España) for providing seismic sections. We are indebted to Seismic Micro-Technology and Midland Valley, which generously provided Kingdom Suite and Move software. We should also like to express our gratitude to E. Tesón, F. Roure, A. Mora and G. von Knorring, who helped to improve the manuscript.

References

Alonso, J. L., Pulgar, F. J., García-Ramos, J. C. & Barba, P. 1996. Tertiary basins and alpine tectonics in the Cantabrian Mountains. *In*: Friend, P. F. & Dabrio, C. J. (eds) *Tertiary Basins of Spain: The Stratigraphic Record of Crustal Kinematics*, Cambridge University Press, Cambridge, 214–227.

Alonso, J. L., Marcos, A. & Suárez, A. 2009. Paleogeographic inversion resulting from large out of sequence breaching thrusts: the León Fault (Cantabrian Zone, NW Iberia). A new picture of the external Variscan Thrust Belt in the Ibero-Armorican Arc. *Geologica Acta*, **7**, 451–473.

Álvarez-Marrón, J. A., Pérez-Estaún, J. J. *et al.* 1996. Seismic structure of the northern continental margin of Spain from ESCIN deep seismic profiles. *Tectonophysics*, **264**, 153–174.

Amilibia, A., McClay, K. R., Sàbat, F., Muñoz, J. A. & Roca, E. 2005. Analogue modelling of inverted oblique rift systems. *Geologica Acta*, **3**, 251–271.

Amilibia, A., Sàbat, F., McClay, K. R., Muñoz, J. A., Roca, E. & Chong, G. 2008. The role of inherited tectono-sedimentary architecture in the development of the central Andean mountain belt: Insights from the Cordillera de Domeyko. *Journal of Structural Geology*, **30**, 1520–1539.

Arthaud, F. & Matte, P. 1977. Late Paleozoic strike-slip faulting in southern Europe and northern Africa: result of a right-lateral shear zone between the Appalachians and the Urals. *Bulletin Geological Society of America*, **88**, 1305–1320.

Aurell, M., Robles, S., Bádenas, B., Rosales, I., Quesada, S., Meléndez, G. & García-Ramos, J. C. 2003. Transgressive-regressive cycles and Jurassic paleogeography of northeast Iberia. *Sedimentary Geology*, **162**, 239–271, http://dx.doi.org/10.1016/S0037-0738(03)00154-4

Bahroudi, A. & Koyi, H. A. 2003. Effect of spatial distribution of Hormuz salt on deformation style in the Zagros fold and thrust belt: an analogue modelling approach. *Journal of the Geological Society*, **160**, 719–733, 10.1144/0016-764902-135.

Barrón, E., Gómez, J. J., Goy, A. & Pieren, A. P. 2006. The Triassic–Jurassic boundary in Asturias (northern Spain): palynological characterisation and facies. *Review of Paleobotany and Palynology*, **138**, 187–208.

Beaumont, C., Muñoz, J. A., Hamilton, J. & Fullsack, P. 2000. Factors controlling the Alpine Evolution of the Central Pyrenees inferred from a comparison of observations and geodynamical models. *Journal of Geophysical Research*, **105**, 8121–8145, http://dx.doi.org/10.1029/1999JB900390

Boillot, G. & Malod, J. 1988. The north and NW Spanish continental margin: a review. *Revista Sociedad Geológica de España*, **1**, 295–316.

Bois, C., Pinet, B. & Gariel, O. 1997. The sedimentary cover along the ECORS Bay of Biscay deep seismic reflection profile. A comparison between the Parentis basin and other European rifts and basins. *Mémoires de la Societé Géologique de France*, **171**, 143–165.

Boyer, S. E. & Elliot, D. 1982. Thrust systems. *AAPG Bulletin*. **66**, 1196–1230.

Buchanan, J. G. & Buchanan, P. G. (eds) 1995. *Basin Inversion*. Geological Society, London, Special Publications, **88**.

Butler, R. W. H., Tavarnelli, E. & Grasso, M. 2006. Structural inheritance in mountain belts: an Alpine–Apennine perspective. *Journal of Structural Geology*, **28**, 1893–1908, http://dx.doi.org/10.1016/j.jsg.2006.09.006

Cámara, P. 1997. The Basque–Cantabrian basin's Mesozoic tectono-sedimentary evolution. *Mémoires de la Societé Géologique de France*, **171**, 187–191.

Castañares, L. M. & Robles, S. 2004. El vulcanismo del Albiense–Santoniense en la Cuenca Vasco-Cantábrica. *In*: Vera, J. A. (ed.) *Geología de España*. SGE-IGME, Madrid, 306–308.

Choukroune, P. 1992. Tectonic evolution of the Pyrenees. *Annual Review of Earth and Planetary Sciences*, **20**, 143–158.

Choukroune, P. & ECORS Team 1989. The ECORS Pyrenean deep seismic profile reflection data and the overall structure of an orogenic belt. *Tectonics*, **8**, 23–39, http://dx.doi.org/10.1029/TC008i001p00023

Choukroune, P., Roure, F., Pinet, B. & ECORS Pyrenees Team 1990. Main results of the ECORS Pyrenees profile. *Tectonophysics*, **173**, 411–423.

Cooper, M. A. & Williams, G. D. (eds) 1989. *Inversion Tectonics*. Geological Society, London, Special Publications, **44**.

Corretgé, L. G. & Suárez, O. 1991. Igneous rocks of the Cantabrian/Palentian Zone. *In*: Dallmeyer, R. D. & Martínez-García, E. (eds) *Pre-Mesozoic Geology of Iberia*. Springer, Berlin, 72–79.

Coward, M. P. 1994. Inversion tectonics. *In*: Hancock, P. L. (ed.) *Continental Deformation*. Pergamon, Oxford, 289–304.

Cuevas, J., Aranguren, A., Badillo, J. M. & Tubía, J. M. 1999. Estudio estructural del sector central del

Arco Vasco (Cuenca Vasco-Cantábrica). *Boletín Geológico y Minero España*, **110**, 3–18.

DAHLEN, F. A. 1984. Noncohesive critical Coulomb wedges: an exact solution. *Journal of Geophysical Research*, **89**, 10125–10133.

DALLMEYER, R. D. & MARTÍNEZ-GARCÍA, E. 1990. *Pre-Mesozoic Geology of Iberia*. Springer, Berlin.

DALLMEYER, R. D., MARTÍNEZ CATALÁN, J. R. *ET AL.* 1997. Diachronous Variscan tectonothermal activity in the NW Iberian Massif: evidence from $^{40}Ar/^{39}Ar$ dating of regional fabrics. *Tectonophysics*, **227**, 307–337, http://dx.doi.org/10.1016/S0040-1951(97)00035-8

DAVIS, D. M. & ENGELDER, T. 1985. The role of salt in fold-and-thrust belts. *Tectonophysics*, **119**, 67–88.

DAVIS, F. A., SUPPE, J. & DAHLEN, D. 1983. Mechanics of fold-and-thrust belts and accretionary wedges. *Journal of Geophysical Research*, **88**, 1153–1172.

DE SITTER, L. U. 1962. The structure of the southern slope of the Cantabrian Mountains. *Leidse Geologische Mededelingen*, **26**, 255–264.

DEWEY, J. F. & BIRD, J. M. 1970. Mountain belts and the new global tectonics. *Journal of Geophysical Research*, **75**, 2625–2647, http://dx.doi.org/10.1029/JB075i014p02625

ESPINA, R. G. 1997. *La estructura y evolución tectonoestratigráfica del borde occidental de la Cuenca Vasco-Cantábrica (Cordillera Cantábrica, NO de España)*. PhD thesis, University of Oviedo.

ESPINA, R. G., ALONSO, J. L. & PULGAR, J. A. 1996*a*. Growth and propagation of buckle folds determined from syntectonic sediments (the Ubierna Fold Belt, Cantabrian Mountains, N Spain). *Journal of Structural Geology*, **18**, 431–441, http://dx.doi.org/10.1016/0191-8141(95)00103-K

ESPINA, R. G., DE VICENTE, G. & MUÑOZ MARTÍN, A. 1996*b*. Análisi poblacional de fallas alpinas en el borde occidenteal de la Cuenca Vasco-Cantábrica (Cordillera Cantábrica, NO de España). *Geogaceta*, **20**, 936–938.

ESPINA, R. G., ALONSO, J. L. & PULGAR, J. A. 2004. Extensión Triásica en la Cuenca Vasco-Cantábrica. *In*: VERA, J. A. (ed.) *Geología de España*. SGE-IGME, Madrid, 338–339.

FERRER, O., ROCA, E., BENJUMEA, B., ELLOUZ, N., MUÑOZ, J. A. & MARCONI TEAM 2005. The north Pyrenean front and related foreland basin along the Bay of Biscay: Constraints from the Marconi deep seismic reflection survey. *Thrust belts and Foreland Basins, International Meeting*, 161–164.

FERRER, O., ROCA, E., BENJUMEA, B., MUÑOZ, J. A., ELLOUZ, N. & MARCONI TEAM 2008. The deep seismic reflection MARCONI-3 profile: role of extensional Mesozoic structure during the Pyrenean contractional deformation at the eastern part of the Bay of Biscay. *Marine and Petroleum Geology*, **25**, 714–730, http://dx.doi.org/10.1016/j.marpetgeo.2008.06.002

FLOQUET, M. 2004. El Cretácico Superior de la Cuenca Vasco-Cantábrica y áreas adyacentes. *In*: VERA, J. A. (ed.) *Geología de España*. SGE-IGME, Madrid, 299–306.

GALLASTEGUI, J. 2000. Estructura cortical de la Cordillera y Margen Continental Cantábricos: perfiles ESCI-N. *Trabajos Geología*, **22**, 9–234.

GALLASTEGUI, J., PULGAR, J. A. & GALLART, J. 2002. Initiation of an active margin at the North Iberian continent-ocean transition. *Tectonics*, **21**, http://dx.doi.org/10.1029/2001TC901046

GARCÍA DE CORTÁZAR, A. & PUJALTE, V. 1982. Litoestratigrafía y facies del grupo Cabuérniga (Malm-Valanginiense Inferior?) al S deCantabria–NE de Palencia. *Cuadernos Geología Ibérica*, **8**, 5–21.

GARCÍA-MONDÉJAR, J. 1987. Aptian-Albian carbonate episode of Basque-Cantabrian Basin, northern Spain. *AAPG Bulletin*, **71**, 558.

GARCÍA-MONDÉJAR, J., PUJALTE, V. & ROBLES, S. 1986. Características sedimentológicas, secuenciales y tectoestratigráficas del Triásico de Cantabria y Norte de Palencia. *Cuadernos de Geología Ibérica*, **10**, 151–172.

GARCÍA-MONDÉJAR, J., FERNÁNDEZ-MENDIOLA, P. A., AGIRREZABALA, L. M., ARAMBURU, A., LÓPEZ-HORGUE, M. A., IRIARTE, E. & MARTÍNEZ DE RITUERTO, S. 2004. El Aptiense–Albiense de la Cuenca Vasco-Cantábrica. *In*: VERA, J. A. (ed.) *Geología de España*. SGE-IGME, Madrid, 291–296.

GARCÍA-RAMOS, J. C. & GUTIÉRREZ-CLAVEROL, M. 1995. La cobertera Mesozoico-Terciaria. *In*: ARAMUBURY Y, C. & BASTIDA, F. (eds) *Geología de Asturias*. Trea, Gijón, 81–94.

GARCÍA-RAMOS, J. C., COLMENERO, J. R., VARGAS, I., MANJÓN, M., CRESPO, A. & MATAS, J. 1982. *Mapa geológico 1:50 000, Hoja 132 (Guardo)*. IGME, Madrid.

GÓMEZ, M., VERGÉS, J. & RIAZA, C. 2002. Inversion tectonics of the northern margin of the Basque Cantabrian Basin. *Bulletin de la Société Géologique de France*, **173**, 449–459.

GUTIÉRREZ-ALONSO, G., FERNÁNDEZ-SUÁREZ, J., WEIL, A. B., MURPHY, J. B., NANCE, R. D., CORFÚ, F. & JOHNSTON, S. T. 2008. Self-subduction of the Pangaean global plate. *Nature Geoscience*, **1**, 549–553, http://dx.doi.org/10.1038/ngeo250

GUTIÉRREZ-CLAVEROL, M. & TORRES ALONSO, M. 1995. *Geología de Oviedo. Descripción, recursos y aplicaciones*. Paraíso, Ayuntamiento de Oviedo.

HARDING, T. P. 1985. Seismic characteristics and identification of negative flower structures, positive flower structures and positive structural inversion. *AAPG Bulletin*, **69**, 582–600.

HARRY, D. L., OLDOW, J. S. & SAWYER, D. S. 1995. The growth of orogenic belts and the role of crustal heterogeneities in decollement tectonics. *Geological Society of American Bulletin*, **107**, 1411–1426, http://dx.doi.org/10.1130/0016-7606(1995)107

HEREDIA, N. 1998. Los Cabalgamientos del sector suroriental de las unidades del Ponga y de la Cuenca Carbonífera Central (Zona Cantábrica, NO de España). *Trabajos de Geología*, **20**, 53–127.

HEREDIA, N., ALONSO, J. L. & RODRÍGUES FERNÁNDEZ, L. R. 1990. *Mapa geológico 1:50 000, Hoja 105 (Riaño)*. IGME, Madrid.

HERNAIZ, P. P. 1994. La falla de Ubierna (margen SO de la cuenca Cantábrica). *Geogaceta*, **16**, 39–42.

HERNAIZ, P. P. & SOLÉ, J. 2000. Las estructuras del diapiro de Salinas del Rosío y del alto de San Pedro–Iglesias y sus implicaciones en la evolución tectónica de la transversal burgalesa de la Cordillera

Vascocantábrica–Cuenca del Duero. *Revista de la Sociedad Geológica de España*, **13**, 471–486.

Hernaiz, P. P., Serrano, A., Malagón, J. & Rodríguez Cañas, C. 1994. Evolución estructural del margen SO de la cuenca Vasco Cantábrica. *Geogaceta*, **15**, 143–146.

Holdsworth, R. E. 2004. Weak faults, rotten cores. *Science*, **303**, 181–182, http://dx.doi.org/10.1126/science.1092491

Jammes, S., Manatschal, G., Lavier, L. & Masini, E. 2009. Tectonosedimentary evolution related to extreme crustal thinning ahead of a propagating ocean: the example of the western Pyrenees. *Tectonics*, **28**, TC4012, http://dx.doi.org/10.1029/2008TC002406

Julivert, M., Ramírez del Pozo, J. & Truyols, J. 1971. Le réseau de failles et la couverture post-hercynienne dans les Asturies. *In*: *Historie Structurale du Golfe de Gascogne, Tome 2*. Technip, París.

Lacombe, O., Mouthereau, F., Angelier, J. & Deffontaines, B. 2001. Structural, geodetic and seismological evidence for tectonic escape in SW Taiwan. *Tectonophysics*, **333**, 323–345.

Lamplugh, G. W. 1920. Structure of the Weald and analogous tracts. *Quarterly Journal of the Geological Society*, **15**, LXXIII–XCV.

Lanaja, J. M. 1987. *Contribución de la exploración petrolífera al conocimiento de la Geología de España*. IGME, Madrid,

Larrasoaña, J. C., Parés, J. M., Millán, H., del Valle, J. & Pueyo, E. L. 2003. Paleomagnetic, structural, and stratigraphic constraints on transverse fault kinematics during basin inversion: the Pamplona Fault (Pyrenees, north Spain). *Tectonics*, **22**, 1071–1092, http://dx.doi.org/10.1029/2002TC001446

Le Pichon, X. & Sibuet, J. C. 1971. Western extension of boundary between European and Iberian plates during the Pyrenean orogeny. *Earth and Planetary Science Letters*, **12**, 83–88, http://dx.doi.org/10.1016/0012-821X(71)90058-6

Lepvrier, C. & Martínez-García, E. 1990. Fault development and stress evolution of the post-Hercynian Asturian Basin (Asturias and Cantabria, northwestern Spain). *Tectonophysics*, **184**, 345–356, http://dx.doi.org/10.1016/0040-1951(90)90447-G

López-Fernández, C., Pulgar, J. A., González-Cortina, J. M., Gallart, J., Díaz, J. & Ruiz, M. 2004. Actividad sísmica en el Noroeste del a Península Ibérica observada por la red sísmica local del Proyecto GASPI (1999–2002). *Trabajos de Geología*, **24**, 91–106.

Luján, M., Storti, F., Balanyá, J. C., Crespo-Blanc, A. & Rossetti, F. 2003. Role of décollement material with different rheological properties in the structure of the Aljibe thrust imbricate (Flysch Trough, Gibraltar Arc): an analogue modelling approach. *Journal of Structural Geology*, **25**, 867–881, http://dx.doi.org/10.1016/S0191-8141(02)00087-1

Malagón, J., Hernaiz, P. P., Rodríguez Cañas, C. & Serrano, A. 1994. Notas sobre la inversión tectónica y aloctonia de la cuenca Vasco-Cantábrica. *Geogaceta* **15**, 139–142.

Marshak, S. 2004. Salients, recesses, arcs, oroclines, and syntaxesda review of ideas concerning the formation of map-view curves in fold-thrust belts. *In*: McClay, K. R. (ed.) *Thrust Tectonics and Hydrocarbon Systems*. AAPG, Memoirs, **82**, 131–156.

Martín-González, F. & Heredia, N. 2011*a*. Complex tectonic and tectonostratigraphic evolution of an Alpine foreland basin: the western Duero Basin and the related Tertiary depressions of the NW Iberian Peninsula. *Tectonophysics*, **502**, 75–89, http://dx.doi.org/10.1016/j.tecto.2010.03.002

Martín-González, F. & Heredia, N. 2011*b*. Geometry, structures and evolution of the western termination of the Alpine-Pyrenean Orogen reliefs (NW Iberian Peninsula). *Journal of Iberian Geology*, **37**, 103–120, http://dx.doi.org/10.5209/rev_JIGE.2011.v37.n2.1

Martínez-Torres, L. M. 1993. Corte balanceado de la Sierra Cantabria (cabalgamiento de la Cuenca Vasco-Cantábrica sobre la Cuenca del Ebro). *Geogaceta*, **14**, 113–115.

Mathieu, C. 1986. Histoire géologique du sous-basin de Parentis. *Bulletin des Centres de Recherches Elf-Aquitaine (Production)*, **10**, 33–47.

Maurin, J.-C. & Niviere, B. 2000. Extensional forced folding and décollement of the pre-rift series along the Rhine graben and their influence on the geometry of the syn-rift sequences. *In*: Cosgrove, J. W. & Ameen, M. S. (eds) *Forced Folds and Fractures*. Geological Society, London, Special Publications, **169**, 73–86.

McClay, K. R. 1992. Glossary of thrust tectonics terms. *In*: McClay, K. R. (ed.) *Thrust Tectonics*. Chapman & Hall, London, 419–433.

McClay, K. R. 1995. The geometries and kinematics of inverted fault systems: a review of analogue model studies. *In*: Buchanan, J. G. & Buchanan, P. G. (eds) *Basin Inversion*. Geological Society, London, Special Publications, **88**, 97–119.

Menéndez-Casares, E., González-Fernéndez, B., Gutiérrez-Claverol, M. & García-Ramos, J. C. 2004. Precisiones sobre los acuíferos de la cuenca jurásica asturiana (NO de España). *Trabajos de Geología*, **24**, 119–126.

Mouthereau, F., Tensi, J., Bellahsen, N., Lacombe, O., Boisgrollier, T. & Kargar, S. 2007. Tertiary sequence of deformation in a thin- skinned/thick-skinned collision belt: the Zagros Folded Belt (Fars, Iran). *Tectonics*, **26**, TC5006, http://dx.doi.org/10.1029/2007TC002098

Muñoz, J. A. 1992. Evolution of a continental collision belt: ECORS–Pyrenees crustal balanced section. *In*: McClay, K. R. (ed.) *Thrust Tectonics*. Chapman & Hall, London, 235–246.

Muñoz, J. A. 2002. The Pyrenees. *In*: Gibbons, W. & Moreno, T. (eds) *The Geology of Spain*. Geological Society, London, 370–385.

Nielsen, S. B. & Hansen, D. L. 2000. Physical explanation of the formation and evolution of inversion zones and marginal troughs. *Geology*, **28**, 875–878.

Pedreira, D., Pulgar, J. A., Gallart, J. & Díaz, J. 2003. Seismic evidence of Alpine crustal thickening and wedging from the western Pyrenees to the Cantabrian Mountains (north Iberia). *Journal of Geophysical Research*, **108**, 2204, http://dx.doi.org/10.1029/2001JB001667

Pedreira, D., Pulgar, J. A., Gallart, J. & Torné, M. 2007. Three-dimensional gravity and magnetic

modeling of crustal indentation and wedging in the western Pyrenees–Cantabrian Mountains. *Journal of Geophysical Research*, **112**, B12405, http://dx.doi.org/10.1029/2007JB005021

Pérez-Estaún, A., Martínez-Catalán, J. R. & Bastida, F. 1991. Crustal thickening and deformation sequence in the footwall to the suture of the Variscan belt of NW Spain. *Tectonophysics*, **191**, 243–253, http://dx.doi.org/10.1016/0040-1951(91)90060-6

Pérez-Estaún, A., Bastida, F. *et al.* 1988. A thin-skinned tectonics model for an arcuate fold and thrust belt: the Cantabrian Zone (Variscan Ibero-Armorican Arc). *Tectonics*, **7**, 517–537, http://dx.doi.org/10.1029/TC007i003p00517

Pfiffner, O. A. 2006. Thick-skined and thin-skined styles of continental contraction. *In*: Mazzoli, S. & Butler, R. W. H. (eds) *Styles of Continental Contraction*. Geological Society of America Special Paper, **414**, 153–177. doi: 10.1130/2006.2414(09)

Portero, J. M., Ramírez del Pozo, J. & Aguilar, M. 1979. *Mapa geológico 1:50 000, Hoja 170 (Haro)*. IGME, Madrid.

Pujalte, V. 1979. Control tectónico de la sedimentación 'purbeck-weald' en las provincias de Santander y N. de Burgos. *Acta Geològica Hispànica*, **14**, 216–222.

Pujalte, V. 1982. La evolución paleogeográfica de la cuenca 'Wealdense' de Cantabria. *Cuadernos de Geología Ibérica*, **8**, 65–83.

Pujalte, V., Robles, S. & Hernández, J. Mª. 1996. La sedimentación continental del Grupo Campóo (Malm-Cretácico basal de Cantabria, Burgos y Palencia): testimonio de un reajuste hidrográfico al inicio de una fase rift. *Cuademos de Geologia Ibérica*, **21**, 227–251.

Pujalte, V., Robles, S., García-Ramos, J. C. & Hernández, J. M. 2004. El Malm-Barremiense no marinos de la Cordillera Cantábrica. *In*: Vera, J. A. (ed.) *Geología de España*. SGE-IGME, Madrid, 288–291.

Pulgar, J. A., Gallart, J., Fernández-Viejo, G., Pérez-Estaún, A. & Álvarez-Marrón, J. 1996. Seismic image of the Cantabrian Mountains in the western extension of the Pyrenees from integrated ESCIN reflection and refraction data. *Tectonophysics*, **264**, 1–19.

Pulgar, J. A., Alonso, J. L., Espina, R. G. & Marín, J. A. 1999. La deformación alpina en el basamento varisco de la Zona Cantábrica. *Trabajos de Geolología*, **21**, 283–294.

Quesada, S., Robles, S. & Pujalte, V. 1993. El Jurásico Marino del margen suroccidental de la Cuenca Vasco-Cantábrica y su relación con la exploración de hidrocarburos. *Geogaceta*, **13**, 92–96.

Quintana, L., Alonso, J. L., Pulgar, J. A. & Rodríguez-Fernández, L. R. 2006. Transpressional inversion in an extensional transfer zone (the Saltacaballos fault, northern Spain). *Journal of Structural Geology*, **28**, 2038–2048.

Ranalli, G. 2000. Rheology of the crust and its role in tectonic reactivation. *Journal Geodynamics*, **30**, 3–15, http://dx.doi.org/10.1016/S0264-3707(99)00024-1

Rat, P. 1988. The Basque–Cantabrian basin between the Iberian and European plates; some facts but still many problems. *Revista de la Sociedad Geologica de España*, **1**, 327–348.

Ratschbacher, L., Frisch, W., Neubauer, F., Schmid, S. M. & Neugebauer, J. 1989. Extension in compressional orogenic belts: the eastern Alps. *Geology*, **17**, 404–407.

Ratschbacher, L., Frisch, W., Linzer, H. G. & Merle, O. 1991. Lateral extrusion in the Eastern Alps, Part 2. Structural analysis. *Tectonics*, **10**, 257–271.

Roca, E., Muñoz, J. A., Ferrer, O. & Ellouz, N. 2011. The role of the Bay of Biscay Mesozoic extensional structure in the configuration of the Pyrenean orogen: constraints from the MARCONI deep seismic reflection survey. *Tectonics*, **30**, TC2001, http://dx.doi.org/10.1029/2010TC002735

Rodríguez Cañas, C., Hernaiz, P. P., Malagón, J. & Serrano, A. 1994. Notas sobre la estructura cabalgante de Rojas-Santa Casilda. *Geogaceta*, **15**, 135–138.

Roure, F., Choukroune, P. *et al.* 1989. Ecors deep seismic data and balanced cross sections: geometric constraints on the evolution of the Pyrenees. *Tectonics*, **8**, 41–50, http://dx.doi.org/10.1029/TC008i001p00041.

Ruiz, M. 2007. *Caracterització estructural i sismotectònica de la litosfera en el Domini Pirenaico-Cantàbric a partir de mètodes de sísmica activa i passiva*. PhD thesis, University Barcelona, Barcelona.

Sandiford, M. 1999. Mechanics of basin inversion. *Tectonophysics*, **305**, 109–120.

Serrano, A., Hernaiz, P. P., Magalón, J. & Rodríguez-Cañas, C. 1994. Tectónica distensiva y halocinesis en el margen SO de la cuenca Vasco-Cantábrica. *Geogaceta*, **15**, 131–134.

Sibson, R. H. 1985. A note on fault reactivation. *Journal of Structural Geology*, **7**, 751–754.

Sibson, R. H. 1995. Selective fault reactivation during basin inversion: potential for fluid redistribution through fault-valve action. *In*: Buchanan, J. G. & Buchanan, P. G. (eds) *Basin Inversion*. Geological Society, London, Special Publications, **88**, 3–19.

Sperner, B., Ratschbacher, L. & Nemcok, M. 2002. Interplay between subduction retreat and lateral extrusion: tectonics of the Western Carpathians. *Tectonics*, **21**, 1051, http://dx.doi.org/10.1029/2001TC901028

Storti, F., Soto-Marin, R., Rossetti, F. & Casas-Sainz, A. 2007. Evolution of experimental thrust wedges accreted from along-strike tapered, silicone-floored multilayers. *Journal of the Geological Society*, **164**, 73–85.

Tapponnier, P., Peltzer, G., Le Dain, A. Y., Armijo, R. & Cobbold, P. 1982. Propagating extrusion tectonics in Asia: new insights from simple experiments with Plasticine. *Geology*, **10**, 611–616.

Tavani, S. & Cifelli, F. 2010. Deformation pattern analysis and tectonic implications of a décollement level within the Central Apennines (Italy). *Geological Journal*, **45**, 582–596, http://dx.doi.org/10.1002/gj.1198

Tavani, S. & Muñoz, J. A. 2012. Mesozoic rifting in the Basque-Cantabrian Basin (Spain): inherited faults,

transversal structures and stress perturbation. *Terranova*, **24**, 70–76. http://dx.doi.org/10.1111/j.1365-3121.2011.01040.x

TAVANI, S., MENCOS, J., BAUSÀ, J. & MUÑOZ, J. A. 2011*a*. The fracture pattern of the Sant Corneli-Bóixols oblique inversion anticline (Spanish Pyrenees). *Journal of Structural Geology*, **33**, 1662–1680, http://dx.doi.org/10.1016/j.jsg.2011.08.007.

TAVANI, S., QUINTÀ, A. & GRANADO, P. 2011*b*. Cenozoic right-lateral wrench tectonics in the Western Pyrenees (Spain): the Ubierna Fault System. *Tectonophysics*, **509**, 238–253, http://dx.doi.org/10.1016/j.tecto.2011.06.013

TEIXELL, A. 1998. Crustal structure and orogenic material budget in the west central Pyrenees. *Tectonics*, **17**, 395–406.

THINON, I., MATIAS, L., RÉHAULT, J. P., HIRN, A., FIDALGO-GONZÁLEZ, L. & AVEDIK, F. 2003. Deep structure of the Armorican Basin (Bay of Biscay): a review of Norgasis seismic reflection and refraction data. *Journal Geological Society of London*, **160**, 99–116.

TURNER, J. P. & WILLIAMS, G. A. 2004. Sedimentary basin inversion and intra-plate shortening. *Earth Science Reviews*, **65**, 277–304.

VAN WEES, J. D. & BEEKMAN, F. 2000. Lithosphere rheology during intraplate basin extension and inversion: inferences from automated modelling of four basins on western Europe. *Tectonophysics*, **320**, 219–242.

VERGÉS, J. & GARCÍA-SENZ, J. 2001. Mesozoic evolution and Cainozoic inversion of the Pyrenean Rift. *In*: ZIEGLER, P. A., CAVAZZA, W., ROBERTSON, A. H. F. & CRASQUIN-SOLEAU, S. (eds) *Peri-Tethys Memoir 6: Peri-Tethyan Rift/Wrench Basins and Passive Margins*. Mémoires du Muséum National d'Histoire Naturelle, Paris, **186**, 187–212.

WILLIAMS, G. A., TURNER, J. P. & HOLFORD, S. P. 2005. Inversion and exhumation of the St. George's Channel basin, offshore Wales, UK. *Journal Geological Society of London*, **162**, 97–110.

ZIEGLER, P. A. (ed.) 1987. Compressional intra-plate deformation in the Alpine Foreland. *Tectonophysics*, **137**, 420.

Chapter 2

The Mesozoic rifting stage in the Burgalesa Platform. The development of forced folding, salt migration and the subsequent inversion

This chapter contains the second scientific paper that constitutes this thesis, in it we describe the decoupling effect of the Upper Triassic salts during the Early Cretaceous extension and as a consequence, the development of extensional forced folds and associated syn-rift growth geometries onlapping the pre-rift succession. The present article has been published in the Tectonics journal volume 32 and it is cited as follows:

Tavani, S., Carola, E., Granado, P., Quintà, A., Muñoz, J.A. 2013. Transpressive inversion of a Mesozoic extensional forced fold system with an intermediate décollement level in the Basque-Cantabrian Basin (Spain). ***Tectonics 32 DOI:10.1002/tect.20019.***

Resum

El segon article presentat en aquesta Tesi tracte sobre el període extensiu que va tenir lloc durant el Mesozoic així com també sobre les geometries sedimentaries que presenta la successió sin-extensiva. A més a més, com aquestes geometries varen ésser preservades durant la inversió de les falles que va tenir lloc durant el Cenozoic.

A la conca Basco-Cantàbrica (Espanya), el desenvolupament de falles normals i els plecs associats va tenir lloc durant l'extensió Juràssic terminal - Cretaci Inferior. La deformació de pell gruixuda produïda durant la inversió transpresiva associada al Cenozoic, va preservar l'arquitectura extensiva en el sector oest de la conca. La integració de mapes geològics i perfils de sísmica permet restringir l'estil de deformació durant l'extensió i la subseqüent inversió al sector oest de la conca Basco-Cantàbrica.

Les falles extensives afecten des del basament Paleozoic fins a les roques pertanyents al Triàsic Inferior. La presència d'un nivell de desenganxament eficaç representat per les evaporites del Triàsic produeixen la desconnexió de la deformació entre les roques del basament i la seqüència de cobertora post-extensives definides per el Triàsic Superior fins al Juràssic Mig. Plecs forçats en extensió es van desenvolupar a la cobertora a causa de l'activitat de les falles afectant al basament i per la migració de les evaporites cap als blocs superiors de les falles extensives, produint-se soldadures de sal. Els sediments del Juràssic Superior - Cretaci Inferior es van dipositar sincrònicament al desenvolupament dels plecs forçats produint geometries de creixement extensives associades tant a les falles principals com a les falles transversals del sistema.

Les seqüències de creixement sin-extensives estan caracteritzades per les relacions de *downlap* i *onlap* amb la successió pre-extensiva situada immediatament per sota. Aquestes geometries han estat interpretades com al resultat de la variació entre la quantitat de desplaçament extensional allarg de les falles principals del sistema. La compressió durant el Cenozoic va produir la inversió transpressiva dextrògira de les falles de basament i la reactivació a favor del cabussament de les falles extensives transversals.

Abstract

The second paper presented in this Thesis deals with the rifting stage that occurred during the Mesozoic and the sedimentary geometries that the syn-rift succession presents. In addition, how these geometries were preserved during the inversion of the faults that took place in Cenozoic times.

In the Basque-Cantabrian Basin (Spain), normal faulting and associated folding occurred during Late Jurassic to Early Cretaceous rifting. Cenozoic Pyrenean thick-skinned transpressive inversion in the western parts of the basin preserved the first-order extensional architecture. Integration of geological maps and seismic profiles has permitted to fully constrain the style of extensional deformation and subsequent inversion in the western portion of the Basque-Cantabrian Basin.

Extensional faults offset the Paleozoic basement up to Lower Triassic rocks. The presence of an efficient décollement level represented by Triassic evaporites produced the decoupling between basement rocks and the Upper Triassic to Middle Jurassic pre-rift cover sequence. Extensional forced folding occurred in the cover, driven by basement faulting and the migration of evaporites towards the hanging wall of the extensional faults, with salt welds developing away from them. Upper Jurassic to Lower Cretaceous syn-rift sediments deposited synchronously with forced folding, which led to the development of extensional growth geometries associated with both master faults and nearly-transverse faults.

Syn-rift growth sequences are characterized by downlap and onlap relationships with the underlying pre-rift units, interpreted as the result of along strike variations of master fault extensional displacement rate. Cenozoic Pyrenean contraction generated the right-lateral transpressive inversion of basement master faults and the almost dip-slip reactivation of transverse extensional faults.

TECTONICS, VOL. 32, 1–13, doi:10.1002/tect.20019, 2013

Transpressive inversion of a Mesozoic extensional forced fold system with an intermediate décollement level in the Basque-Cantabrian Basin (Spain)

Stefano Tavani,[1] Eloi Carola,[2,3] Pablo Granado,[2] Anna Quintà,[2] and Josep Anton Muñoz[2]

Received 3 September 2012; revised 14 December 2012; accepted 1 February 2013.

[1] In the Basque-Cantabrian Basin (Spain), normal faulting and associated folding occurred during Late Jurassic to Early Cretaceous rifting. Cenozoic Pyrenean thick-skinned transpressive inversion in the western parts of the basin preserved the first-order extensional architecture. Integration of geological maps and seismic profiles has permitted to fully constrain the style of extensional deformation and subsequent inversion in the western portion of the Basque-Cantabrian Basin. Extensional faults offset the Paleozoic basement up to Lower Triassic rocks. The presence of an efficient décollement level represented by Triassic evaporites produced the decoupling between basement rocks and the Upper Triassic to Middle Jurassic prerift cover sequence. Extensional forced folding occurred in the cover, driven by basement faulting and the migration of evaporites toward the hanging wall of the extensional faults, with salt welds developing away from them. Upper Jurassic to Lower Cretaceous syn-rift sediments deposited synchronously with forced folding, which led to the development of extensional growth geometries associated with both master faults and nearly-transverse faults. Syn-rift growth sequences are characterized by downlap and onlap relationships with the underlying prerift units, interpreted as the result of along-strike variations of master fault extensional displacement rate. Cenozoic Pyrenean contraction generated the right-lateral transpressive inversion of basement master faults and the almost dip-slip reactivation of transverse extensional faults.

Citation: Tavani, S., E. Carola, P. Granado, A. Quintà, and J. A. Muñoz (2013), Transpressive inversion of a Mesozoic extensional forced fold system with an intermediate décollement level in the Basque-Cantabrian Basin (Spain), *Tectonics*, *32*, doi:10.1002/tect.20019.

1. Introduction

[2] Extensional forced folds (Figure 1) represent a particular class of the wide range of fault-related folds that occur in extensional basins [e.g., *White et al*., 1986; *Dula*, 1991; *Schlische*, 1992; *Xiao and Suppe*, 1992; *Gawthorpe et al*., 1997; *Janecke et al*., 1998; *Sharp et al*., 2000; *Khalil and McClay*, 2002; *Jackson et al*., 2006; *Kane et al*., 2010 among others]. Extensional forced folds commonly form due to the decoupling effect of a ductile level, which divides a shallow folded multilayer from a deeper faulted basement [e.g., *Brown*, 1980; *Laubscher*, 1982; *Colleta et al*., 1988; *Withjack et al*., 1989; *Cosgrove and Ameen*, 1999; *Maurin and Niviere*, 1999; *Keller and Lynch*, 1999; *Richardson et al*., 2005]. Such a folding mechanism has been recently proposed for the Mesozoic Basque-Cantabrian Basin of Northern Spain (Figure 2a) [e.g., *Soto et al*., 2011; *Tavani et al*., 2011; *Tavani*, 2012], where Triassic evaporites would have represented the ductile level responsible for the decoupling between Paleozoic to Lower Triassic faulted rocks and prerift Upper Triassic to Middle Jurassic folded sediments. Cenozoic Pyrenean contractional stage largely modified the extensional architecture of the basin in its central and eastern portions, where the postevaporitic Mesozoic sequence has been detached above Triassic evaporites and has overridden the adjacent Cenozoic Ebro Foreland Basin for several kilometers [*Martínez-Torres*, 1993]. Early works have proposed a similar Cenozoic framework also for the western portion of the basin, with thin-skinned [e.g., *Malagón et al*., 1994], thick-skinned [e.g., *Alonso et al*., 1996], and mixed scenarios [e.g., *Hernaiz and Solé Pont*, 2000] resulting from the postulation of south-directed thrusting of the western portion of the Mesozoic Basque-Cantabrian Basin onto the Cenozoic Duero Foreland Basin. However, no surface or subsurface data exist confirming this assumption and, actually, both seismic lines across the Duero Basin [*Tavani et al*., 2011] and recently acquired mesostructural data [*Tavani et al*., 2011; *Quintà and Tavani*, 2012] indicate its inconsistency,

[1]Dipartimento di Scienze della Terra, dell'Ambiente e delle Risorse (DISTAR), Università Federico II, Napoli, Italy.
[2]Geomodels, Departament de Geodinàmica i Geofísica, Universitat de Barcelona, Barcelona, Spain.
[3]Fundación Ciudad de la Energía, CIUDEN, Ponferrada, Spain.

Corresponding author: S. Tavani, Dipartimento di Scienze della Terra, dell'Ambiente e delle Risorse, Università degli Studi di Napoli Federico II, Largo San Marcellino 10, 80138 Napoli, Italy. (stefano.tavani@unina.it)

0278-7407/13/10.1002/tect.20019

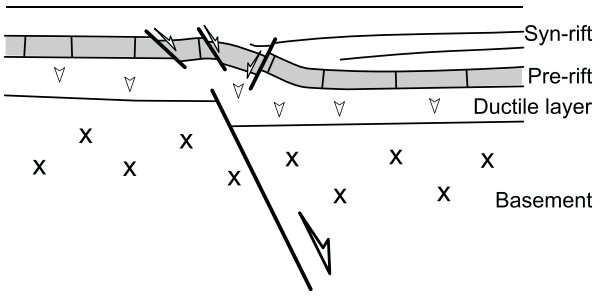

Figure 1. Scheme of an extensional forced fold.

supporting instead a strike-slip right-lateral scenario, and preventing the possibility of extrapolating in the study area those geometries observed in the Basque Pyrenees located to the east. As detailed in the recent review of *Tavani* [2012], the Cenozoic inversion stage in the south-western portion of the basin was characterized by thick-skinned right-lateral reactivation of the WNW-ESE striking Ubierna and Ventaniella crustal scale faults [*Tavani et al*., 2011]. Most of the deformation concentrated in the 100 km long and 15 km wide overstep area between these two faults (Figure 2b), with a right-lateral displacement exceeding 10 km in the central part of the system [*Tavani et al*., 2011], and largely preserved the Mesozoic extensional architecture of the basin in the surrounding areas. Mesozoic extensional geometry is well-recognizable in publicly available seismic profiles. In addition, a regional plunge striking almost parallel to the basement extensional structures developed in the area during the contractional stage of deformation, allowing for faulted Paleozoic rocks and folded Mesozoic sediments to be well exposed. This represents an interesting situation for the aim of this study, because well-preserved cross-sections of the extensional geometries are nicely imaged in map view (Figure 2b).

[3] This work has the twofold purpose of (1) describing the outstanding evidence of extensional forced folding in the Mesozoic Basque-Cantabrian Basin, including the existence of an intimate link between syn-growth geometries and along-strike variability of the fault slip rate, (2) illustrating how the extensional system has been inverted during Pyrenean orogeny.

2. Geological Framework

[4] The area of study is located in the western and southern portions of the Mesozoic Basque-Cantabrian Basin (Figure 2). The Meso-Cenozoic deformation history of the basin started with a Permo-Triassic extensional stage, which led to the development of WNW-ESE and E-W striking faults [e.g., *Ziegler*, 1989; *García-Mondéjar et al*., 1996]. This stage predated the main Late Jurassic to Early Cretaceous extensional event, during which the Basque-Cantabrian Basin developed as part of the southern passive margin of the Bay of Biscay-Pyrenean rift system [e.g., *Le Pichon and Sibuet*, 1971; *Muñoz*, 2002]. Inherited extensional faults were reactivated during this second rifting stage [e.g., *Pulgar et al*., 1999; *Espina et al*., 2004], with an extension direction oriented about NNE-SSW and forming an angle of 75°–80° with the major WNW-ESE striking faults [*Tavani and Muñoz*, 2012], and were later inverted during the Pyrenean compression [e.g., *Muñoz*, 1992; *Espina*, 1997; *Vergés et al*., 2002; *Barnolas and Pujalte*, 2004]. This Cenozoic contractive stage was characterized by a complex deformation partitioning in time and space, consisting of reverse, right-lateral and left-lateral reactivation of WNW-ESE and E-W striking inherited faults [*Tavani et al*., 2011]. The Asturian Massif and the westernmost Basque-Cantabrian Basin (Figure 2a) were characterized by the thick-skinned transpressional reactivation of basement faults, while in the central and eastern portions of the Basque-Cantabrian Basin inherited elements underwent thin-skinned dip-slip inversion [*Tavani*, 2012, and references therein]. Thin-skinned inversion in the central and eastern portions of the basin detached the Meso-Cenozoic sedimentary pile above Triassic evaporites, and determined the overthrusting of the Mesozoic sequence above the Cenozoic Ebro foreland basin for several tens of kilometers [*Martínez-Torres*, 1993]. In the western portion of the basin, the Cenozoic transpressional tectonics was mainly concentrated along the WNW-ESE striking Ubierna Fault System [*Hernaiz*, 1994; *Tavani et al*., 2011], and the other inherited structures have been largely preserved (Figures 2b and 2c). The Ubierna Fault System is known to represent the southern boundary of the Mesozoic basin [*Rat*, 1988; *Hernaiz et al*., 1994; *Malagón et al*., 1994]. Only limited inversion occurred along other WNW-ESE striking elements, like the Golobar and Rumaceo fault systems [*Espina et al*., 2004]. Moreover, the same northern block of the Ubierna Fault System has been poorly affected by Cenozoic deformation. This area underwent a westward increasing uplift, with associated gently folding and limited internal deformation [see *Tavani*, 2012, Figure 19]. Three main structures striking from NE-SW to NNE-SSE, i.e., at a high angle to the Ubierna Fault, are present in this area, being the Ayoluengo ridge, the Hontomín flexure and the Rojas structure (Figures 2b and 2c). The latter is a particularly important and well-constrained structure, which includes two anticlines and represents the Cenozoic contractional horsetail termination of the Ubierna Fault. The well Rojas NE-1 was drilled in its northern sector and, as the other deep wells of the area, encountered Paleozoic rocks below the Triassic evaporitic Keuper facies (Figure 2d).

[5] The polyphasic deformation history of the study area favored a complex stratigraphic architecture (Figure 3). Two paleogeographic domains can be individuated, locating to the north and to the south of the Ubierna Fault System, respectively. The Basque-Cantabrian Basin domain consists of thousands of meters of sediments deposited from Late Carboniferous times onward recording the two phases of Mesozoic rifting and subsequent basin inversion [*García-Mondéjar et al*., 1996; *Espina et al*., 2004; *Beroiz and Permanyer*, 2011]. Permo-Triassic conglomerates and sandstones of the Buntsandstein facies unconformably overlie the Paleozoic basement of the basin, and were deposited during the first rifting event. Triassic postrift sediments consist of dolostones and carbonates of the Muschelkalk facies, and evaporites and clays of the Keuper facies [*Lanaja*, 1987; *García-Mondéjar et al*., 1996; *Espina*, 1997]. Upper Triassic to Middle Jurassic postrift rocks include limestones, dolostones, evaporites, and marls [e.g., *Quesada et al*., 1993]. Late Jurassic to Early Cretaceous syn-rift siliciclastic sediments, including fluvio-deltaic conglomerates, sandstones, and clays, were sourced from the southern emerged lands

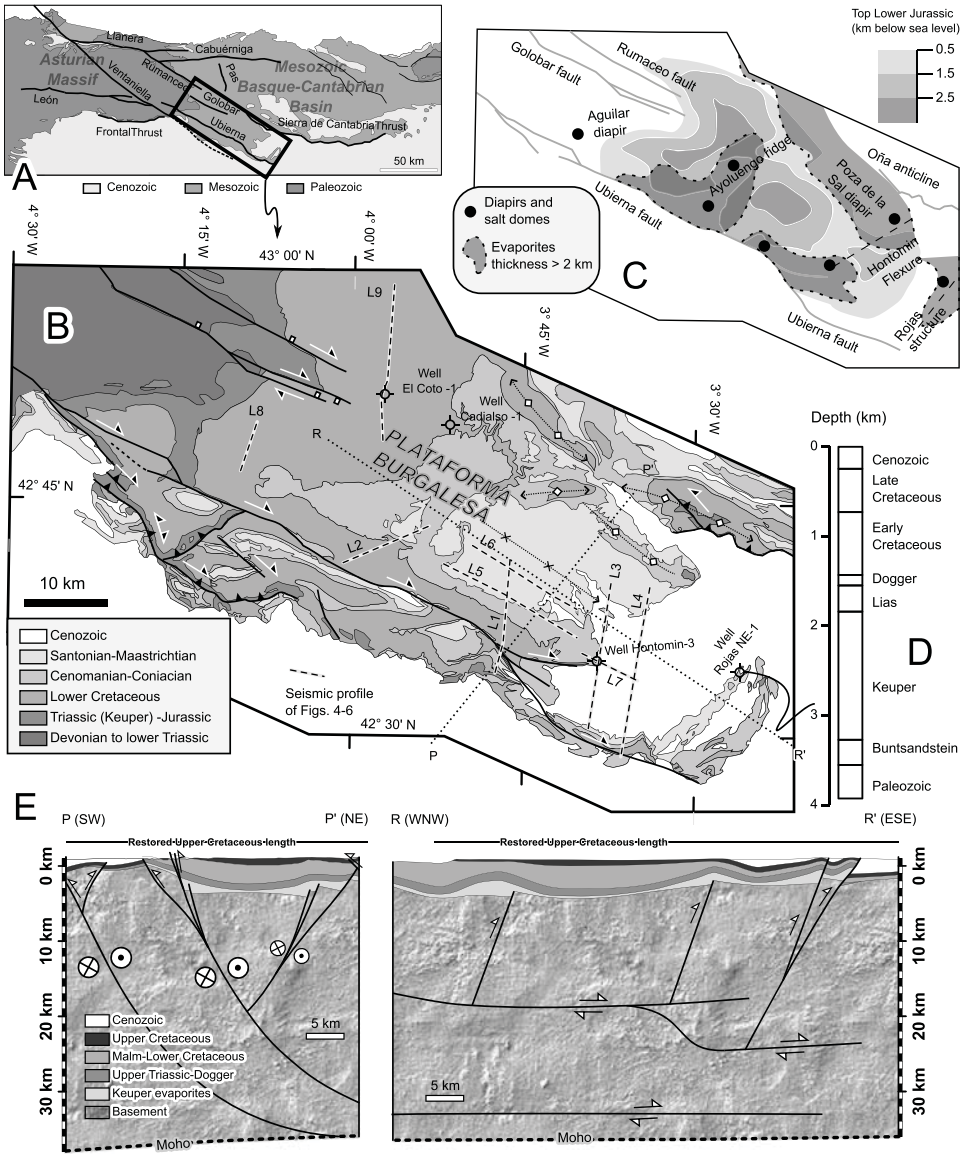

Figure 2. (A) Geological map of the Basque-Cantabrian Basin and Asturian Massif area with labels of the main features. (B) Geological map of the southern portion of the Basque-Cantabrian Basin (modified from *Tavani et al*. [2011]), with traces of seismic lines and geological cross-sections in Figure 2E. (C) structural scheme of the area with: labeling, location of main diapirs (named in the map) and salt domes, depth of the top of Lower Jurassic rocks in the northern block of the Ubierna Fault (modified from *Beroiz and Permanyer* [2011]), thickness of Triassic evaporites (modified from *Serrano and Martínez del Olmo* [1989] and *Pinto et al*. [2005]). (D) Rojas NE-1 well. (E) Schematic crustal-scale cross-sections across and along the Plataforma Burgalesa and Ubierna Fault. Notice that: (1) nearly horizontal lines in the *R-R'* section represent the intersection between the NNE-dipping faults and the section plane; (2) in the same cross-section, WNW-dipping faults terminate onto these nearly horizontal faults trace because WNW-dipping faults are located in the hanging wall of the NNE-dipping faults.

[*Lanaja*, 1987; *Pujalte et al*., 1996]. Upper Cretaceous postrift sediments consist of limestones and marls that unconformably overlay Paleozoic to Lower Cretaceous rocks. The Cenozoic syn-orogenic sediments are mostly represented by conglomerates and sandstones that span from Paleocene to Miocene age [*Hernaiz and Solé Pont*, 2000]. On the other hand, the Duero Basin to the south of the Ubierna Fault System is characterized by a thinner Mesozoic cover, mainly represented by Cretaceous sediments related with several transgressive-regressive cycles [*Floquet*, 2004]. Evidences of Mesozoic rifting are restricted to fault bounded Triassic deposits located along the eastern basin boundary [*Lanaja*, 1987; *Hernaiz and Solé Pont*, 2000]. Cenozoic sediments of the Duero Basin span as well from Paleocene to Miocene times.

[6] In relation to the seismic character of the above mentioned units, the pre-evaporitic basement is characterized

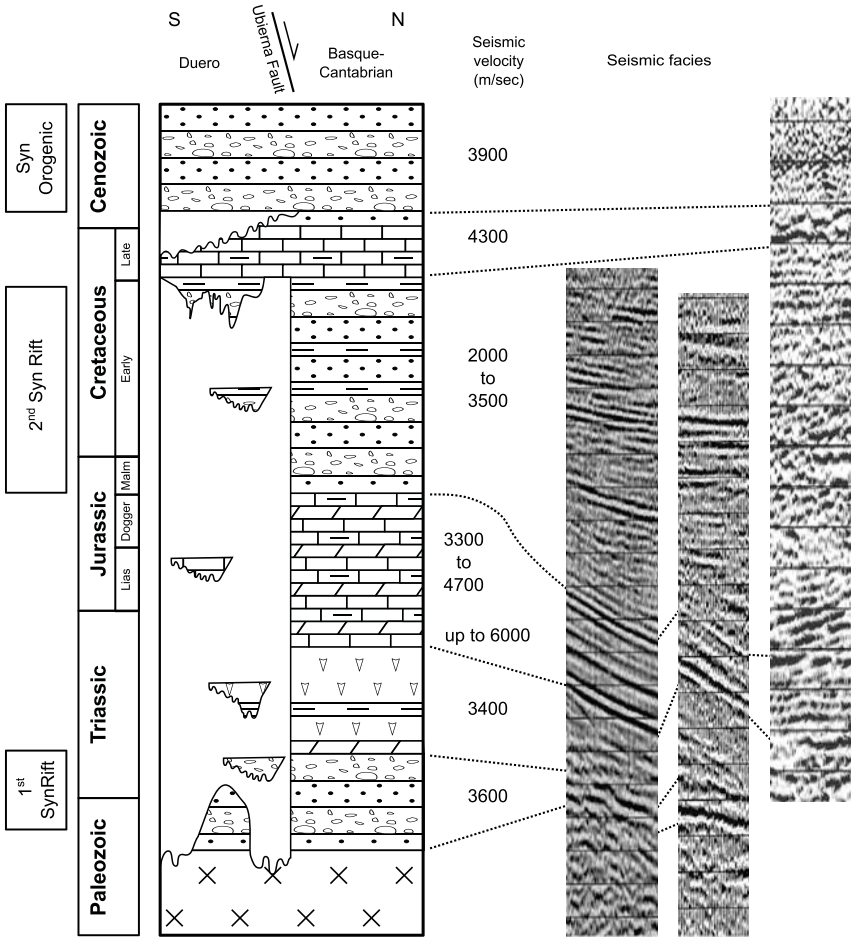

Figure 3. Synthetic stratigraphy of the area, with seismic velocities of the different packages and examples illustrating their seismic facies.

by extremely variable seismic facies, laterally passing from chaotic to transparent. A remarkable exception is represented by the Permo-Triassic Buntsandstein sediments, which correspond to almost continuous reflectors. These underlay the diagnostic transparent facies of the Upper Triassic evaporites (Figure 3), which may include some subordered reflective layers. These two Permo-Triassic units have been encountered in a few wells of the area, as well as in the "El Coto-1" well (Figure 1), their seismic velocities being about 3500 m/s. Upper Triassic to Middle Jurassic carbonates always appear as bright parallel reflectors, and generally continuous along large parts of the seismic sections. The measured velocity of the seismic signal across these sediments reaches 6000 m/s in the lowermost part, but it generally ranges between 3300 m/s and 4700 m/s. Upper Jurassic to Lower Cretaceous syn-rift sediments are also characterized by a strong reflectivity. However, it is generally lower than that of the underlying prerift package. This, together with the several internal unconformities and, above all, the major unconformity with the underlying prerift package, makes the syn-rift sediments always well recognizable in all the seismic sections of the area. Seismic velocities of these syn-rift sediments range between 2000 and 3500 m/s. Upper Cretaceous carbonates are characterized by continuous and parallel reflectors. Their average velocity is about 4000 m/s, but the seismic interpretation of these rocks must be always accompanied by surface constraints, because the strong karstification locally can imply an abrupt velocity drop. Finally, the overlying Cenozoic sediments are characterized by both chaotic and well defined continuous reflectors and, as for Upper Cretaceous materials, seismic interpretation of these sediments is highly favored by the surface control.

3. Data

[7] To the north of the Ubierna Fault, the Plataforma Burgalesa Domain is represented by a system of WNW-ESE striking and ESE plunging open synclines and anticlines of Upper Cretaceous postrift sediments (Figure 2). Progressively older rocks are exposed toward the west due to the eastward regional plunge. The NW-SE oriented Hontomín Flexure represents the eastern boundary of the wide and (at a regional scale) almost flat-lying central portion of the Plataforma Burgalesa Domain, and to the east Cenozoic sediments are largely exposed. Upper Cretaceous layers in the central portion of the Plataforma Burgalesa dip toward NNW when approaching the Ubierna Fault, while Lower Cretaceous sediments are exposed close to it. Seismic profiles striking

about perpendicular to the Ubierna Fault highlight a strong decoupling between surface and subsurface geometries. The N-S running seismic section L1 crosses the Ubierna Fault in an easterly location (Figures 2b and 4a) and shows flat-lying Upper Cretaceous layers that become slightly north-dipping close to the Ubierna Fault. Upper Jurassic to Lower Cretaceous syn-rift sediments are also almost flat-lying and are represented by strongly north thickening reflectors (Figure 4a). This seismic profile displays well-imaged syn-rift reflectors onlapping onto the underlying north-dipping prerift Upper Triassic to Middle Jurassic layers. Below these, the transparent seismic facies attributable to the evaporitic Keuper are well recognizable. Triangularly-shaped bodies of evaporites divide north-dipping Upper Triassic to Middle Jurassic layers from underlying subhorizontal reflectors (Figure 4c) that are interpreted as belonging to the Permo-Triassic Buntsandstein facies. Notice that these basement reflectors are displaced in a normal sense across the Ubierna Fault, as shown in the inset of Figure 4b, indicating that if any, Cenozoic reverse component of displacement has not recuperated the extensional one. The same hanging wall geometries are imaged in the NE-SW striking L2 section, which is located in the central portion of the Ubierna Fault (Figure 4d). North-dipping Upper Triassic to Middle Jurassic layers are onlapped by subhorizontal northward thickening syn-rift sediments. In both lines L1 and L2, onlap geometries are present close to the Ubierna Fault, while in the northern portion of both lines prerift and syn-rift sediments are almost parallel.

[8] Seismic lines L3 and L4 image the Ubierna Fault and one of its fault splay (Figures 2b and 5). These two N-S striking seismic lines run along the area where the Ubierna Fault trace bends and splays. Particularly important for this work is the presence of two wells along the L3 section, allowing to fully confirm that the major unconformity observed in the seismic sections marks the limit between prerift Middle Jurassic and syn-rift Upper Jurassic sediments.

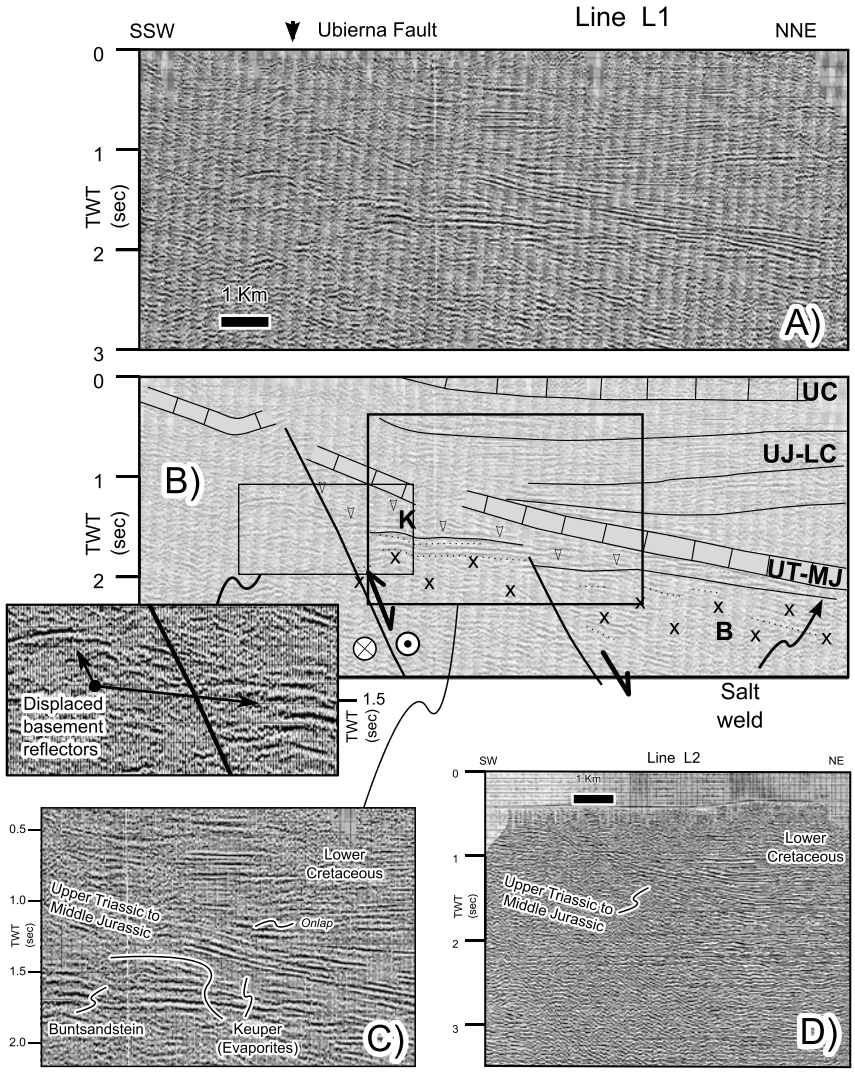

Figure 4. (A) N-S striking seismic line L1 with (B) line drawing and (C) detail illustrating the relationships between cover, evaporites and basement. (D) NE-SW striking seismic line L2. Here and in the following, C is Cenozoic; UC is Upper Cretaceous; UJ-LC is syn-rift Upper Jurassic to Lower Cretaceous; UT-MJ is prerift Upper Triassic to Middle Jurassic; K is Keuper evaporites; B is basement.

Syn-tectonic relationships between syn-rift Upper Jurassic to Lower Cretaceous sediments and prerift Upper Triassic to Middle Jurassic units are similar to those observed to the east (Figure 4). In detail, prerift and syn-rift reflectors are almost parallel in the area between the Ubierna Fault and its splay, onlap geometries are imaged in the central portion of line L3 (Figure 5a), while to the north downlap geometries are present, which are interpreted as tilted onlaps. Although the syn-rift sequence includes fluvio-deltaic facies, which may suggest an alternative interpretation of these downlaps as sedimentary features, this second hypothesis is ruled out by the evidence that both regional and local paleocurrents were roughly from the southerly located mainland to the northern marine basin [*Pujalte et al*., 1996]. The thickness of the syn-rift portion of the multilayer drastically increases northward across both the Ubierna Fault and the splay fault, although in the splay fault case, the northward thickening occurs along a wider cross-sectional region. Upper Cretaceous reflectors show short wavelength tight anticlines located onto the tips of the Ubierna Fault and its splay, separated by a syncline filled with Cenozoic sediments onlapping onto the Upper Cretaceous fold limbs. As revealed by the seismic data, both faults penetrate into the syn-rift sequence. However, the folded structure formed by the postrift Upper Cretaceous layers and Cenozoic syn-orogenic materials filling the synclinal areas witness that faulting of the cover sequence (syn-rift included) occurred during the Cenozoic contractional stage.

[9] Folding of the entire multilayer related with the inversion of an oblique basement fault is well-imaged in seismic profiles oriented perpendicular (Figure 5b) and parallel (Figures 6a–6c) to the Ubierna Fault. WNW-ESE striking seismic lines L5 and L6 (Figures 6a and 6b) show the along-strike geometry of the hanging wall of the Ubierna Fault. Reflectors immediately below the evaporitic seismic facies and those corresponding to Upper Triassic to Middle Jurassic layers are subparallel, at least in the western and central portion of the two line, whereas in the easternmost portion of these lines, many almost horizontal subevaporitic reflectors are present. Seismic line L7 of Figure 6c shows the eastern prolongation of these geometries. Upper Triassic to Middle Jurassic layers define an anticline cored by Triassic evaporites. In the eastern limb, prerift and postrift layers are parallel to the prerift ones, and Cenozoic material filling the synclinal low to the east indicates the Cenozoic age of folding. In the western limb, both postrift and syn-rift layers are subhorizontal. In detail, the thickness of the syn-rift sequence reduces from the western limb toward the crest, with onlapping geometries being present. Below the salt body coring the anticline, reflectors corresponding to the Permo-Triassic Buntsandstein facies are subhorizontal. Onlap geometries, syn-rift thickness variations, and Cenozoic folding observed along the Hontomín flexure (Figures 3, 6b, and 6c) indicate that this NE-SW oriented structure is the surface expression of an inverted NW-dipping extensional fault, as shown in the line drawing of Figure 6c.

[10] The N-S striking seismic section L8 along the western termination of the Ubierna Fault (Figure 6d) shows similar hanging wall geometries to those observed in correspondence of the bend of the Ubierna Fault (lines L3 and L4 of Figures 5a and 5b). In this section reflectors attributed to the Upper Jurassic-Lower Cretaceous syn-rift sequence downlap southward onto prerift Upper Triassic to Middle Jurassic reflectors, and become progressively parallel to each other toward the northern portion of the seismic line. The last seismic section presented in this work is located in the western portion of the Plataforma Burgalesa, where Lower

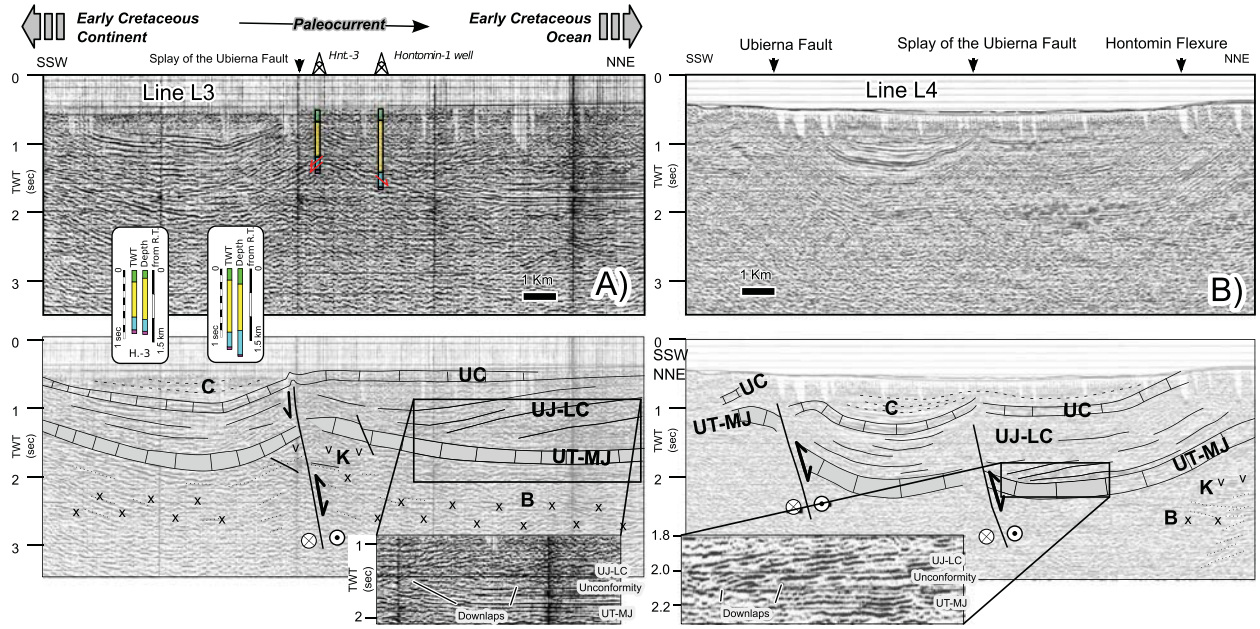

Figure 5. N-S striking seismic lines (A) L3 and (B) L4, with interpretation and detail of downlap relationships between syn-rift and prerift reflectors. Partially modified from *Tavani et al*. [2011]. Hontomín-1 and Hontomín-3 wells are reported along L3 line, with postrift, syn-rift, prerift, and evaporites indicated. Main boundaries encountered in these wells are reported, in both TWT and depth.

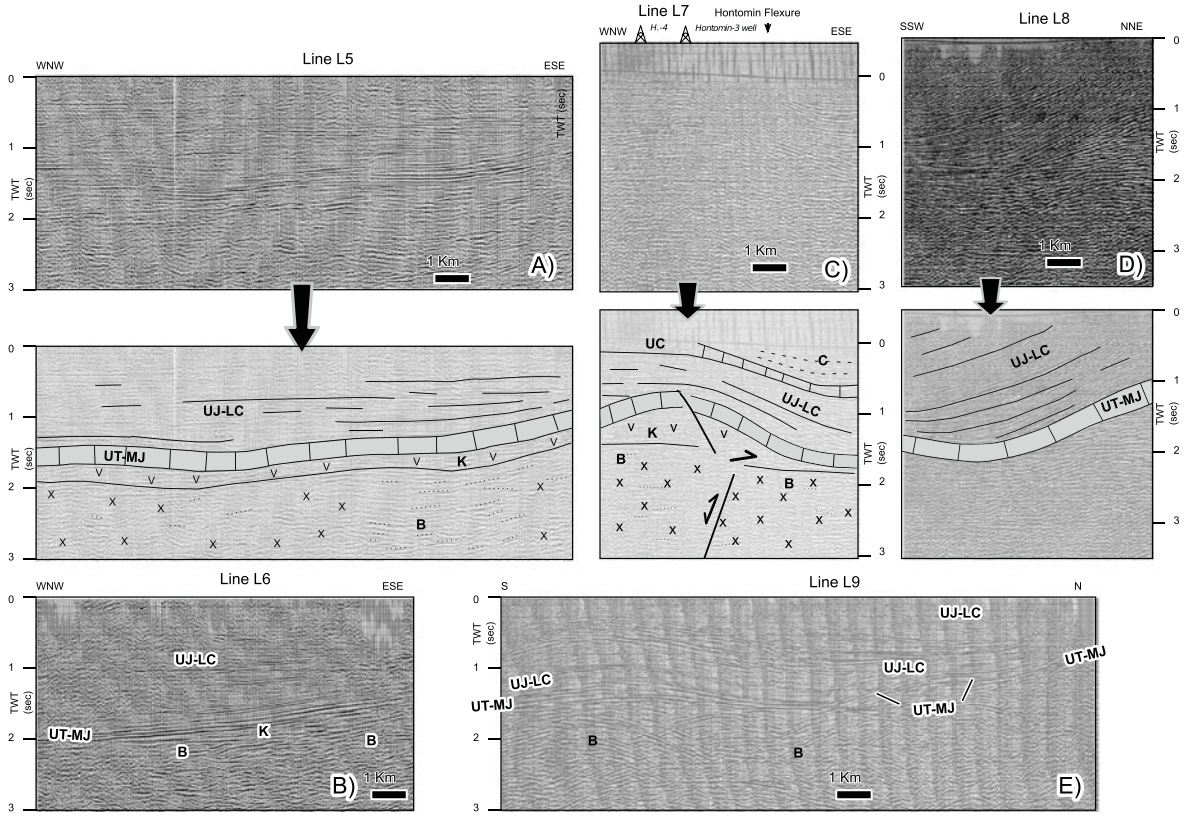

Figure 6. WNW-ESE striking seismic lines (A) L5, (B) L6, and (C) L7 and N-S striking lines (D) L8 and (E) L9. Partially modified from *Tavani et al*. [2011].

Cretaceous syn-rift sediments are exposed (Figure 6e). The N-S striking section shows a gentle anticline whose crestal sector corresponds to a Mesozoic depocenter as shown by syn-rift sequence thickening in this area. Toward the north, the same syn-rift sequence is severely thinned.

[11] Geometries observed in this last section are nicely exposed along the western boundary of the basin due to the presence of the mentioned regional ESE plunge (Figure 7). This area is affected by the Rumaceo and Golobar faults and allows for the evaluation of the pre-evaporite and postevaporite units relationships. A strong decoupling exists between these portions of the multilayer. Major faults mostly affect the basement and have a Triassic origin, as evidenced by thickness variation of the Buntsandstein facies [e.g., *Espina et al*., 2004]. On the other hand, the Upper Triassic to Middle Jurassic sequence is poorly faulted and regionally drapes the evaporites. Cenozoic inversion of the major basement faults [*Espina et al*., 2004] has occurred within a right-lateral transpressive framework [*Tavani et al*., 2011], and led to the development of anticlines and synclines formed due to the buttressing effect of the extensional faults (Figure 7d). These faults penetrate into the cover sequence, but with relatively limited displacements (i.e., less than a few hundreds of meters). The fact that faults preserve their integrity across the evaporites, and that the latter accumulated in the synclinal areas between anticlines cored by inherited faults, indicates that evaporites played a locally important role during Cenozoic inversion, but did not act as a regionally important décollement level.

4. Discussion

[12] In agreement with data and observations presented in this work, with previously published mesostructural data [*Tavani et al*., 2011; *Quintà and Tavani*, 2012], with computed depths of reference layers in the area [e.g., *Beroiz and Permanyer*, 2011], and with Triassic evaporites thickness distribution [*Serrano and Martínez del Olmo*, 1989; *Pinto et al*., 2005] (Figure 2c), two schematic 3-D block diagrams with related schematic maps have been constructed (Figure 8). These illustrate the present-day (Figure 8a) and Late Cretaceous (Figure 8b) geometries of the area. The present-day geology is interpreted as the result of the Cenozoic reactivation of the deeply rooted Mesozoic extensional system. In detail, WNW-ESE striking master faults and NNE-SSW to NE-SW striking transverse extensional elements underwent right-lateral strike-slip and dip-slip reactivation, respectively. The present day Ubierna Fault is interpreted as resulting from the Cenozoic strike-slip linkage of two Mesozoic extensional master faults. The Mesozoic northern Ubierna Fault included the present day segment of the fault located to the west of the main bend and the Hontomín splay fault. The Southern Mesozoic Ubierna Fault included the easternmost segment of the present day Ubierna Fault. Such an interpretation is consistent with the observed northward thickening of the syn-rift sequence, which is observed across the Hontomín splay fault (seismic lines L3 and L4 in Figure 5). The Hontomín flexure displays all the evidences of a NE-SW striking and NW-dipping inverted extensional fault (Figure 6c).

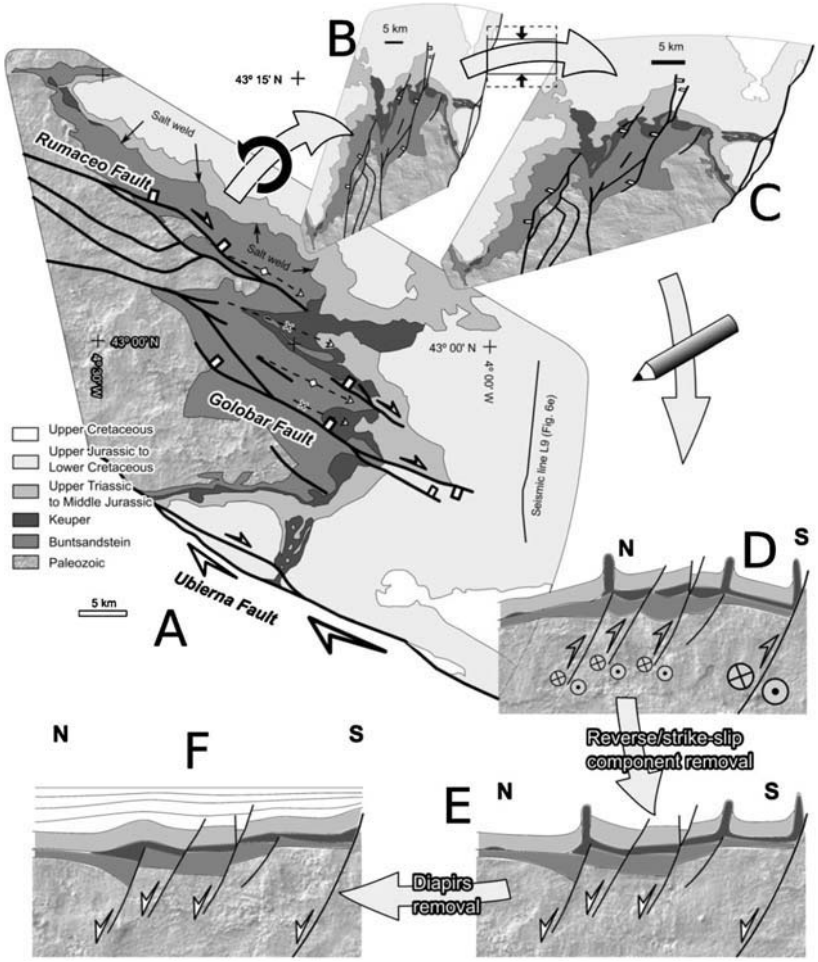

Figure 7. (A) Geological map of the westernmost sector of the Basque-Cantabrian Basin, at its transition with the Asturian Massif (modified and rearranged from *Tavani* [2012]). The presence of an ESE dipping plunge makes this area almost a natural cross-section for evaluating relationships between pre-evaporitic rocks and postevaporitic cover. This is done by (B) rotating and (C) stretching the geological map, and then "smoothing" the resulting geometries (D), particularly at the border of the map (i.e., Rumaceo and Ubierna faults). The obtained N-S oriented scheme represents a roughly N-S oriented cross-section displaying provides insights about both the present-day geology and the Mesozoic extensional architecture of the area. From this scheme it is qualitatively removed the effects of compression stage (E), and then that of the salt diapirs (F). The result is a deep geological scheme resembling the first-order cross-sectional geometry of the basin at the end of the extensional stage.

The same can be inferred for the Rojas structure located further ESE. In fact, well data in the Rojas area indicate the presence of a syn-rift sequence that is strongly reduced, even absent, immediately to the east [e.g., *Muñoz-Jiménez and Casas-Sainz*, 1997]. This interpretation also matches with the transverse roughly NE-SW to NNE-SSW striking trend of the Ayoluengo ridge [*Beroiz and Permanyer*, 2011]. Consistently with the structural style of the elements described in this work, these transverse elements are interpreted to be the result of Mesozoic basement faulting and coeval cover forced folding, whose geometry would have been later amplified and modified upon Cenozoic reactivation. Such an interpretation is surely valid for the Hontomín Transfer Fault, as recognized in seismic profiles crossing this area. It is also strongly supported for the Rojas and Ayoluengo structures (Figure 2c), where the anomalously thick evaporites accumulated along the hanging wall of basement faults are interpreted to be the result of Mesozoic forced folding in the presence of a decoupling evaporitic layer [e.g., *Stewart et al*., 1997; *Maurin and Niviere*, 1999; *Keller and Lynch*, 1999; *Richardson et al*., 2005]. The geometries imaged in the hanging wall of the Ubierna Fault, along with the presence of evaportites accumulation, diapirs, and salt domes along the trace of the fault (Figure 2c), provide an additional evidence of forced folding associated with the Northern Mesozoic Ubierna Fault.

[13] This reconstruction is in agreement with the documented ESE-directed movement of the Plataforma Burgalesa Domain during Cenozoic times [*Tavani et al*., 2011]. The amount of Cenozoic shortening associated with the inversion of the Mesozoic Ayoluengo, Hontomín, and Rojas transverse extensional faults, in fact, is about 2.5 km, as resulting from line-length restoration of the Upper Cretaceous layer along

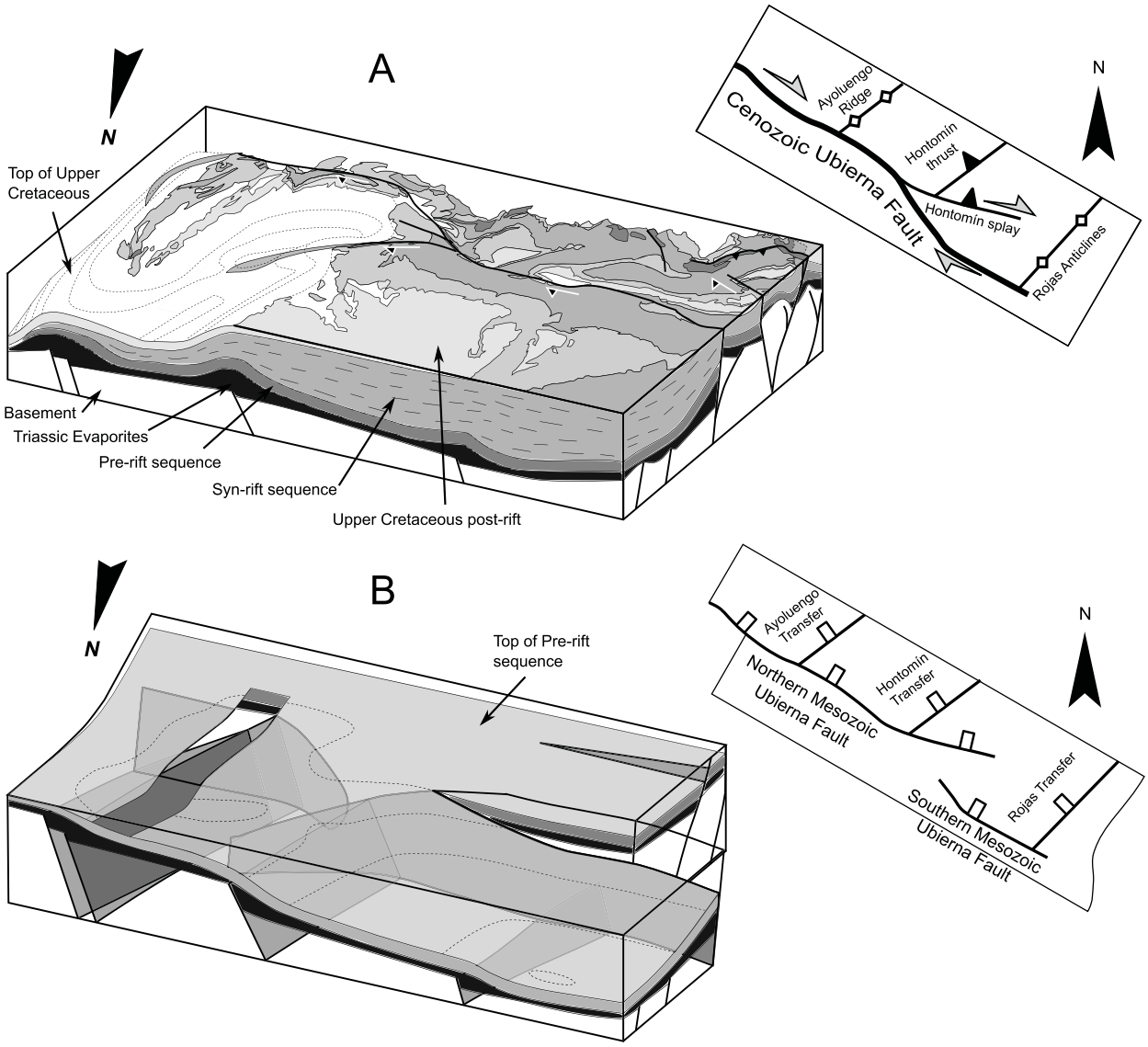

Figure 8. View from the north of 3-D block diagrams of the area (with relative map views), (A) illustrating the present-day geology and (B) the reconstructed geometries at the end of Early Cretaceous.

the *R*-*R*′ section of Figure 2e. This value forms part of the right-lateral displacement of the Ubierna Fault, whose cumulative value includes also the certainly higher contribution of the southern, heavily deformed, block of the fault. There, as an example, subsidiary right-lateral faults displacing up to hundreds of meters many recent (Pliocene?-Quaternary) morphological features are present (see supplementary material in *Tavani et al*. [2011]). In conclusion, the estimation of more than 10 km of right-lateral displacement made by *Tavani et al.* [2011] appears to be consistent with data from the northern block of the fault that we have presented in this work.

[14] Seismic lines illustrated in this work display another important and intriguing feature related with the prerift and syn-rift depositional megasequence boundaries. Downlap and onlap relationships between syn-rift and prerift sequences are observed on the hanging wall of the Northern Mesozoic Ubierna Fault. As previously discussed, syn-rift sediments were supplied from emerged lands located to the south, thus preventing the interpretation of south-dipping downlaps as sedimentary features. Hence, a salt expulsion rollover hypothesis [*Ge et al.*, 1997; *Brun and Maudit*, 2008] cannot be invoked, because in this case the downlaps should dip toward the north too. In contrast, geometries of syn-rift strata somehow resemble those of extensional rollovers developing above listric faults that commonly occur during extensional deformation in the presence of a salt décollement [e.g., *Davison*, 1986; *White et al*., 1986; *Soto et al*., 2007]. This solution, however, requires documenting the presence of a regionally important lower décollement located either at the prerift to syn-rift transition or within the evaporitic layer, where many kilometers of extensional displacement should have occurred. The observation that some exposed faults located immediately to the north of the seismic line L8 (where downlap relationships are present) are not displaced

across the evaporites, and penetrate upward into the lowermost part of the syn-rift package (Figure 7), evidences that such an extensional rollover hypothesis must be discarded too.

[15] A key observation to interpret the origin of syn-rift downlapping relationships is that these occur only in correspondence of the fault tips of the Northern Mesozoic Ubierna Fault (seismic lines L3 and L4 of Figure 5 and line L7 of Figure 6), and are not present in the central portion of such fault (Figure 4). Our interpretation, which is illustrated by the end of this section, is that these depositional relationships are intimately linked to the behavior of the Triassic evaporites during the extensional activity of the Northern Mesozoic Ubierna Fault, which deformed at varying strain rates along the strike of the fault. The structural styles associated with basement extensional faulting and decoupled cover deformation are known to be controlled, among other factors, by the displacement rate of the basement fault and the thickness and mechanical properties of the evaporitic unit [e.g., *Koyi et al*., 1993; *Stewart et al*., 1996, 1997]. In particular, increasing the displacement rate along the basement fault reduces the decoupling between the basement and the cover [e.g., *Withjack and Callaway*, 2000; *Richardson et al*., 2005]. As illustrated in Figure 8b, and in agreement with the extensional faults growth models [e.g., *Walsh and Watterson* 1988; *Cartwrigth et al*., 1995; *Willemse et al*., 1996; *Cowie and Shipton*, 1998; *Walsh et al*., 2003; *Kim and Sanderson*, 2005] and experimental research [e.g., *Koyi et al*., 1993; *Withjack and Callaway*, 2000], we infer that the Ubierna Fault had its largest displacement and, likely, slip rate in its central portion, where it would have been able to propagate into the cover sequence across the evaporite layers. Displacement rates diminished laterally toward the tip regions, and the fault would progressively not affect the cover sequences. Using simple kink-band geometry, the effect of fault propagation vs. nonpropagation onto the geometry of syn-rift sediments is illustrated in Figure 9. When decoupled extensional forced folds form, displacement along the master fault creates a space located adjacent to the fault where ductile material becomes accumulated. Cover sequences are folded and domed due to the combined effect

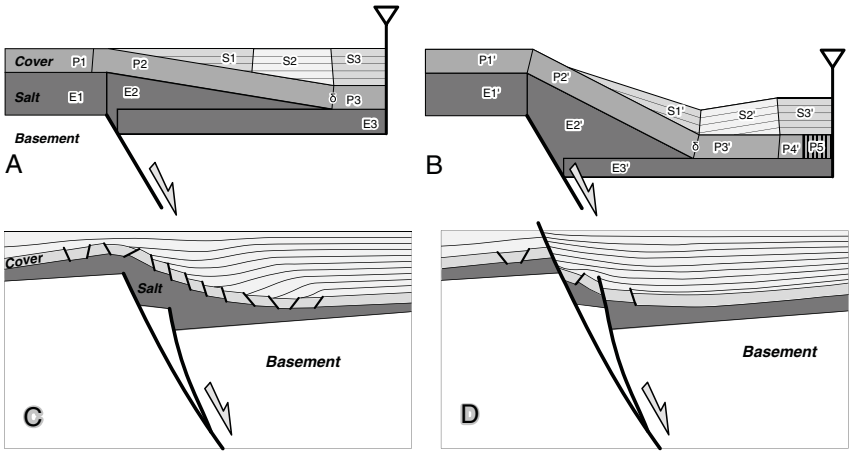

Figure 9. (A-B) Kink-band construction for an extensional forced fold, illustrating the relationships between fault movement, salt migration, cover sequence folding, and syn-kinematic sedimentation. See text for details. Expected pattern of syn-kinematic sediments for an extensional forced fold (C) without and (D) with fault propagation into the cover.

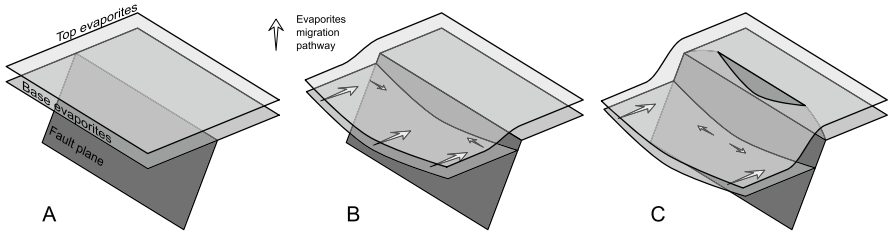

Figure 10. Schematic evolution of the Triassic evaporites (top and bottom layers are drawn) during the extensional activity of the Ubierna Fault. In the early stages of fault activity, forced folding has occurred along the entire strike of the fault. This implied, in the hanging wall of the fault, evaporites migration toward the fault and, subordinated movements from the tip regions toward the centre of the fault, where a huge amount of evaporites is required to ensure folding of the cover. Later, propagation of the fault into the cover sequence has occurred only in the central portion of the fault, which implies the termination of evaporites accumulation in that area. Forced folding continued at the tips, which implies migration of evaporites from the central part of the fault toward the tips.

of hanging wall downthrow and salt being drawn in toward the basement fault. Salt evacuation is favored by the differential load exerted on the hanging wall by the deposition of the syn-kinematic sediments. For sake of simplicity, in the presented model it is assumed that salt migrates only from the downthrown hanging wall [e.g., *Koyi et al*., 1993]. This is illustrated in our model by the thickness change between panels E3 and E3′ and E2 and E2′ of Figure 9. The model also assumes that folding of the cover sequence occurs by rigid limb rotation. Accordingly, the sum of the areas of polygons E2 and E3 of Figure 9a must equal that of the areas of E2′ and E3′ of Figure 9b. Thickness preservation of the cover sequence draping the salt layer is assumed in the model just to ensure a simple geometrical construction (Figures 9a and 9b). Synchronous fault slip and broadening of the polygon E2 (which transforms into E2′) implies the steepening of the cover sequence panel P2. As a result, onlapping syn-kinematic sediments of panel S1 deposited onto panel P2 rotate to form the panel S1′, where tilted onlap geometries become downlap. It is unlikely that broadening of panel E2 occurs only by thinning of E3 (which is also geometrically impossible after a certain displacement value). It is much more suitably expected for polygon E2 to reduce its width to minimize required salt mobilization. The effect of this on the cover sequence is that the axial surface δ, which divides panels P2 and P3 of the cover, migrates toward the fault with increasing displacement. Accordingly, δ is an active axial surface [*Suppe*, 1983]. The consequence is that panel P3′ of Figure 9b is flat-lying as the panel P4′, but the former hosts twice tilted layers (i.e., material that belonged to panel P2 of Figure 9a and had been crossed by the migrating axial surface δ). P3′ is geometrically indistinguishable from P4′, but the attitude change of syn-kinematic sediments above reflect the existence of an active axial surface. In particular, P3′ is overlain by S2′, which was part of S2 and includes downlap geometries, while P4′ is overlain by S3′, where prekinematic and syn-kinematic layers are parallel to each other. Assumption of both thickness preservation in the prerift layers and vertical pin on the downthrowning hanging wall impose an area gain represented by polygon P5 (Figure 9b). A more geologically reasonable assumption is area preservation, which accounts for the stretching observed in prerift layers as intense boundinage of incompetent lithologies and extensional faulting for more competent ones. Such geometrical necessity is supported by natural examples [e.g., *Maurin and Niviere*, 1999; *Keller and Lynch*, 1999] and analogue models of extensional forced folds [e.g., *Cosgrove and Ameen*, 1999].

[16] To summarize, progressive hanging wall downthrowning and synchronous narrowing of the triangularly shaped body of evaporites produces the tilting of onlap geometries, which transform in downlaps, and drastic stretching of the prekinematic cover sequence (Figure 9c). This occurs when the fault does not propagate into the cover. On the contrary, when the stage of forced folding is rapidly followed by the propagation of the fault into the cover sequence, downlap geometries do not develop and the amount of stretching in the prekinematic cover is reduced (Figure 9d).

[17] According to the above described simple geometric model, the presence of downlap geometries at the tips of the Northern Mesozoic Ubierna Fault and their absence in its central portion, suggests that during Late Jurassic-Early Cretaceous extension the fault propagated into the cover only in its central portion, where both slip rate and total displacement were largest. From this arises a two-stage syn-rift salt mobilization history (Figure 10). In the first stage (Figure 10b) the salt is evacuated toward the fault, with salt migration directions oriented almost perpendicular to the fault strike. A certain centripetal component can be inferred, because the central portion of the fault requires a higher supply of evaporites to ensure folding of the cover. As the master fault propagates into the cover (Figure 10c), the system locks up in the central portion of the fault; salt accumulation in the hanging-wall continues at the fault tips, implying the along-strike migration of evaporites from the central portion of the fault toward its tips.

5. Conclusions

[18] The Mesozoic Basque-Cantabrian Basin of northern Spain is a thick-skinned extensional domain inverted during Cenozoic Pyrenean contraction. During Late Jurassic to Early Cretaceous rifting, extensional forced folds developed due to the decoupling effect of Triassic evaporites, which divided a folded Upper Triassic to Middle Jurassic cover sequence and a faulted Paleozoic to Lower Triassic faulted sequence. Forced folding developed in association both WNW-ESE striking master faults and NE-SW to NNE-SSW striking transverse faults. During Mesozoic rifting, the most important structure was the WNW-ESE striking and NNE-dipping Northern Ubierna Fault, which represented the southern basin boundary. In the hanging wall of the fault, syn-kinematic layers are characterized by onlap geometries near the fault, as a result of progressive tilting of underlying cover sequence during forced folding. Toward the northern part of the hanging wall, away from the fault, syn-kinematic and prekinematic layers are almost parallel in the central portion of the fault, while at the tips of the fault, onlap geometries are followed, toward the north, by downlap relationships. We have shown that this is coherent with a longer stage of forced folding at the fault tips. Accordingly, a higher displacement rate in the central portion of the fault implied the propagation of the Ubierna Fault into cover sequence after a relatively short period of forced folding. On the contrary, lower slip rates at the fault tips implied the nonpropagation of the fault into the cover.

[19] Cenozoic Pyrenean inversion implied the right-lateral, slightly transpressive, reactivation of WNW-ESE striking master faults. Strike-slip linkage of the southern and northern Mesozoic Ubierna faults occurred during this stage. The westernmost portion of the Northern Ubierna Fault was reactivated as a splay fault of the Cenozoic Ubierna Fault. In the northern block of the latter, ESE to SE directed movements associated with this right-lateral transpressive stage caused the inversion of inherited transverse extensional faults, namely the Rojas, Hontomín, and Ayoluengo transverse faults. Thick-skinned, almost dip-slip, inversion of these deeply rooted transverse elements implied the almost rigid uplift of the area preserving the extensional geometries. As a result, triangularly shaped bodies of evaporites, which accumulated in the hanging wall of these transverse faults during Mesozoic forced folding, acquired dome-like geometries.

[20] **Acknowledgments**. Antonio Pedrera and Antonio Casas are warmly thanked for reviewing the manuscript and for constructive comments. This work was carried within the framework of CIUDEN

(FBG305657) and INTECTOSAL (CGL2010-21968-C02- 01/BTE) projects and the "Grup de Recerca de Geodinàmica i Anàlisi de Conques" (2009SGR-1198). The I.G.M.E. (INSTITUTO GEOLÓGICO Y MINERO DE ESPAÑA) is thanked for providing seismic profiles and geological maps.

References

Alonso, J. L., J. A. Pulgar, J. C. García-Ramos, and P. Barba (1996), Tertiary basins and Alpine tectonics in the Cantabrian Mountains (NW Spain), in *Tertiary basins of Spain: Tectonics, Climate and Sea-Level Changes*, edited by P. F. Friend, and C. J. Dabrio, pp. 214–227, Cambridge University Press, Cambridge.

Barnolas, A., and V. Pujalte (2004), La Cordillera Pirenaica, in *Geología de España*, edited by J. A. Vera, pp. 233–343, SGE-IGME, Madrid.

Beroiz, C., and A. Permanyer (2011), Hydrocarbon habitat of the Sedano Trough, Basque-Cantabrian Basin, Spain, *J. Pet. Geol*, *34*, 387–410, doi:10.1111/j.1747-5457.2011.00511.x.

Brown, R. N. (1980), History of exploration and discovery of Morgan, Ramadan, and July oilfields, Gulf of Suez, Egypt, *Canadian Society of Petroleum Geologists, Memoir*, **6**, in: A. D. Miall, Editor, *Facts and principles of world petroleum occurrence*, 733–764.

Brun, J. P., and T. P. O. Maudit (2008), Rollovers in salt tectonics: The inadequacy of the listric fault model, *Tectonophysics*, *457*, 1–11, doi:10.1016/j.tecto.2007.11.038.

Cartwrigth, J. A., B. D. Trudgill, and C. S. Mansfield (1995), Fault growth by segment linkage: an explanation for scatter in maximum displacement and trace length data from Canyonlands Grabens of SE Utah, *J. Struct. Geol.*, *17*, 1319–1326.

Colleta, B., P. Le Quellec, J. Letouzey, and I. Moretti (1988), Longitudinal evolution of the Suez rift structure (Egypt). *Tectonophysics*, *153*, 221–233.

Cosgrove, J. W., and M. S. Ameen (1999), A comparison of the geometry, spatial organization and fracture patterns associated with forced folds and buckle folds, *Geological Society of London Special Publication*, **169**, in: J.W. Cosgrove, M.S. Ameen, Editors, *Folds and Fractures*, 7–21.

Cowie, P. A., and Z. K. Shipton (1998), Fault tip displacements gradients and process zone dimensions. *J. Struct. Geol.*, *20*, 983–997.

Davison, I. (1986), Listric normal fault profiles: calculation using bed-length balance and fault displacement, *J. Struct. Geol.*, *8*, 209–210

Dula, W. F. (1991), Geometric models of listrc normal faults and rollover folds, *AAPG Bull.*, *75*, 1609–1625.

Espina, R. (1997), La estructura y evolución tectonoestratigráfica del borde occidental de la Cuenca Vasco-Cantábrica (Cordillera Cantábrica, NO de España), Ph.D. Thesis, Univerity of Oviedo. 230 pp.

Espina, R., J. L. Alonso, and J. A. Pulgar (2004), Extensión Triásica en la Cuenca Vasco-Cantábrica, in *Geología de España*, edited by J. A. Vera, 338–339, SGE-IGME, Madrid.

Floquet, M. (2004), El Cretácico Superior de la Cuenca Vasco-Cantábrica y áreas adyacentes, in *Geología de España*, edited by J. A. Vera, pp. 299–306, SGE-IGME, Madrid.

García-Mondéjar, J., L. M. Agirrezabala, A. Aranburu, P. A. Fernández-Mendiola, I. Gómez-Pérez, M. López-Horgue, and I. Rosales (1996), Aptian-Albian tectonic pattern of the Basque-Cantabrian Basin (Northern Spain), *Geol. J.*, *31*, 13–45.

Gawthorpe, R. L., I. Sharp, J. R. Underhill, and S. Gupta (1997), Linked sequence stratigraphic and structural evolution of propagating normal faults, *Geology.*, *25*, 795–798.

Ge, H., M. P. A. Jackson, and B. C. Vendeville (1997), Kinematics and dynamics of salt tectonics driven by progradation, *AAPG Bull. 81*, 398–423.

Hernaiz, P. P. (1994), La falla de Ubierna (margen SO de la cuenca Cantabrica). *Geogaceta*, *16*, 39–42.

Hernaiz, P. P., A. Serrano, J. Malagón, and C. Rodríguez-Cañas (1994), Evolución estructural del margen SO de la Cuenca Vasco-Cantábrica, *Geogaceta*, *15*, 143–146.

Hernaiz, P. P., and J. Solé Pont (2000), Las estructuras del Diapiro de Salinas del Rosío y del alto de San Pedro-Iglesias y sus implicaciones en la evolución tectónica de la transversal Burgalesa de la Cordillera Vascocantábrica-Cuenca del Duero, *Rev. Soc. Geol. España*, *13*, 471–486.

Jackson, C. A. L., R. L. Gawthorpe, and I. Sharp (2006), Style and sequence of deformation during extensional fault-propagation folding: examples from the Hammam Faraun and El-Qaa fault blocks, Suez Rift, Egypt, *J. Struct. Geol.*, *28*, 519–535, doi:10.1016/j.jsg.2005.11.009.

Janecke, S. U., C. J. Vanderburg, and J. J. Blankenau (1998), Geometry, mechanisms and significance of extensional folds from examples in the Rocky Mountain Basin and Range province, U.S.A, *J. Struct. Geol.*, *20*, 841–856.

Kane, K. E., C. A.-L. Jackson, and E. Larsen (2010), Normal fault growth and fault-related folding in a salt-influenced rift basin: South Viking Graben, offshore Norway, *J. Struct. Geol.*, *32*, 490–506, doi:10.1016/j.jsg.2010.02.005.

Keller, J. V. A., and G. Lynch (1999), Displacement transfer and forced folding in the Maritimes basin of Nova Scotia, Eastern Canada, *Geological Society of London Special Publication*, **169**, in: J.W. Cosgrove, M.S. Ameen, Editors, *Folds and Fractures*, 87–101.

Khalil, S. M., and K. R. McClay (2002), Extensional fault-related folding, northwestern Red Sea, Egypt, *J. Struct. Geol.*, *24*, 743–762, doi:10.1016/S0191-8141(01)00118-3.

Kim, Y.-S., and D. J. Sanderson (2005), The relationship between displacement and length of faults: a review. *Earth Sci. Rev.*, *68*, 317–334, doi:10.1016/j.earscirev.2004.06.003.

Koyi, H., M. K. Jenyon, and K. Peterson (1993), The effect of basement faulting on diapirism, *J. Pet. Geol.*, *16*, 285–312.

Lanaja, J. M. (1987), Contribución de la exploracíon petrolífera al conocimiento de la geología de España Istituto Tecnólogico GeoMinero de España, Madrid, 1–465.

Laubscher, H. P. (1982), Die Sudostecke des Rheingrabens-ein kinematisches und dynamisches problem, *Eclogae Geol. Helv.*, *75*, 101–116.

Le Pichon, X., and J. C. Sibuet (1971), Western extension of boundary between European and Iberian plates during the Pyrenean orogeny, *Earth Planet. Sci. Lett.*, *12*, 83–88.

Malagón, J., P. P. Hernaiz, C. Rodríguez Cañas, and A. Serrano (1994), Notas sobre la inversión tectónica y aloctonía de la cuenca Vasco-Cantábrica, *Geogaceta*, *15*, 139–142.

Martínez-Torres, L. M. (1993), Corte balanceado de la Sierra Cantabria (cabalgamiento de la Cuenca Vasco-Cantábrica sobre la Cuenca del Ebro), *Geogaceta*, *14*, 113–115.

Maurin, J.-C., and B. Niviere (1999), Extensional forced folding and décollement of the pre-rift series along the Rhine Graben and their influence on the geometry of the syn-rift sequences, *Geological Society of London Special Publication*, **169**, in: J.W. Cosgrove, M.S. Ameen, Editors , *Folds and Fractures*, 73–86.

Muñoz-Jiménez, A., and A. M. Casas-Sainz (1997), The Rioja Trough (N Spain): tectosedimentary evolution of a symmetric foreland basin, *Basin Res.*, *9*, 65–85.

Muñoz, J. A. (1992), Evolution of continental collision belt: ECORS Pyrenees crustal balanced cross-section, *Thrust Tectonics*, edited by K. R. McClay, pp. 235–246, Chapman and Hall, London, United Kingdom.

Muñoz, J. A. (2002), Alpine tectonics I: the Alpine system north of the Betic Cordillera: The Pyrenees, *The Geology of Spain*, edited by W. Gibbons, T. Moreno, Geological Society, London, United Kingdom, 370–385.

Pinto, V., A. Casas, L. Rivero, and M. Torné (2005), 3D gravity modeling of the Triassic salt diapirs of the Cubeta Alavesa (northern Spain), *Tectonophysics*, *405*, 65–75, doi:10.1016/j.tecto.2005.05.010.

Pujalte, V., S. Robles, and J. M. Hernández (1996), La sedimentación continental del Grupo Campóo (Malm-Cretácico basal de Cantabria, Burgos y Palencia): testimonio de un reajuste hidrográfico al inicio de una fase rift, *Cuad. Geol. Ibérica*, *21*, 227–251.

Pulgar, J. A., J. L. Alonso, R. G. Espina, and J. A. Marín (1999), La deformación alpina en el basamento varisco de la Zona Cantábrica, *Trabajos de Geologia*, *21*, 283–294.

Quesada, S., S. Robles, and V. Pujalte (1993), El Jurasico Marino del margen suroccidental de la Cuenca Vasco-Cantábrica y su relación con la exploración de hidrocarburos, *Geogaceta*, *13*, 92–96.

Quintà, A., and S. Tavani (2012), The foreland deformation in the south-western Basque-Cantabrian Belt (Spain), *Tectonophysics*, *576–577*, 4–19, doi:10.1016/j.tecto.2012.02.015.

Rat, P. (1988), The Basque-Cantabrian Basin between the Iberian and European plates some facts but still many problems. *Rev. Soc. Geol. España*, *1*, 327–348.

Richardson, N. J., J. R. Underhill, and G. Lewisw (2005), The role of evaporite mobility in modifying subsidence patterns during normal fault growth and linkage, Halten Terrace, Mid-Norway, *Basin Res.*, *17*, 203–223, doi:10.1111/j.1365-2117.2005.00250.x.

Schlische, R. W. (1992), Anatomy and evolution of the Jurassic continental rift system, Eastern North America, *Tectonics*, *12*, 1026–1042.

Serrano, A., and W. Martínez del Olmo (1989), Diapirismo del Trías Salino en el Dominio Cántabro-Navarro, Libro homenaje a Rafael Soler, A.G.G. E.E.P., 115–121.

Sharp, I., R. L. Gawthorpe, J. R. Underhill, and S. Gupta (2000), Fault-propagation folding in extensional settings: examples of structural style and synrift sedimentary response from the Suez rift, Sinai,Egypt, *Bull. Geol. Soc. Am.*, *112*, 1877–1899.

Soto, R., A. M. Casas-Sainz, and J. J. Villalaín (2011), Widespread Cretaceous inversion event in northern Spain: evidence from subsurface

and paleomagnetic data, *J. Geol. Soc.*, *168*, 899–912, doi:10.1144/0016-76492010-072.

Soto, R., A. M. Casas-Sainz, and P. Del Río (2007), Geometry of half-grabens containing a mid-level viscous décollement, *Basin Res.*, *19*, 437–450, doi:10.1111/j.1365-2117.2007.00328.x.

Stewart, S. A., M. J. Harvey, S. C. Otto, and P. J. Weston (1996), Influence of salt on salt geometry: examples from the UK salt basins, *Geological Society of London Special Publication*, **100**, in: G.I. Alsop, D.J. Blundell and I. Davison, Editors, *Salt Tectonics*, 175–202.

Stewart, S. A., A. H. Ruffell and M. J. Harvey (1997), Relationship between basement-linked and gravity-driven fault systems in the UKCS salt basins. *Marine Petrol. Geol.*, *14*, 581–604.

Suppe, J. (1983), Geometry and kinematics of fault-bend folding, *Am. J. Sci.*, *283*, 684–721.

Tavani, S., A. Quintà, and P. Granado (2011), Cenozoic right-lateral wrench tectonics in the Western Pyrenees (Spain): The Ubierna Fault System. *Tectonophysics*, *509*, 238–253, doi:10.1016/j.tecto.2011.06.013.

Tavani, S., and J. A. Muñoz (2012), Mesozoic rifting in the Basque-Cantabrian Basin (Spain): Inherited faults, transversal structures and stress perturbation. *Terra Nova*, *24*, 70–76, doi:10.1111/j.1365-3121.2011.01040.x.

Tavani, S. (2012), Plate-kinematics in the Cantabrian Domain of the Pyrenean Orogen, *Solid Earth*, *3*, 265–292, doi:10.5194/se-3-265-2012.

Vergés, J., M. Fernández, and A. Martínez (2002), The Pyrenean orogen: pre-, syn-, and post-collisional evolution, *Journal of the Virtual Explorer*, **8**, in: G. Rosenbaum, G.S. Lister, Editors, *Reconstruction of the Evolution of the Alpine-Himalayan Orogen*, 57–76, doi:10.3809/jvirtex.2002.00058.

Walsh, J. J., and J. Watterson (1988), Analysis of the relationship between the displacements and dimensions of faults, *J. Struct. Geol.*, *10*, 239–247.

Walsh, J. J., W. R. Bailey, C. Childs, A. Nichol, and C. G. Bonson (2003), Formation of segmented normal faults: a 3-D perspective, *J. Struct. Geol.*, *25*, 1251–1262, doi:10.1016/S0191-8141(02)00161-X.

White, N. J., J. A. Jackson, and D. P. McKenzie (1986), The relationships between the geometry of normal faults and that of the sedimentary layers in their hangingwall, *J. Struct. Geol.*, *8*, 897–909.

Willemse, E. J. M., D. D. Pollard, and A. Aydin (1996), Three-dimensional analysis of slip distributions on normal fault arrays with consequences for fault scaling, *J. Struct. Geol.*, *18*, 295–309.

Withjack, M. O., K., Meisling, and L. Russell (1989), Forced folding and basement-detached normal faulting in the Haltenbanken area, offshore Norway. *American Association of Petroleum Geologists Memoir*, **46**, in A.J. Tankard, H.R. Balkwill, Editors, *Extensional Tectonics and Stratigraphy of the North Atlantic Margins*, 567–575.

Withjack, M. O., and J. S. Callaway (2000), Active normal faulting beneath a salt layer - an experimental study of deformation in the cover sequence, *AAPG Bull.*, *84*, 627–651.

Xiao, H., and J. Suppe (1992), Origin of rollover, *AAPG Bull.*, *76*, 509–529.

Ziegler, P. A. (1989), Evolution of the North Atlantic: An Overview. *American Association of Petroleum Geologists Memoir*, **46**, in A.J. Tankard, H.R. Balkwill, Editors, *Extensional Tectonics and Stratigraphy of the North Atlantic Margins*, 111–129.

Chapter 3

The transition between thin-skinned and thick-skinned styles of deformation present in the study area

This chapter contains the third scientific article carried out for this thesis, in it we describe the new proposed evolution model for the Burgalesa Platform with thin-skinned to the east and thick-skinned to the west. This model is supported by the surface geology, the subsurface data and the mechanical stratigraphy of the study area. The actual Burgalesa Platform configuration is the result of the partitioning of deformation through space and time and highly influenced by the pre-configuration of the extensional basin and the interaction between different structural units during the Cenozoic contractional stage. The present article has been submitted to the International Journal of Earth Science and it is cited as follows:

Carola, E., Muñoz, J.A., Roca, E. submitted. The transition from basement-involved thick-skinned to detachment thin-skinned tectonics in the Basque-Pyrenees: The Burgalesa Platform and vicinities. ***International Journal of Earth Science.***

Resum

El tercer article presentat en aquesta Tesi es presenta el nou model proposat per explicar l'evolució de la Plataforma Burgalesa durant el Cenozoic i els condicionants que varen actuar resultant en la distribució actual de la zona.

La interpretació de les línies sísmiques als marges de la Plataforma Burgalesa als Pirineus Basco-Cantàbrics ha permès proposar un nou model estructural que combina diferents models de deformació durant la inversió obliqua, condicionada per la distribució dels nivells salins triàsics. La deformació va esser desacoblada per la presència del nivell salí entre els encavalcaments involucrant el sòcol, invertint les falles extensives triàsiques i Juràssic tardà-Cretaci Inferior, i el sistema d'encavalcaments desenganxat el qual involucra les successions sedimentàries des del Triàsic Superior fins al Neogen. Aquests diferents estils de deformació no van ser només superposats a la vertical per sobre i per sota el nivell de desenganxament sinó que aquest canvi d'un estil a l'altre també es dona allarg de la transversal del límit de les sals triàsiques.

El sistema d'encavalcaments que desenganxa la Plataforma Burgalesa va estar confinat entre les estructures involucrant basament del Massís Asturià situat a l'oest i l'extrem més al nord-oest de les estructures que involucren el sòcol de la Cadena Ibèrica (estructura de San Pedro) situat al sud. Aquest fet juntament amb la obliqüitat entre la direcció d'escurçament degut a la contracció Pirenaica i la direcció de les estructures extensives desenvolupades prèviament va determinar la reactivació en direcció de les falles invertides de basament i l'extrusió lateral de la Plataforma Burgalesa, desenganxada sobre el nivell salí, desplaçant-la cap al sud-est formant un arc prominent el qual té una direcció obliqua a la tendència general dels Pirineus. El model proposat combina l'estil estructural *thick-skinned* amb el *thin-skinned* durant la inversió tectònica obliqua i és consistent amb les dades de superfície, incloent el patró de fractures, les dades de subsòl disponibles i l'estratigrafia mecànica.

Abstract

The third paper presented in this Thesis proposed a new model in order to explain the evolution of the Burgalesa Platform during the Cenozoic and the elements that acted resulting in the actual distribution of the studied area.

Interpretation of seismic data at the margins of the Burgalesa Platform in the Basque-Cantabrian Pyrenees has allowed proposition of a new structural model that combines different modes of deformation during oblique tectonic inversion, conditioned by the distribution of Triassic salts. Deformation was decoupled by the presence of the salt horizon between basement-involved thrusts inverting formerly Triassic and Late Jurassic-Early Cretaceous extensional faults and a detached thrust system involving the Upper Triassic to Neogene sedimentary package. Such different styles of deformation were not only stacked vertically above and below the salt, but most importantly, they change from one to the other along strike across the transversal edges of the Triassic salts.

The Burgalesa Platform detached thrust system was confined between the basement-involved structures of the Cantabrian Mountains westward and the NW tip of the Iberian basement-involved structures (San Pedro) southward. This together with the obliquity between the Pyrenean contractional shortening direction and the strike of the previous extensional faults, mostly at the late stages of deformation, determined the strike-slip reactivation of the basement-involved inverted faults and the lateral extrusion of the Burgalesa Platform detached Mesozoic successions above the salt toward the SE to form a prominent thrust salient oblique to the main Pyrenean trend. The proposed model combines thick-skinned with thin-skinned structural styles during oblique tectonic inversion and is consistent with the surface data, including the fracture system, the available subsurface data and the mechanical stratigraphy.

The transition from basement-involved thick-skinned to detachment thin-skinned tectonics in the Basque-Pyrenees: The Burgalesa Platform and vicinities.

Eloi Carola[1]*, Josep Anton Muñoz[1], Eduard Roca[1]

[1]*GEOMODELS Research Institute, Departament de Geodinàmica i Geofísica, Universitat de Barcelona. C/ Martí Franquès s/n. 08028 Barcelona, Spain*

* Corresponding author: Eloi Carola.
e.carola@ub.edu; eloicarola@gmail.com
Universitat de Barcelona, Facultat de Geologia.
C/ Martí Franquès s/n
08028 Barcelona
Tel.: +34 934034028

Bullets:

- Determination of the transition from thick-skinned to thin-skinned in the Burgalesa Platform of the Basque-Pyrenees.

- New interpretation model for the Burgalesa Platform with thick-skinned tectonics at the western boundary and thin-skinned tectonics at the eastern one.

- Thickness distribution of the Upper Triassic salt allowed the detachment of the Mesozoic succession.

Keywords: Thick-skinned; Thin-skinned; Inversion Tectonics; Basque-Pyrenees; Cantabrian Mountains; Burgalesa Platform.

Abstract

Interpretation of seismic data at the margins of the Burgalesa Platform in the Basque-Cantabrian Pyrenees has allowed proposition of a new structural model that combines different modes of deformation during oblique tectonic inversion, conditioned by the distribution of Triassic salts. Deformation was decoupled by the presence of the salt horizon between basement-involved thrusts inverting formerly Triassic and Late Jurassic-Early Cretaceous extensional faults and a detached thrust system involving the Upper Triassic to Neogene sedimentary package. Such different styles of deformation were not only stacked vertically above and below the salt, but most importantly, they change from one to the other along strike across the transversal edges of the Triassic salts. The Burgalesa Platform detached thrust system was confined between the basement-involved structures of the Cantabrian Mountains westward and the NW tip of the Iberian basement-involved structures (San Pedro) southward. This together with the obliquity between the Pyrenean contractional shortening direction and the strike of the previous extensional faults, mostly at the late stages of deformation, determined the strike-slip reactivation of the basement-involved inverted faults and the lateral extrusion of the Burgalesa Platform detached Mesozoic successions above the salt toward the SE to form a prominent thrust salient oblique to the main Pyrenean trend. The proposed model combines thick-skinned with thin-skinned structural styles during oblique tectonic inversion and is consistent with the surface data, including the fracture system, the available subsurface data and the mechanical stratigraphy.

1 Introduction

Structural style of orogenic systems depends on many factors such as crustal rheology, inherited structure or distribution of weak horizons (Ellis *et al.*, 1998; Beaumont *et al.*, 2000; Bug and Greya, 2005; Butler *et al.*, 2006; James and Huismans, 2012). Positive inversion tectonics, understood as the contractional reactivation of an extensional fault, has been documented since the 1980's in sedimentary basins using seismic data (e.g. Badley *et al.*, 1989; Chapman, 1989), field studies (e.g. Schröder, 1987; Butler, 1989) and analogical modelling (e.g. Koopman *et al.*, 1987; McClay, 1989). During the inversion and with the progressive incorporation of the basin into the fold and thrust belt, several geological features must be taken into account. Among others: i) the position of inherited extensional faults causing weak points within the crust and acting these as preferential deformational paths (e.g. Coward, 1994; Holdsworth, 2004; Sepher and Cosgrove, 2005; Carrera *et al.*, 2006;

Mouthereau and Lacombre, 2006, Amilibia *et al.*, 2008, among others); ii) the rheology of materials and the presence of weak layers promoting the partition of deformation and controlling the evolution during inversion or the decoupling between the cover and the basement (e.g. Davis and Engelder, 1985, Bassi G. 1995; Steward *et al.*, 1997; Steward and Argent, 2000); iii) the variation in stratigraphic thickness or lateral changes in facies inside the basins, due to differential subsidence, fault activity, salt mobilization or erosion controlling the spacing and distribution of main faults as well as the position of lateral structures and its propagation in space (e.g. Davis and Engelder 1985; Jaumé and Lillie, 1988; Calassou *et al.*, 1993; Boyer, 1995; Mitra, 1997; Corrado *et al.*, 1998; Macedo and Marshak, 1999; Fischer and Jackson, 1999; Soto *et al.*, 2002; Spratt *et al.*, 2004; Marshak, 2004; Pfiffner, 2006). All these parameters result in two different styles of deformation during the evolution of the thrust belt. Thick-skinned tectonics, in which the basement is involved such as the inner parts of some orogens like the Alps, the Pyrenees or the Andes contrasting with the thin-skinned tectonics in which the cover is detached from the basement such as the external parts of the Pyrenees or the Zagros among others. Additionally, some orogens present along-strike or along-time variation in the style of deformation (Hill *et al.*, 2002; Mazzoli *et al.*, 2008).

These two styles of deformation are present in the Basque-Pyrenees and the Cantabrian Mountains of the Pyrenees. The first, with thin-skinned tectonics with the Mesozoic cover detached from the basement at the Upper Triassic salt layer. The second, with thick-skinned tectonics with the basement involved within the structures (Muñoz, 1992, 2002; Alonso *et al.*, 1996, Pulgar *et al.*, 1999; Vergés *et al.*, 2002; Gallastegui, 2000; Roca *et al.*, 2011). The Burgalesa Platform is the area where the along-strike transition between the two styles occurs. Both thin-skinned and thick-skinned tectonic models have been proposed in order to explain the evolution of the area either with surface geology or subsurface data thus explaining the surface geology (Hernaiz, 1994; Hernaiz *et al.*, 1994; Malagón *et al.*, 1994; Rodríguez-Cañas *et al.*, 1994; Serrano *et al.*, 1994; Espina *et al.*, 1996; Espina, 1997; Pulgar *et al.*, 1999; Gallastegui, 2000; Tavani *et al.*, 2011; Quintana, 2012). The aim of this work is in one hand, to integrate the surface and subsurface data with the observations and constraints reported by other authors in order to propose a new evolution model for the Burgalesa Platform. This model contains the transition between the two styles of deformation present along-strike of the studied area. On the other hand, to better characterise the configuration of the extensional basin that controlled the contractional deformation during the Pyrenean Orogeny and the implication that it had.

2 Geological setting

The structural evolution of the doubly-vergent Pyrenean Orogen was controlled by the inversion of Lower Cretaceous extensional basins (Beaumont *et al*., 2000; Jammes *et al.*, 2014). The extensional event related to the opening of the North Atlantic and the Bay of Biscay during Late Jurassic-Early Cretaceous resulted in the development of intracontinental basins at the rift margins, the exhumation of continental mantle at the last stages of rifting, and the spreading of oceanic crust at the western Bay of Biscay ridge (Roca *et al*., 2011). This event allowed the local deposition of more than 10 km of syn-rift sediments overlying the Jurassic carbonates and the stretched and thinned continental crust (e.g. Le Pichon and Sibuet, 1971; Montadert *et al*., 1979; García de Cortázar and Pujalte, 1982; Pujalte, 1982; Mathieu, 1986; Ziegler, 1987; García-Mondéjar *et al.*, 1996; Bois *et al.*, 1997; Pedreira *et al.*, 2007; Ruiz, 2007; Ferrer *et al.*, 2008; Jammes *et al.*, 2009, Roca *et al.*, 2011). The convergence between the Eurasian and the Iberian plates during Late Cretaceous-Cenozoic produced the subduction of Iberia towards the north, with the subsequent inversion of the inherited Mesozoic basins (e.g. Le Pichon and Sibuet, 1971; Muñoz, 1992, 2002; Alonso *et al.*, 1996; Vergés and García-Senz, 2001). The along strike structural changes of the Pyrenean orogen resulted from the inversion of a segmented rift system at the northern Iberian margin (Roca *et al.*, 2011). Thus, the Cantabrian Mountains, the Basque-Pyrenees and the Pyrenees s.s. are distinct structural domains of the Pyrenean orogen bounded by transfer faults inherited from the previous Early Cretaceous extensional system (Fig. 1A).

The Cantabrian Mountains, at the western part of the Pyrenean orogen (Fig. 1A and B), are constituted by Paleozoic rocks deformed during both the Variscan Orogeny (Pérez-Estaún *et al.*, 1991) and the Pyrenean Orogeny, as well as by the Permian, Triassic and Late Jurassic-Early Cretaceous extensional events. Pyrenean contractional deformation caused the reactivation of the Variscan faults and the tightening and steepening of previously developed folds (Pérez-Estaún *et al.*, 1988; Alonso *et al.*, 1996; Pulgar *et al.*, 1999; Alonso *et al.*, 2009). Most of the contractional deformation has been accommodated into the northern retro-wedge along the Cantabrian margin. In the southern part (pro-wedge) the thrust system involves the Variscan basement and displaced the Cantabrian Mountains towards the south over the Duero foreland basin (Álvarez-Marrón *et al.*, 1996; Pulgar *et al.*, 1997; Gallastegui, 2000; Gallastegui *et al.*, 2002; Pedreira, *et al.*, 2003; Pedreira *et al.*, 2007; Roca *et al.*, 2011; Martín-González and Heredia, 2011, among others). The thrust front mostly corresponds to a fault propagation

fold with its related frontal thrust only outcropping in some areas (Fig. 1A and B). As a result, the Duero basin shows a major syncline geometry.

Further east the Basque-Pyrenees (Fig. 1A and C) resulted from the inversion of the W-E striking Upper Jurassic-Lower Cretaceous Basque-Cantabrian Basin during the Pyrenean deformation. This is one of the basins that were developed at the southern passive margin of the Bay of Biscay. The Basque-Pyrenees are displaced southward more than 15 km over the Ebro Foreland Basin by means of a south-directed low-angle thrust detached into the Upper Triassic evaporites (Martínez-Torres, 1993; Carola *et al.*, 2013). The frontal structure (Sierra de Cantabria Frontal Thrust) and associated folds present a north-facing concave shape in map view where in the central parts they strike almost W-E whereas, at the edges they progressively rotate to a more WSW-ENE and NW-SE orientation in the east and west respectively (Fig. 1A).

In continuation with the Cantabrian Mountains and to the southwest of the Basque-Pyrenees there is a distinct structural domain known as Burgalesa Platform (Fig. 1A). It consists of a moderately deformed succession of Triassic to Upper Cretaceous sediments with some preserved syn-tectonic Miocene continental rocks. The Burgalesa Platform shows a thrust salient with a prominent bend at its eastern edge where structures change the trend from WNW-ESE to NE-SW (Fig. 1A).

There is not a consensus as far as the tectonic style and the structural evolution of the Burgalesa Platform are concerned. Different structural models have been proposed during the last decades, among them the most distinct ones are: i) low-angle thin-skinned; ii) low-angle thick-skinned, and iii) transpressive high-angle thick-skinned (Fig. 1D). In the thin-skinned model, the Jurassic-Cretaceous succession is detached from the Variscan basement into the Triassic evaporites and transported at least 10 km southward (Hernaiz, 1994; Hernaiz *et al.*, 1994; Malagón *et al.*, 1994; Rodríguez-Cañas *et al.*, 1994; Serrano *et al.*, 1994).

The low-angle thick-skinned model is based on the existence of a basement-involved low-angle thrust below the Mesozoic succession, in continuation with the floor thrust of the thrust system deforming the Cantabrian Mountains (Espina *et al.*, 1996; Alonso *et al.*, 1996; Espina, 1997; Pulgar *et al.*, 1999; Gallastegui, 2000; Alonso *et al.*, 2007; Quintana, 2012). Finally, in the third model the contractional structures are transpressive elements related with high-angle and deeply-rooted right-lateral strike-slip faults, such as the Ubierna fault (Tavani *et al.*, 2011). The

implication of this third model is that the Burgalesa Platform Domain would represent an uplifted area of the deformed Duero foreland.

These contrasting models are based on different data sets, mostly from surface geology, that at least partially support the proposed structural evolution for each model. A question arises about which of these models is the most consistent with all the available data in the area (surface and subsurface) and compatible with other considerations such as the inherited structures, the mechanical stratigraphy of the rocks involved or the kinematics of the area. This work brings together subsurface and surface data in order to discuss a new model. Any proposed structural model would have to consider the Late Jurassic-Early Cretaceous extensional faults that deformed the area as well as the presence of a thick layer of Triassic salts as drilled by numerous wells.

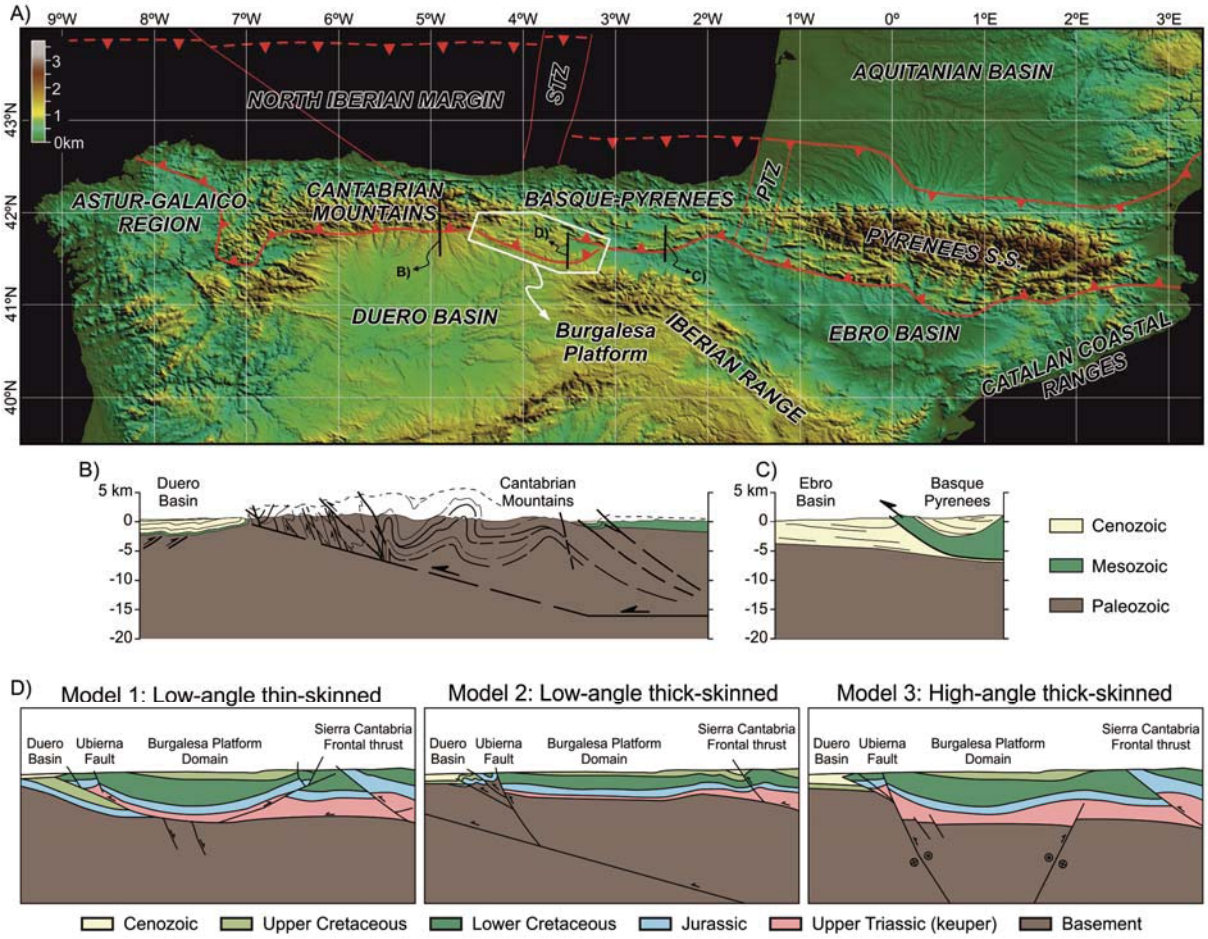

Figure 1: A) Elevation map of the W-E Pyrenean Orogen and surroundings with the major domains labelled. STZ and PTZ corresponds to Santander and Pamplona Transfer Zones respectively. B and C) S-N cross-sections of the Cantabrian Mountains and the Basque-Pyrenees (Modified from Pulgar *et al.*, 1999; Riba and Jurado, 1992). D) Schematic S-N models purposed by different authors in order to explain the main features and the deformation style of the Burgalesa Platform Domain and adjacent areas.

3 Tectonostratigraphic units of the Burgalesa Platform

The stratigraphic succession of the study area can be divided into several units, which are associated to the different tectonics events that took place from Triassic to Cenozoic times (Fig. 2).

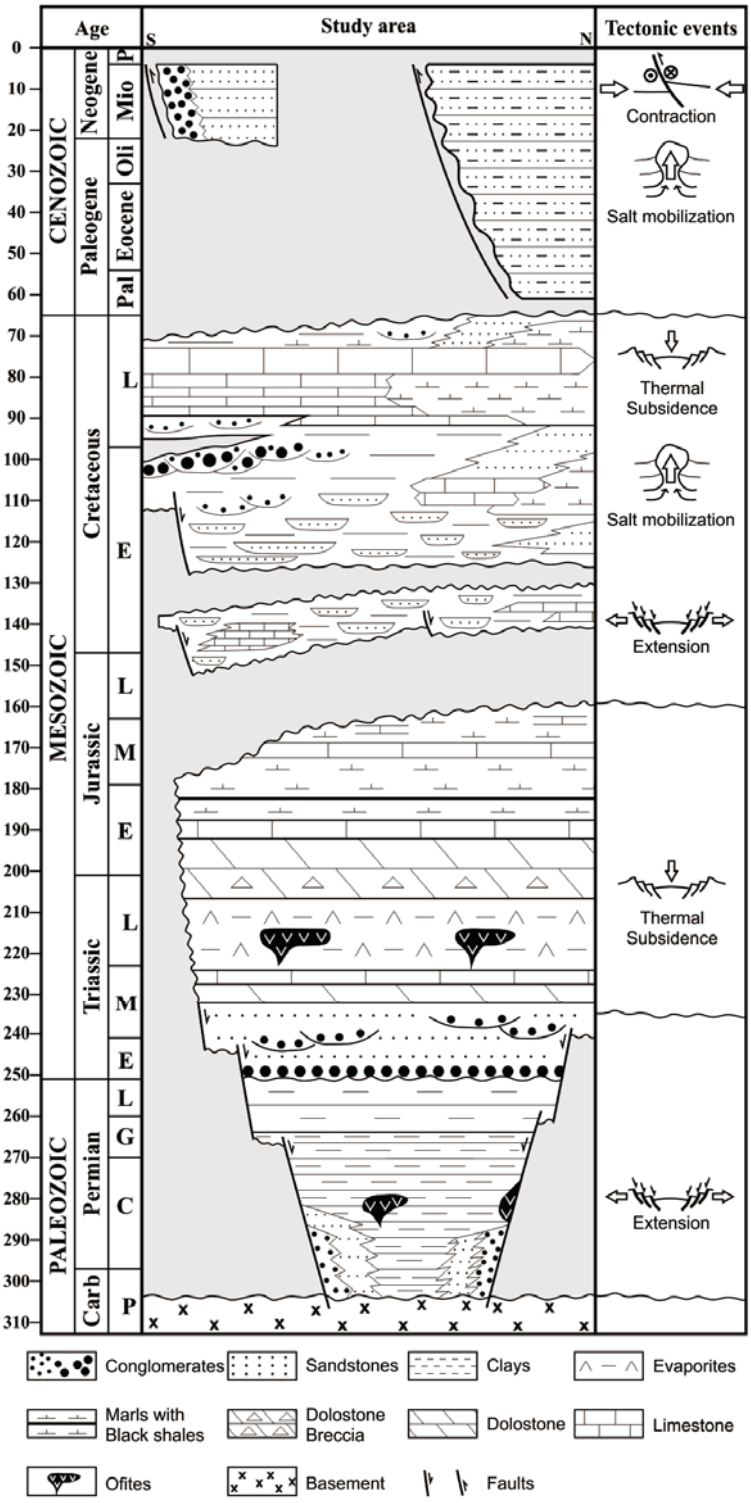

Figure 2: Cronostratigraphic column of the study area with the main tectonic events that took place. (Partially modified from Barnolas and Pujalte, 2004).

The Paleozoic succession is made up of Ordovician quartzites and phyllites , Devonian ferruginous sandstones, Carboniferous limestones and Permian clays. The Lower to Middle Triassic sediments are constituted by conglomerates and sandstones of the Buntsandstein facies and dolostones of the Muschelkalk facies, which are associated to the rifting stage that produced the breakup of Pangea (Van Veen, 1965; Wagner *et al.*, 1971; García-Mondéjar *et al.*, 1986; Alonso, 1987). All the pre-Upper Triassic succession is referred as basement throughout the paper.

Above, the Upper Triassic Keuper facies consists of salt, anhydrite, gypsum and shales with sub-volcanic basic intrusions. This unit is the most important detachment level. Its ability to flow under the right conditions is the responsible of its irregular distribution as evidenced by the amount of diapirs present in the study area (i.e. Aguilar (Serrano and Martínez del Olmo, 2004), Poza de la Sal (Hempel, 1967; Quintà *et al.*, 2012), Salinas del Rosío (Hernáiz and Solé, 2000), among others). This unit is widespread all along the Pyrenees, although it is absent in significant areas (i.e. eastern Pyrenees, aragonese western Pyrenees) as well as in the Cantabrian Mountains.

After the Triassic extensional event, a quiescence stage took place during the Jurassic. This period of time is characterised by the development of a carbonate ramp, mainly limestones and dolostones with interbedded evaporites at the lower parts of the unit. Whereas, deep marine hemipelagic sediments with limestones, marls and shales characterise the upper portions of this unit (Pujalte *et al.*, 1988; Robles *et al.*, 1989, 2004; Quesada *et al.*, 1991, 1993, 2005; Aurell *et al.*, 2003).

The second and main extensional event is related to the opening of the North Atlantic and the Bay of Biscay during the Late Jurassic to Early Cretaceous. The stratigraphic record of this period in the Burgalesa Platform is characterised by fluvio-deltaic siliciclastic sandstones that locally reach more than 4 km (Pujalte, 1981, 1982; Pujalte *et al.*, 1996, 2004; Hernández *et al.*, 1999). Forced folding of the Jurassic succession and salt mobilization took place during this extensional event (Tavani *et al.*, 2013).

The upper Albian-Upper Cretaceous succession is made up of conglomerates and sandstones at the base and limestones and marls at the top post-dating the Early Cretaceous extension. It is associated to a gradual deepening of the succession passing from continental to marine environment during several transgressive events (Aguilar, 1971; Ramirez del Pozo, 1971; Portero, 1979).

The Cenozoic syn-orogenic sediments are mainly constituted by conglomerates, sandstones and red clays. The pebbles and cobbles are mainly from the Upper Cretaceous limestones and dolostones (Portero *et al.*, 1979). This unit is restricted to the border of the study area (i.e. Ebro and Duero foreland basins) and also in the Bureba Sub-basin and Villarcayo syncline (Fig. 3).

4. Structure of The Burgalesa Platform

The internal structure of the Burgalesa Platform is dominated at surface by wide and gentle folds with very shallow dips affecting the Upper Cretaceous limestones. Most of the contractional structures are located between the thrust front and the Ubierna fault where they define a narrow belt of folds and related thrusts (Folded Band, Fig. 3). North of the Ubierna fault there is a structural continuity between the Cantabrian Mountains and the Burgalesa Platform at surface as evidenced by a continuous tilted panel towards the ESE of Triassic to Upper Cretaceous rocks overlying the Variscan basement (Fig. 3). To the north, there is also an apparent structural continuity with the Basque-Pyrenees, although a series of anticlines and faults connect the structures in the Ebro reservoir area with the Sierra de Cantabria Frontal Thrust, thus representing the northern edge of the Burgalesa Platform (Fig. 3). The SE part of the Burgalesa Platform is characterised by NE-SW trending folds (Hontomín flexure, Rojas), along which salt structures occur (Poza de la Sal, Hontomín and Rojas domes). These folds developed during the sedimentation of the Miocene fluvial deposits that finally covered them, masking the relationships between the NE-SW structures, the Ebro Basin and the Sierra de Cantabria frontal thrust. The upper and younger Miocene conglomerates define a re-entrant in map view between the Sierra de Cantabria thrust front and the Burgalesa Platform (Fig. 3).

At surface the significance of such re-entrant cannot be deciphered, mostly if it is only the result of the unconformable disposition of the Miocene conglomerates over the NE-SW structures that would connect with the Sierra de Cantabria thrust or if, alternatively, represents a structural re-entrant of the Ebro Basin between the Basque-Pyrenees and the Burgalesa Platform. The solution given to this uncertainty has a strong impact on the structure and the deduced structural evolution of the Burgalesa Platform and can only be resolved by subsurface data as will be discussed later on. The Miocene syn- to post-tectonic sediments of the Duero Basin also mask the frontal structure of the Burgalesa Platform and also the available subsurface data is crucial for its proper understanding.

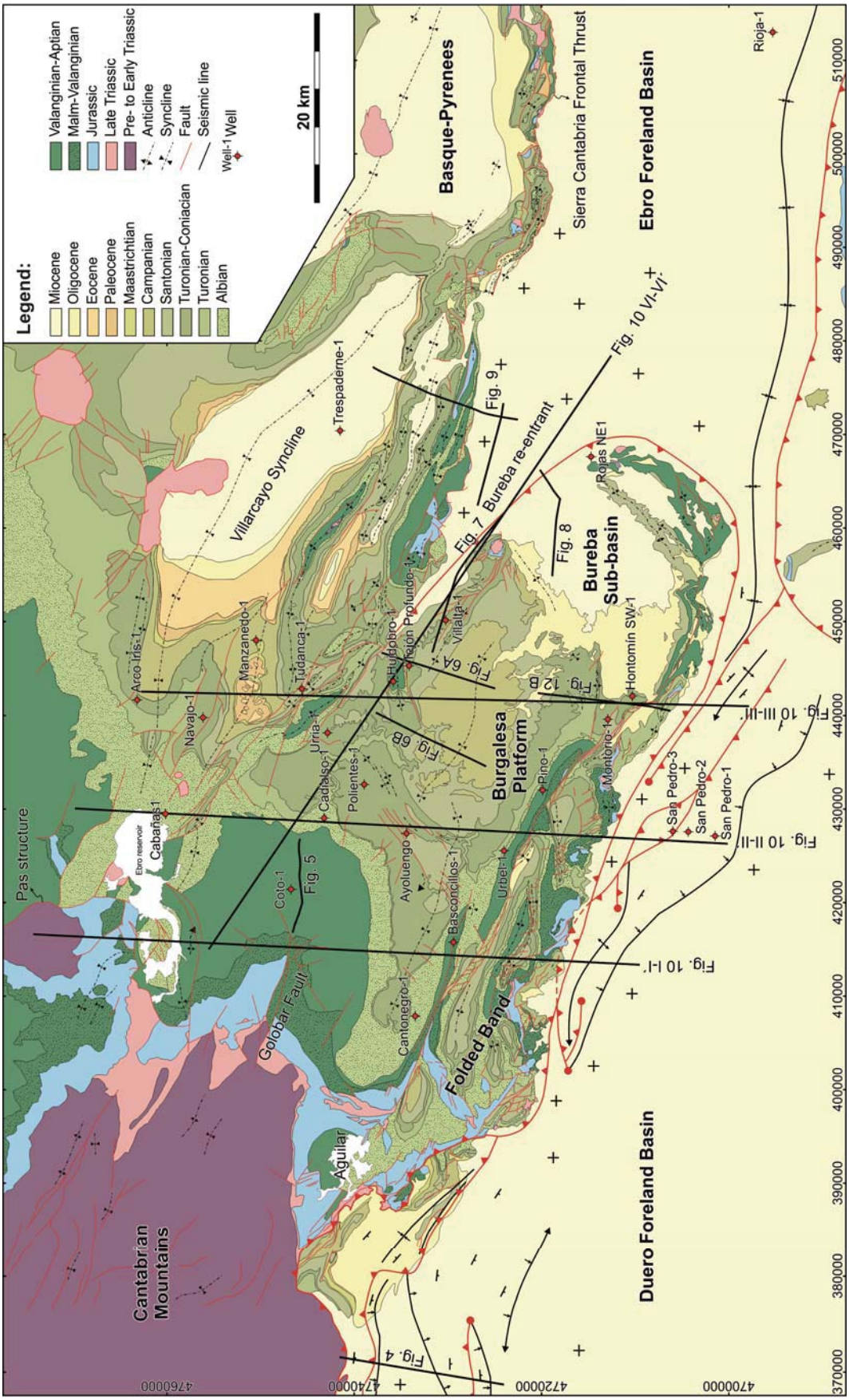

Figure 3: Geological map of the Burgalesa Platform and surroundings with the location of the different seismic lines, wells and cross-sections shown in this work as well as the foreland deformation interpreted from the seismic sections.

Here below the main structural features of the Burgalesa Platform and its relationships with the surrounding units will be discussed in detail taken advantage of the available seismic sections and well data acquired in the area for hydrocarbon exploration.

4.1. Interpretation of the seismic and well data

A seismic profile across the Cantabrian Mountains thrust front, west of the Burgalesa Platform, shows the thick-skinned structural style of this unit as well as its relationships with the Duero foreland basin (Fig. 4). The floor of the Paleogene-Neogene Duero Basin is characterised by a continuous and constant thickness succession of the upper Albian-Upper Cretaceous post-rift sediments (sandstones of the Utrillas Fm. and limestones) unconformably overlying the Paleozoic basement rocks (Gallastegui, 2000). These sediments crop out at surface in the hangingwall of the frontal thrust with subvertical to overturned northward steeply dipping beds structurally above the Devonian rocks. The bedding attitude of the Cretaceous sediments in the hangingwall together with the location of the south-dipping reflections of the equivalent succession in the seismic section define the frontal syncline of a fault propagation fold and demonstrate the reduced displacement of the frontal thrust in the subsurface. Moreover, this thrust does not reach the surface as the younger syn-orogenic Neogene conglomerates, adjacent to the thrust front, show a progressive unconformity above the Paleogene vertical conglomerates that overlie the Upper Cretaceous limestones (Fig. 4). Thrusts and related folds also affect the basement and the Upper Cretaceous sediments in the Duero foreland basin. Their displacement caused growth geometries in the younger Neogene clastic sediments (Fig. 4).

An E-W seismic profile across the eastward tilted panel of Triassic to Lower Cretaceous stratigraphic units illustrates the transition between the eastern edge of the Cantabrian Mountains and the Burgalesa Platform Domain (Fig. 5). In this section, the east-dipping panel of continuous and strong reflections attributed to the Jurassic and to the Lower Cretaceous terminates in a syncline. Below the Mesozoic tilted panel, a set of west-dipping reflections has been imaged into the chaotic seismic facies of the basement between 3,5 and 2 TWT seconds (Fig. 5). It has been considered as a continuous seismic event, which merges with the axial surface of the above described syncline at the bottom of the Mesozoic succession, and interpreted as a thrust involving the basement of the Cantabrian Mountains, climbing up section laterally into the Upper Triassic evaporites of the Burgalesa Platform.

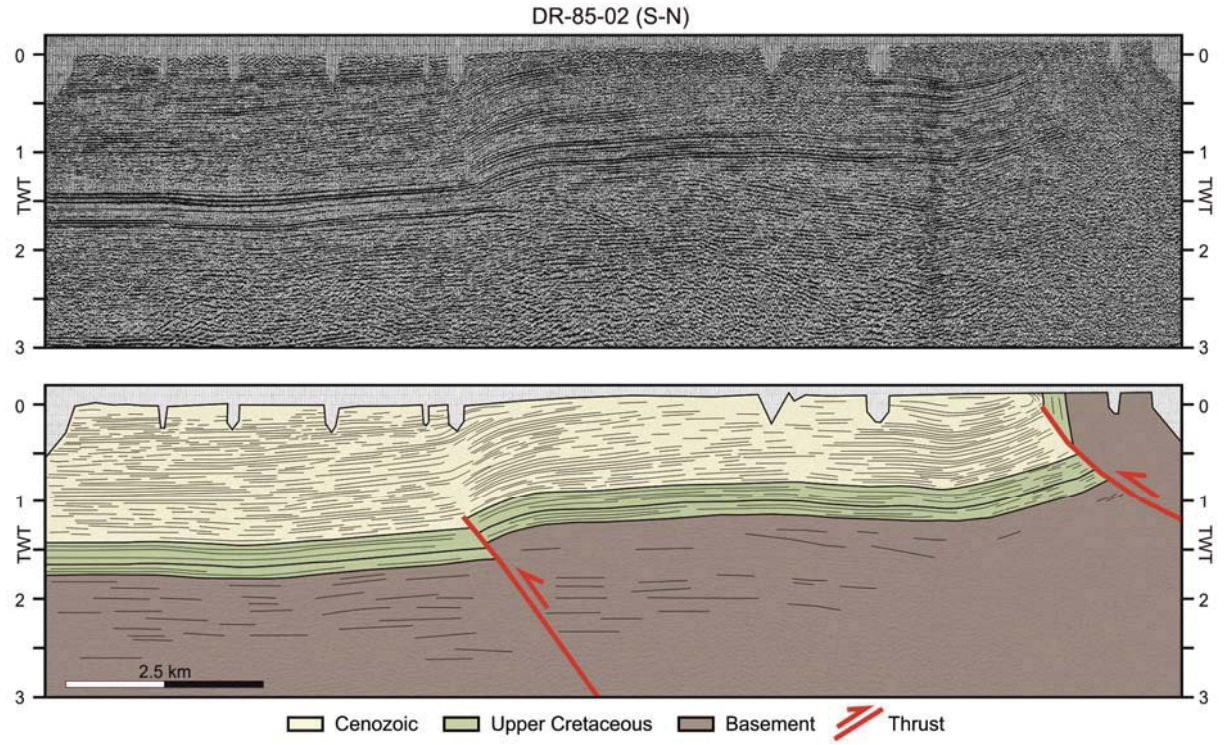

Figure 4: S-N seismic section of the Duero Foreland Basin and the eastern part of the Cantabrian Mountains with thrusts affecting the Cenozoic succession as well as the Mesozoic and the basement. See figure 3 for location.

This structure has the same structural position as the frontal anticline of the Cantabrian Mountains in the hangingwall of the floor thrust of the basement-involved thrust system, but differently with respect to the Duero basin the thrust was not emergent as it detached into the Triassic salts. Thus, east of the syncline, the Mesozoic succession of the Burgalesa Platform has been detached above the basement.

Detachment of the Burgalesa Platform from the basement can also be deduced from the interpretation of the seismic lines located further east. Two seismic lines across the Huidobro anticline, at the northern edge of the Burgalesa Platform, reveal a significant structural relief of the Jurassic succession above a continuous set of gently northward-dipping reflectors interpreted as the top of the basement (Fig. 6). The identification of the different packages of reflectors relies not only on their seismic facies, but also on the data supplied by the Tejón Profundo-1 well in the S-84-110 seismic line (Fig. 6A). The Tejón Profundo-1 well, drilled in the Huidobro anticline, encountered a repetition of the Mesozoic succession at 1700 meters below the surface.

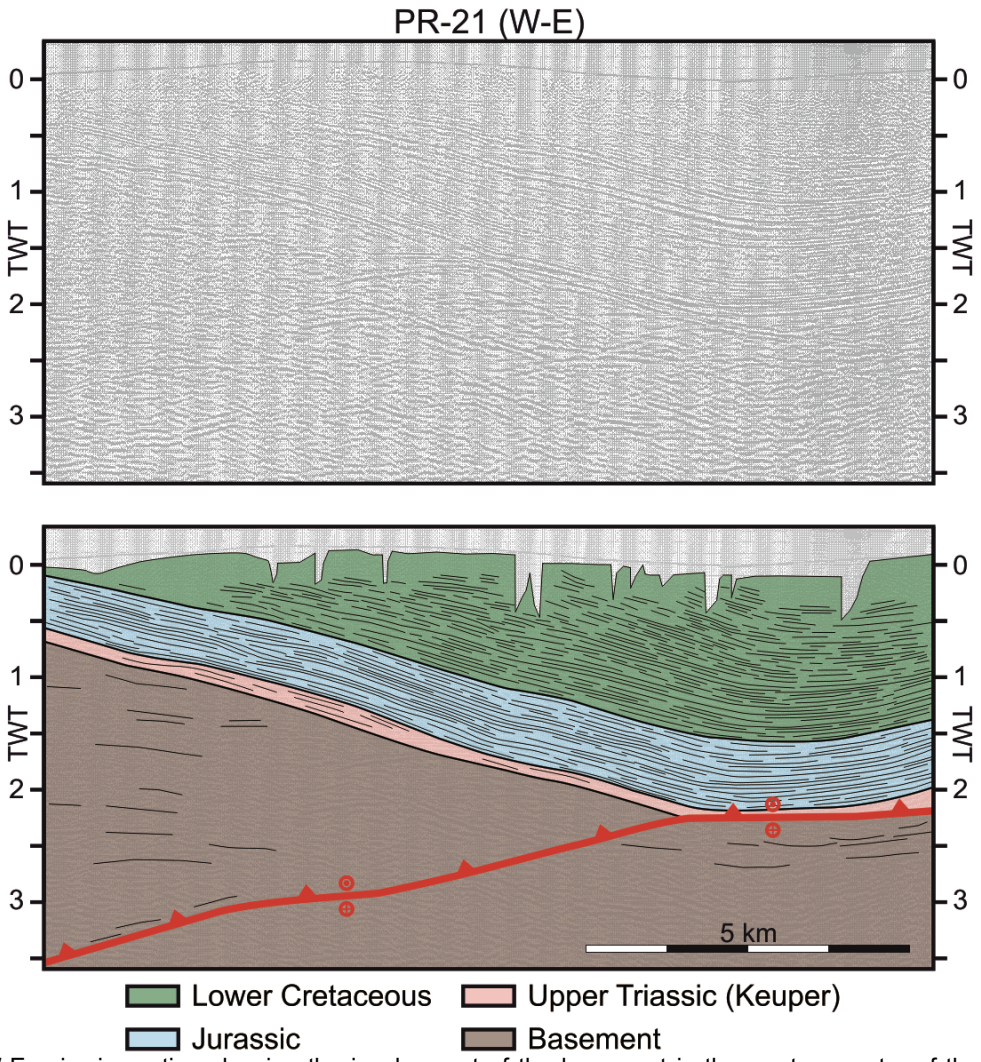

Figure 5: W-E seismic section showing the involvement of the basement in the western sector of the Burgalesa Platform producing the plunge observable in the Mesozoic succession at surface. See figure 3 for location.

In addition, the register shows a thick salt succession (1200 m) underneath the lower Jurassic without reaching the bottom of the Keuper at the end of the well (3800 m.b.s.). The most puzzling geometry revealed by these seismic lines and the well is the mismatch of the positive structural relief when comparing the top of the Jurassic succession and the bottom of the Upper Cretaceous sediments. The amplitude of the anticline related to the back-thrust that duplicated the Jurassic and Lower Cretaceous beds decreases significantly in the Upper Cretaceous succession. Moreover, there are no evidence of growth sediments into this succession and, most importantly, these sediments where deposited before the onset of the Pyrenean convergence. The Lower Cretaceous succession presents a thickening towards the south being this succession almost twice thicker than the succession in the Huidobro anticline where, in its turn, the Upper Triassic is significantly thicker. These relationships reveal salt withdrawal and salt inflation (Fig. 6).

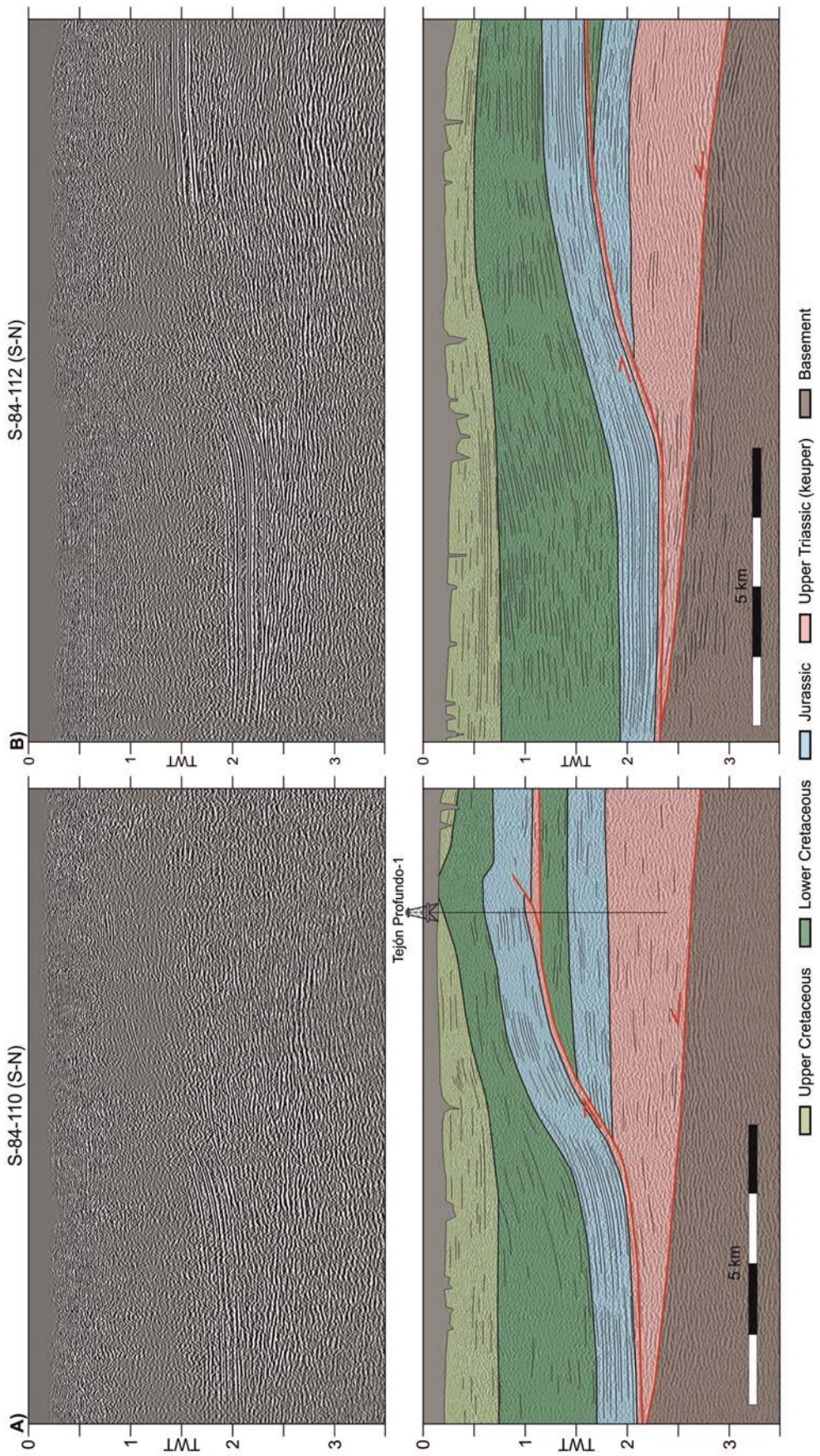

Figure 6: S-N seismic sections located in the Huidobro area where the Tejón Profundo-1 well testifies a repetition of the Mesozoic succession and how this back-thrust is imaged in the lines. Note how the structural relief decreases westwards. See figure 3 for location.

East of the Huidobro anticline, the northern edge of the Burgalesa Platform is characterised by the NW-SE trending Villalta anticline (Fig. 3). An oblique seismic section across it shows its structure at depth (Fig. 7). The Upper Triassic to Jurassic succession of the NE limb of the anticline is involved into a hangingwall ramp above a flat-lying thrust that would be the eastward continuation of the back-thrust imaged in the Huidobro anticline by N-S trending seismic profiles (Figs. 6 and 7). The flat-lying reflections in the footwall would be in continuation with the Lower Cretaceous to Triassic succession drilled by the Tejón Profundo-1 well underneath the Huidobro back-thrust. These sediments are involved in the Poza de la Sal antiform and the related salt structure (Figs. 3 and 7). In the central sector of the seismic profile the shallower Mesozoic-Cenozoic reflectors appear folded in contrast with the flat-lying reflectors underneath at 2 TWT seconds. In the easternmost part, the Cenozoic and Upper Cretaceous sediments of the foreland basin have been imaged by more than 2 TWT seconds of strong, continuous and parallel reflections. They present similar signature and seismic facies as shown by seismic profiles in the Duero Basin further to the west.

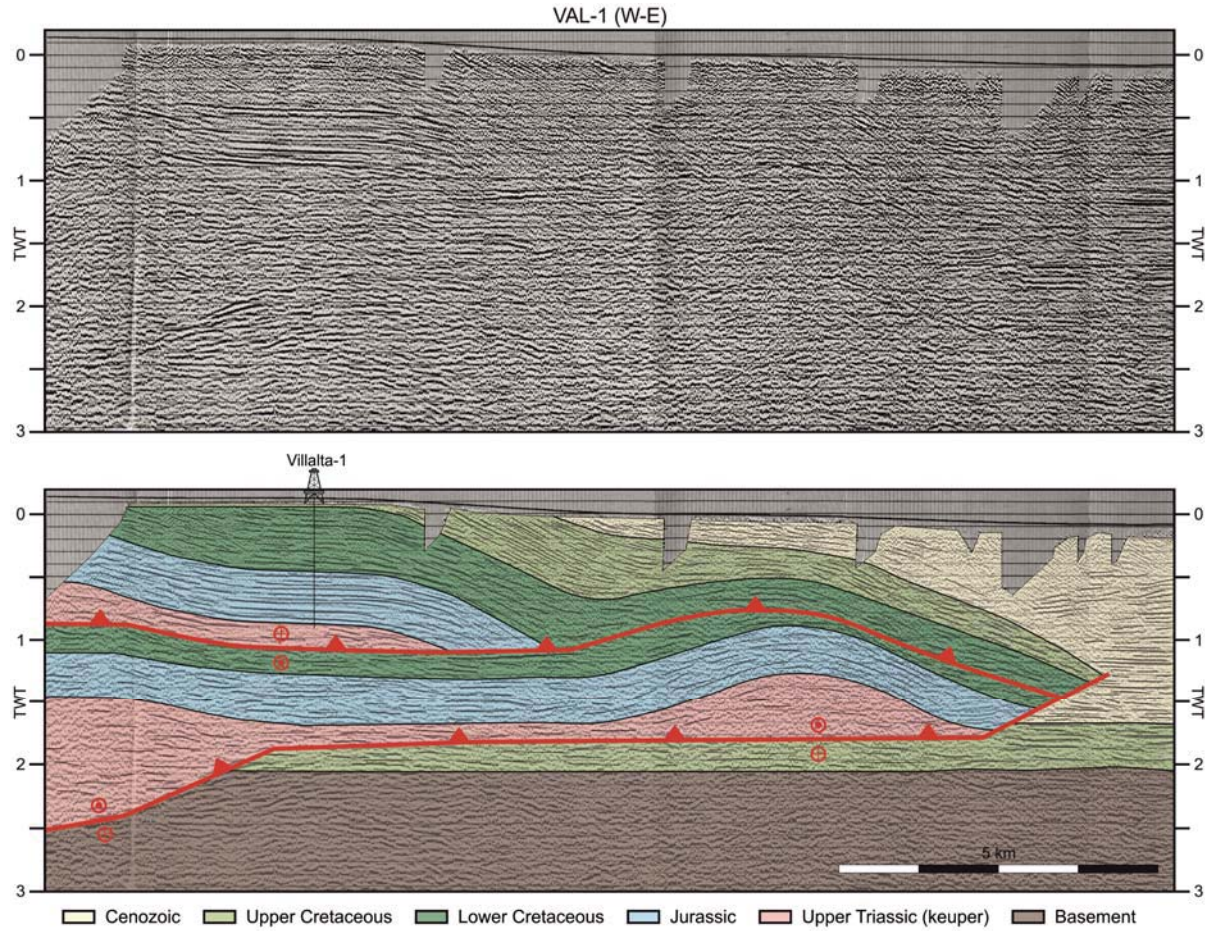

Figure 7: W-E seismic section in the Villalta area showing the hangingwall cutoff of the back-thrust present in this sector of the Burgalesa Platform. The deeper reflectors show the transversal extensional fault delimiting the former Basque-Cantabrian Basin and how during the inversion of the basin, the Mesozoic succession was south-eastwards displaced favoured by the presence of the Upper Triassic salts acting as a detachment level. See figure 3 for location.

The lower reflections are characterised by an upper continuous and high amplitude set of reflectors above a semitransparent unit and a lowermost unit of continuous reflections lying above the acoustic basement. These 3 seismic units correspond to the Upper Cretaceous succession of the Duero Basin, which has been drilled by numerous exploration wells (compare Figs. 7 and 4, Gallastegui, 2000). The Cenozoic sediments progressively cover the allochtonous Mesozoic units towards the west, although the sole thrust truncates the lower ones. West of the thrust front the reflectors corresponding to the autochthonous Upper Cretaceous are difficult to follow westward underneath the sole thrust. They are truncated at the western edge of the profile by a strong west-dipping reflection that has been interpreted as a footwall ramp of the sole thrust.

The SE edge of the Burgalesa Platform corresponds to the NE-SW trending Rojas anticline (Fig. 3). A seismic section across the northern continuation of the Rojas anticline below the Miocene sediments shows a frontal thrust and a related anticline similar to and in continuation with the frontal structure described in the previous seismic section (Figs. 7 and 8). As a result, the geometry of the thrust front at the SE edge of the Burgalesa Platform would show a significant thrust salient, concave to the WNW, if the younger Miocene sediments would be removed. The seismic section of Figure 8 shows the relationships between the Burgalesa Platform and the Ebro foreland basin at its westernmost reentrant between the Burgalesa Platform and the Basque-Pyrenees (Fig. 3). In the eastern portion of the section, the foreland is imaged as a layer cake succession of strong and continuous reflectors of the Cenozoic and Upper Cretaceous sediments. The thrust truncates the lower part of the Cenozoic succession and its related anticline shows growing relationships with the middle to upper part of the Cenozoic foreland basin sediments corresponding to the Early to Middle Miocene. The western part of the seismic section is dominated by a wedge of Lower Cretaceous sediments sandwiched between lower subhorizontal reflectors, Jurassic in age, and an upper east-dipping panel of Upper Cretaceous sediments. The Lower Cretaceous wedge thins eastward and the reflectors onlap onto the Jurassic succession.

A seismic section located northeastward of the Burgalesa Platform and crossing the Sierra de Cantabria Frontal Thrust shows the thin-skinned tectonic style of deformation in this part of the orogen (Fig. 9).

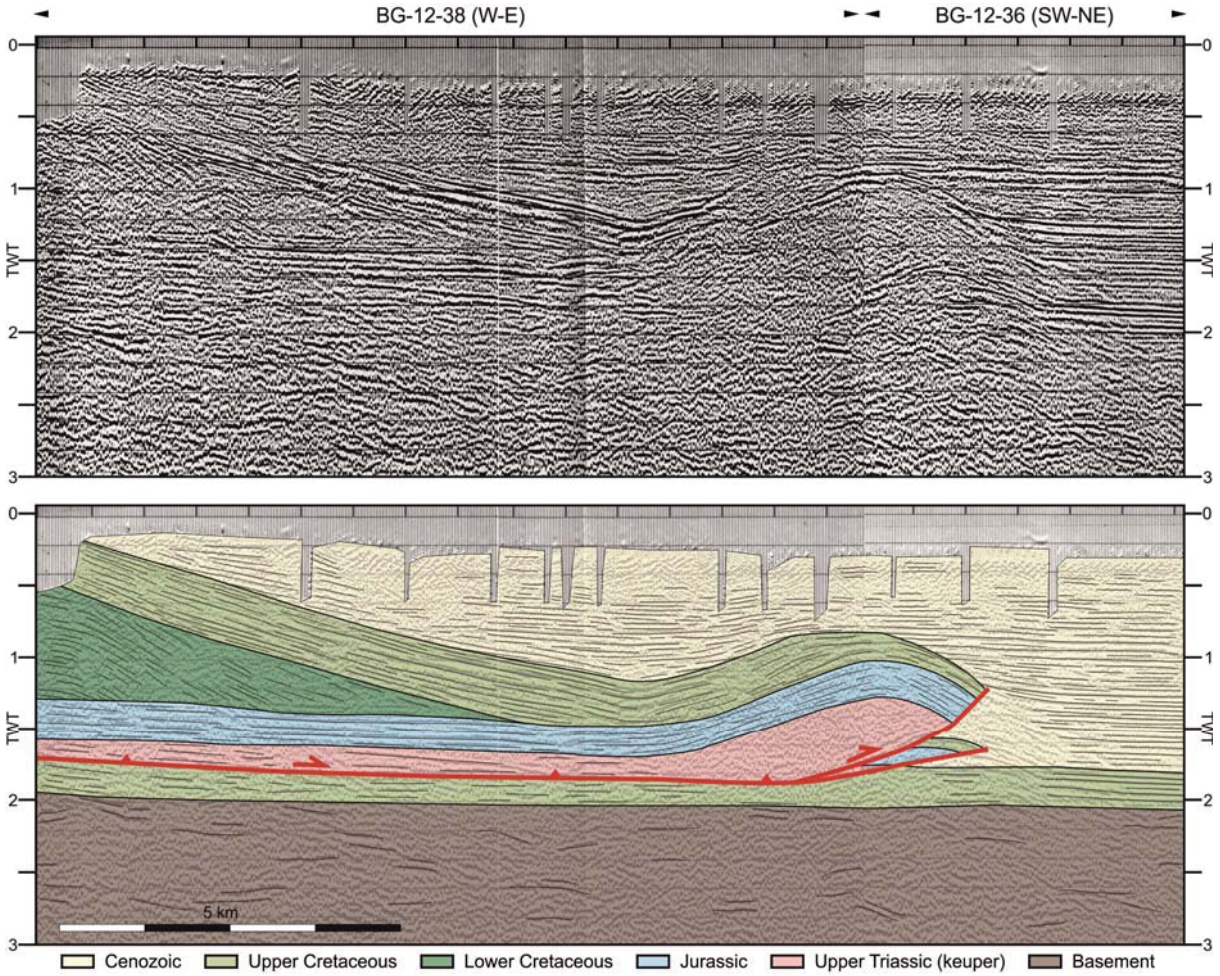

Figure 8: Composed W-E and SW-NE seismic section in the Bureba sub-basin reflecting the eastward thinning of the Lower Cretaceous succession related to the extensional event that produced forced folding of the Jurassic units. The contractional structure, displacing the Mesozoic succession towards the SE, is fossilised by the Cenozoic sediments of the Bureba and the Ebro Foreland Basin. See figure 3 for location.

The Jurassic to Cenozoic succession has been detached above the Upper Triassic salts and thrusted on top of the flat-lying Cretaceous to Cenozoic sediments of the Ebro foreland basin in continuation with the foreland described in previous seismic sections. The foreland is imaged as a layer cake parallel succession at all directions as shown by the W-E and S-N sections in which no deformation is visible. In this area, more than 1.5 seconds TWT thick succession of strong and continuous reflections alternate with weak reflections attributed to the Cenozoic foreland basin infill. Additionally in the Rioja 1 well, located towards the south-east in the Ebro foreland basin, more than 3 km of Cenozoic succession was testified (Lanaja, 1987). Below the Cenozoic, strong and continuous reflections characteristic of the Upper Cretaceous seismic facies and the upper Albian overlie the basement. In the hangingwall, the Lower Cretaceous succession experiences a thickening towards the north. The northern part of the section is characterised by the Villarcayo syncline filled with Cenozoic sediments and where the Trespaderne-1 well is located.

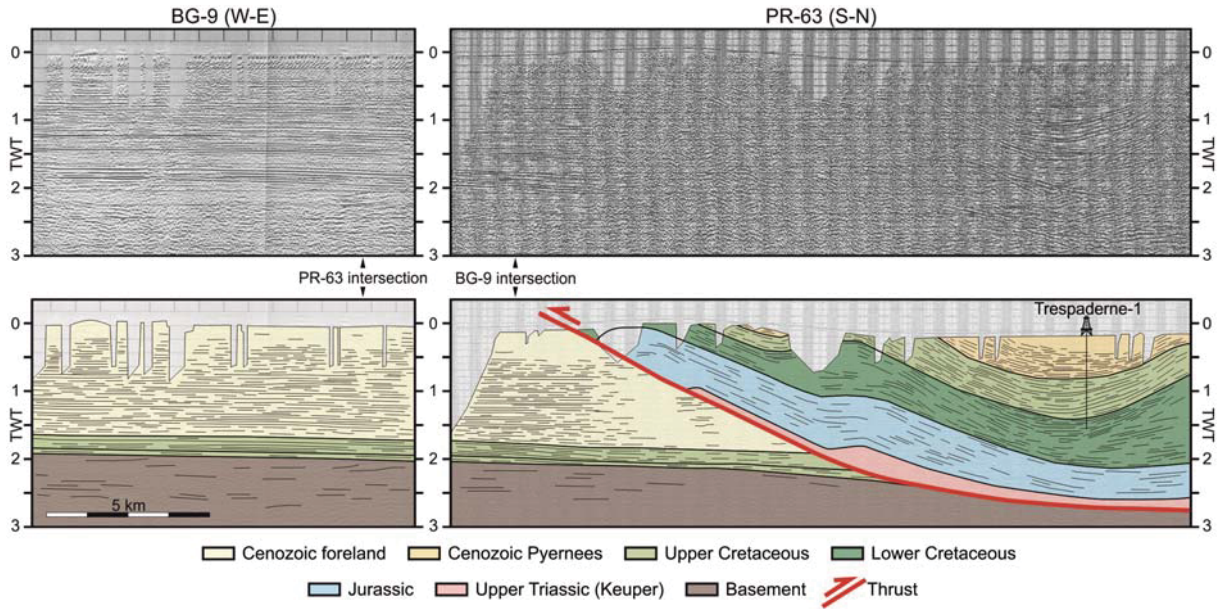

Figure 9: W-E seismic section of the Bureba re-entrant displaying flat-lying Mesozoic and Cenozoic successions and S-N seismic section of the western part of the Basque-Pyrenees with the Mesozoic and Cenozoic succession southward displaced by a thrust detached at the Upper Triassic salt that overrides the Ebro Foreland Basin.

4.2. Interpretation of the structure: integration of surface and subsurface data

Three south-north and one northwest-southeast cross-sections integrating the surface geology and the subsurface data, allow to determine on one hand, the transition between the two styles of deformation and on the other hand, the structural significance of the Burgalesa Platform with respect to the Pyrenean Orogen (Fig. 10).

The westernmost S-N cross-section is characterised by basement involved structures, outcropping in the northern sector, whereas, detached structures occur in the southern part (I-I' in figure 10). The transition between the two domains occurs southwards of the Golobar fault where the depocenter of the syn-extensional sediments is located. South of this transition, the syn-rift succession progressively thins contrasting with the Triassic salts that thickens towards the Ubierna Fault. The wells drilled in the hangingwall of this structure (i.e. Basconcillos-1 and Abar-1) testify both, a strongly incomplete Jurassic succession and the duplication of the syn-rift sediments below the Jurassic. The interpretation for this structure is that of a small back-thrust, rooted into the Triassic salt layer cutting a previously developed extensional fault that produced the partial omission of the Jurassic and the thickening of the Triassic salt. Southwards, in the folded band, both the Jurassic and the syn-rift successions are reduced. The thrust system climbs up southwards being this part of the Burgalesa Platform riding over the Duero Foreland Basin and also over the north-directed and basement involved San Pedro structure.

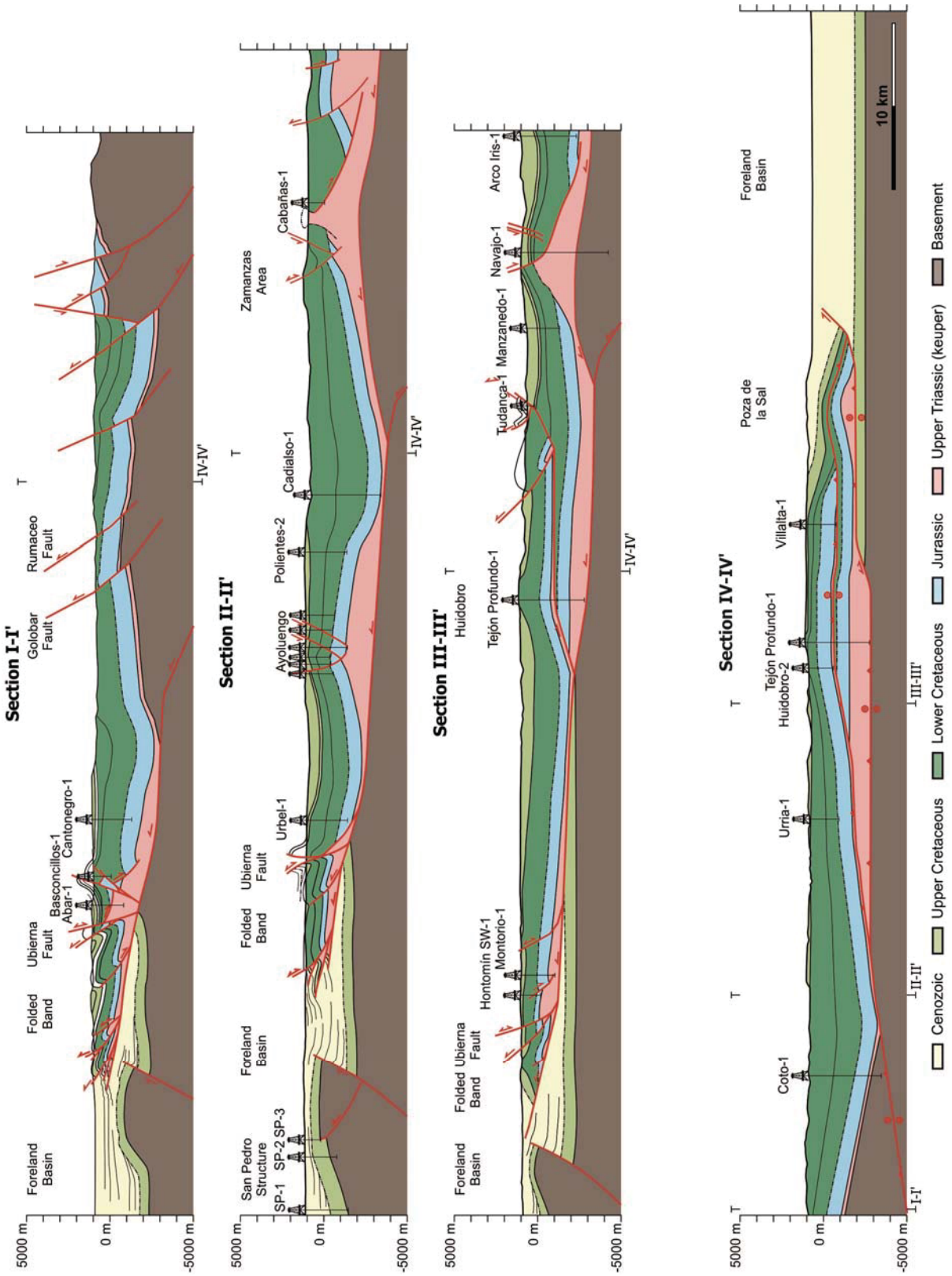

Figure 10: Cross-sections of the study area. Three in a S-N orientation and one in a NW-SE with both, the main areas and wells labelled. See figure 3 for location.

Similar to the previous one, the middle S-N cross-section shows the involvement of the basement in the northern sector and the detachment of the Mesozoic in the southern one (II-II'

in figure 10). The transition between the two styles takes place northwards of the Lower Cretaceous depocenter where the Cadialso-1 well drilled more than 3 km of syn-rift sediments. The northern area is characterised by the presence of a salt wall in the Ebro area in which the Cabañas-1 well testifies the omission of the Jurassic succession. To the north, the surface geology allows to constrain the thrust that uplifts the Jurassic succession outcropping westwards of the trace of the cross-section (Fig. 3). South of the depocenter the syn-rift succession thins until it reaches the Ayoluengo salt-cored structure, where the wells drilled a thickness of *ca.* 1000 meters of Lower Cretaceous rocks. The southern sector of the Burgalesa Platform is characterised by the thrusting over the Duero Foreland Basin and by a thinning of both, the Jurassic and syn-rift successions. The southernmost part of the cross-section is where the San Pedro wells are located, constraining the presence of this structure at depth.

The easternmost S-N cross-section here presented shows the prolongation of the Ebro reservoir salt wall at the northern sector (III-III' in figure 10). In this area, the Navajo-1 well testifies a thin syn-rift succession directly overlying the Triassic salts, with the omission of the Jurassic rocks. The well drilled more than 2000 meters of Triassic salts and reached the top of the basement at 3900 meters below the surface (m.b.s.). Contrasting with this, the adjacent Arco Iris-1 and Manzanedo-1 wells drilled all the Cretaceous and the Jurassic successions. These data suggest that the Navajo antiform resulted from the squeezing of a salt wall related with an Early Cretaceous extensional fault in the hangingwall of a basement involved thrust.

In the Huidobro area, as stated before, the back-thrust duplicates the succession as testified by both, the Tejón Profundo-1 well and the seismic line (Fig. 6). However, a problem arises when comparing the amount of shortening observed in the pre-rift Jurassic horizons and the one observed in the Upper Cretaceous beds (Fig. 10). Part of this mismatch in the amount of shortening can be the result of the obliquity between the cross-section and the thrust transport direction. Nevertheless, this would not explain the observed difference. In addition, this would not also explain the differences in structural relief between the deeper structural levels and the shallower ones (Fig. 6). Such difference in the structural relief results into the unconformity at the bottom of the post-rift upper Albian-Upper Cretaceous sediments and the erosional truncation geometry of the syn-rift horizons below the unconformity, mostly visible in the southern limb of the Huidobro anticline (see details in the seismic lines of Fig. 6). Differences in the structural relief can be partially explained by salt inflation during rifting. The southern limb of the salt body drilled by the Tejón Profundo-1 well will be the locus of the back-thrust during the subsequent contractional deformation at Paleogen-Neogene times (Hernaiz et al.,

1994; Malagón et al., 1994). The other explanation for the observed structural relationships, and mostly the unconformity observed at the bottom of the post-rift succession, would be that part of the observed contractional deformation is pre upper Albian, and thus linked with the extensional system as part of a toe system. The Early Cretaceous extensional basins were transported to the N-NE and detached above the Triassic salts. The structural relief created by salt structures during the extensional deformation, such as salt walls and diapirs along the northern edge of the Burgalesa Platform would have controlled the geometry and location of contractional structures in the northern part of Burgalesa Platform. The possible existence of salt welds basinward the salt structures would have enhanced the contractional reactivation of the flanks of the salt structures facing the rift margin. The existence of Early Cretaceous contractional features were already cited by Serrano *et al.* (1994), although not documented, these contractional structures are commonly related with the distal parts of extensional systems (Peel *et al.*, 1995; Rowan *et al.*, 1999; Rowan *et al.*, 2004; Lacoste *et al.*, 2012; Cartwright *et al*., 2012, among others). Southwards, the thrust system climbs up section and overrides the Duero Foreland Basin. In this part, a narrow corridor between the Burgalesa Platform and the San Pedro Structure is present.

Finally, the NW-SE section illustrates the transition between thick-skinned and thin-skinned styles of deformation in the NW-SE direction (IV-IV' in figure 10). In the north-western part, the basement is involved in the thrust system and as a consequence the Mesozoic sequence is uplifted and tilted towards the SE as described in figure 5. In this portion, the Coto-1 well drilled a thin Triassic salt succession before the top of the basement at *ca*. 3000 m.b.s. Eastward, the Mesozoic succession is detached into the Triassic salts as stated before (Fig. 5). The hangingwall cutoff of the basement coincides with the depocentre of the syn-rift sediments, as does in sections I and II, where Triassic salts were thin, either depositionally or by welding during the salt withdrawal towards the margins of the basins. The syn-rift succession thins above the inflated salt, reaching less than 1000 meters in the Huidobro-2 well. From this sector to the Villalta-1 well, the oblique to the transport view of the back-thrust is the main structural feature as described in figure 7. In this section, the differences in the structural relief between the Upper Cretaceous beds and the Jurassic ones in relation with the thrust that duplicates the pre-rift succession, as well as the lack of evidence of a major back-thrust at surface, reinforces the Early Cretaceous age for part of this structure. The south-eastern edge of the Burgalesa Platform is characterised by the perpendicular view of the salt-cored Rojas structure and the frontal thrust system climbing over the Ebro Foreland Basin.

Determining the main succession boundaries by integrating all the subsurface data allows to characterise the distribution pattern of the main depocenters and thinned areas (Fig. 11). The distribution of the Triassic salt layer has two main trends in the Burgalesa Platform. On the one hand, the NE-SW orientation present in the Ayoluengo and Rojas area where in this latter case a total thickness of 1400 meters was drilled by the well Rojas NE-1. On the other hand, the WNW-ESE orientation present along the northern block of the Ubierna Fault System, where the wells Abar-1 with 1000 meters, the Pino-1 with 300 meters or the Montorio-1 with 450 meters of salt is present, and along the Villalta anticline in where the Tejón Profundo-1 well drilled more than 1200 meters of Upper Triassic salts. All these thicknesses are minimum values because the wells did not drilled the whole Upper Triassic reaching the succession located below. In contrast, the Coto-1 well only drilled 100 meters of Triassic salts and reached the basement at more than 4000 meters below the surface. In contraposition, the Lower Cretaceous distribution can be summarised in an opposite manner of the Upper Triassic salt distribution. The thinned areas corresponds to the thickened salt areas such as the northern block of the Ubierna fault in the Ayoluengo structure and in the Villalta areas. The thickened syn-rift area is located to the NW where the salt accumulation is minimum. Even though in this area the Lower Cretaceous is outcropping and the total thickness cannot be precisely determined, a total thickness of almost 3000 meters is registered by the Coto-1 well.

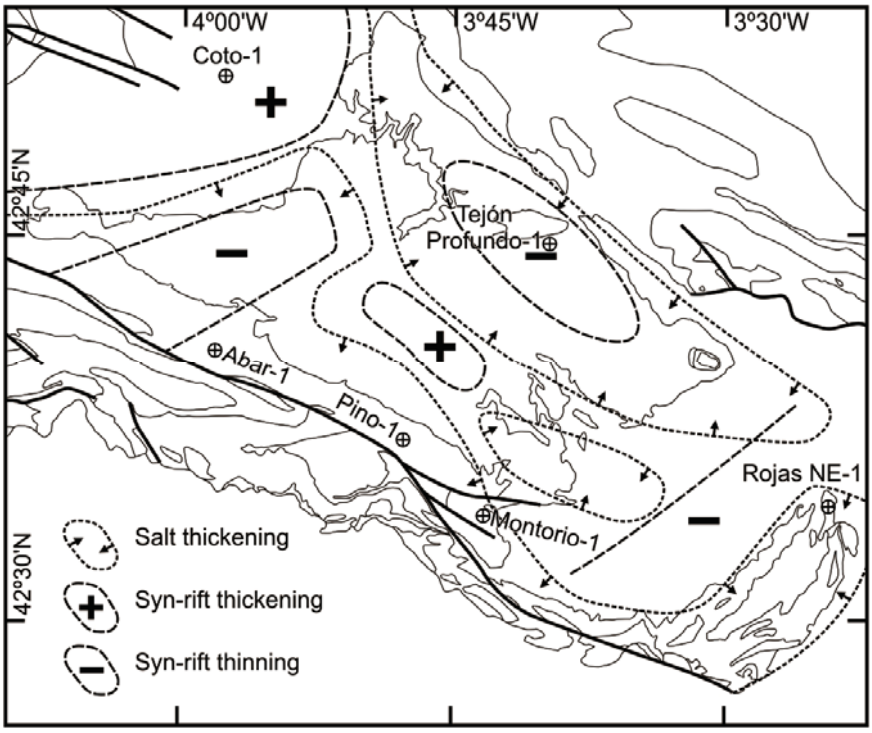

Figure 11: Schematic map with the distribution of the salt thickened areas and the location of the syn-rift depocenters and thinned parts and also the location of some of the wells of the study area.

The thinned south-eastern area is associated with the boundary of the extensional basin during the Cretaceous as demonstrated by the seismic line described in figure 8 where the syn-rift drastically reduces its thickness and also how onlap onto the Jurassic. The onlap stated before, extends in a broad band almost parallel to the Ubierna fault trace displaying a southwards direction of migration (Fig. 12A).

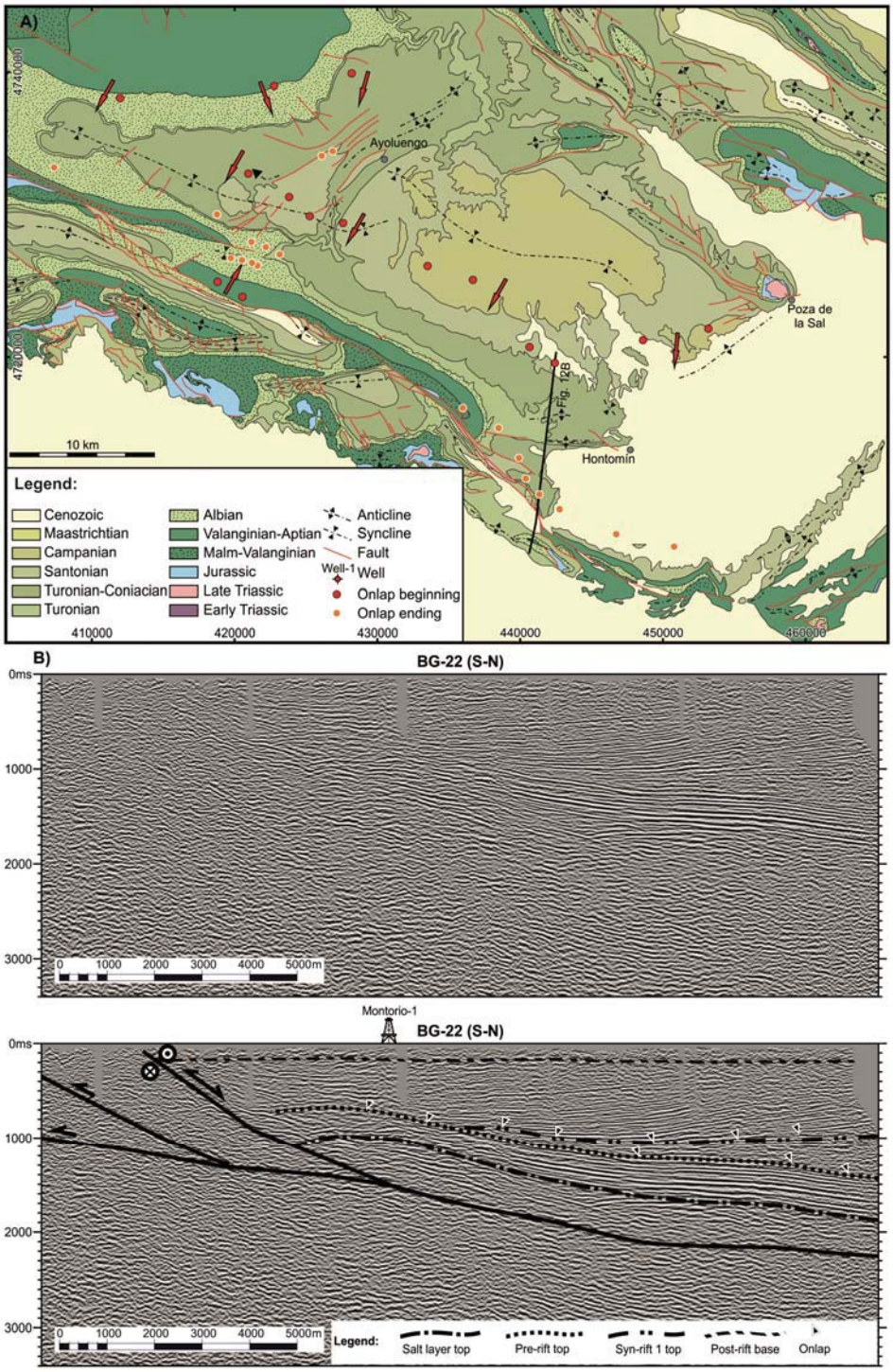

Figure 12: A) Geological map with the distribution of the onlap geometries observed in the seismic sections. Red arrows indicate the direction of migration of the onlaps. B) S-N seismic section crossing the Folded Band and the Burgalesa Platform highlighting the onlaps.

The map view trace of the onlaps has a roughly WNW-ESE orientation with a bend in the middle where it attains a more NW-SE orientation thus similar as the Ubierna fault. A S-N seismic section crossing the southern limit of the Burgalesa Platform shows a southern sector, in which thrusts deform the whole Mesozoic successions and a northern sector where cover deformation is almost absent (Fig. 12B). The southern area corresponds to the Folded Band located southwards of the Burgalesa Platform and the seismic facies do not allow to interpret the Mesozoic successions. Whereas, the northern area is characterised by north-dipping pre-rift panel, a sedimentary wedge constituted by syn-rift successions and an almost horizontal post-rift succession eroding the one located immediately below (Fig. 12B). Within the sedimentary wedge, the sedimentary geometry observable onlaps both the pre-rift and the syn-rift successions with a southwards direction of migration extending from the northern limit of the seismic and ending close to the Ubierna fault.

5 Discussion

The data and structural interpretations herein included demonstrate the strong decoupling of the Mesozoic successions from the basement rocks located below the Upper Triassic salts in the Burgalesa Platform and, in general, in the Basque-Pyrenees. Decoupling occurred during both the Late Jurassic-Early Cretaceous extensional deformation and the subsequent tectonic inversion and fold and thrust development at Paleogene-Neogene times.

The scarcity of extensional faults bounding the main depocenters of the syn-rift sequences, the onlap geometries of the syn-rift beds onto the Jurassic carbonates lying above the Triassic salts and all the observed salt structures that developed during the extensional deformation suggest that salt decoupled deformation above and below. Of particularly relevance are the contractional structures described in the northern part of the Burgalesa Platform (Fig. 6). They involve a few kilometres of shortening and demonstrate decoupling and a significant detachment of the cover of the Burgalesa Platform to the N-NE during thin-skinned extensional deformation.

Extensional faults affecting the cover mostly emerged at the rift margins, at present inverted along the thrust front southward the Ubierna fault system. These faults marked a sharp transition in the stratigraphic record. Thus, at the rift shoulders, at present the Duero and Ebro foreland basins, the Mesozoic pre-rift sequences are not preserved, the syn-rift sediments were not deposited and the upper Albian post-rift sequences unconformably overlie the basement rocks. This stratigraphy is constant in the foreland all along the thrust front including in the

Bureba re-entrant at the NE edge of the Burgalesa Platform (Fig. 7 and 9). In the hangingwall of the marginal extensional detachment a gap in the pre-rift Jurassic should be expected to account for the onlap geometries in the Burgalesa Platform, as observed in the most frontal preserved thrust imbricates. Such Jurassic gaps related with the extensional detachment have also been observed and described further east in the Basque-Pyrenees and in the Bay of Biscay (Jammes *et al.*, 2009; Rowan, 2014).

The extensional faults affecting the Upper Triassic salts as well as the cover in the Burgalesa Platform produced the migration of salt. The sedimentation of the syn-rift successions accentuated the salt mobilisation (Vendeville and Jackson, 1992; Hudec and Jackson, 2007, among others). At the end of the extensional deformation, the salt thickness distribution pattern was characterised by two areas of major accumulation surrounded by areas where the thickness of the salt layer was depleted and even welded (Fig. 11). The WNW-ESE orientation was associated to inherited Late Permian-Triassic extensional structures reactivated during the Late Jurassic-Early Cretaceous extensional event and the NE-SW orientation associated to newly develop extensional faults (Tavani and Muñoz, 2012 and Tavani *et al.*, 2013). The Ubierna, Huidobro and Navajo areas are characteristic of the first orientation whereas, the Rojas area at the easternmost boundary is characteristic of the second orientation. As a consequence, this salt distribution has a strong impact during the inversion of the basin. This characteristic is well known and the configuration of the former basin, the mechanical stratigraphy and the thickness and the spatial distribution of the ductile levels can determine differential advance of the thrust system towards the foreland basin with respect to areas where this level is absent or strongly reduced (Jaumé and Lille, Davis and Engelder, 1985; Bahroudi and Koyi, 2003; Luján *et al.*, 2003; Sepehr *et al.*, 06; Vidal *et al.*, 2009; among others).

Extensional faults thinning the basement below the Triassic salt should be expected to occur northward the emergent marginal extensional fault system. The Ubierna fault and related salt structure would be located above a basement-involved high-angle extensional fault offsetting the base of the salt. However, the salt was thick enough to allow decoupling during northward-directed detachment and developed drape folds above the basement step. A northward displacement of more than 10 km above the extensional detachment is necessary to explain the width of the observed onlap geometries north of the Ubierna structure as shown in figure 12. This would be also consistent with the described syn-extensional contractional features northwards and the distribution of the syn-rift depocenters.

The spatial and thickness distribution of the Triassic pre-rift salt was dependent on the geometry of the Triassic extensional faults, which controlled the topography at the time of evaporite deposition during the late to sag phase of the Triassic rifting. In the western part of the Basque-Pyrenees Triassic extensional faults (Ubierna, Golobar and Rumaceo faults among others) were arranged in a left stepped way. Rely ramps connecting the extensional faults were characterised by eastward dipping panels, some of them probably breached as suggested by Espina (1997), and defined an approximately north trending western edge of the Triassic salts.

Decoupling did not occur at the western edge of the Burgalesa Platform because of the absence of the Upper Triassic salts, either by no deposition or by erosion during the Late Jurassic-Early Cretaceous rifting. The western edge of the Triassic salts coincides with the transition from the thin-skinned tectonic style of the frontal part of the Basque-Pyrenees and the Burgalesa Platform eastward to the thick-skinned tectonic style of the Cantabrian Mountains westward. There, coupling of the basement and cover during the Pyrenean deformation resulted in an increase of the structural relief and the eastward plunge of the structures at the eastern termination of the Cantabrian Mountains (Alonso *et al.*, 1996; Espina, 1997; Tavani *et al.*, 2013). Recent AFT and ZHe thermochronological data by Fillon (2012) along a cross-section in the eastern part of the Cantabrian Mountains yield a Late Eocene age for the onset of the exhumation of the basement involved during the inversion of the Cabuérniga and Rumaceo faults. Exhumation continued southward into the hangingwall of the Golobar fault at Oligocene times. A youngest Early Miocene exhumation age was acquired in the basement rocks in the hangingwall at the western termination of the Ubierna fault once uplift ended further north. Southward migration of basement exhumation is consistent with a forward propagating thrust system involving both basement and cover rocks and inverting the previously developed Triassic and Late Jurassic-Early Cretaceous extensional faults (Alonso *et al.*, 1996; Fillon, 2012). Moreover, the old exhumation ages (Jurassic to Paleocene) recorded in Cretaceous and Stephanian rocks along the thrust front (Fillon, 2012) demonstrate the limited amount of uplift and related displacement of the frontal thrust in agreement with the fault-propagation fold model suggested by Alonso *et al.* (1996).

As stated before, this N-S western boundary of the Burgalesa Platform has an eastward plunge, for this reason, the map view allows to project the surface geology towards the east and to extrapolate the subsurface geology downwards as shown by Tavani *et al.* (2013). However, in the light of the surface and subsurface data provided in this work, we must clarify that this down-plunge projection cannot be extrapolated eastward the transition between the two styles

of deformation. This is because more to the east the Upper Triassic salt layer detaches the Mesozoic succession from the basement (Fig. 5). This disharmony between the cover and the basement is denoted by the surface geology in the area east of Aguilar where the cover structures are not reflected into the basement and with the amount of contractional and salt structures aligned along this N-S boundary such as the Aguilar, the Reinosa or the Pas structures from south to north (Espina, 1997, Fig. 3). The only structure that partially truncates the décollement level at the western Burgalesa Platform is the Golobar fault (Fig. 3). This would be in agreement with the right-lateral strike slip reactivation of the formerly inverted Golobar extensional fault during the last stages of deformation (Tavani *et al.*, 2011), coeval with the progression of deformation into the basement below the Burgalesa Platform (Fig. 5 and 10). Uplift and exhumation of the hangingwall of the Golobar fault during tectonic inversion occurred at Oligocene times (Fillon, 2012) and the right-lateral reactivation with reduced uplift would be younger.

Integration of all the observations, constraints and data presented in this work together with the data reported by several authors in the last years, requires a new model to explain the structural evolution of the Burgalesa Platform. The proposed model is a combination of thin-skinned and thick-skinned modes of deformation. Decoupling and related thin-skinned structures have been controlled by the initial distribution of Triassic salts. On the contrary, basement-involved structures have mostly determined by the reactivation of extensional faults. Oblique inversion tectonics played also a significant role. The increase of the obliquity between the strike of the faults and the shortening direction as the Pyrenean deformation progressed would have favoured strike-slip reactivation, both in the cover and in the basement, and lateral extrusion of the Burgalesa Platform (Tavani *et al.*, 2011; Quintà and Tavani, 2012).

The thick-skinned domain is characterised by the WNW-ESE to W-E basement-involved thrust structures of the Cantabrian Mountains (Alonso *et al.*, 1996; Gallastegui, 2000; Tavani *et al.*, 2013) and the Duero foreland basin (Fig. 4, Gallastegui, 2000). In addition, in this area, Tavani *et al.* (2011) reported the transpressive reactivation of outcropping faults (i.e. Ubierna, Golobar, Rumaceo). The thin-skinned domain spans eastwards of the basement cutoff along most of the entire Burgalesa Platform and also in the Basque-Pyrenees. This domain is characterised by the detachment and south-eastwards extrusion of the Burgalesa Platform as previously pointed out by Rodríguez Cañas *et al.* (1994) and Tavani *et al.* (2011).

The moderate deformation of the Upper Cretaceous sediments, with predominant subhorizontal beds at a roughly similar height, and the strong deformation along the southern and eastern edges of the Burgalesa Platform (Folded Band and Rojas structure respectively) are consistent with a fold and thrust belt detached on salt, being its edges determined by the abrupt termination of the Triassic salts in the hangingwall of previous extensional faults. The interpretation of the seismic data in the Bureba re-entrant of the Ebro foreland basin at the northern edge of the Rojas structure is crucial for the thin-skinned interpretation of the Burgalesa Platform (Fig. 3). The continuity of the seismic stratigraphy of the Bureba re-entrant with the Ebro and Duero basins, the salient geometry of the Rojas structure and the attitude of the different tectonostratigraphic packages there demonstrate detachment and thrusting of the Mesozoic successions of the Burgalesa Platform above the Duero-Ebro basins (Figs. 8 and 9). Thrust transport direction would be to the SE as suggested by the geometry of the Rojas salient (Rodríguez Cañas *et al.*, 1994). The geometry of the Bureba re-entrant prevents any attempt to connect the NE-SW trending Rojas structure with the Sierra de Cantabria frontal thrust with a continuous NE trend (Fig. 3) as it is done in many published structural sketches of the area. Moreover, a NW-SE trending thrust connecting the Rojas and Poza de la Sal is required to account for the stratigraphic differences between the foreland and the Burgalesa Platform, as observed in seismic sections (Fig. 7 and Fig. 8). The resulting geometry of the SE edge of the Burgalesa Platform can be hardly explained by a thick-skinned structural style. It would require the tectonic inversion of three different extensional faults: the Ubierna fault southward, the Rojas one eastward and a northern SW dipping one. There are evidence for the first two, but not for the latter. In addition, inversion of such fault system involving the basement would require vertical tectonics and piston-like deformation mode. This is not compatible with surface data neither with the geometries observed in seismic lines.

The attitude of the autochthonous Upper Cretaceous top cutoff line, located in the footwall of the sole thrust, gives an idea of the allochthony of the Burgalesa Platform. To know the position of such line, the NW tip of the Bureba re-entrant (Figs. 3 and 9) can be connected with the northernmost outcropping Upper Cretaceous folded sediments of the Duero foreland basin that are located to the south of the eastern Cantabrian Mountains basement rocks tip (Figs. 3 and 13). Such a line has an almost W-E trend in continuation with the equivalent cutoff line in the footwall of the Sierra de Cantabria frontal thrust (Fig. 13). The quality of the available seismic data does not allow to fully constrain the position of this line at depth below the Burgalesa Platform.

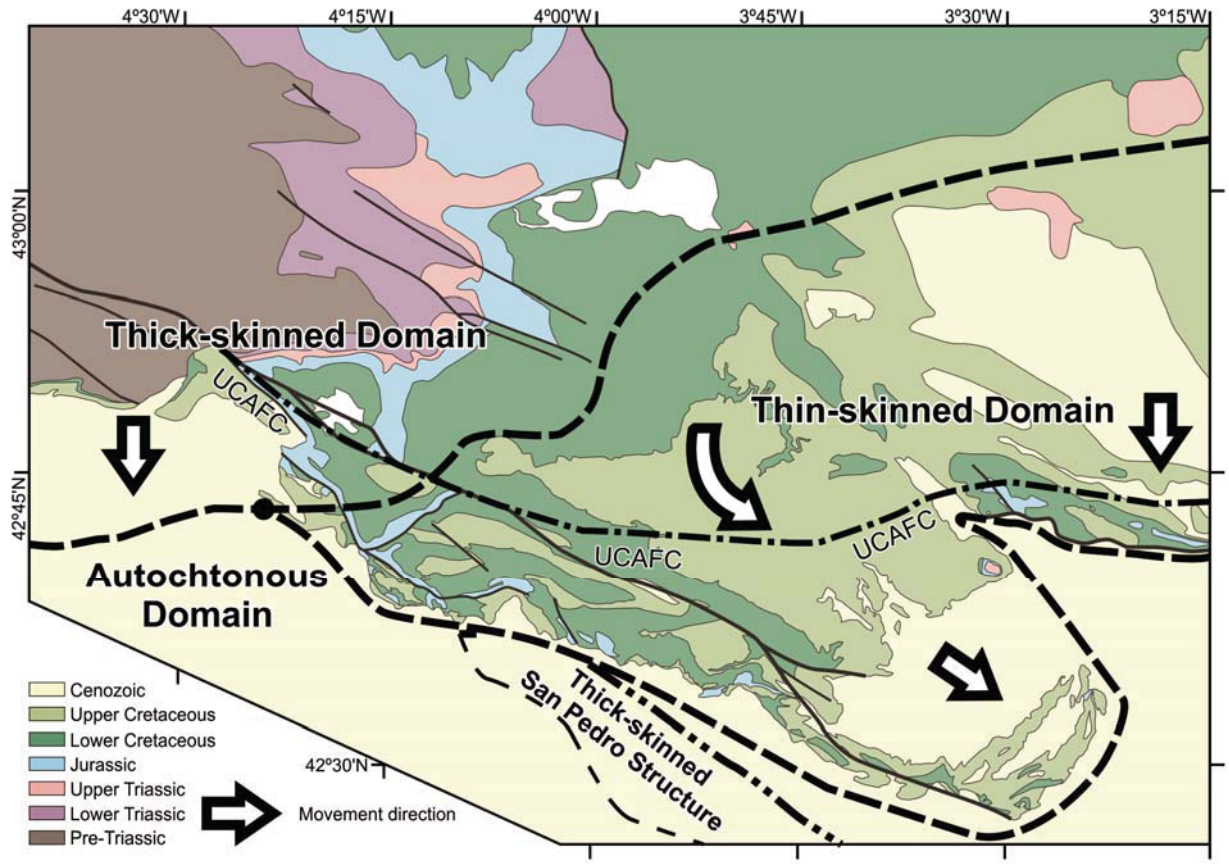

Figure 13: Map of the study area and surrounding with the movement directions of each area and also the main domains (i.e. Thick-skinned, Thin-skinned and Autochtonous) described in the text and present in the area. UCAFC corresponds to Upper Cretaceous Autochtonous Footwall Cutoff.

As shown in many tectonic settings (i.e. contractional, extensional or strike-slip) when a ductile level like salt or even shales is present the deformation is decoupled between the basement and the cover (Jaumé and Lille, 1988; Peel *et al.*, 1995; Coward and Stewart, 1995; Rowan *et al.*, 1999; Withjack and Callaway, 2000; Durand-Riard *et al.*, 2013; among others). This fact would make difficult to explain that in the study area, where a thick salt succession is present, the deformation was not decoupled across this layer thus resulting in a thick-skinned deformation.

With the proposed model, the amount of overlap between the allochthonous Mesozoic succession of the Burgalesa Platform and the autochthonous Mesozoic of the Ebro and Duero Foreland increase towards the southeast. This is denoted in figure 13 where the actual thrust front limit of the Burgalesa Platform and the limit of the Upper Cretaceous Autochthonous Footwall Cutoff (UCAFC) are overlapped. As shown for the south-eastern part of the cross-section IV-IV' (Fig. 10) and at the seismic section (Fig. 7) the amount of south-east displacement of the Burgalesa Platform with respect to the autochthonous is almost 15 km

being this value close to the right-lateral displacement for the Ubierna Fault System pointed by Tavani *et al.* (2011). This south-east displacement is also in agreement with the Upper Cretaceous fracture pattern of the Burgalesa Platform (Quintà and Tavani, 2012).

This proposed model reflects the actual configuration of the studied area but it resulted from the partitioning of deformation through time. For such reason, the evolution is subdivided into three main stages each one characterised by a different kinematic of the structures. During the early stages of deformation, the north-directed basement-involved thrusts deforming the San Pedro structure were developed. At this time, the Burgalesa Platform was southward displaced thus reactivating and inverting the former extensional faults detaching the whole Mesozoic succession above the Upper Triassic salts. At the end of this deformational period, the San Pedro structure resulted in a NW-SE orientation in map view (Fig. 13). As deformation continued, the Burgalesa Platform was displaced towards the south until it overrode the San Pedro structure (Fig. 3). At this point, and may be because this latter structure acted as a backstop for the southward displacement of the Burgalesa Platform, the WNW-ESE Ubierna fault was reactivated in a right-lateral sense thus forcing the Burgalesa Platform to extrude towards the south-east overriding the Ebro Foreland Basin. During the last stages of deformation, the reactivation of basement structures deformed the Duero foreland and also the western Burgalesa Platform. Regarding to the reactivation of the Golobar fault, it would be in agreement with the deformation of the inner parts of the fold and thrust belt in order to preserve the tapper (Davis *et al.*, 1983; Dahlen, 1990; Boyer, 1995, among others). In addition, the oblique inversion of basement structures located below the detached Mesozoic succession could be expected during the late stages of deformation as it progressed south-eastwards.

Even though the similarities in structural style between the San Pedro structure and the structures deforming the Duero foreland basin south of the Cantabrian Mountain front they were disconnected and are related to different thrust belts during the Cenozoic contractional stage. This asseveration is supported by the foreland deformation map pattern and by the relative timing between the different structures of both sectors partially constrained by the relative age of growth sediments and the exhumation ages of the eastern Cantabrian Mountains. On the one hand, the NW-SE San Pedro structure would be related to the Iberian Range. The north-directed basement-involved thrust of the San Pedro structure and the decrease of deformation westwards of this structure would be in agreement with the attribution of this structure as the westward continuation of the northern wedge of the Iberian Range in which the same characteristics are described (Álvaro *et al.*, 1979; Guimerà, 1984; Guimerà *et al.*, 1995;

Salas *et al.*, 2001; Guimerà *et al.*, 2004). In addition, the obliquity between the NW-SE San Pedro structure and the WNW-ESE Burgalesa Platform together with the relative timing, being the San Pedro structure overrode by the Burgalesa Platform, also supports the disconnection between the two structural units. On the other hand, the southern deformation of the Cantabrian Mountain would be related to the Pyrenees instead of the Iberian Range. The eastwards decrease of deformation of the W-E orientated south-directed basement-involved structures described in the foreland together with the relative timing between the structures and the thermochronological ages of the Cantabrian Mountains are in agreement with the southward propagation of deformation of the Pyrenees.

6 Conclusions

The data presented in this study allowed to propose a new evolution model for the Burgalesa Platform which fully match with all the surface, subsurface and mechanical stratigraphic constraints. It supports the interpretation of the Burgalesa Platform as a result of the interference between thick- and thin-skinned styles of deformation, both in time and space, during the Cenozoic contractional stage. The western part or the Burgalesa Platform, close to the Cantabrian Mountains, is characterised by south-directed basement-involved structures whereas, the eastern part is characterised by thrusts detached at the Upper Triassic salts overriding the foreland basin. These differences are related to the distribution of the Upper Triassic salt layer, resulted from the Triassic and Late Jurassic-Early Cretaceous extensional events, that controlled the deformation during the Pyrenean Orogeny. The boundary that divides the two styles of deformation connects the easternmost deformation of Cantabrian Mountains in the Duero foreland basin with the western area of the Basque-Pyrenees. This boundary crosses the Burgalesa Platform between the Golobar and Ayoluengo areas with a SW-NE orientation.

The confined location of the Burgalesa Platform with respect to the Cantabrian Mountains and the San Pedro structure together with the obliquity between the strike of extensional faults and the shortening direction of the Pyrenean Orogeny conditioned the evolution of the Burgalesa Platform. During the early stages of deformation, the southward displacement of the whole Basque-Cantabrian Pyrenees was coeval with the northward-directed San Pedro structure. As deformation continued, the right-lateral reactivation of the Ubierna Fault System, due to the backstop produced by the San Pedro Structure, resulted in the more than 15 km of south-east lateral extrusion of the Burgalesa Platform over the Ebro Foreland Basin. At the last stage of

contraction reactivation of basement thrusts at the western sector deformed the Duero Foreland Basin as well as the Burgalesa Platform.

7 Acknowledgments

This work was carried out under the financial support of INTECTOSAL (CGL2010-21968-C02- 01/BTE) and CIUDEN (FBG305657) projects and also the "Grup de Recerca de Geodinàmica i Anàlisi de Conques" (2009SGR-1198). Stefano Tavani is thanked for fruitful discussions. The Instituto Geológico y Minero de España (I.G.M.E.) is thanked for providing seismic sections. We also thank Seismic Micro-Technology and Midland Valley which generously provided Kingdom Suite and Move software.

8 References

Aguilar, M.J. 1971. Correlaciones por ciclos de aporte en el Albense de la Cuenca Cantábrica. *Acta Geológica Hispánica* **6**, 92-96.

Alonso, J.L. 1987. Estructura y evolución tectonoestratigráfica de la región del Manto del Esla (Zona Cantábrica NW de España). Tesis Doctoral. Universidad de Oviedo. 276pp.

Alonso, J.L., Pulgar, J.A., García-Ramos, J.C., Barba, P., 1996. Tertiary Basins and Alpine Tectonics in the Cantabrian Mountains. In: Friend, P.F., Dabrio, C.J., (eds.). Tertiary basins of Spain: The stratigraphic record of crustal kinematics. Cambridge, Cambridge University Press, 214-227.

Alonso, J.L., Pulgar, J.A., Pedreira, D. 2007. Relieve de la Cordillera Cantábrica. *Enseñanza de las Ciencias de la Tierra*, **15.2**, 151-163.

Alonso, J.L., Marcos, A., Suárez, A. 2009. Paleogeographic inversion resulting from large out of sequence breaching thrusts: The León Fault (Cantabrian Zone, NW Iberia). A new picture of the external Variscan Thrust Belt in the Ibero-Armorican Arc. *Geologica acta,* **7**, 451-473.

Álvarez-Marrón, J., A. Pérez-Estaún, J.J. Danñobeitia, J.A. Pulgar, R. Martínez Catalán, A. Marcos, F. Bastida, P. Ayarza Arribas, J. Aller, A. Gallart, F. Gonzalez-Lodeiro, E. Banda, M.C. Comas and D. Córdoba. 1996. Seismic structure of the northern continental margin of Spain from ESCIN deep seismic profiles. *Tectonophysics*. vol. 264, pp. 153-174.

Álvaro, M., Capote, R., Vegas, R. 1979. Un modelo de evolución geotectónica para la cadena Celtibérica. *Acta Geologica Hispanica*, **14**, 172-181.

Amilibia, A., Sàbat, F., McClay, K.R., Muñoz, J.A., Roca, E., Chong, C. 2008. The role of inherited tectono-sedimentary architecture in the development of central Andean mountain

belt: Insights from the Cordillera de Domeyko. *Journal of Structural Geology.* **30**, 1520-1539.

Aurell, M., Robles, S., Bádenas, B., Rosales, I., Quesada, S., Meléndez, G., García-Ramos, J.C. 2003. Transgressive-regressive cycles and Jurassic paleogeography of northeast Iberia. *Sedimentary Geology,* **162**, 239-271. doi:10.1016/S0037-0738(03)00154-4.

Badley, M.E., Price, J-D., Backshall, L.C. 1989. Inversion, reactivated faults and related structures: seismic examples from the southern North Sea. In: Inversion tectonics Cooper, M.A. and Williams, G.D. (eds). *Geological Society Spececial Publications*. **44**, 201-219.

Bahroudi, A. and Koyi, H.A., 2003. Effect of spatial distribution of Hormuz salt on deformation style in the Zagros fold and thrust belt: an analogue modelling approach. *Journal of the Geological Society of London* **160**, pp. 719-733. doi: 10.1144/0016-764902-135.

Barnolas, A., Pujalte, V., 2004. La Cordillera Pirenaica. In: Vera, J.A. (Ed.), Geología de España. Madrid, SGE-IGME, 233–343.

Bassi, G. 1995. Relative importance of strain rate and rheology for the mode of continental extension. *International Journal Geophysics.* **122**, 195-210.

Beaumont, C., Muñoz, J.A., Hamilton J., Fullsack, P., 2000. Factors controlling the Alpine evolution of the central Pyrenees inferred from a comparison of observations and geodynamical models. *Journal of Geophysical Research*, **105**, 8121-8145.

Bois, C.; Pinet, B., Gariel, O. 1997. The sedimentary cover along the ECORS Bay of Biscay deep seismic reflection profile. A comparison between the Parentis basin and other European rifts and basins. *Mémoires de la Societé Géologique de France*, **171**, 143-165.

Boyer, S. 1995. Sedimentary basin taper as a factor controlling the geometry and advance of thrust belts. *American Journal of Science.* **295**, 1220-1254.

Bug, J.P., Greya, T.V. 2005. The role of viscous heating in Barrovian metamorphism of collisional orogens: thermomechanical models and application to the Lepontine Dome in the Central Alps. *Journal Metamorphic Geology*, **23**, 75-95.

Butler, R.W.H., Tavarnelli, E., Grasso, M. 2006. Structural inheritance in mountain belts: an Alpine–Apennine perspective, *Journal of Structural Geology* **28**, pp. 1893-1908. doi:10.1016/j.jsg.2006.09.006.

Butler, R.W.H. 1989. The influence of pre-existing basin structure on thrust system evolution in the Western Alps. In: Inversion tectonics Cooper, M.A. and Williams, G.D. (eds). *Geological Society Spececial Publications*. **44**, 105-122.

Calassou, S., Larroque, C., Malavielle, J. 1993. Transfer zones of deformation in thrust wedges: An experimental study. *Tectonophysics*, **221**, 325-344.

Carola, E.; Tavani, S.; Ferrer, O.; Granado, P.; Quintà, A.; Butillé, M.; Muñoz, J.A. 2013. Along-strike extrusion at the transition between thin- and thick-skinned domains in the Pyrenean Orogen (northern Spain). In *Thick-skin-dominated Orogens: From initial inversion to full accretion*. Nemcok,M.; Mora, A.R.; Cosgrove, J.W. (eds). *Geological Society of London Special Publications* **377**, DOI:10.1144/SP377.3.

Carrera, N., Muñoz, J.A., Sàbat, F., Mon, R., Roca, E. 2006. The role of inverion tectonics in the structure of the Cordillera Oriental (NW Argentinean Andes). *Journal of Structural Geology*, **28**, 1921-1932.

Cartwright, J., Jackson, M., Dooley, T., Higgins, S. 2012. Strain partitioning in gracity-driven shortening of a thick, multilayered evaporite sequence. In: *Salt Tectonics, Sediments and Prospectivity.* Alsop, G.I., Archer, S.G., Hartley, A.J., Grant, N.T., Hodgkinson, R. (eds). *Geological Society of London Special Publications* **363**, 449-470.

Chapman, T.J. 1989. The Permian to Cretaceous structural evolution of the Western Approaches Basin (Melville sub-basin), UK. In: Inversion tectonics Cooper, M.A. and Williams, G.D. (eds). *Geological Society Spececial Publications*. **44**, 177-200.

Corrado, S., Bucci, D., Naso, G., Faccenna, C. 1998. Influence of paleogeography on thrust system geometries: an analogue modelling approach from the Abruzzi-Molise (Italy) case history. *Tectonophysics*, **296**, 437-453.

Coward, M.P., 1994. Inversion Tectonics. In: Hancock, P.L. (Ed.), Continental Deformation, Pergamon Oxford, 289-304.

Coward, M.P., Stewart, S. 1995. Salt-induced structures in the Mesozoic-Tertiary cover of the southern North Sea U.K. *In:* M.P.A. Jackson, D.G. Roberts, and S. Snelson (eds). Salt tectonics: a global perspective. *AAPG Memoir*, **65**, 229-250.

Dahlen, F.A. 1990. Critical taper model of dold-and-thrust belts and accretionary wedges. *Annual reviews earth and planetary science.* **18**, 55-99.

Davis, D., Suppe, J., Dahlen, F.A. 1983. Mechanics of Fold-and-Thrust belts and accretionary wedges. *Journal of Geophysical Research,* **88**, 1153-1172.

Davis, D.M., Engelder, T. 1985. The role of salt in fold-and-thrust belts. *Tectonophysics* 119, 67-88.

Durand-Riard, P., Shaw, J.H., Plesch, A., Lufadeju, G. Enabling 3D geomechanical restoration of strike- and oblique-slip faults using geological constraints, with applications to the deep-

water Niger Delta. *Journal of Structural Geology*, **48,** 33-44. DOI: 10.1016/j.jsg.2012.12.2009.

Ellis, S., Beaumont, C., Jamieson, R.A., Quinlan, G. 1998. Continental collision including a weak zone: the vise model and its application to the Newfoundland Appalachians. *Canadian Journal of Earth Science*, **35**, 1323-1346.

Espina, R.G. 1997. La estructura y evolución tectonoestratigráfica del borde occidental de la Cuenca Vasco-Cantábrica (Cordillera Cantábrica, NO de España) Ph.D. Thesis, Univerity of Oviedo. 230pp.

Espina, R.G., De Vicente, G., Muñoz Martín, A. 1996. Análisi poblacional de fallas alpinas en el borde occidenteal de la Cuenca Vasco-Cantábrica (Cordillera Cantábrica, NO de España). *Geogaceta.* **20** 936-938.

Ferrer, O., E. Roca, B. Benjumea, J. A. Muñoz, N. Ellouz, and MARCONI Team. 2008. The deep seismic reflection MARCONI-3 profile: role of extensional Mesozoic structure during the Pyrenean contractional deformation at the eastern part of the Bay of Biscay. *Marine and Petroleum Geology,* **25(8)**, 714-730. doi:10.1016/j.marpetgeo.2008.06.002.

Fillon, C. 2012. Spatial and temporal variation in Cenozoic exhumation of the Pyrenean-Cantabrian mountain belt: coupling between tectonics and surface processes. PhD Thesis. Institut des Sciences de la Terre de Grenoble (ISTerre), Grenoble, France. 202p.

Fischer, M.P., Jackson, P.B., 1999. Stratigraphic controls on deformation patterns in fault-related folds: a detachment fold example from the Sierra Madre Oriental, northeast Mexico. *Journal of Structural Geology* **21**, 613-633.

Gallastegui, J. 2000. Estructura cortical de la Cordillera y Margen Continental Cantábricos: Perfiles ESCI-N. *Trabajos Geología,* **22**, 9-234.

Gallastegui, J., J. A. Pulgar, and J. Gallart. 2002. Initiation of an active margin at the North Iberian continent-ocean transition. *Tectonics,* **21(4)**, doi: 10.1029/2001TC901046.

García de Cortázar, A., Pujalte, V., 1982. Litoestratigrafía y facies del grupo Cabuérniga (Malm-Valanginiense Inferior?) al S deCantabria-NE de Palencia. *Cuadernos Geología Ibérica* **8**, 5-21.

García-Mondéjar, J., Pujalte, V., Robles, S. 1986. Características sedimentológicas secuenciales y tectoestratigráficas del Triásico de Cantabria y Norte de Palencia. *Cuadernos de Geología Ibérica,* **10**. 151-172.

García-Mondéjar, J., Agirrezabala, L.M., Aranburu, A., Fernández-Mendiola, P.A., Gómez-Pérez, I., López-Horgue, M., Rosales, I. 1996. Aptian-Albian tectonic pattern of the Basque-Cantabrian Basin (northern Spain). *Geological Journal* **31**, 13-45.

Guimerà, J. 1984. Palaeogene evolution of deformation in the north-east Iberian Peninsula. *Geological Magazine*, **121**, 413-420.

Guimerà, J., Alonso, A., Mas, R. 1995. Inversion of an extensional-ramp basin by a newly formed thrust: The Cameros Basin (N Spain). *In:* Buchanan, J.G. and Buchanan, P.G. (eds). *Basin Inversion.* Geological Society of London Special Publications, **88**, 433-453.

Guimerà, J., Mas, R., Alonso, Á. 2004. Intraplate deformation in the NW Iberian Chain: Mesozoic extension and Tertiary contractional inversion. *Journal of the Geological Society of London* **161**, 291-303.

Hempel, P.M. 1967. Der diapir von Poza de la Sal (Nordspanien). *Beiheft Geologisches Jahrbuch* **66**, 95-126.

Hernáiz, P.P., Solé, J. 2000. Las estructuras del diapiro de Salinas del Rosío y del alto de San Pedro-Iglesias y sus implicaciones en la evolución tectónica de la transversal burgalesa de la Cordillera Vascocantábrica-Cuenca del Duero. *Rev. Soc. Geol. España* **13** 471-486.

Hernáiz, P.P., Serrano, A., Malagón, J., Rodríguez Cañas, C. 1994. Evolución estructural del margen SO de la cuenca Vasco Cantábrica. *Geogaceta*. V15. pp. 143-146.

Hernáiz, P.P. 1994. La falla de Ubierna (margen SO de la cuenca Cantábrica). *Geogaceta.* **16**. 39-42.

Hernández, J.Mª., Pujalte, V., Robles, S., Martín-Closas, C. 1999. División estratigráfica genética del grupo Campóo (Malm-Cretácico Inferior, SW Cuenca Vascocantábrica). *Rev. Soc. Geol. España* **12** 377-396.

Hill, K.C., Kendrick, R.D., Crowhurst, P.V., Gow, P.A. 2002. Copper-gold mineralisation in New Guinea: tectonics, lineaments, thermochronology and structure. *Australian Journal of Earth Sciences*. **49**, 737-752.

Holdsworth, R.E., 2004. Weak faults, rotten cores. *Science* **303**, 181-182. doi: 10.1126/science.1092491.

Hudec, M.R., Jackson, M.P.A. 2007. Terra infima: Understanding salt tectonics. *Earth Science reviews* **82**, 1-28. DOI: 10.1016/j.earscirev.2007.01.001.

Jammes, S., G. Manatschal, L. Lavier, and E. Masini. 2009. Tectonosedimentary evolution related to extreme crustal thinning ahead of a propagating ocean: the example of the western Pyrenees, *Tectonics,* **28**, TC4012, doi:10.1029/2008TC002406.

James, S., Huismans, R.S. 2012. Structural styles of mountain building: controls of lithospheric rheologic stratification and extensional inheritance. *Journal of Geophysical Research*, **117**, 1978-2012.

Jammes, S., Huismans, R.S., Muñoz, J.A. 2014. Lateral variations in structural style of mountain guilding: controls of rheological and rift inheritance. *Terra Nova* DOI:10.1111/ter.12087.

Jaumé, S. C., R. J. Lillie. 1988. Mechanics of the Salt Range-Potwar Plateau, Pakistan: A fold-and-thrust belt underlain by evaporites, *Tectonics*, **7**, 57- 71.

Koopman, A., Speksnijder, A., Horsfield, W.T. 1987. Sandbox model studies of inversion tectonics. *Tectonophysics*, **137**, 379-388.

Lacoste, A., Vendeville, B.C., Mourgues, R., Loncke, L., Lebacq, M. 2012. Gravitational instabilities triggered by fluid overpressure and downslope incision - Insights from analytical and analogue modelling. *Journal of Structural Geology*, **42**, 151-162. DOI: 10.1016/j.jsg.2012.05.011.

Lanaja, J. M. 1987. *Contribución de la exploración petrolífera al conocimiento de la Geología de España.* IGME, Serv. Oubl. Min. Indust. Energ., Madrid. 465 pp.

Le Pichon, X., Sibuet, J.C., 1971. Western extension of boundary between European and Iberian plates during the Pyrenean orogeny. *Earth and Planetary Science Letters* **12**, 83-88. doi:10.1016/0012-821X(71)90058-6.

Luján, M., Storti, F., Balanyá, J.C., Crespo-Blanc, A. and Rossetti, F., 2003. Role of décollement material with different rheological properties in the structure of the Aljibe thrust imbricate (Flysch Trough, Gibraltar Arc): an analogue modelling approach. *Journal of Structural Geology* **25**, pp. 867–881. doi:10.1016/S0191-8141(02)00087-1.

Macedo, J., Marshak, S. 1999. Controls on the geometry of fold-thrust belt salients. *Geological Society of America Bulletin*, **111**, 1808-1822.

Malagón, J., Hernáiz, P.P., Rodríguez Cañas, C., Serrano. 1994. Notas sobre la inversión tectónica y aloctonia de la cuenca Vasco-Cantábrica. *Geogaceta.* **15**. 139-142.

Marshak, S., 2004. Salients, recesses, arcs, oroclines, and syntaxesda review of ideas concerning the formation of map-view curves in fold-thrust belts. In: McClay, K.R. (Ed.), Thrust tectonics and hydrocarbon systems. *Memoir of the American Association of Petroleum Geologists* **82**, pp. 131-156.

Martínez-Torres, L. M. 1993. Corte balanceado de la Sierra Cantabria (cabalgamiento de la Cuenca Vasco-Cantábrica sobre la Cuenca del Ebro), *Geogaceta,* **14**, 113-115.

Martín-González, F. & Heredia, N. 2011. Complex tectonic and tectonostratigraphic evolution of an Alpine foreland basin: The western Duero Basin and the related Tertiary depressions of the NW Iberian Peninsula. *Tectonophysics* 502, 75-89. doi:10.1016/j.tecto.2010.03.002.

Mathieu, C. 1986. Histoire géologique du sous-basin de Parentis. *Bulletin des Centres de Recherches Elf-Aquitaine (Production)*, **10**, 33-47.

Mazzoli, S., D'Errico, M., Allega, L., Corrado, S., Invernizzi, C., Shiner, P., Zattin, M., 2008. Tectonic burial and 'young' (b10 Ma) exhumation in the southern Apennines fold and thrust belt (Italy). *Geology* **36**, 243-246.

McClay, K.R. 1989. Analogue models of inversion tectonics. In: Inversion tectonics Cooper, M.A. and Williams, G.D. (eds). *Geological Society Spececial Publications*. **44**, 41-59.

Mitra, G. 1997. Evolution of salients in a fold-and-thrust belt: the effects of sedimentary basin geometry, strain distribution and critical taper. In: Sengupta, S. (Ed.) Evolution of Geological Structures in Micro- to Macro-scales, Chapman and Hall, London. 59-90.

Montadert, L., Charpal, O., Roberts, D. G., Guennoc, P., Sibuet, J. C. 1979. Northeast Atlantic passive margins: rifting and subsidence processes. *American Geophysics Union, Revue*, **3**, 154-186.

Mouthereau, F., Lacombre, O. 2006. Inversion of the Paleogene Chinese continental margin and thick-skinned deformation in the Western Foreland of Taiwan. *Journal of Structural Geology*. **28**, 1977-1993.

Muñoz, J. A. 1992. Evolution of a continental collision belt: ECORS-Pyrenees crustal balanced section, in *Thrust Tectonics*, edited by K. R. McClay, pp. 235-246, Chapman and Hall, London.

Muñoz, J. A. 2002. The Pyrenees, in *The Geology of Spain*, edited by W. Gibbons and T. Moreno, pp. 370-385. Geological Society of London, London.

Pedreira, D., J. A. Pulgar, J. Gallart, and J. Díaz. 2003. Seismic evidence of Alpine crustal thickening and wedging from the western Pyrenees to the Cantabrian Mountains (north Iberia). *Journal of Geophysical Research,* **108**(B4), doi: 10.1029/2001JB001667.

Pedreira, D., Pulgar, J. A., Gallart, J., Torné, M. 2007. Three-dimensional gravity and magnetic modeling of crustal indentation and wedging in the western Pyrenees- Cantabrian Mountains, *J. Geophys. Res.,* **112**(B12405), doi: 10.1029/2007JB005021.

Peel, F., Travis, C.J., Hossack, J.R. 1995. Genetic structural provinces and salt tectonics of the Cenozoic offshore US gulf of Mexico: a preliminary analysis. *In:* M.P.A. Jackson, D.G. Roberts, and S. Snelson (eds). Salt tectonics: a global perspective. *AAPG Memoir*, **65**, 153-175.

Pérez-Estaún, A., Bastida, F., Alonso, J.L., Marquinez, J., Aller, J., Álvarez-Marrón, J., Marcos, A., Pulgar, J. 1988. A thin-skinned Tectonics Model for an arcuate fold and thrust belt: The Cantabrian Zone (Variscan Ibero-Armorican Arc). *Tectonics* **7**, 517-537.

Pérez-Estaún, A., Martínez-Catalán, J.R., Bastida, F. 1991. Crustal thickening and deformation sequence in the footwall to the suture of the Variscan belt of northwest Spain. *Tectonophysics.* **191**. 243-253. doi:10.1016/0040-1951(91)90060-6.

Pfiffner, O. A. 2006. Thick-skined and thin-skined styles of continental contraction. In:Mazzoli, S. and Butler, R. W. H. (eds) *Styles of Continental Contraction. Geological Society of America Special Paper*, **414**, 153-177. doi: 10.1130/2006.2414(09).

Portero, J.M., Ramírez del Pozo, J., Aguilar, M. 1973. Mapa geológico 1:50.000, Hoja 170 (Haro). IGME.

Pujalte, V., Robles, S., Valles, J.C. 1988. El Jurásico marino de las zonas de alto sedimentario relativo del borde SW de la Cuenca Vasco–Cantábrica (Rebolledo de la Torre, Palencia). *In: III Coloquio de Estratigrafía y Paleogeografía del Jurásico de España. Libro guía de las excursiones*. Ciencias de la Tierra (Instituto de Estudios Riojanos), **11**, 85–94.

Pujalte, V., Robles, S., Hernández, J.Mª. 1996. La sedimentación continental del Grupo Campóo (Malm-Cretácico basal de Cantabria, Burgos y Palencia): testimonio de un reajuste hidrográfico al inicio de una fase rift. *Cuad. Geol. Ibérica*, **21** 227-251.

Pujalte, V., Robles, S., García-Ramos, J.C., Hernández, J.M. 2004. El Malm-Barremiense no marinos de la Cordillera Cantábrica. *In:* Vera, J.A. (ed.) *Geología de España.* SGE-IGME, Madrid, 288-291.

Pujalte, V. 1981. Sedimentary succession and palaeonvironments within fault-controlled basin: the "Wealden" of the Santander area, Northern Spain. *Sedimentary Geology* **28**, 293-325.

Pujalte, V. 1982. La evolución paleogeográfica de la cuenca "Wealdense" de Cantabria. *Cuadernos de Geología Ibérica*, **8** 65-83.

Pulgar, J.A., Pérez-Estaún, A., Gallart, J., Álvarez-Marrón, J., Gallastegui, J., Alonso, J.L. and ESCIN Group. 1997. The ESCIN-2 deep seismic reflection profile: a traverse across the Cantabrian Mountains and adjacent Duero basin. *Revista Sociedad Geológica de España*. **8**, 383-394.

Pulgar, J. A., Alonso, J. L., Espina, R. G., Marín, J. A. 1999. La deformación alpina en el basamento varisco de la Zona Cantábrica, *Trabajos de Geolología.* **21**, 283-294.

Quesada, S., Robles, S., Pujalte, V. 1991. Correlación secuencial y sedimentológica entre registros de sondeos y series de superficie del Jurásico Marino de la Cuenca de Sanander (Cantabria, Palencia y Burgos). *Geogaceta* **10**, 3-10.

Quesada, S., Robles, S., Pujalte, V., 1993. El Jurásico Marino del margen suroccidental de la Cuenca Vasco-Cantábrica y su relación con la exploración de hidrocarburos. *Geogaceta* **13**, 92-96.

Quesada, S., Robles, S., Rosales, I., 2005. Depositional architecture and transgressive–regressive cycles within Liassic backstepping carbonate ramps in the Basque–Cantabrian basin, northern Spain. *Journal Geological Society of London*. **162**, 531-548.

Quintà, A., Tavani, S., Roca, E. 2012. Fracture pattern analysis as a tool for constraining the interaction between regional and diapir-related stress field: Poza de la Sal Diapir (Basque Pyrenees, Spain). In: *Salt Tectonics, Sediments and Prospectivity.* Alsop, G.I., Archer, S.G., Hartley, A.J., Grant, N.T., Hodgkinson, R. (eds). *Geological Society of London Special Publications* **363**, 521-532.

Quintà, A., Tavani, S. 2012. The foreland deformation in the south-western Basque-Cantabrian Belt (Spain). *Tectonophysics.* **576-577**. 4-19. DOI: 10.1016/j.tecto.2012.02.015.

Quintana, L. 2012. Extensión e inversión tectónica en el sector central de la región Vasco-Cantábrica (Cantabria, Vizcaya, norte de España). PhD Thesis. Universidad de Oviedo, Oviedo. Spain. 560pp.

Ramírez del Pozo, J. 191. Bioestratigrafía y Microfacies del Jurássico y Cretácico del Norte de España (Región Cantábrica). *Memorias Instituto Geológico y Minero de España* **78**, 1-357.

Riba, O. and Juardo, M. J. 1992. Reflexiones sobre la geología de la parte occidental de la Depresión del Ebro. *Acta Geologica Hispanica*, **27**, 177-193.

Robles, S., Pujalte, V., Valles, J.C. 1989. Sistemas sedimentarios del Jurásico de la parte occidental de la Cuenca Vasco-Cantatábrica. *Cuadernos Geología Ibérica*. **13**, 185-198.

Robles, S., Quesada, S., Rosales, I., Aurell, M., García-Ramos, J.C. 2004. El Jurásico marino de la Cordillera Cantábrica. In: Vera, J.A. (ed.) Geología de España. SGE IGME, Madrid, 279-285.

Roca, E., Muñoz, J.A., Ferrer, O., Ellouz, N. 2011. The role of the Bay of Biscay Mesozoic extensional structure in the configuration of the Pyrenean orogen: Constraints from the MARCONI deep seismic reflection survey. *Tectonics.* **30**. TC2001. doi: 10.1029/2010TC002735.

Rodríguez Cañas, C., Hernáiz, P.P., Malagón, J., Serrano, A. 1994. Notas sobre la estructura cabalgante de Rojas-Santa Casilda. *Geogaceta* **15**, 135-138.

Rowan, M.G., Jackson, M.P.A., Trudgill, B.D. 1999. Salt-Related fault families and fault welds in the Northern Gulf of Mexico. *AAPG Bulletin*, **83**, 1454-1484.

Rowan, M.G., Peel, F.J., Vendeville, B.C. 2004. Gravity-driven Fold Belts on passive Margins. *In:* McClay (eds). Thrust tectonics and hydrocarbon systems. *AAPG Memoir*, **82**, 157-182.

Rowan, M. 2014. Passive-margin salt basins: hyperextension, evaporite depositioon, and salt tectonics. *Basin Research*, **26**, 154-182. DOI: 10.1111/bre.12043.

Ruiz, M. 2007. Caracterització estructural i sismotectònica de la litosfera en el Domini Pirenaico-Cantàbric a partir de mètodes de sísmica activa i passiva, Ph.D. thesis, Univ. Barcelona, Barcelona, Spain.

Salas, R., Guimerà, J., Mas, R., Martín-Closas, C., Meléndez, A., Alonso, Á. 2001. Evolution of the Mesozoic Central Iberian Rift System and its Cainozoic inversion (Iberian Chain). *In:* Ziegler, P.A., Cavazza, W., Robertson, A.H.F., Crasquin-Soleau, S. (eds). *Peri-Tethys Memoir 6: Peri-Tethyan Rift/Wrench Basins and PAssive Margins. Mémories du Muséum National de l'Historie Naturelle*, **186**, 145-185.

Schröder, B. 1987. Inversion tectonics along the western margin of the Bohemian Massif. *Tectonophysics*, **137**, 93-100.

Sepehr, M., Cosgrove, J., Moieni, M. 2006. The impact of cover rock rheology on the style of folding in the Zagros fold-thrust belt. *Tectonophysics*, **429**, 265-281. DOI: 10.1016/j.tecto.2006.05.021.

Sepher, M., Cosgrove, J.W. 2005. The role of the Kazerun fault zone in the formation and deformation of the Zagros fold-thrust belt, Iran. *Tectonics.* **28**. TC5005.

Serrano, A., Martínez del Olmo, W. 2004. Estructuras diapíricas de la zona meridional de la Cuenca Vasco-Cantábrica. In: Vera, J.A. (Ed.), Geología de España. SGE-IGME Madrid, pp. 334–338.

Serrano, A., Hernáiz, P.P., Magalón, J. Rodríguez-Cañas, C. 1994. Tectónica distensiva y halocinesis en el margen SO de la cuenca Vasco-Cantábrica. *Geogaceta.* **15**. 131-134.

Soto, R., Casas, A.M., Storti, F., Faccenna, C. 2002. Role of lateral thickness variations on the development of oblique structures at the Western end of the South Pyrenean Central Unit. *Tectonophysics*, **35**, 215-235.

Spratt, D.A., Dixon, J.M., Beattie, E.T. 2004. Changes in structural style controlled by lithofacies contrast across transverse carbonate bank margins - Canadian Rocky Mountains and scaled physical models. In: McClay, K.R. (Ed.), *Thrust tectonic and hydrocarbon systems: AAPG Memoir*, **82**, 259-275.

Steward, S.A., Argent, J.D. 2000. Relationship between polarity of extensional fault arrays and presence of detachments. *Journal of Structural Geology*. **22,** 693-711.

Steward, S.A., Ruffell, A.H., Harvey, M.J. 1997. Relationship between basement-linked and gravity-driven faults systems in the UKCS salt basins. *Marine and Petroleum Geology,* **14**, 581-604.

Tavani, S., Muñoz, J.A. 2012. Mesozoic rifting in the Basque-Cantabrian Basin (Spain): Inherited faults, transversal structures and stress perturbation. *Terranova*. **24**, 70-76. DOI: 10.1111/j.1365-3121.2011.01040.x.

Tavani, S., Quintà, A., Granado, P. 2011. Cenozoic right-lateral wrench tectonics in the Western Pyrenees (Spain): The Ubierna Fault System. *Tectonophysics*, **509**, 238-253. DOI: 10.1016/j.tecto.2011.06.013.

Tavani, S.; Carola, E.; Granado, P.; Quintà, A.; Muñoz, J.A. 2013. Transpressive inversion of a Mesozoic extensional forced fold system with an intermediate décollement level in the Basque-Cantabrian Basin (Spain). *Tectonics* v32. DOI:10.1002/tect.20019.

Veen, V. 1965. The tectonic and strarigraphic history of the Cardaño area, Cantabrian Mountains, northern Spain. *Leisde. Geol. Meded.* **35**, 45-104.

Vendeville, B.C., Jackson, M.P.A. 1992. The rise of diapirs during thin-skinned extension. *Marine and Petroleum Geology.* **9**, 331-353.

Vergés, J., García-Senz, J. 2001., Mesozoic evolution and Cainozoic inversión of the Pyrenean Rift, in *Peri-Tethys Memoir 6: Peri-Tethyan Rift/Wrench Basins and Passive Margins*, edited by P. A. Ziegler et al., *Mém. Mus. National Hist. Nat.,* **186**, 187-212.

Vergés, J., Fernàndez, M., Martínez, A., 2002. The Pyrenean origen: pre-, syn-, and post-collisional evolution. In: Rosenbaum, G., Lister, G.S., (Eds.), Reconstruction of the Evolution of the Alpine-Himalayan Orogen. Journal of the Virtual Explorer 8, 57–76.

Vidal-Royo, O., Koyi, H.A., Muñoz, J.A. 2009. Formation of orogen-perpendicular thrusts due to mechanical contrasts in the basal décollement in the Central External Sierras (Southern Pyrenees, Spain). *Journal of Structural Geology* **31**, 523-539.

Wagner, R.H., Winkler Prins, C.F., Riding, R.E., Wagner-Gentis, C.H.T. 1971. Lithostratigraphic units of the lower part of the Carboniferous in northern León, Spain. *Trabajos de Geología* **4**, 603-663.

Whithjack, M.O., Callaway, S. 2000. Active normal faulting beneath a salt layer: An experimental study od deformation patterns in the Cove Sequence. *American Association of Petroleum Geologists Bulletin.* **84**, 627-651.

Ziegler, P.A. (Ed.), 1987. Compressional Intra-Plate Deformation in the Alpine Foreland. *Tectonophysics*, vol. 137, 420 pp.

Chapter 4

The paleomagnetic study of the Burgalesa Platform Domain and surrounding areas

This chapter is subdivided into two subsections. The first part, gives a brief overview of the fundamentals of the paleomagnetic method focussed to understand the following results and further discussions. The second part, points out the results of the vertical axis rotation paleomagnetic study carried in the Burgalesa Platform and surrounding areas.

4.1 Fundamentals of paleomagnetism

The paleomagnetism is the study of the magnetic field vector at the earth surface, acquired by the ferromagnetic minerals of rocks. The magnetic field of the Earth is mainly produced by the convection in the outer core of iron rich material. In addition, other secondary magnetic fields are present on Earth but representing less than 10% (Langereis *et al.*, 2010). The geomagnetic field presents changes in magnitude and in direction ranging from short periods to long periods. The short periods (i.e. milliseconds to days) such as short-term fluctuations, daily magnetic variations or magnetic storms. The long periods (i.e. centuries to millions of years) with secular variations, magnetic excursions or polarity reversals. The polarity reversals with periods ranging from 10^4 to 10^6 years consist on the change of the north and south magnetic poles. The magnetic field vector recorded in the rocks at the surface is explained by the Geocentric Axial Dipole (GAD) hypothesis that simplifies the Earth as a dipole aligned to the Earth rotation axis (Hospers, 1954). However, the best fit for the GAD model corresponds to an inclined dipole that nowadays is tilted about 11º.

The magnetic field vector (F) can be defined by two angles that describe the inclination and the declination (Fig. 4.1). The inclination (I) is the vertical angle, ranging from -90º to 90º, being positive downwards, between the horizontal plane and the magnetic field vector (F). The declination (D) is the horizontal angle, ranging from 0º to 360º, between the geographic north and the horizontal projection of magnetic field vector (F').

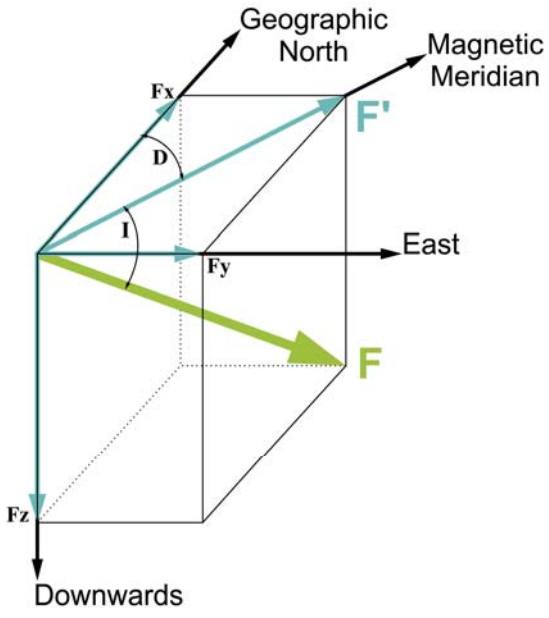

Fig. 4.1: Decomposition of the magnetic field vector (F) into the two different components inclination (I) and declination (D). Modified from Butler, 1992.

The mineralogy susceptible to lock the magnetic field is enclosed in three different ferromagnetic mineral groups: iron-titanium oxides with magnetite, titano-magnetite, hematite and titano-hematite as the main minerals; iron oxyhydroxides like goethite; and iron sulphides like pyrrhoite. All these minerals can preserve the Natural Remanent Magnetisation (NRM) that is the magnetisation present in a rock under natural conditions. In order to identify the minerals present in the rocks, three different procedures can be done:

1) **Microscopy** consisting on determining the ferromagnetic minerals by means of optical observations using reflected light and SEM. The major difficulties of this procedure are the low concentration of ferromagnetic minerals and the time required to prepare the samples.

2) **Curie temperature determination** consisting on monitoring a concentrated powder sample, exposed to a strong magnetic field, while the temperature increases. After that, the mineralogy is determined by visual inspection of the inflections in the heating and cooling trajectories. In some cases, a detailed petrographical study is needed in order to determine the exact mineralogy present in the specimen.

3) **Coercivity spectrum analysis** consist on inducing isothermal remanent magnetisation (IRM) to a sample. Two different analysis can be done. In one hand, **IRM acquisition curve analysis**, the sample is induced with increasing steady fields and the intrinsic coercivity spectrum is measured and plotted (Fig. 4.2).

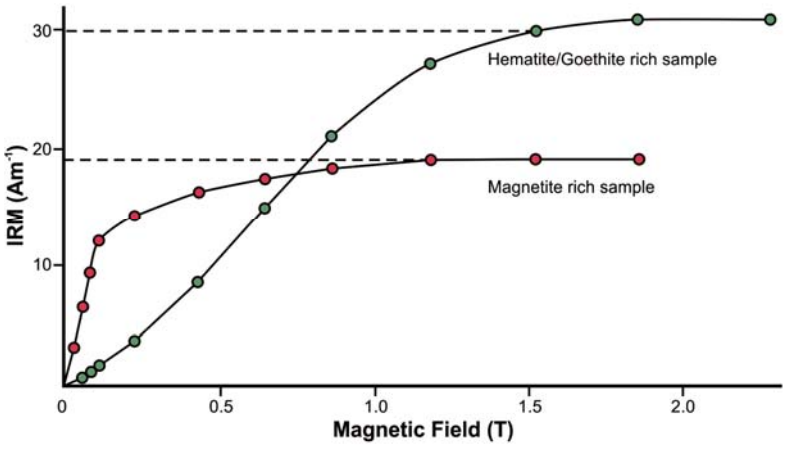

Fig. 4.2: Examples of IRM acquisition curves of a magnetite rich rock and of a hematite/goethite rich rock.

Coercivities lower than 0.1T are mostly due to magnetite, between 0.1T and 0.3T are due to detrital hematite, and those greater than 0.3T are due to authigenic hematite and goethite. On the other hand, the **three-axis IRM analysis**, the sample is induced with three different fields (soft, medium and hard) each one in a different and perpendicular axis (Lowrie, 1990). The resultant thermal demagnetisation of the sample is then analysed. This process is repeated stepwise increasing the heating temperature. The identification of the mineralogy consists of plotting and visual evaluating the thermal decay of each component separately. Table 4.1 shows the different characteristic maximum coercitivity and unblocking temperatures of the most common ferromagnetic minerals.

Table 4.1: Maximum coercitivity and unblocking temperature of the ferromagnetic minerals. (From Lowrie, 1990).

Ferromagnetic mineral	Maximum coercitivity (T)	Unblocking temperature (ºC)
Magnetite	0.3	575
Maghemite	0.3	350
Titanomagnetite (0.3)	0.2	350
Titanomagnetite (0.6)	0.1	150
Pyrrhoite	0.5-1	325
Hematite	1.5-5	675
Goethite	>5	80-120

The NRM is affected by geological processes during rock formation and its subsequent evolution. The NRM acquired during the formation of rocks is known as primary NRM. In addition, secondary NRMs can be acquired during the history of the rock resulting in a partly or total alteration of the NRM. In nature, there are three different forms of NRM acquisition depending on the operating mechanism:

1) **Thermoremanent Magnetism** (TRM) is produced when cooling a rock volume that crosses the Curie temperature. This process locks the ferromagnetic minerals with the magnetic field present. This type of NRM is characteristic of igneous rocks.

2) **Chemical Remanent Magnetism** (CRM) is acquired during mineral growth or alteration of previous minerals below the Curie temperature. It

can occur during the early stages of burial or during the exhumation of the rocks. It is commonly related to sedimentary rocks.

3) **Detrital Remanent Magnetism** (DRM) is developed by the alignment of detrital ferromagnetic minerals in a sedimentary rock with the presence of a magnetic field. After the sedimentation of the grains, the lithification processes compact the rock locking the orientation of the ferromagnetic minerals.

The laboratory treatment of the paleomagnetic studies is focused to isolate the stable component of the magnetisation known as the characteristic remanent magnetisation (ChRM). This is performed by demagnetising the rock specimens using stepwise thermal or alternating field demagnetisations and measuring the resultant component at each step. The data are plotted into a vector component diagram in which the progressive demagnetisation is represented (Fig. 4.3) (Zijderveld, 1967).

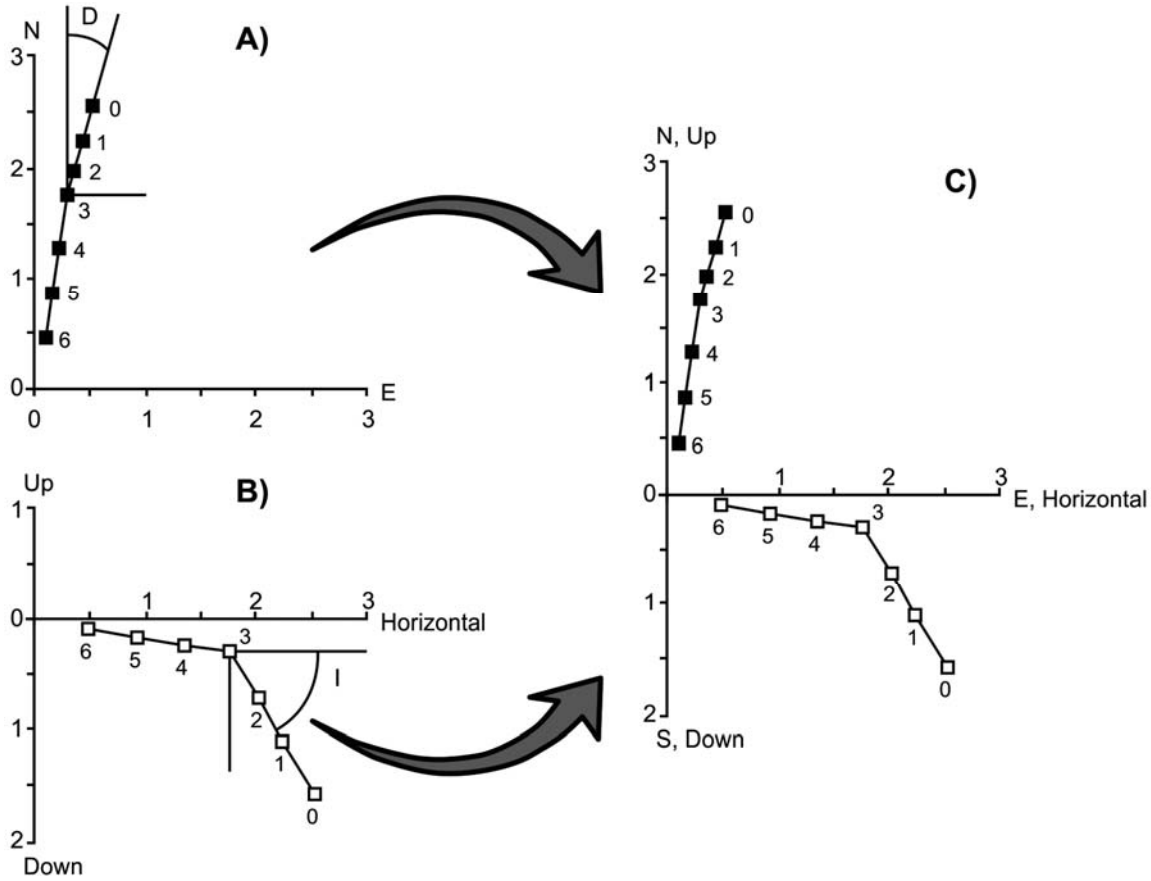

Fig. 4.3: Decomposition of the Zijderveld diagram. A) projection of the NRM onto the horizontal plane. B) Projection of the NRM onto the vertical plane. C) Combination of the previous diagrams into a single one. Solid points corresponds to the projection onto the horizontal plane whereas, open points corresponds to the projection onto the vertical plane. D corresponds to declination, I to inclination and the numbers next to the points are the different demagnetisation steps. Modified from Butler, 1992.

Zijderveld diagrams are the result of the combination of two orthogonal projections. On one hand, the projection onto the horizontal plane in which the declination at each demagnetisation step can be calculated (Fig. 4.3A). This projection can be oriented either N-S as in the example of Fig. 4.3A or W-E. On the other hand, the projection onto the vertical plane of each demagnetisation step, in this diagram, the inclination can be calculated (Fig. 4.3B). The combination of these two diagrams into a single one allows to display the information about the direction and intensity of the demagnetised specimen (Fig. 4.3C). Using Zijderveld diagrams the different NRM directions can be directly determined by visual fitting the best trend for each NRM direction observable in the diagram. In the example of Fig. 4.3C two different NRM directions are present. One, from demagnetisation step 0 to 3 and the other from 3 to 6.

The calculated characteristic remanent magnetisation (ChRM) direction is then analysed in order to test its primary origin. Stability field tests allow to know the relative timing of magnetisation. Among others, the conglomerate test, the reversal test, the baked contact test, the consistency test and the fold test. The latter one used in this thesis is commonly used in magnetotectonic studies and it is explained below.

- **Fold test:** This test allows to evaluate the relative timing of ChRM acquisition respect to folding. The method consists on calculating the characteristic directions of a determined unit in both limbs of a fold. Once the directions are calculated, the directions tectonically corrected and uncorrected are plotted and compared. If the data converge after unfolding respect to the original folded directions, the test is positive revealing that the magnetisation was acquired prior to deformation (Fig. 4.4A). On the contrary, if the directions are scattered once unfolded, the test is negative denoting that the magnetisation was acquired after folding (Fig. 4.4B). Magnetisation can also occur synchronically to the folding. In this particular case both, the corrected and the uncorrected data remain scattered and the data only cluster if the structure is partially restored. The fold test can be either used in a small scale fold, sampling both limbs in the same site, or in a more regional scale fold sampling two or more different sites, in both limbs, with the same age and lithology.

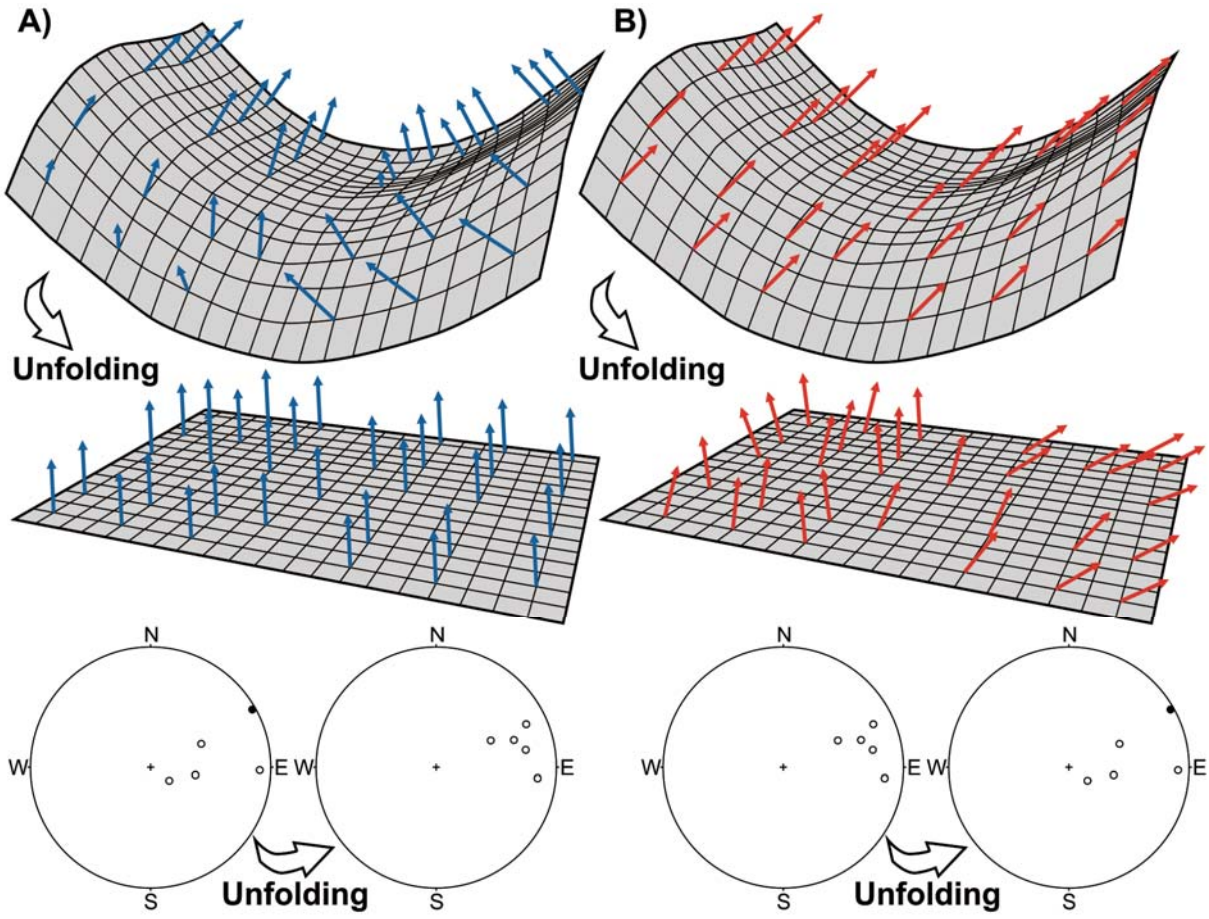

Fig. 4.4: Simplified examples of the fold test. A) Positive fold test in which magnetisation occurred previously to the folding and where the data cluster after tectonic correction. B) Negative fold test with post-folding magnetisation with a scattering of the data after unfolding the limbs. Modified from McFadden (1998) and Butler (1992).

McFadden fold test: In 1990, McFadden developed the test based on the relationship between the tectonic data and the paleomagnetic mean directions. The test stepwise unfold the structure and determines the K value that is the precision parameter of scattering of the data in both limbs. This test is represented plotting the percentage or Fisher concentration of unfolding against the K value. Once the K is maximum it is reached the minimum scattering of the directions determining the percentage of unfolding most suitable for the fold (Fig. 4.5A).

Direction-correction tilt test: Purposed by Enkin (2003) determines the relationship between the dipping of the beds and the paleomagnetic mean direction. This test determines the degree of untilting that gives the minimal dispersion of the direction by means of analytical methods (Fig. 4.5B).

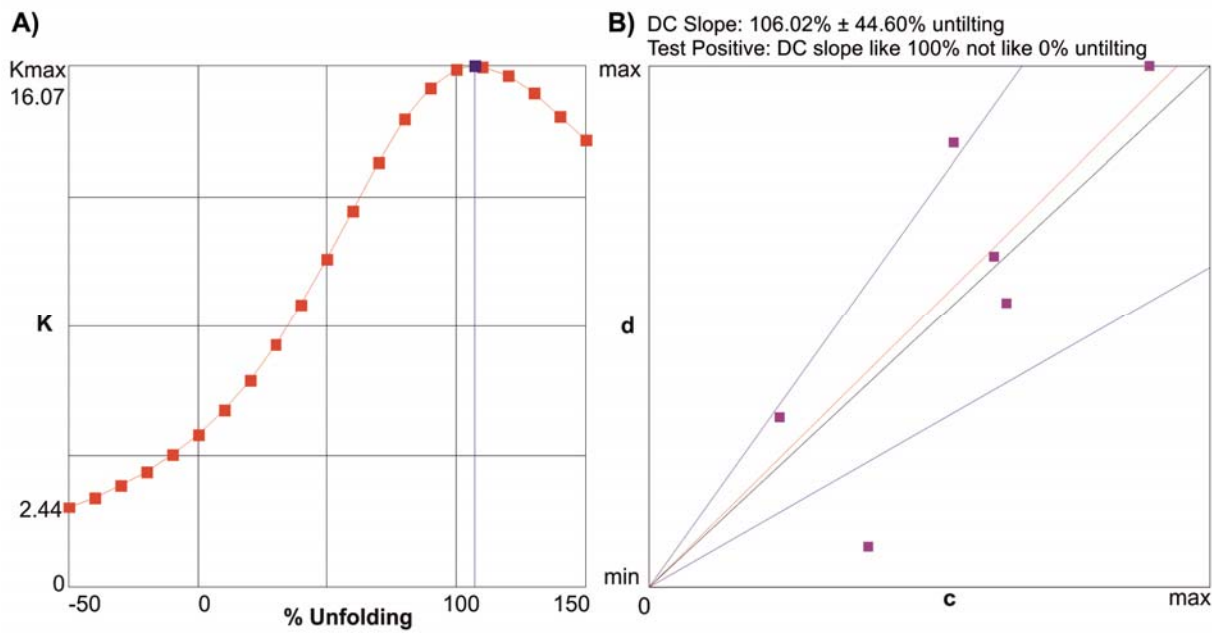

Fig. 4.5: Two example of fold tests. A) McFadden fold test plot with 16.07Kmax value and around 110% unfolding. B) Enkin direction-correction tilt test with a 106.02% ± 44.6% unfolding.

From all the possible applications of paleomagnetism, only the studies applied to solve tectonic problems at a sub-continental scale, also known as magnetotectonics (McClelland *et al.*, 1985), are explained in this chapter.

The ability of paleomagnetism of recording the original paleomagnetic field direction has been used to characterise the origin of the salients and recesses by means of the study of vertical axis rotations (Van der Voo & Channell, 1980, Schwartz & Van de Voo, 1984; Eldredge & Van der Voo, 1988; Butler *et al.*, 1995; Gray & Stamatakos, 1997; Allerton, 1998; Sussman and Weil, 2004; Weil *et al.*, 2010; Muñoz *et al.*, 2013 among others). The procedure carried out in this studies consists on comparing the measured directions of a determined unit in a deformed plate with the direction, for the same unit, in a stable area. The presence of an angular difference in the declination direction implies that rotation about a vertical axis of the deformed plate has occurred (Fig. 4.6). The theoretical model of the development of arcs by rotating the limbs around the vertical axis predicts that the rotation direction must point towards the inner parts of the arc, resulting in clockwise rotation in one limb, counter clockwise rotation in the other and no rotation in the centre of the arc with respect to the direction from the stable plate (Fig. 4.6).

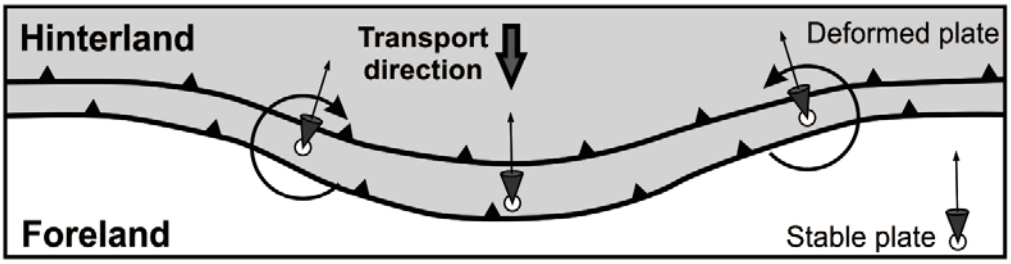

Fig. 4.6: Representation of the expected rotations at both limbs of the salient compared to the stable and undeformed foreland.

Three different types of curvatures can be determined depending on the kinematics of the structure by means of Vertical Axis Rotation (VAR) studies (Fig. 4.7). The **Primary Arcs** (Fig. 4.7A) are developed by inherited curved structures without tightening during the evolution. During the development of the new structures, no vertical axis rotation of the foreland is produced. Usually, the curved structures are developed by inhomogeneities either in the stratigraphic record (i.e. lateral pinch-outs or lateral facies changes) or in the inherited trend of the structures (i.e. irregular limit of the basin, different trend of the faults). In this case, the measured direction of the rocks in the thrust and fold belt must be equal to the stable direction of the rocks in the foreland basin. The **Secondary Arcs** (Fig. 4.7B) are folded linear structures developed previously to the deformation. In this case, the amount of VAR must be equal to the present day angle of the structures in the thrust and fold belt. The **Progressive Arcs** (Fig. 4.7C) are formed by both, inherited curved structures and vertical axis rotations during the emplacement of the thrusts. Studying the pre-, syn- and post-orogenic sediments, the amount of vertical axis rotation and its timing can be determined.

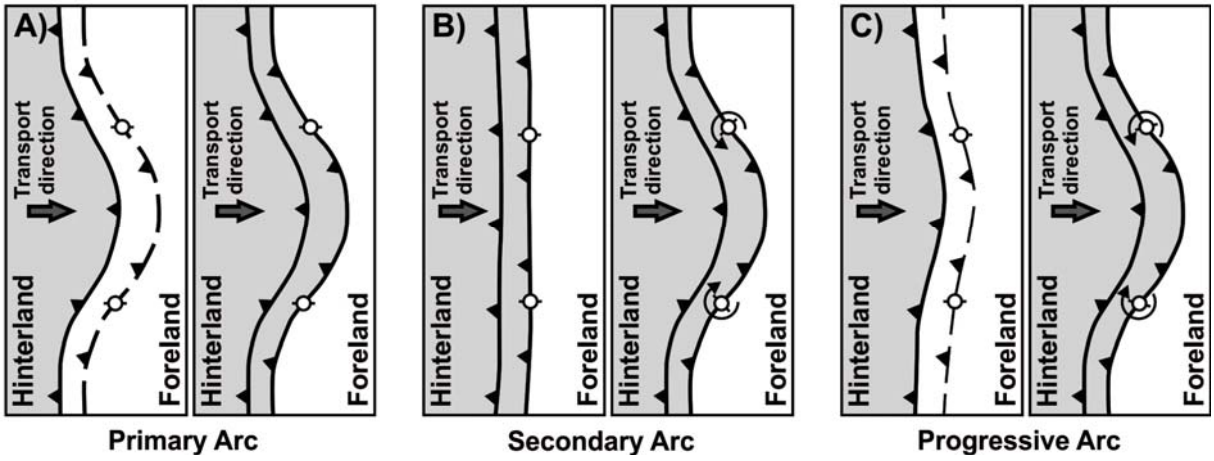

Fig. 4.7: Origin of curvatures present in most of the orogens worldwide. A) Primary curvature with non-rotational structures. B) Secondary curvature developed by limb rotation around the vertical axis. C) Progressive curvature with both, primary curved structures and vertical axis rotation.

The difference between the final angle of the structures in the thrust and fold belt and the angle of VAR results in the original curvature of the inherited structures. For a progressive arc, this VAR angle cannot be zero and must be less than the present angle of the thrust and fold belt. The first scenario would correspond to a primary arc, the second case, would correspond to a secondary arc.

4.2 The paleomagnetic study at the Burgalesa Platform and surroundings

The paleomagnetic study carried out in the Burgalesa Platform and surroundings, is made up of sixty-two sampled sites with a mean of ten samples per site. The main objective was to determine the vertical axis rotation occurred during the Cenozoic. For such purpose, forty-three sites where drilled in Eocene to Miocene units, eighteen in the Upper Cretaceous and one in the Lower Cretaceous. In this sub-chapter are presented: 1) The mineralogical characterisation in twelve different sites using the combined analysis of IRM acquisition and three-axis IRM; 2) The quality of the data depending on the lithology of each age; 3) The fold tests (i.e. two local and two regional fold tests) in order to know the stability of the magnetisation; and, 4) The characteristic direction of the different sites in order to know the vertical axis rotation occurred during the Cenozoic.

4.2.1 Mineralogy

The study of both, IRM acquisition and three-axis IRM analysis, allow to determine the ferromagnetic mineralogy of the sampled rocks. Two different groups have been identified depending on the magnetic carriers of the sampled sites: (titano)magnetite and hematite groups.

The (titano)magnetite group is characterised by an abrupt saturation increase from 0 up to 0.2T, point in which the sample is almost saturated. Then the saturation follows a flat trend up to 1.2T. The three-axis plot shows that the predominant axis is the soft one (axis induced with 0.1T). It experiences a decrease from 0ºC to 360ºC and then the trend smoothes up to 680ºC (Fig. 4.8 A and B). The (titano)magnetite dominant mineralogy is the main remanence carrier of the Upper Cretaceous and Miocene limestones and grey clays.

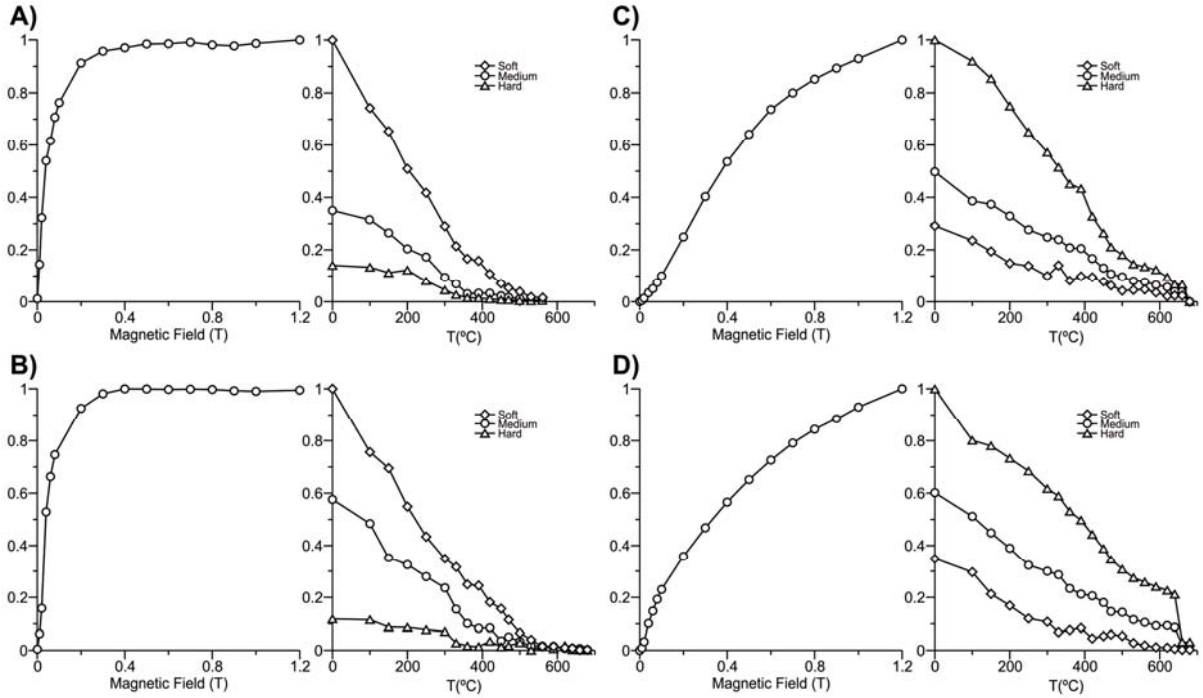

Fig. 4.8: IRM acquisition and three-axis analysis normalised to one and corresponding to: A) Miocene grey clays of the FC02 site; B) Upper Cretaceous dark shales of the FC21 site; C) Lower Miocene red clays of the FC07 site; and, D) Oligocene red clays of the FC22 site. A and B are enclosed in the (titano)magnetite group whereas, C and D are enclosed in the hematite group.

On the other hand, the hematite group is characterised by a progressive increase up to 1.2T, point in which the saturation of the sample is not reached. In the three-axis plot, the predominant axis is the hard one (induced with 1.2T) and presents a constant decrease up to 640ºC, temperature in where the magnetisation decreases abruptly (Fig. 4.8 C and D). The hematite dominant mineralogy is the predominant remanence carrier of the Lower Cretaceous and Oligocene-Miocene fine grain sandstones and red clays.

4.2.2 Quality of the data

In order to calculate orientations from the data, an accurate analysis of the quality of the data is required. The quality of the samples has differences depending on their lithology and age.

The Upper Cretaceous samples consists of limestones, marls and dark shales. The quality of the limestones cannot be generalised, as some sites have good quality data whereas other sites are characterised by bad quality data. This is due to the small amount of magnetic minerals in limestones. For the same reason, it is difficult to obtain good quality data from the marls. Finally, the dark shales data usually presents regular or bad quality due to the presence of sulphurs (Fig. 4.9).

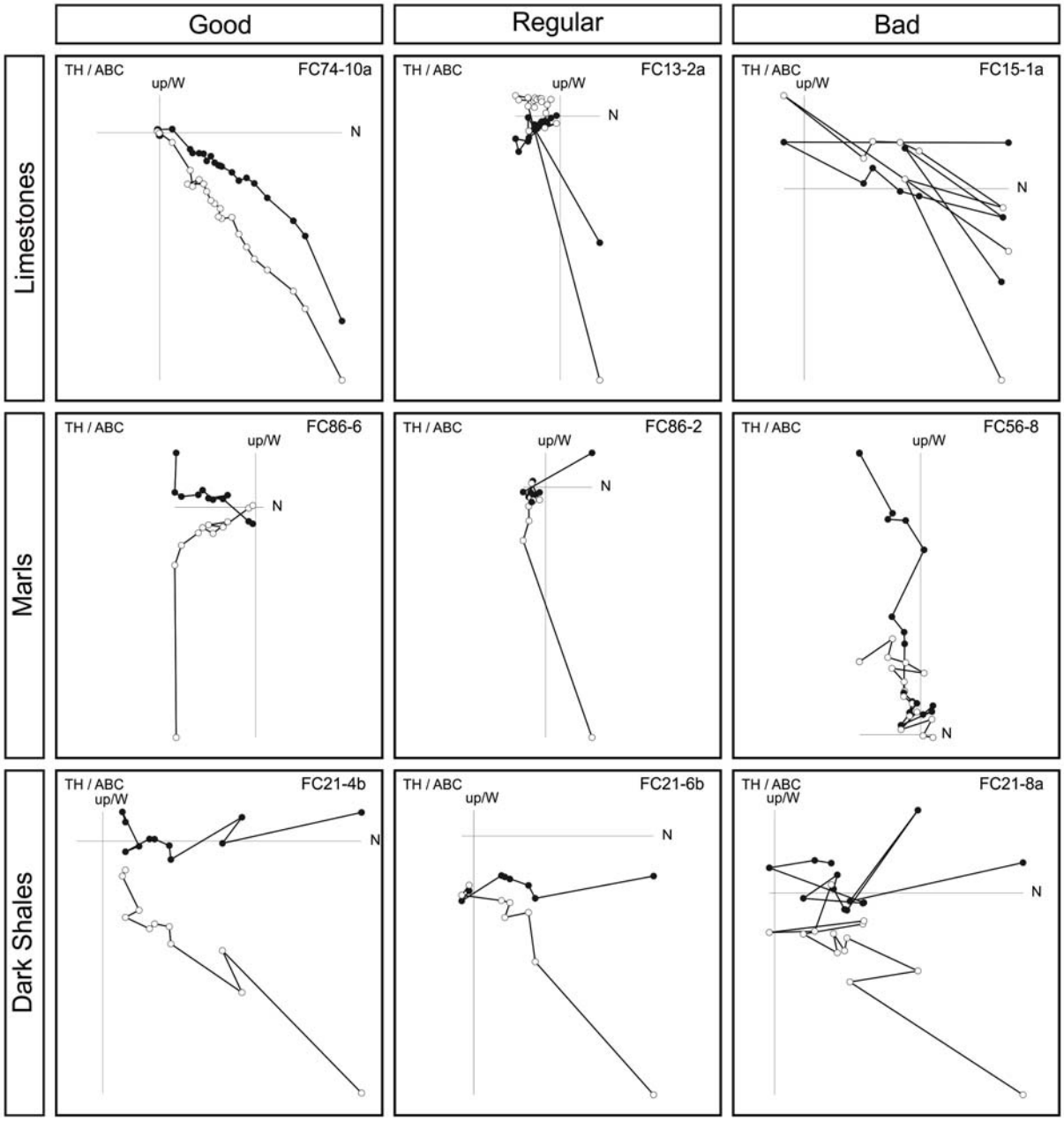

Fig. 4.9: Zijderveld diagrams showing quality examples of the Upper Cretaceous lithologies.

The Cenozoic sampled sites are characterised by red clays, grey clays and white clays. The first two lithologies usually have good to regular quality, although bad quality data is obtained in a few samples. Red clays have shown better results than the other lithologies due to the presence of hematite. White clays show a tendency similar to limestones, in which the small amount of magnetic minerals results in regular quality data (Fig. 4.10).

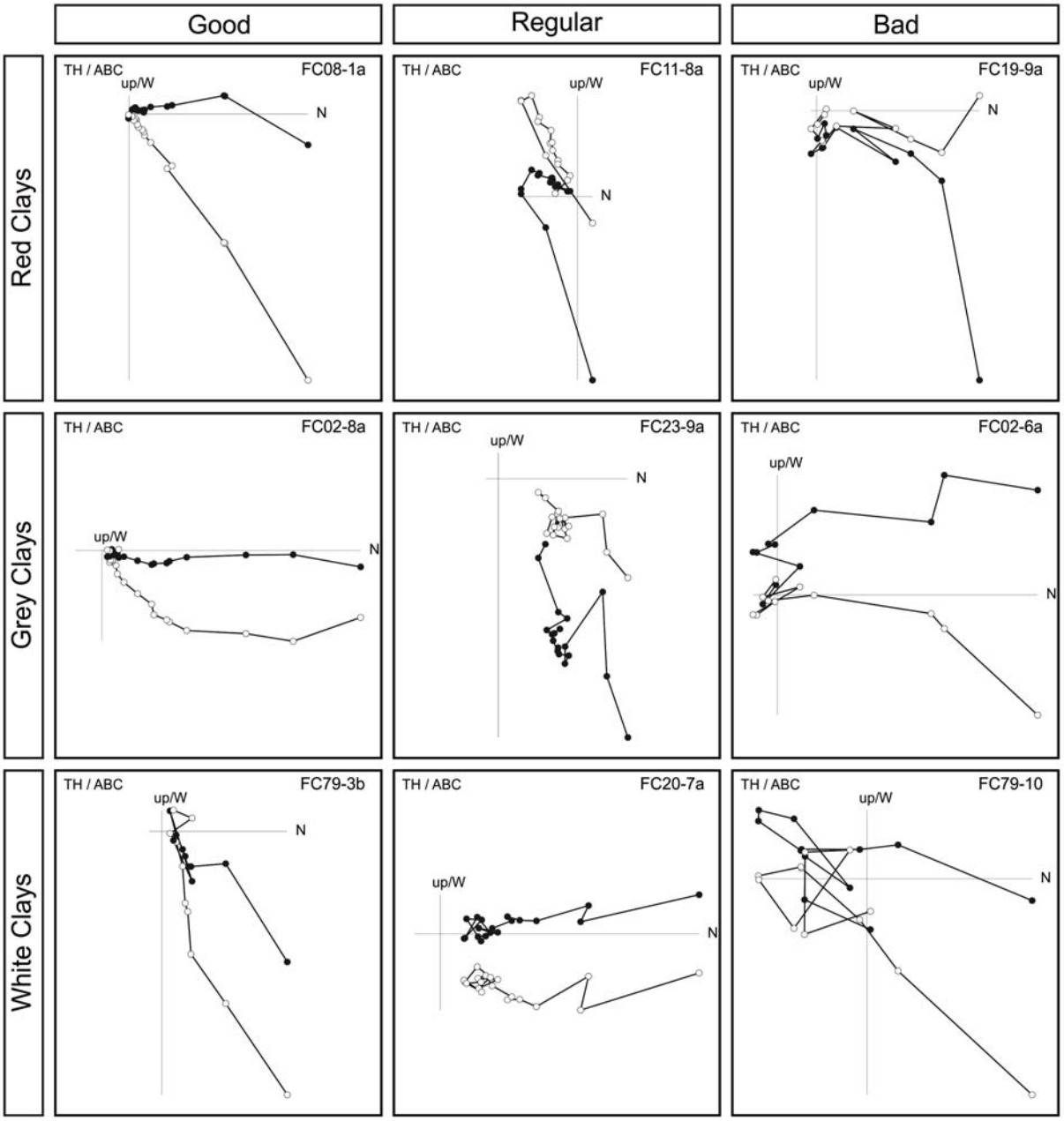

Fig. 4.10: Zijderveld diagrams showing quality examples of the Cenozoic lithologies.

4.2.3 Fold tests

In order to test and evaluate the relative timing of acquisition of the characteristic remanent magnetisation respect to folding, two local fold tests, one in Upper Cretaceous limestones and another one in Miocene clays and sandstones, have been carried out. Even though the good exposure quality of the Upper Cretaceous FC-66 site, in which the fold test was performed (Fig. 4.11), the scattered and bad quality data do not allow to apply the fold test neither to obtain the characteristic direction for this site.

Fig. 4.11: Field image of the FC-66 Upper Cretaceous limestones site sampled in order to perform a fold test.

In contrast, the quality of the data in the Miocene sampled FC-01 site (Fig. 4.12) allowed to test the timing of magnetisation. The stereographic projections show that the data are scattered before bedding correction and clustered after bedding correction (Fig. 4.13A). In addition, applying the McFadden fold test, the best fit is reached with a 90% unfolding being the Kmax 16.34 (Fig. 4.13B). Finally, testing with the Enkin direction-correction tilt test, the best fit is reached at 85.33% ±17.16% (Fig. 4.13C). All the evidence point towards a positive fold test in which magnetisation was acquired before the folding of the strata.

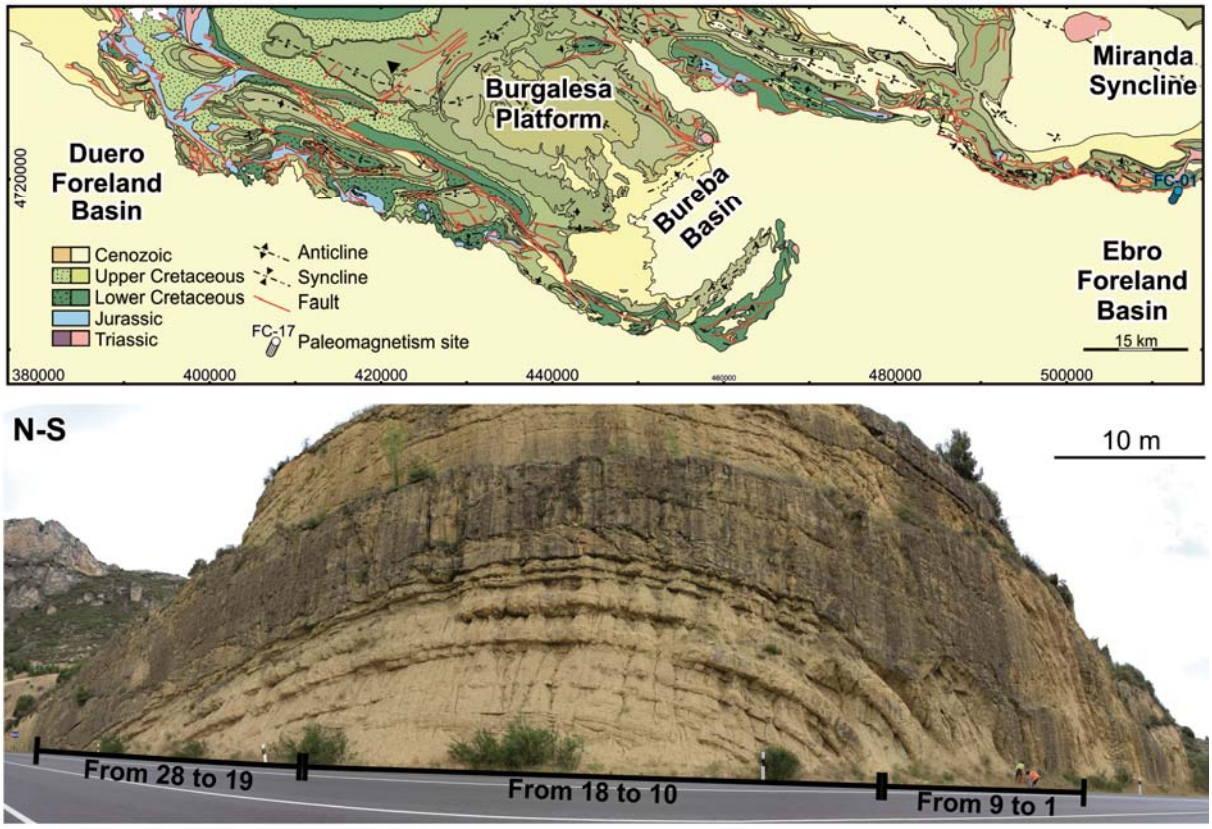

Fig. 4.12: Map and field image of site FC-01 located in the Miocene units of the foreland basin, where the local fold test was performed. The numbers in the photograph correspond to the numbers of the samples obtained in the field.

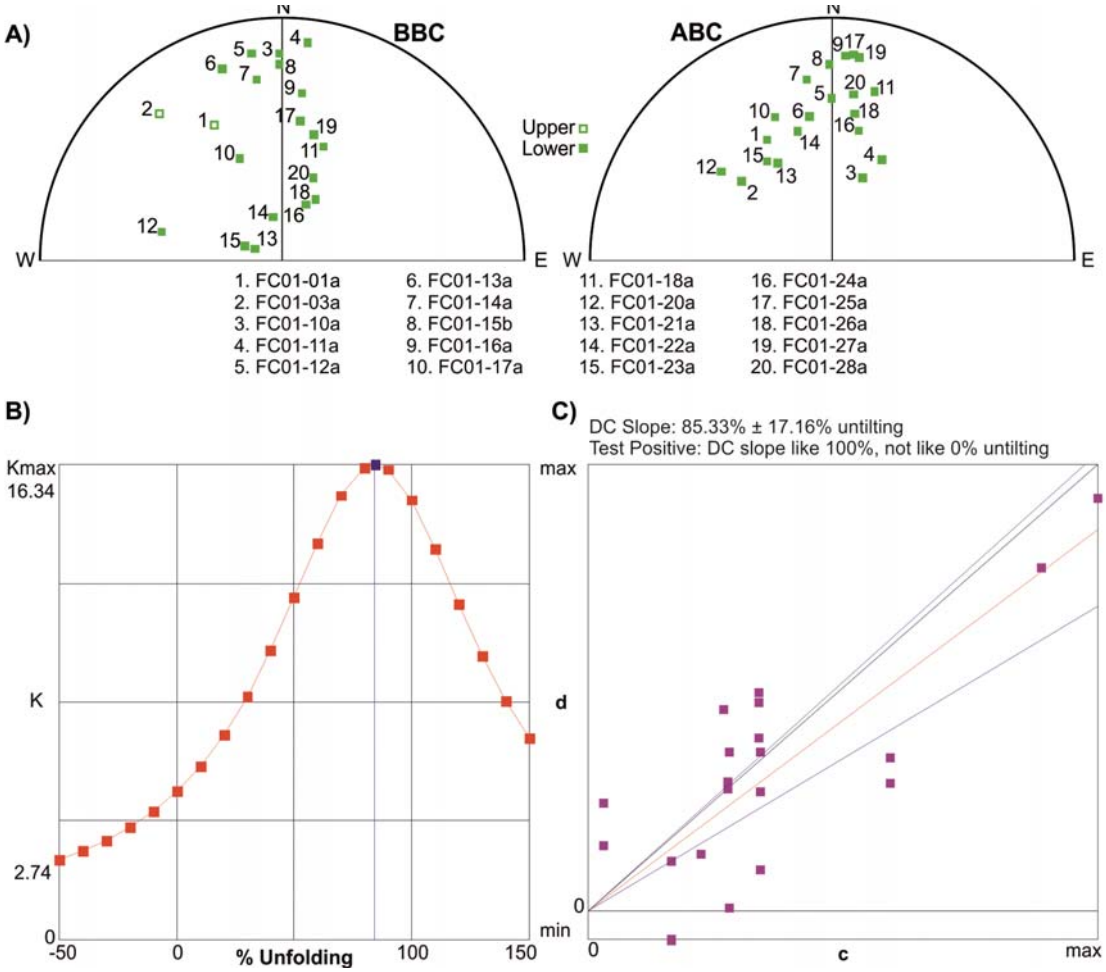

Fig. 4.13: Results of the local fold test of the site FC-01. A) Stereographic projection of the directions Before Bedding Correction (BBC) and After Bedding Correction (ABC) B) McFadden fold test. C) Enkin direction-correction tilt test.

Additionally, two regional fold test have been carried out. One with the Miocene sites in the Miranda syncline area located to the west of the Burgalesa Platform and another one with all the Miocene sites of the study carried out in the southern sector (Fig. 4.14).

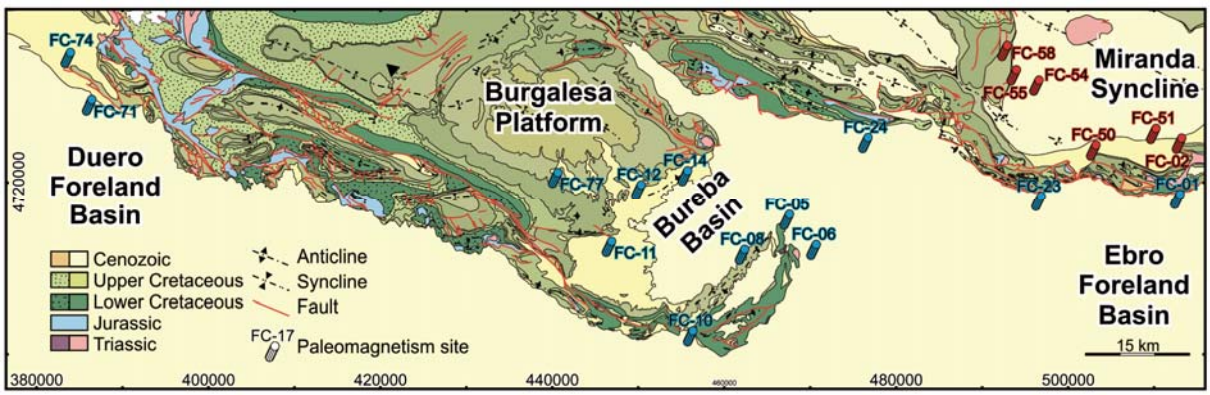

Fig. 4.14: Schematic map of the Western Pyrenees showing the sites of the two regional fold tests carried out within the Miocene units. Red paleomagnetic symbol corresponding to the Miranda syncline fold test. Blue and red paleomagnetic symbols corresponding to all Miocene sites of the 1) Miranda syncline; 2) Ebro Foreland Basin; 3) Bureba Basin; 4) Burgalesa Platform; and, 5) Duero Foreland Basin.

The results of the Miranda regional fold test show how in the stereographic projections of the six sites are scattered before bedding correction and clustered after bedding correction in the lower hemisphere of the first quadrant and in the upper hemisphere of the third quadrant (Fig. 4.15A). The McFadden fold test reaches a Kmax of 16.07 with a 110% unfolding (Fig. 4.15B) and the Enkin direction-correction tilt test presents the best fit at 106% ± 44% unfolding (Fig. 4.15C). The McFadden and Enkin tests resulted positive showing that the magnetisation was acquired before the folding of the Miranda syncline.

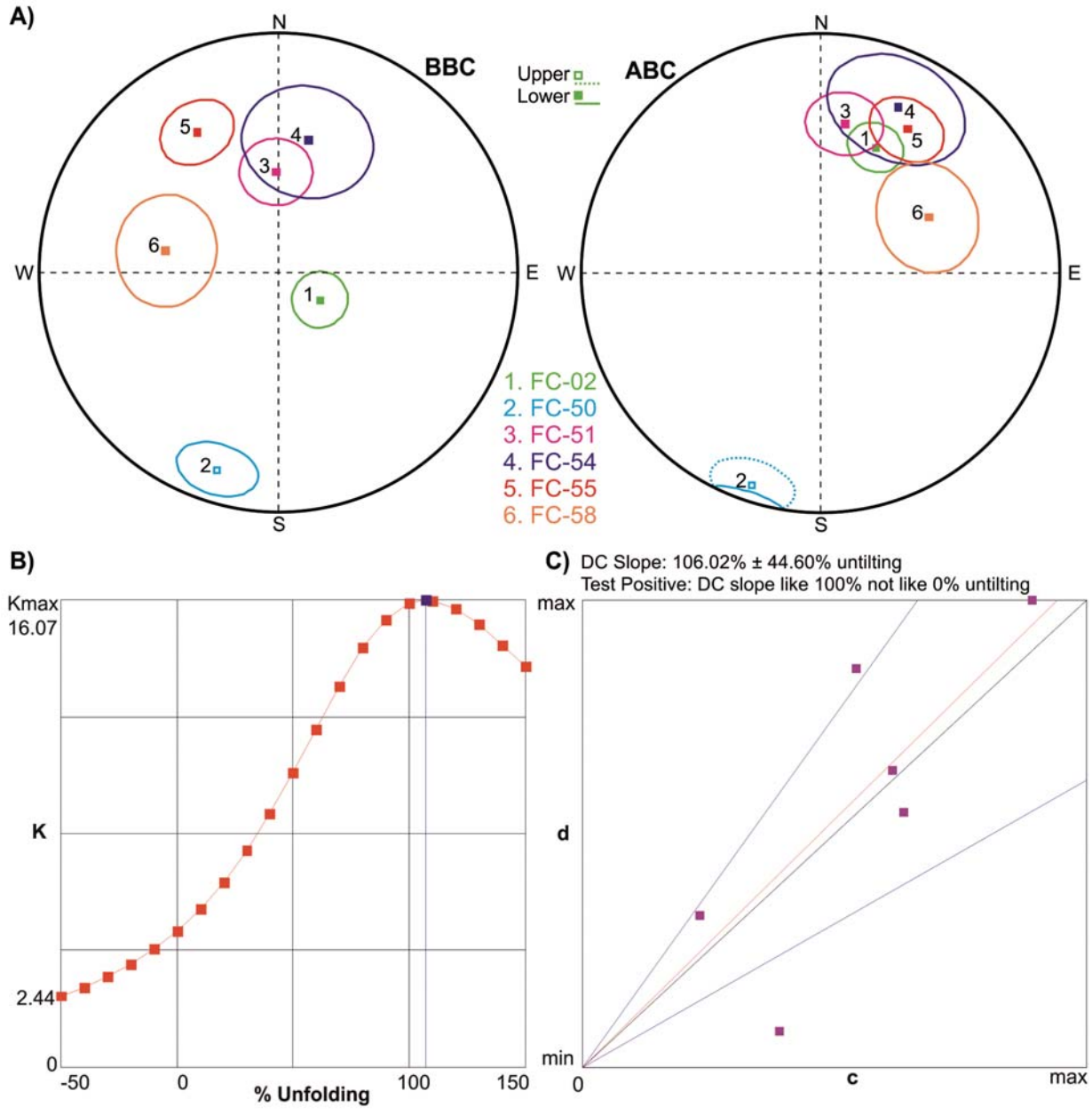

Fig. 4.15: Results of the regional fold test with all the Miocene sites within the Miranda syncline area. A) Stereographic projection of the directions Before Bedding Correction (BBC) and After Bedding Correction (ABC) B) McFadden fold test. C) Enkin direction-correction tilt test.

Finally, the stereographic projections taking into account all the Miocene sites of the southern limit of the Basque Pyrenees show how the sites are scattered before bedding correction. Once corrected, the sites roughly clusters into the lower hemisphere of the first quadrant and in the upper hemisphere of the third quadrant (Fig. 4.16A). The scattering in the corrected stereographic plot could be caused because the sites are not in the same structural domain. In the McFadden test, the Kmax of 19.46 is reached with a 82% unfolding (Fig. 4.16B). The Enkin test presents the best fit with 85.8% ± 25.4% unfolding (Fig. 4.16C). Although the sites are distant and from different sectors, the fold test resulted positive reaffirming that the Miocene magnetisation was acquired before deformation.

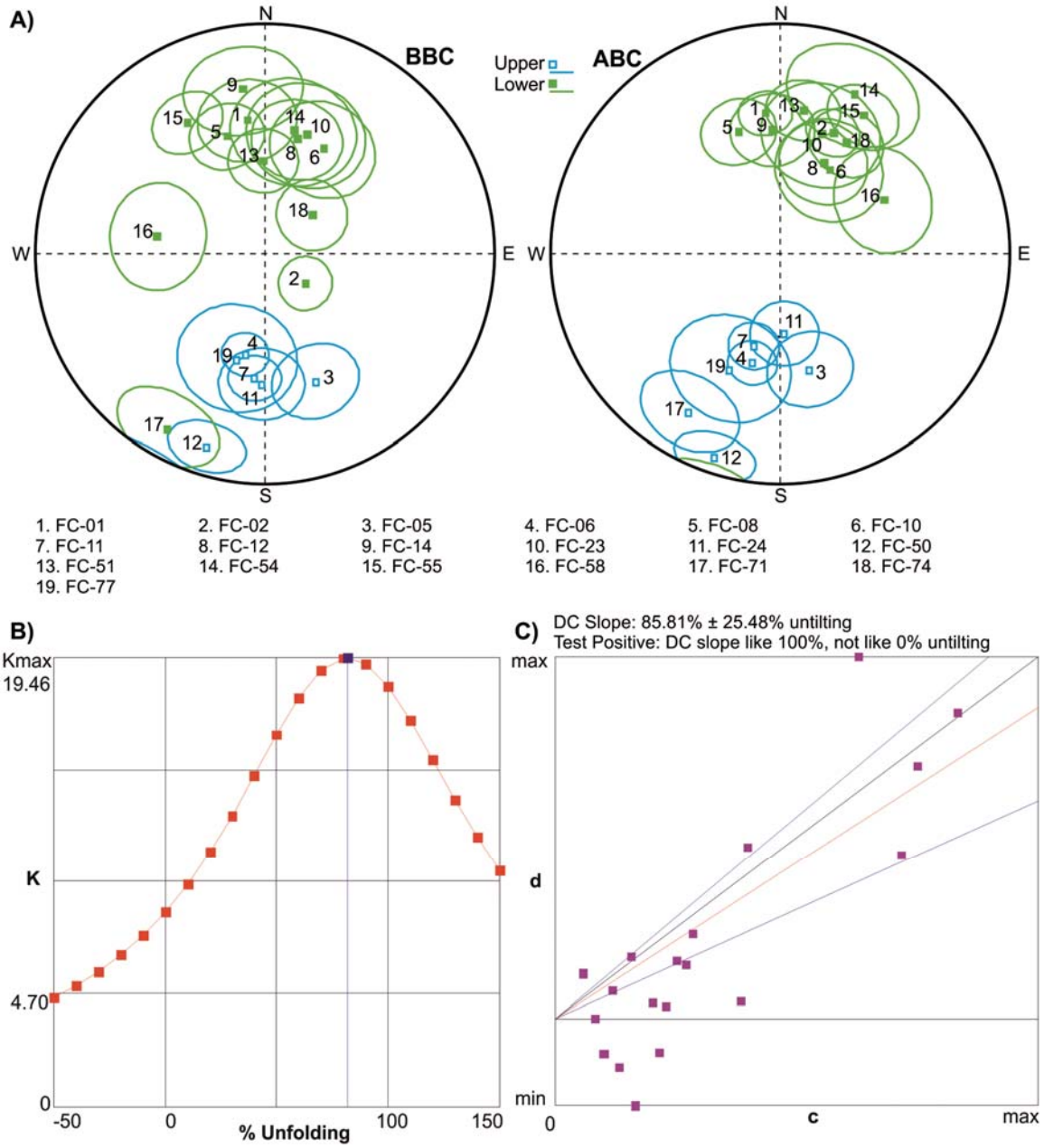

Fig. 4.16: Results of the regional fold test with all the Miocene sites. A) Stereographic projection of the directions Before Bedding Correction (BBC) and After Bedding Correction (ABC) B) McFadden fold test. C) Enkin direction-correction tilt test.

4.2.4 Vertical axis rotations in the different sectors of the studied area

From the sixty-two sampled, analysed and calculated sites twenty-six gave good results being the α_{95} value close to 20 or below. The results show that the different sites experienced clockwise and counter-clockwise rotations (Table 4.2).

Table 4.2: Summary table of the paleomagnetic sites divided into the different structural units. ID corresponds to the site number of Fig. 4.17; Dg/ig to the paleomagnetic direction calculated without tectonics correction; Ds/is to the paleomagnetic direction with tectonics correction; and V.A.R. to the Vertical Axis Rotation.

Structural Unit	Site	ID	Age	Lithology	S0	Dg/ig	Ds/is	α_{95}	V.A.R
Burgalesa P	FC05	14	Lower Miocene	Red Clays	115/10	158/-40	165/-46	14.3	**-17.1**
Burgalesa P	FC06	15	Lower Miocene	Red Clays	045/05	191/-53	194/-49	8.2	**11.4**
Burgalesa P	FC08	16	Lower Miocene	Red Clays	320/02	342/45	341/43	12.5	**-21.5**
Burgalesa P	FC09	17	Upper Cretaceous	Limestones	017/39	346/69	003/32	13.2	**3**
Burgalesa P	FC10	18	Miocene	Red Clays	202/11	029/46	031/55	17.9	**28.8**
Burgalesa P	FC11	19	Lower Miocene	Red Clays	152/14	185/-45	196/-55	8.7	**13.5**
Burgalesa P	FC12	20	Lower Miocene	Red Clays	152/11	016/47	196/-55	15.2	**13.5**
Burgalesa P	FC14	21	Lower Miocene	Red Clays	155/21	352/28	357/45	13.9	**-5.5**
Burgalesa P	FC15	22	Upper Cretaceous	Limestones	022/21	313/28	335/49	16.3	**-25.1**
Burgalesa P	FC67	6	Upper Cretaceous	Limestones	338/16	297/51	306/38	6.3	**-54**
Burgalesa P	FC71	7	Lower Miocene	Red Clays	200/35	209/14	209/-31	15.5	**24.6**
Burgalesa P	FC74	8	Lower Miocene	Red Clays	015/28	051/68	031/43	12.6	**26.6**
Burgalesa P	FC77	9	Lower Miocene	Red Clays	070/10	195/-50	031/43	20.2	**26.6**
Burgalesa P	FC78	10	Upper Cretaceous	Limestones	051/11	176/-49	184/-42	13.7	**4**
Ebro Foreland	FC01	12	Miocene	Clays / Sandstones	FOLD	352/41	354/38	8.7	**-8.4**
Ebro Foreland	FC23	25	Miocene	Grey Clays	000/00	019/44	019/44	19.9	**16.5**
Ebro Foreland	FC24	26	Lower Miocene	Red Clays	192/23	181/-42	177/-61	11.8	**-5.5**
Miranda S.	FC02	13	Miocene	Grey Clays	005/56	126/72	024/42	8.9	**26.4**
Miranda S.	FC50	1	Lower Miocene	Red Clays	063/29	197/-13	198/-7	11.1	**13.6**
Miranda S.	FC51	2	Lower Miocene	Red Clays	032/22	359/56	009/37	11.9	**4.6**
Miranda S.	FC54	3	Lower Miocene	Red Clays	062/26	013/44	025/24	20.7	**21.6**
Miranda S.	FC55	4	Lower Miocene	Red Clays	091/79	329/24	031/30	11.7	**26.6**
Miranda S.	FC58	5	Lower Miocene	Red Clays	082/79	279/51	063/48	11.8	**58.6**
Villarcayo S.	FC17	23	Oligocene	Red Clays	059/16	337/37	342/36	15.7	**-22.2**
Villarcayo S.	FC20	24	Oligocene	White Clays	022/44	287/71	354/44	8.1	**-10.2**
Villarcayo S.	FC85	11	Oligocene	Red Clays	119/19	027/65	062/59	20.5	**57.6**

The stereographic projection of the directions and α_{95} value before bedding correction shows similarities with the projection of the fold tests in which the data are scattered and once the bedding is corrected, the data roughly clusters into two groups, one in the first quadrant located in the lower hemisphere and the second one in the third quadrant in the upper hemisphere (Fig. 4.17).

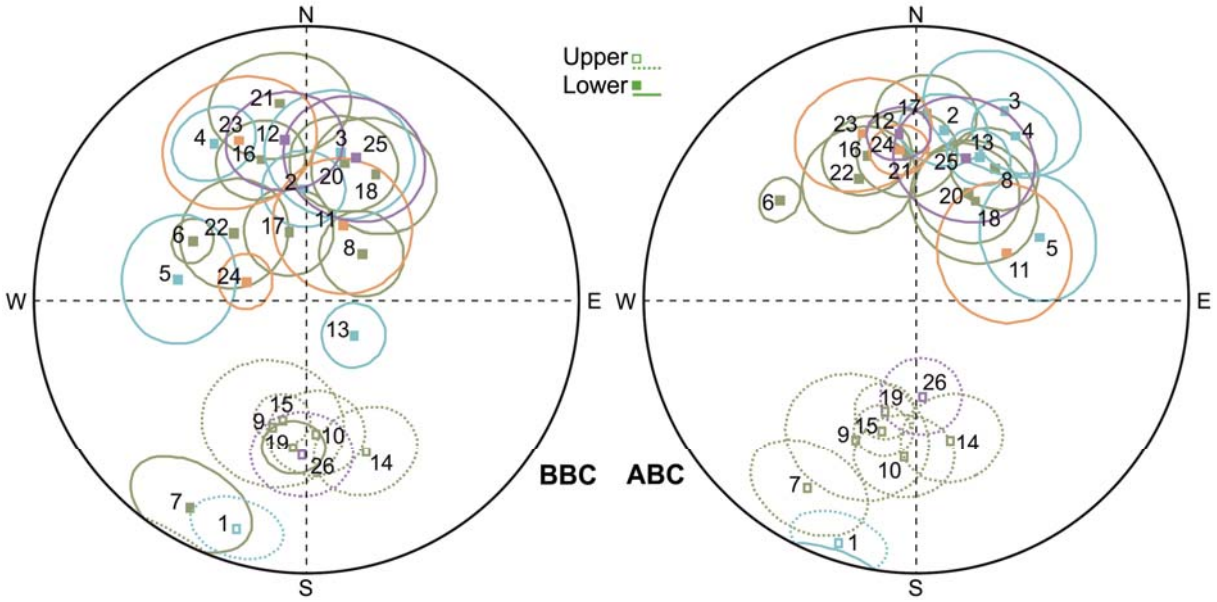

Fig. 4.17: Stereographic projection Before Bedding Correction (BBC) and After Bedding Correction (ABC), respectively of the mean directions and α_{95} associated for all the sites obtained in this study. The reference numbers inside the circles are related to the sites labelled in Table 4.2.

The sites, in which the quality of the data was enough to calculate the characteristic direction, are widely distributed in the different sectors covered by this study (Fig. 4.18). In the Miranda syncline area, the vertical axis rotation registered by the Miocene rocks denotes two different patterns, no rotation in the southern limb of the syncline whereas, clockwise rotation at the western sector with more than 25º of rotation. The Villarcayo syncline area is characterised by three sites in the southern limb, two presenting counter-clockwise rotation of about 10º to 20º and one with a high α_{95} and a clockwise rotation of 57º (FC-85). The northern limb of the syncline was sampled in six different sites but with unreliable directions. In the Rojas area located at the eastern area of the Bureba/Burgalesa Platform, counter-clockwise rotation of 20º is the main trend of the sites. In contrast, the sites located in the western area of the Bureba sub-basin do not register appreciable vertical axis rotation. Finally, the sites located close to the outcropping frontal structures in the Duero and Ebro foreland basin are characterised by clockwise rotation of about 25º in the Duero area and no appreciable rotation within the sites located in the Ebro foreland.

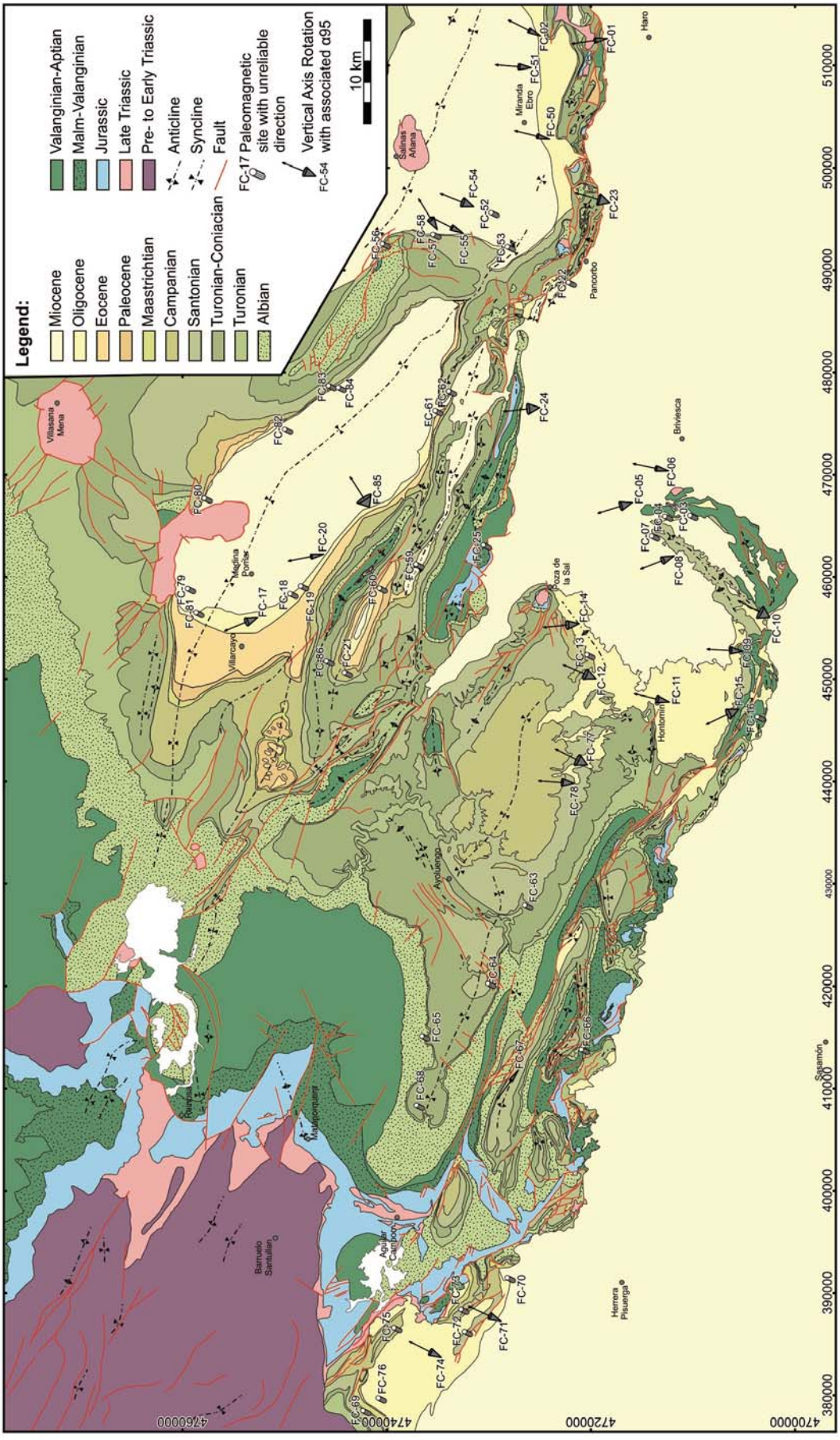

Fig. 4.18: Geological map of the studied area with the location of both, 1) paleomagnetic sites with good quality with the paleomagnetic vector and its associated α_{95} and, 2) sites without enough quality.

Chapter 5

Discussion

In this chapter a global discussion derived from the results of the scientific publications and from the paleomagnetic data is presented in order to provide a complete view of the study area and the implications of the main aspects regarding the structural interpretations of the Burgalesa Platform and vicinities. It has been divided into four different sections, each one covering a different topic:

- 5.1 Integration of foreland seismic data and surface geology with paleomagnetic data
- 5.2 Onlap geometry of the syn-rift sediments and its implications
- 5.3 The Huidobro north-directed thrust and the associated erosional truncation
- 5.4 Reinterpretation of the surface geology in the Zamanzas area

5.1 Integration of foreland seismic data and surface geology with paleomagnetic data

The surface geology of the Duero Foreland Basin adds few constraints about the deformation occurred during the Pyrenean Orogeny because of the horizontal disposition of the Cenozoic sediments of the basin. Only in the areas close to the frontal structures of the Burgalesa Platform, deformation in the Cenozoic sediments can be observed (Fig. 5.1).

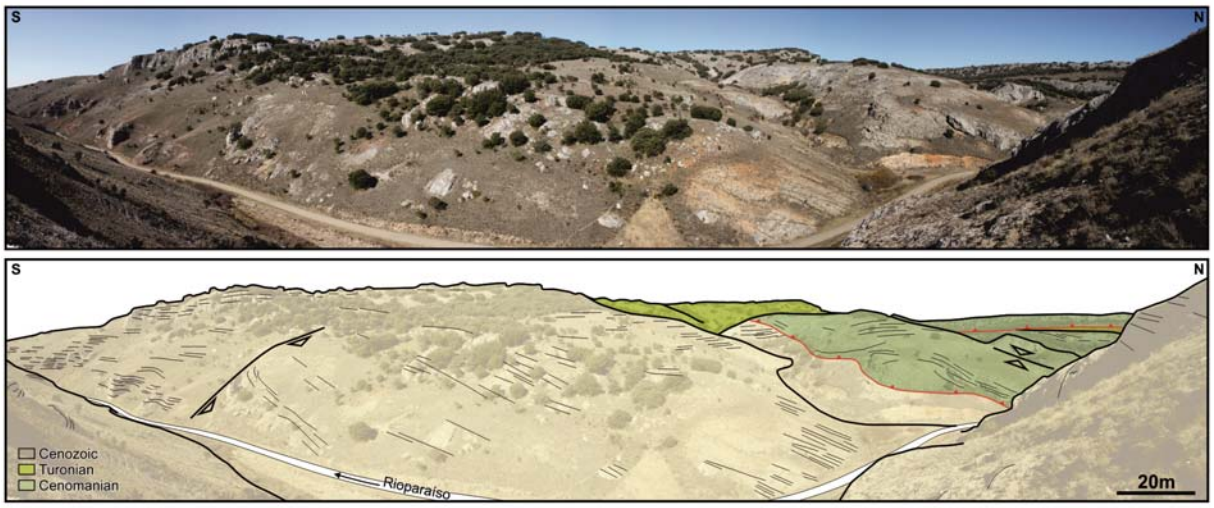

Fig. 5.1: Non interpreted (A) and interpreted (B) S-N photograph of the Duero Foreland Basin and the Burgalesa Platform thrust front. Note the deformation in the hangingwall of the thrust front and the bedding attitude of the Cenozoic succession close to it. Dip of beds diminishes southwards reaching a flat-lying attitude at the southern end of the photograph.

This issue can be overcome using the seismic network available in the foreland. In the seismic sections shown for the Ebro Foreland Basin in chapter 3, no observable deformation occurs below the most recent Cenozoic sediments, being the Mesozoic and Cenozoic successions flat-lying. In contrast, the seismic sections of the Duero Foreland Basin reveal the presence of structures below the outcropping Cenozoic sediments in two different sectors: i) the San Pedro structure located immediately to the south of the central part of the Burgalesa Platform and, ii) the sector situated to the northwest of the Herrera de Pisuerga locality and immediately to the south of the Burgalesa Platform frontal thrust (Fig. 5.2). These two sectors are characterised by basement-involved thrusts that also affect the Cenozoic and the Mesozoic successions.

The deformation in the San Pedro structure is the result of northeast-directed thrusts that involve the basement. The southernmost thrust deforms the succession above, producing a monoclinal flexure that in map view strikes almost parallel to the trace of the thrust (Fig. 5.2).

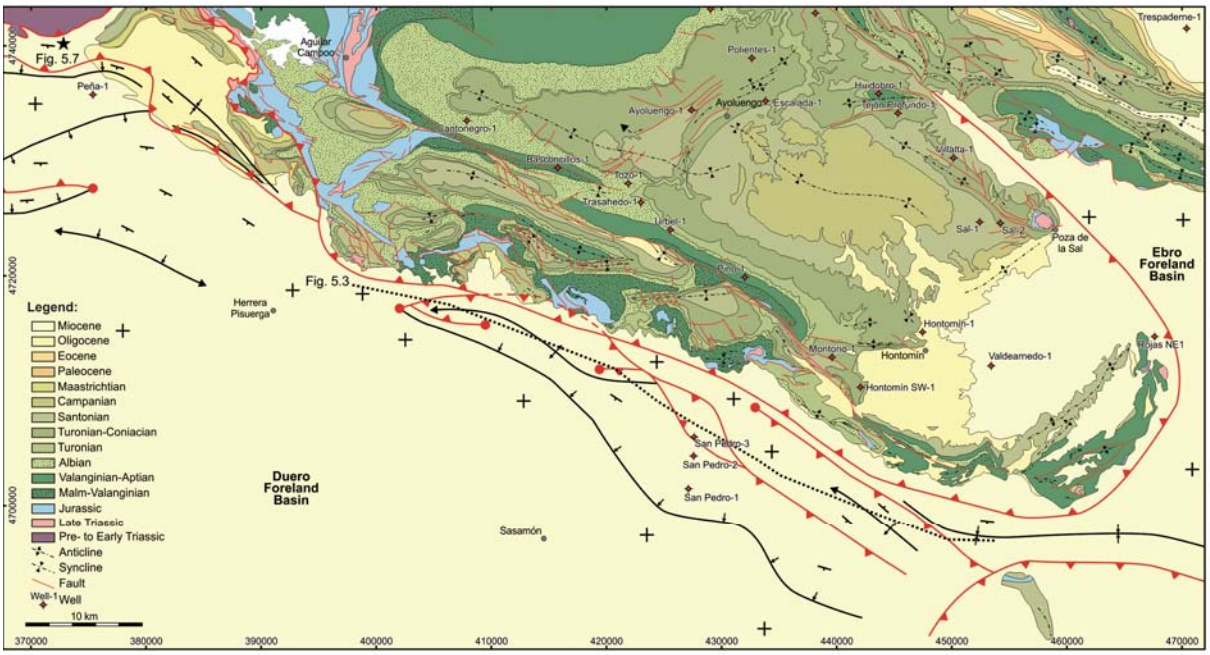

Fig. 5.2: Schematic geological map highlighting the thrusts of the foreland, nowadays covered by the Cenozoic sediments that mask the deformation at surface. Note the contrast between the Ebro Foreland Basin without deformation and the Duero Foreland Basin in which deformation is reported for the San Pedro and the Herrera de Pisuerga sectors.

The NW-SE composite section across the San Pedro structure (Fig. 5.3) allows to characterise the lateral ramps of the thrust system that develops this structure and how at both sides away from these ramps, the Mesozoic and Cenozoic successions are located at the same depth and show flat-lying isopach seismic facies. In contrast, in the central part of the seismic line, the characteristic seismic facies of the Mesozoic and Cenozoic successions appear deformed by several lateral ramps associated to the thrust system with a transport direction towards the northeast. At the north-western part of the San Pedro Structure, the Burgalesa Platform overrides this structure (Fig. 5.2). The detail of the seismic section located more to the south-east allow to determine and constraint the age of the contractional deformation occurred in the San Pedro Structure (Fig. 5.4). In this area, a lateral ramp, affecting the basement, deforms the Mesozoic and part of the Cenozoic successions. Eocene and Oligocene sediments showing growth geometries and Late Oligocene and Miocene fossilising this structure are well observable. These syn-contractional sediments experience an eastwards thickening passing from 0.5 TWT seconds in the hangingwall of the thrust to more than 1 TWT second thick succession in the footwall of this lateral ramp. To the west and below the seismic facies attributed to the syn-contractional sediments, the Mesozoic and basement top reflectors appear uplifted at least 0.6 TWT seconds as a result of the deformation caused by the south-easternmost lateral ramp of the San Pedro thrust system (Fig. 5.4).

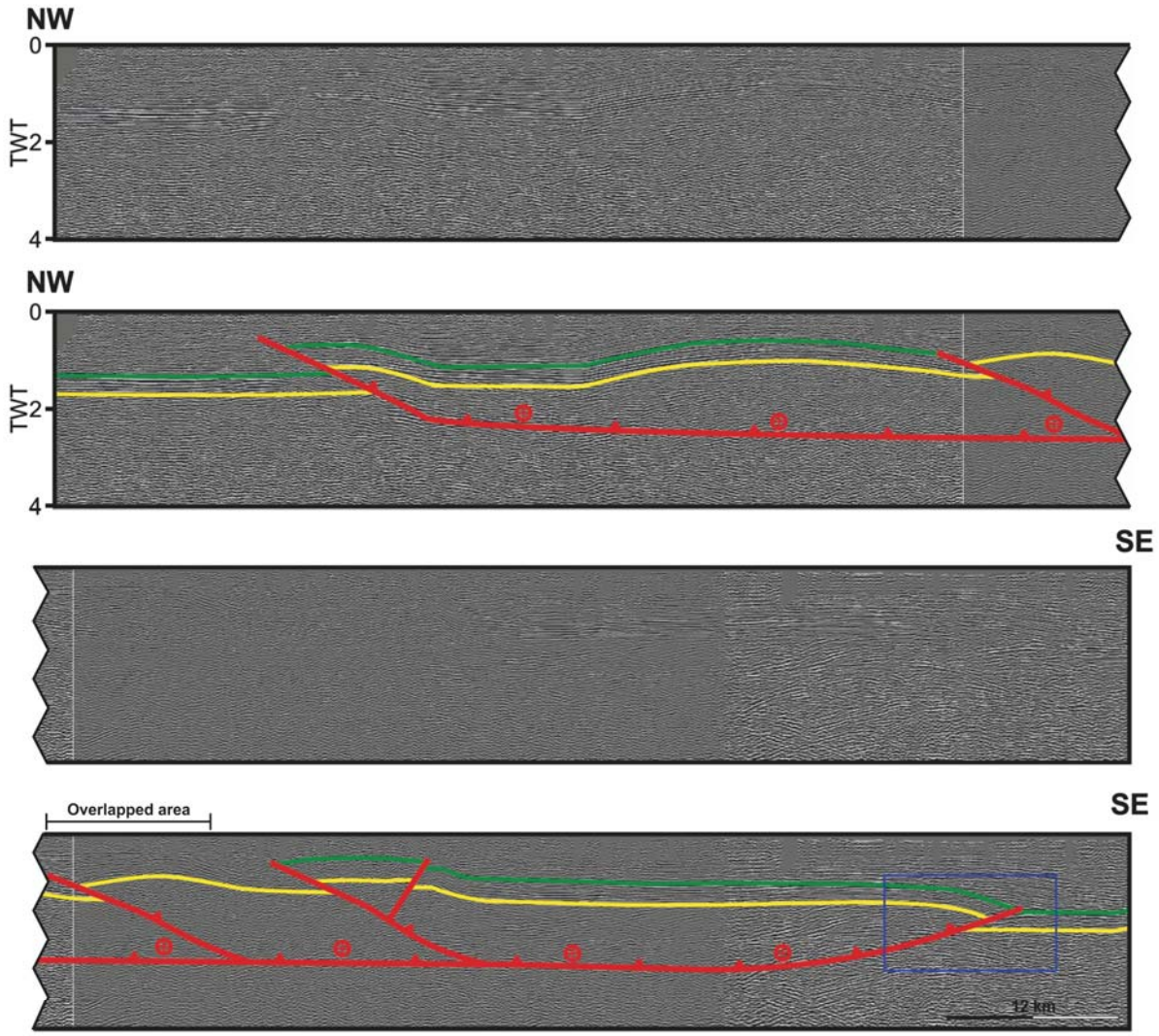

Fig. 5.3: NW-SE composite section located southwards of the Burgalesa Platform in the Duero Foreland Basin showing the deformation caused by the San Pedro thick-skinned structure. Seismic facies below the yellow reflector are attributed to the basement, the facies between the reflectors yellow and green correspond to the Mesozoic succession of the Duero Foreland and the rest of the seismic facies correspond to the Cenozoic succession. Blue square corresponds to detail of figure 5.4. See Fig. 5.2 for location.

These relationships explained above, allows to constrain the relative timing of deformation. The Eocene-Oligocene syn-contractional sediments described in the San Pedro Structure points that the development of this structure was during the early stages of deformation of the Pyrenean Orogeny, but related to the Iberian Range, and thus resulting into a NW-SE striking fault system. In contrast, the southward displacement of the Burgalesa Platform occurred later as denoted by the fact that this latter structural unit is overriding the San Pedro structure at its north-western most tip.

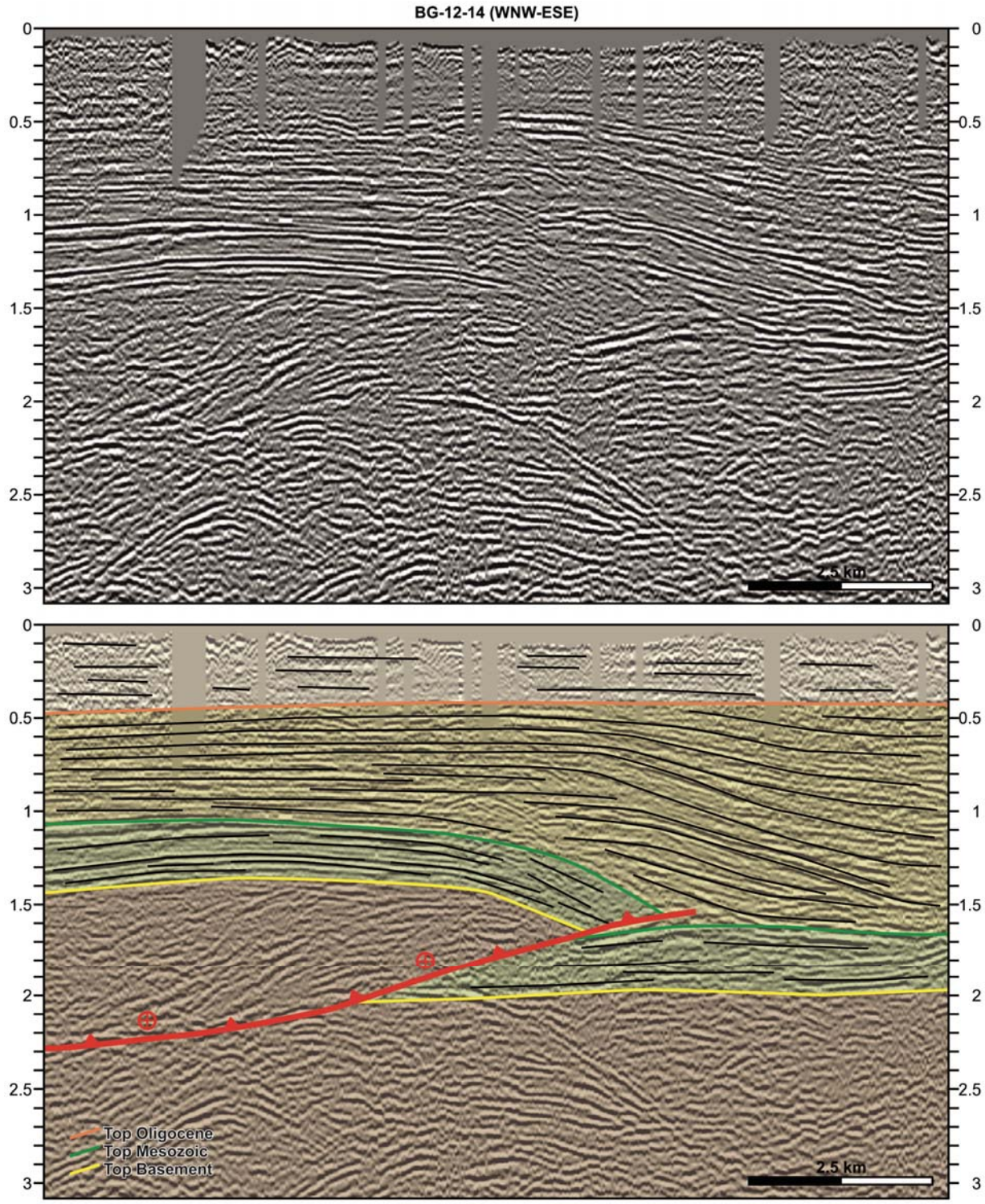

Fig. 5.4: Detail of the seismic section BG-12-14 shown in figure 5.3. Note the Eocene-Oligocene syn-contractional sediments immediately above the Duero Mesozoic succession and how the Late Oligocene-Early Miocene successions lack of deformation.

Regarding the Herrera de Pisuerga sector, structures also involve the basement of the Duero basin, but differently with respect the San Pedro structure they strike roughly W-E and are south-directed (Fig. 5.2). As shown in chapter 3, the thrust system uplifts and deforms the Cenozoic, the Mesozoic and also the basement successions. Moreover, the deformation

diminishes eastwards as can be seen in an oblique to the transport seismic section (Fig. 5.5). In the areas where deformation is absent, the seismic facies show similar characteristics to the ones described in the non-deformed areas of the San Pedro structure.

In addition, the surface geology of the Herrera de Pisuerga sector is characterised by two areas divided by the main frontal thrust. In the southern one, the Upper Albian to Miocene succession of the Duero basin crops out whereas in the northern one the Upper Triassic to Barremian succession appears (Fig. 5.6). The southern area is affected by a thrust with a northwest strike that shows a bend attaining a north-south orientation (Fig. 5.2 and Fig. 5.6). To the west of the area, the thrust is blind and it is constrained by seismic sections whereas, more to the east, it crops out affecting the Upper Cretaceous succession (Fig. 5.6). The Mesozoic succession of this area is characterised by NW-SE anticlines and synclines associated to blind thrusts (Espina *et al.*, 1996). In addition, these authors determined that the age of deformation in this area started during the Late Oligocene. This deformation continued at least during the Miocene as can be deduced from surface geology where Miocene sediments are deformed displaying a progressive unconformity (Fig. 5.6 and 5.7). The northern area is affected by several south-directed thrusts rooted into the main thrust delimiting the Burgalesa Platform. The main south-directed thrust that divides both areas has a sinuous trace. The main bend, with a NE-SW orientation, coincides with the position of the Upper Cretaceous anticlines located in the footwall of the thrust (Fig. 5.6).

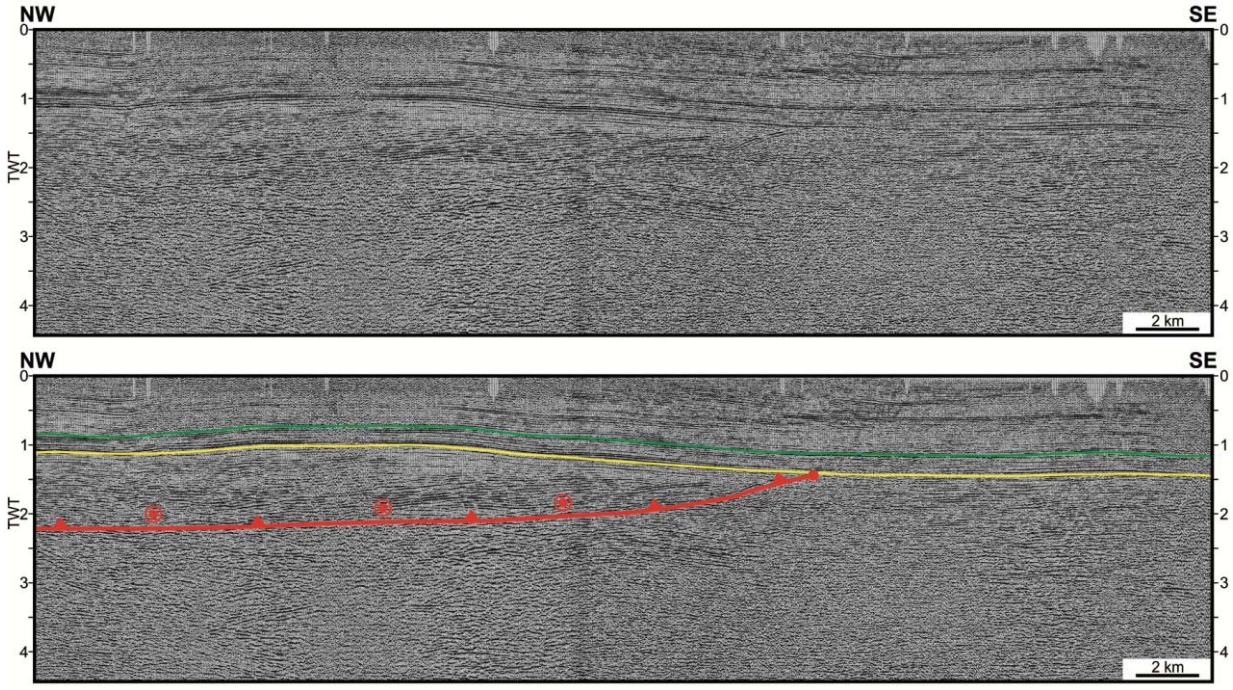

Fig. 5.5: NW-SE seismic section in which thick-skinned tectonics with transport direction towards the south are observed. Note that towards the SE deformation diminishes. See figure 5.2 for location.

This fact points that the deformation caused by the blind thrusts also deformed the main frontal thrust and the Burgalesa Platform thus constraining the timing of deformation. The limited amount of uplift caused by these blind thrusts is in agreement on the one hand with the Late Oligocene and Miocene ages of these structures and on the other hand, with the thermochronological Jurassic to Paleocene exhumation ages reported for the frontal Cantabrian Mountains by Fillon (2012). Furthermore, this interpretation also supports the fault-propagation fold model proposed for the frontal structure of the Cantabrian Mountains by Alonso *et al.* (1996).

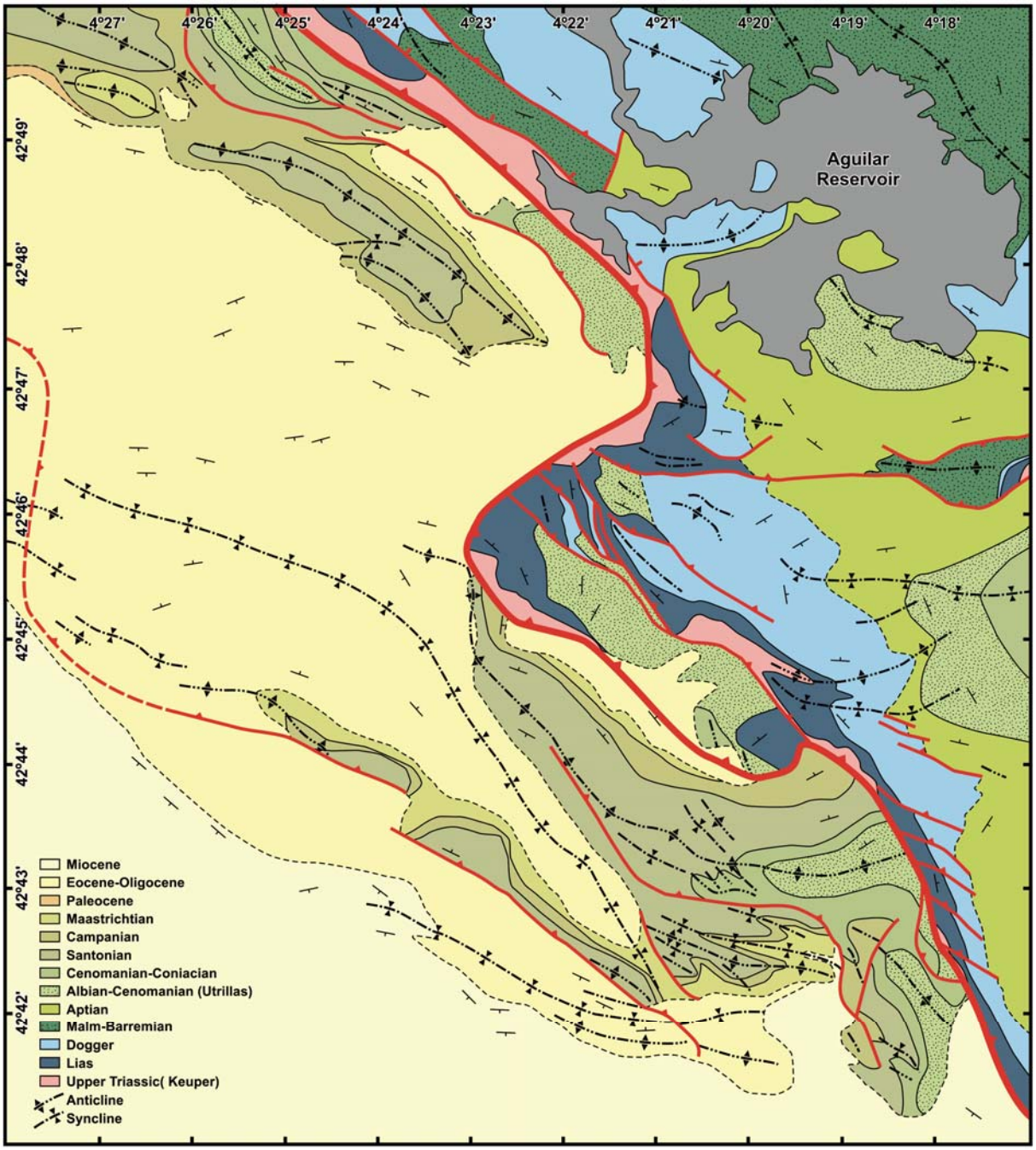

Fig. 5.6: Geological map of the sector located to the north of Herrera de Pisuerga. Modified from IGME (1997).

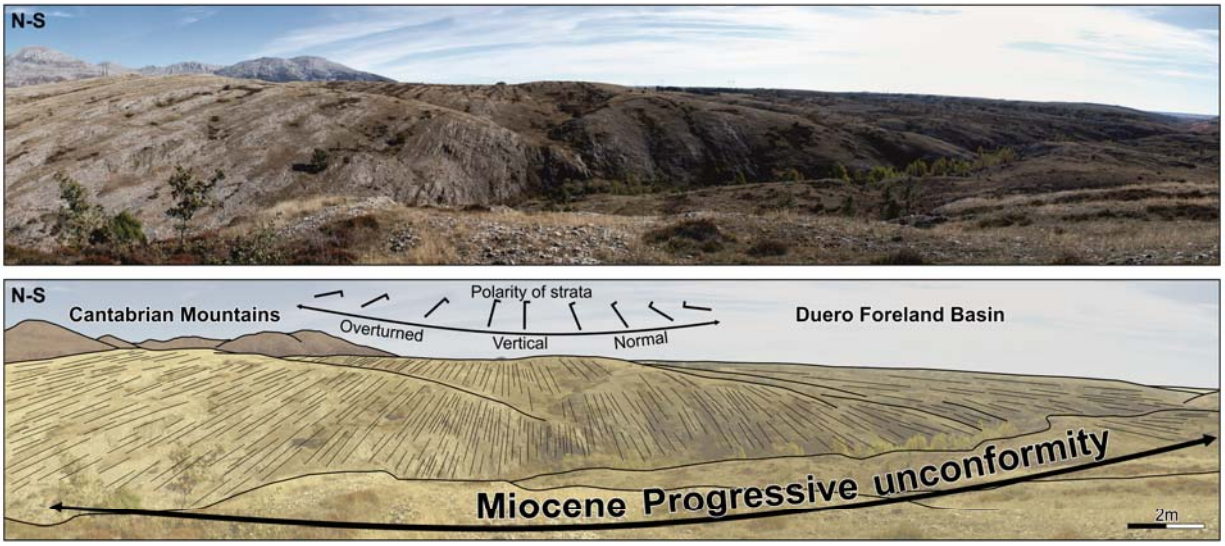

Fig. 5.7: Non interpreted and interpreted N-S field photograph showing the Miocene progressive unconformity. See Fig. 5.2 for location.

Besides the surface geology and the seismic interpretations, paleomagnetic studies have been also carried out in order to know the vertical axis rotations that occurred during the Cenozoic in the Duero Foreland Basin and in the Burgalesa Platform. As shown in chapter 4, the studied area experienced clockwise rotations in the Herrera de Pisuerga sector and counter-clockwise rotations in the south-eastern sector of the Burgalesa Platform (Fig. 5.8).

All the data and observations allow to constrain the contractional evolution of the Burgalesa Platform and Duero Foreland Basin over time. This evolution can be subdivided into three stages. During the early stages of deformation, the San Pedro northeast-directed basement-involved thrusts developed. Coeval with this period, the Burgalesa Platform was southward displaced, inverting the former extensional faults that displayed an arch geometry and detaching the whole Mesozoic succession above the Upper Triassic salts. At the end of this deformational period, the San Pedro structure resulted in a NW-SE orientation in map view (Fig. 5.9A). As deformation continued, the Burgalesa Platform was displaced towards the south until it overrode the San Pedro structure. At this moment, and maybe because this latter structure acted as a backstop for the southward displacement of the Burgalesa Platform, the WNW-ESE Ubierna fault system was reactivated in a right-lateral sense of movement thus forcing the Burgalesa Platform to extrude towards the south-east overriding the Ebro Foreland Basin (Fig. 5.9B).

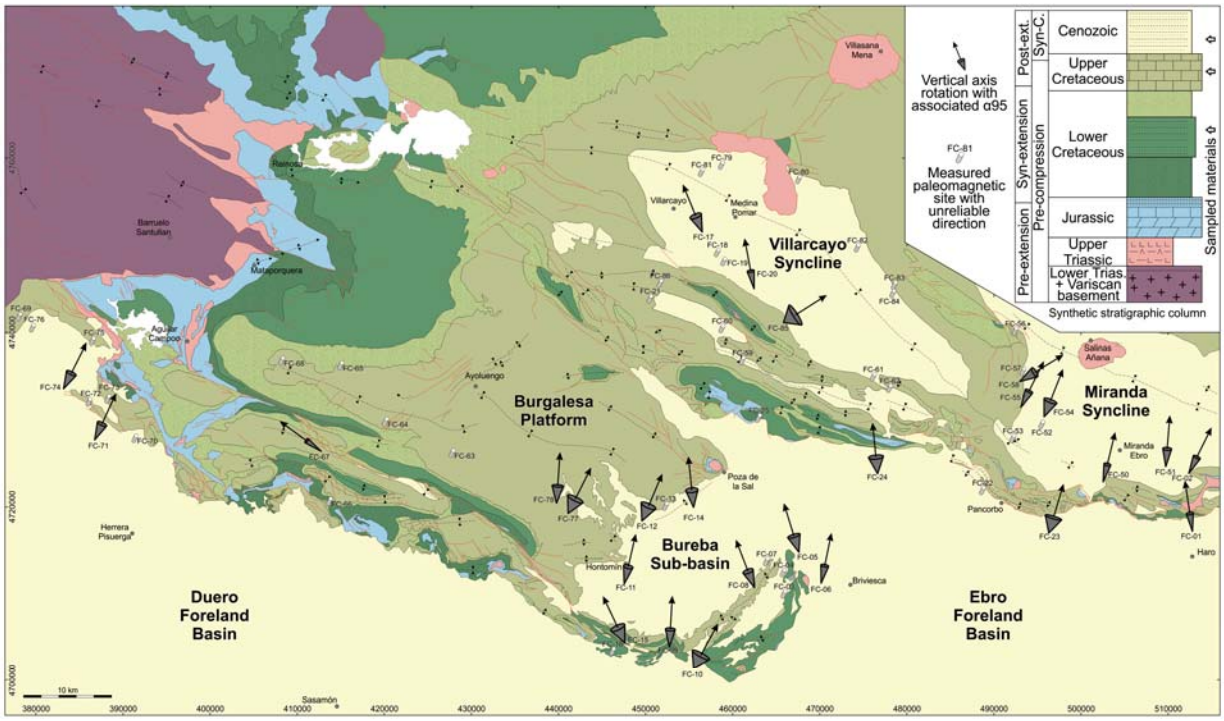

Fig. 5.8: Geological map of the Burgalesa Platform and vicinities with the main areas labelled. Overlapped in this map are shown both, the sampled paleomagnetic sites in which an unreliable direction was obtained and the sites with rotations with its associated α_{95}.

During the last stages of deformation, south-directed basement-involved thrusts deformed the western Burgalesa Platform and also the Duero Foreland Basin. Simultaneously during this stage, the reactivation without decoupling of the Golobar and Ubierna faults occurred. The kinematics during this period resulted in the clockwise and counter-clockwise rotations stated above. The pattern defined by the vertical axis rotation is completely in agreement with the structural model of a tightened arch in which the rotation occurred at the tips are clockwise and counter-clockwise pointing towards the inner parts of the arch whereas, at the central parts of the arch is where rotation is not expected (Sussman and Weil, 2004; Weil and Sussman, 2004; Weil *et al.*, 2010).

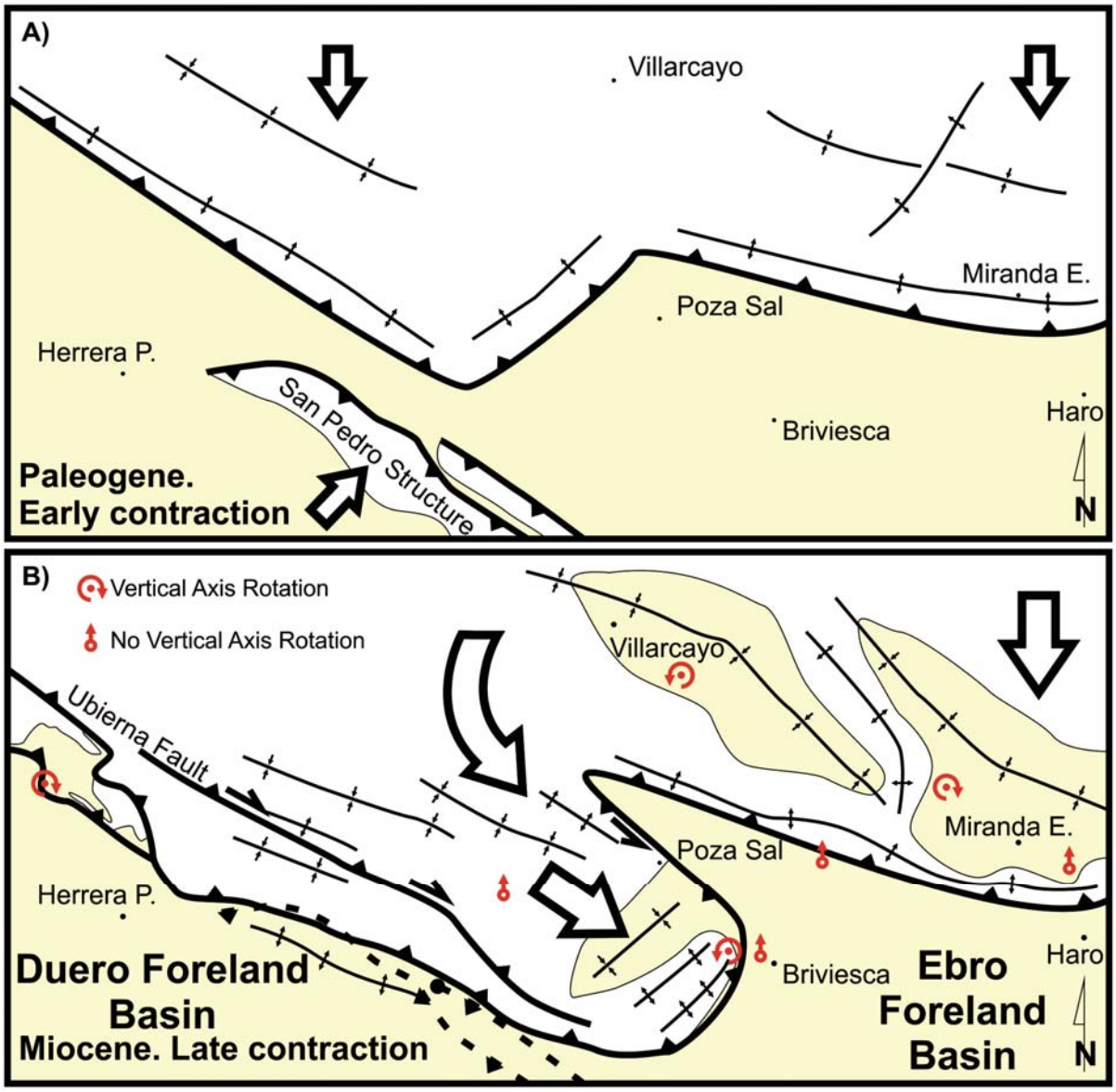

Fig. 5.9: A) Schematic model for the early stages of contraction with the southward displacement of the Burgalesa Platform and the north-eastward displacement and development of the San Pedro Structure. Thick arrows correspond to thrust transport direction. B) Schematic model for the late stages of contraction. The Burgalesa Platform overrides over the Ebro Foreland Basin and over the San Pedro Structure because of the south-east lateral extrusion. In red, the general trend of the paleomagnetic vertical axis rotations. Thick arrows correspond to tectonic transport direction. Dashed and solid line correspond to inactive and active thrust respectively.

Even though the deformation style is quite similar in both San Pedro and Herrera de Pisuerga sectors, the most striking features are the oppositely thrust transport direction and the different age of deformation occurred at both sectors. With all the data and observations provided in this thesis, the most plausible interpretation is that the San Pedro sector corresponds to the north-western tip of the deformation related to the Iberian Range and that the Herrera de Pisuerga sector is related to the Pyrenees. The Eocene-Oligocene ages reported for the first sector and the north-west directed basement-involved thrusts are in agreement with

the main characteristics of the Iberian Range. This double-vergent fold and thrust belt is located immediately to the south of the Pyrenees and resulted from the inversion of the Mesozoic extensional basin during the Cenozoic (Álvaro *et al.*, 1979; Guimerà, 1984; among others). The style of deformation developed during the contractional stage that formed the belt is interpreted as thick-skinned with a thickened crust (Salas *et al.*, 2001; Guimerà *et al.*, 2004). The northern part of the Iberian Range is characterised by north-directed and basement-involved thrusts that override the Ebro Foreland Basin (Guimerà *et al.*, 1995; Guimerà *et al.*, 2004). In contrast, the Late Oligocene to Miocene ages of deformation, the thermochronological ages reported by Fillon (2012) and the W-E south-directed and basement-involved thrusts deforming the Duero Foreland Basin as well as the western part of the Burgalesa Platform supports the attribution of this deformation related with the youngest deformation caused by southernmost thrusts in the Cantabrian Mountains of the Pyrenees. The southern part of the Cantabrian Mountains is characterised by a thrust system that involves the basement and displaces the Cantabrian Mountains towards the south over the Duero Foreland Basin (Álvarez-Marrón *et al.*, 1996; Pulgar *et al.*, 1997; Gallastegui, 2000; Gallastegui *et al.*, 2002; Pedreira, *et al.*, 2003; Pedreira *et al.*, 2007; Roca *et al.*, 2011; Martín-González and Heredia, 2011, among others). All these observations allow to interpret these two sectors as disconnected and independent areas that were developed during different periods and associated to different fold and thrust belts. In addition and derived from this interpretation, the frontal deformation tip line of the Pyrenees would not be connected with the San Pedro Structure as it has been done by some authors (Pulgar *et al.*, 1999; Tavani *et al.*, 2011; Quintana, 2012; Tavani, 2012).

5.2 Onlap geometry of the syn-rift sediments and its implications

During the development of an extensional basin, different sedimentary geometries in the syn-rift package are produced depending on the acting deformation mechanism and also on the mechanical stratigraphy of the pre-rift succession. In this section, the onlap geometries developed in the syn-extensional sediments because of extensional or salt tectonics processes are going to be discussed.

One of the most striking geometric features observed in the seismic lines of the Burgalesa Platform is the onlap of the Lower Cretaceous syn-rift successions above a continuous package of Jurassic pre-rift beds. These geometries are well evident in the southern part of the study area, close to the Ubierna Fault (Fig. 5.10). The seismic lines reveal a northwards thickening of the syn-rift succession with small intraformational unconformities and a southwards migration of the onlap. In addition, an erosional truncation of the syn-rift succession and later unconformable deposition of the post-rift succession can be seen (Fig. 5.10).

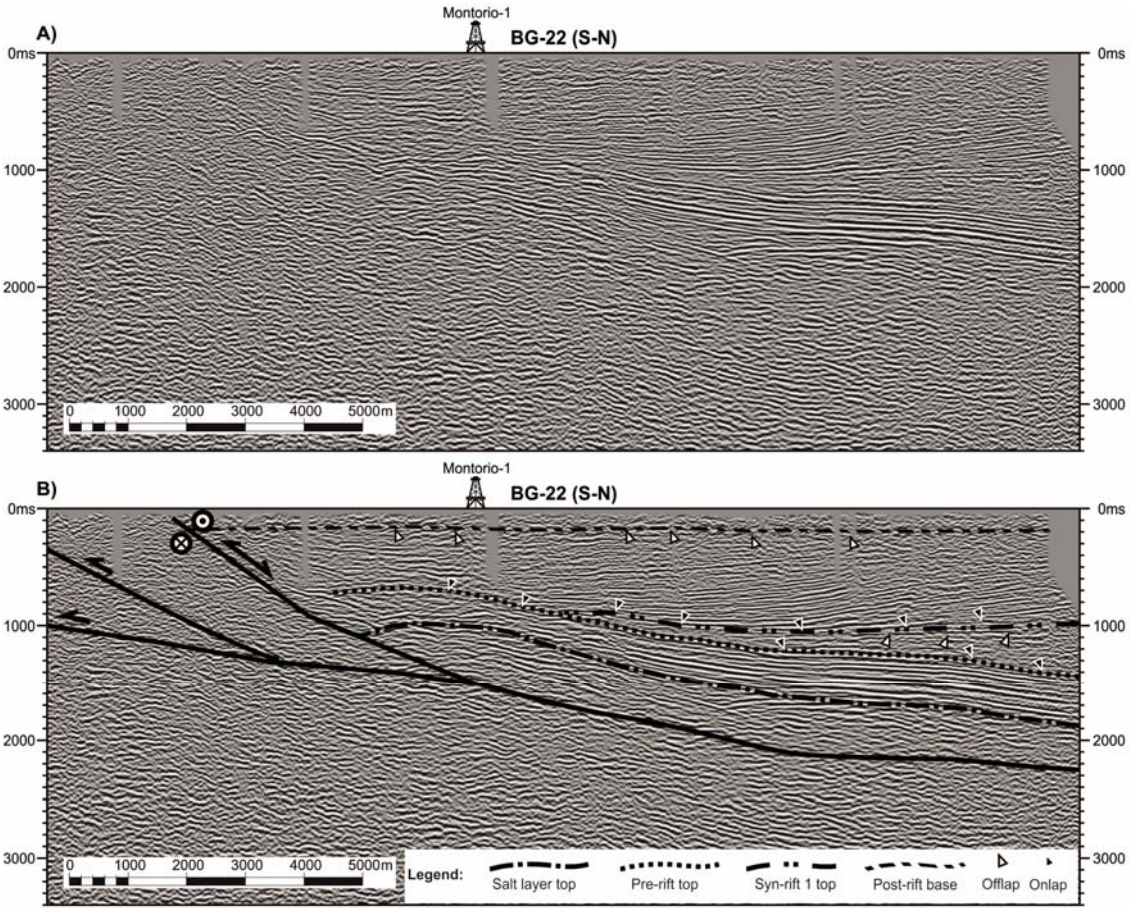

Fig. 5.10: Seismic section of the southern part of the Burgalesa Platform close to the Ubierna Fault with both, onlap and erosional truncation geometries within the syn-rift succession.

These geometries are not restricted to the southern boundary of the study area. More to the north, in the Ayoluengo structure (Fig. 5.11) and in the Hontomín area, similar sedimentary relationships are also observed.

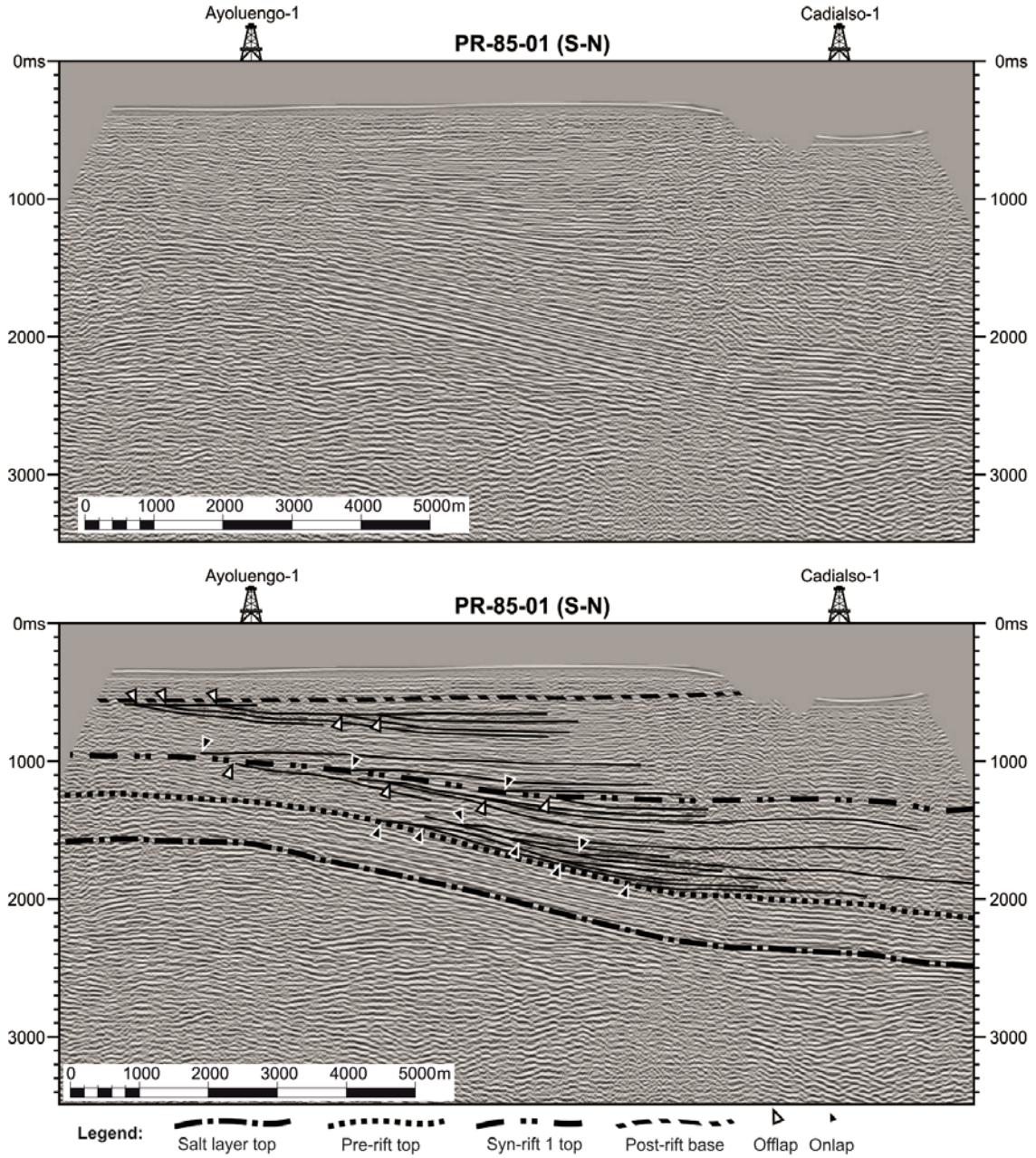

Fig. 5.11: Seismic section of the northern limb of the Ayoluengo structure showing the thickening of the syn-rift succession. This succession shows intraformational unconformities that generate both onlap and erosional truncation geometries.

The interpretation of the distribution of the onlaps and their migration direction has a strong impact in understanding the processes that generated these geometries during the development of an extensional basin (Sharp *et al.*, 2000). The detailed study carried out in the Burgalesa Platform shows, on the one hand, that the region affected by onlaps has a WNW-ESE orientation at the western sector and a more NW-SE orientation to the east. At the

easternmost sector, the length of the onlap map projection increases and attains again a WNW-ESE direction (Fig. 5.12). On the other hand, the migration direction roughly points towards the SW with the exception of the Basconcillos area where it points towards the NE (Fig. 5.12).

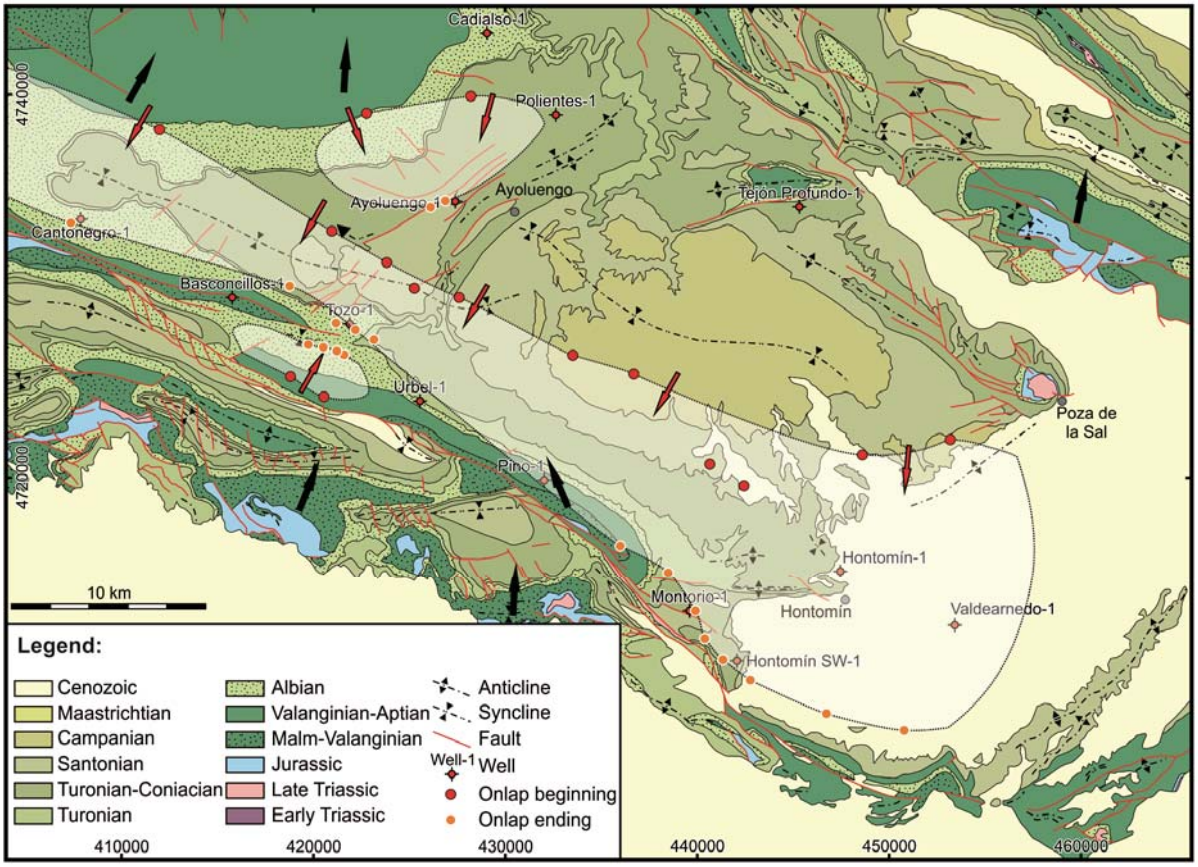

Fig. 5.12: Geological map of the Burgalesa Platform with the location of the beginning and ending of the onlap geometries. The direction of migration of these geometries is marked with red arrows. The paleocurrent data from Pujalte (1981;1982) of the Lower Cretaceous rocks are marked with black arrows. White area corresponds to the onlap extension.

According to these characteristics, seven theoretical models responsible for the development of southwards migrating onlaps are proposed and discussed. These models that invoke only one operating process are grouped in three tectonic settings:

5.2.1 Extensional tectonics

- Extensional planar non-rotational fault
- Extensional planar rotational fault
- Extensional detachment
- Extensional rollover fault

5.2.2 Salt tectonics

- Salt migration triggered by extension
- Salt migration by sedimentary loading

5.2.3 Forced folding

For description simplification, all the theoretical models are oriented taking the left part of the image as the south and being the extensional faults north-directed. In addition, the models have a constant sedimentation rate that is equal to the accommodation space generated during the extension.

5.2.1 Extensional tectonics

Extensional planar non-rotational fault

This model assumes that the extension is produced by a planar fault with only vertical throw that affects the flat pre-rift succession (Fig. 5.13). The resultant geometry of this model is characterised by horizontal pre-rift and syn-rift successions in which the syn-rift is isopach away from the fault. The onlap produced by this model migrates towards the south against the fault.

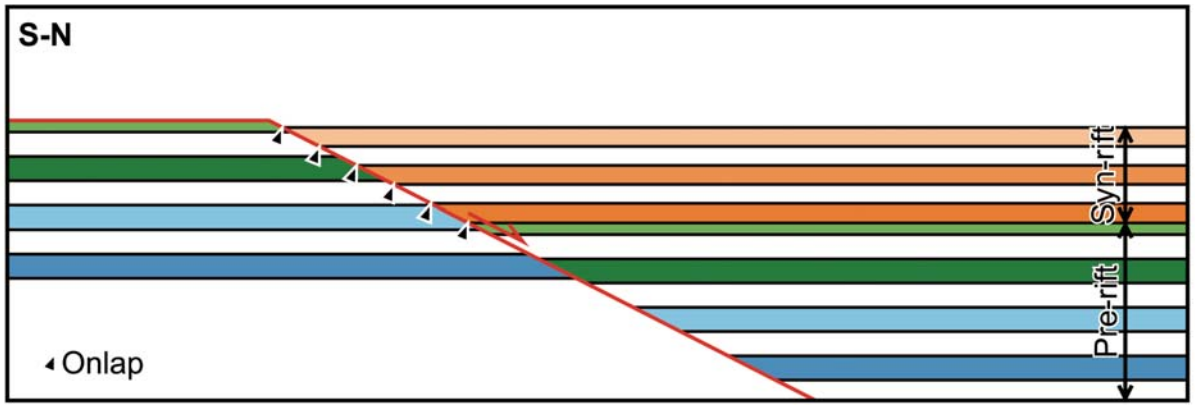

Fig. 5.13: Extensional planar fault model with the main characteristics describing the pre-rift and syn-rift relationship and geometry.

Extensional planar rotational fault

This model is characterised by a planar fault that offsets and tilts the pre-rift succession (Fig. 5.14). Respect to the syn-rift sediments, they experience a southwards thickening, developing a southwards migrating onlap geometry against the fault. The syn-rift succession lacks of parallelism between each strata and both, the pre-rift and the syn-rift successions dip towards the same direction.

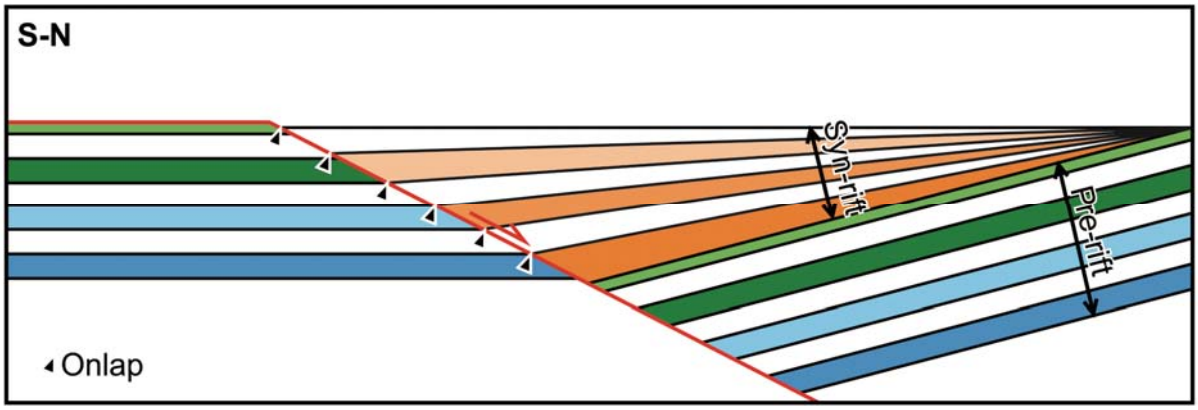

Fig. 5.14: Extensional planar rotational fault model with the main characteristics describing the pre-rift and syn-rift relationship and geometry.

Extensional detachment fault

This model requires extension and translation above the hangingwall of a planar non rotational fault that it is detached into the pre-rift succession at depth (Fig. 5.15). In this theoretical model, the amount of extension must be transferred towards the south to a more external structure in order to balance the extension of the deeper and of the shallower levels. This model produces the southwards migration of the onlap geometries against the pre-rift succession. The syn-rift succession presents parallelism between each strata and dips towards the south when it crosses the active axial surface. Regarding the pre-rift succession, it dips towards the north above the extensional ramp and towards the south or horizontal when it crosses the active axial surface.

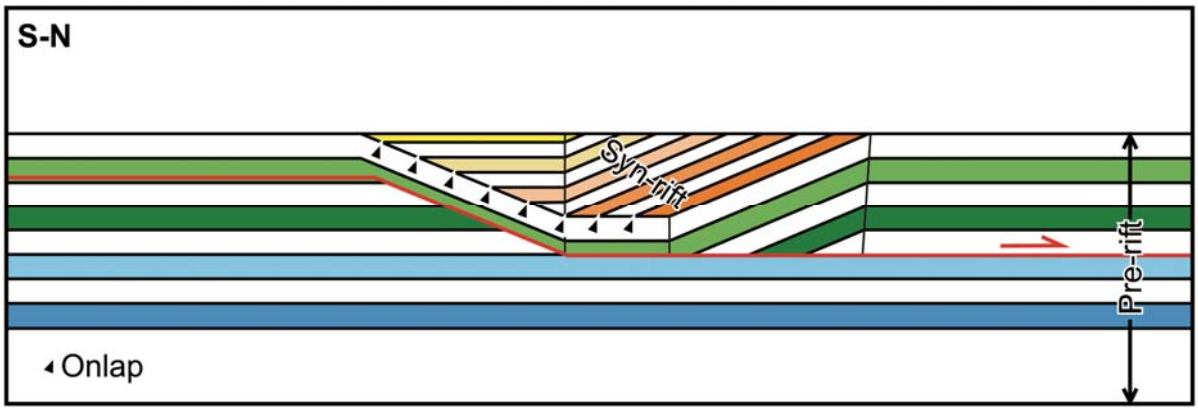

Fig. 5.15: Extensional detachment model with the main characteristics describing the pre-rift and syn-rift relationship and geometry.

Extensional rollover fault

This model is constituted by an extensional fault with a listric geometry affecting and offsetting the pre-rift succession (Fig. 5.16). The onlaps developed during the evolution of the fault migrates southwards against the fault. The syn-rift succession is characterised by southward thickening and by the absence of parallelism between each strata. In addition, the syn-rift and the pre-rift dip towards the same direction. The basal syn-rift and the pre-rift successions develop an anticline geometry as extension continues.

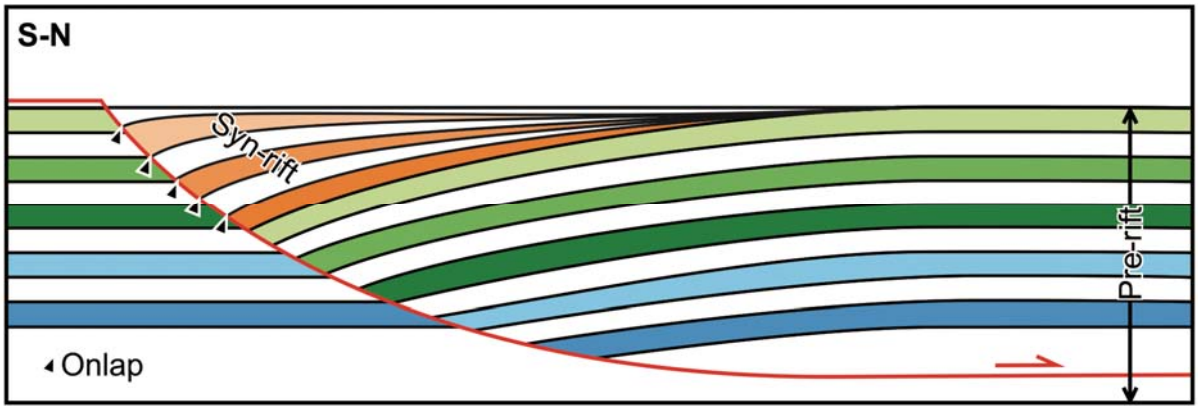

Fig. 5.16: Rollover extensional model with the main characteristics describing the pre-rift and syn-rift relationship and geometry.

5.2.2 Salt tectonics

Salt migration triggered by extension

This model is characterised by an extensional fault rooted into a detachment level (Fig. 5.17). The extension produced into the pre-rift succession triggers the salt mobilisation towards the footwall of the fault. This process generates the uplift of the pre-rift succession located at the footwall, which is eroded by the syn-rift that onlaps northwards. In addition, in the hangingwall of the fault, the syn-rift thickens southwards and the onlaps migrate to the south.

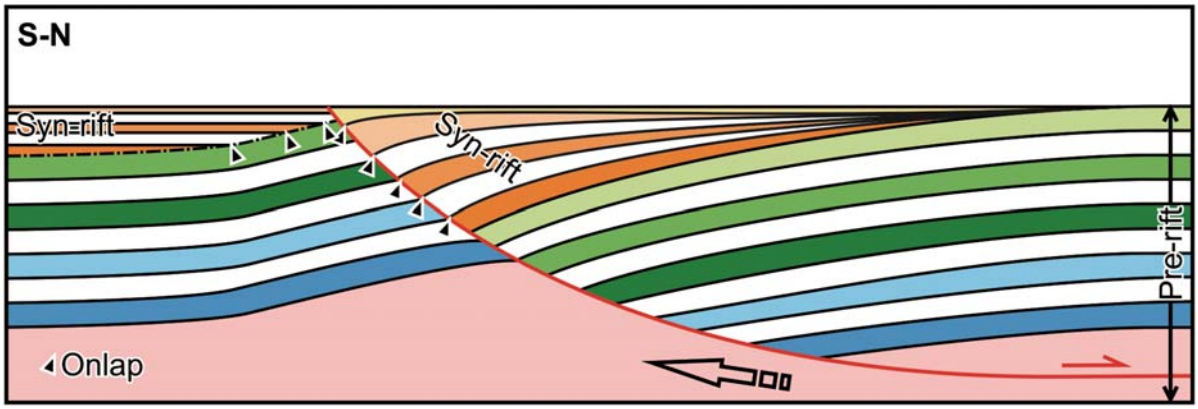

Fig. 5.17: Salt mobilisation triggered by extension model with onlapping geometries against the fault and to the pre-rift succession. Salt is represented by pink colour. The arrow indicates the direction of salt migration.

Salt migration by sedimentary loading

This theoretical model is characterised by a ductile level in between the pre-rift succession. The onlap geometry is not developed due to the activity of a normal fault, rather it is caused by the weight of the syn-rift sedimentation (Fig. 5.18). The onlap migration direction and the sediment supply direction have the same sense (Ge *et al.*, 1997), thus imposing that in this model the source area must be located to the north. The weight of the sediments triggers the mobilisation of salt towards the south and consequently, the southwards migrating onlap geometry. The non planar southward thickened syn-rift succession dips towards the south contrasting with the northward dipping of pre-salt mobilisation succession above the salt level.

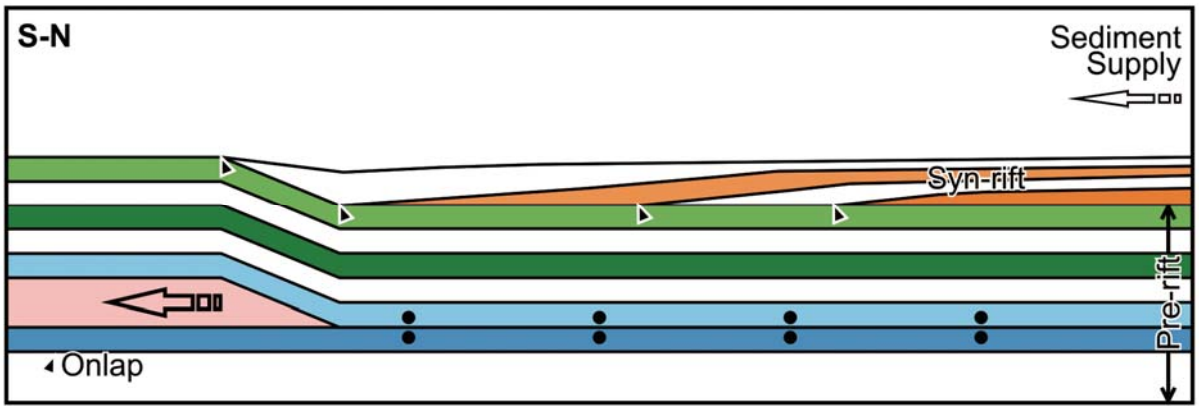

Fig. 5.18: Salt migration and expulsion model with the main characteristics describing the pre-rift and syn-rift relationship and geometry. Pink layer corresponds to salt. The arrow shows the direction of salt mobilisation and the two dots correspond to salt welds produced between the two layers immediately above and below the salt.

Table 5.1 summarises the six theoretical models highlighting the main features of each one. As it has been shown, these models could develop south migrating onlap geometries but some of them are less suitable to be applied in the study area taking into account the different constraints. The fact that in the study area the syn-rift succession lacks of parallelism with respect to the pre-rift one (Fig. 5.10 and Fig. 5.11) allow to discard a non rotational planar fault model, where an isopach syn-rift succession is developed. The detachment model does not fit the constraint of northward thickening of the syn-rift succession. This constraint together with the development of a south-dipping monoclinal at the deepest levels of the hangingwall do not match with the observations of the study area. Moreover, the northward thickening does not fit with the models in which an opposite thickening is described (i.e. extensional planar rotational fault; extensional rollover; and, salt mobilisation towards the footwall of a rollover fault). This fact makes the models unsuitable to explain the Burgalesa Platform development and evolution during the extensional event. In addition, the northward thickening together with the north-directed paleocurrent data reported for the syn-rift units by Pujalte (1981;1982) mismatches

with the theoretical model based on salt migration triggered by sedimentary loading. This mismatch makes difficult to apply this model in which the sediment supply is from the north thus, developing southward migrating onlaps. All these simple layer-cake theoretical models cannot explain the onlap geometries of the study.

Table 5.1: Conceptual models and resultant syn-rift geometries. Conceptual models are oriented with the south to the left. See text for more details.

Process		Conceptual model	Characteristics
Extensional Tectonics	Extensional Planar Fault	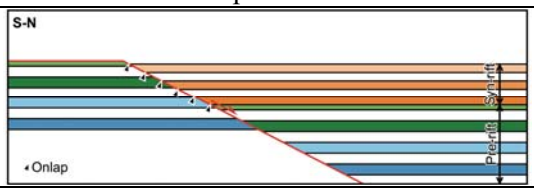	- Southward migrating onlaps against the fault - Planar syn-rift sediments - Pre-rift and syn-rift without dipping
	Extensional Planar Rotational Fault	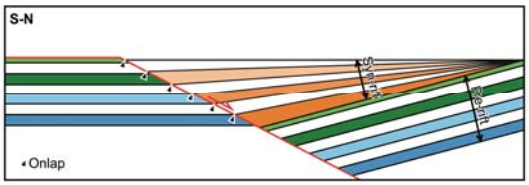	- Syn-rift southward thickening - Southward migrating onlaps against the fault - Planar syn-rift sediments - Pre- and syn-rift dipping towards the same direction
	Extensional Detachment Fault	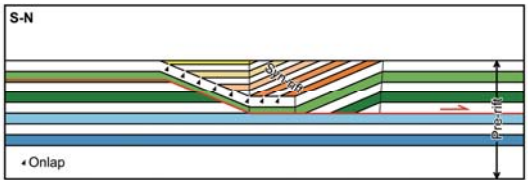	- Southward migrating onlaps against pre-rift succession - Planar syn-rift sediments - Pre- and syn-rift dipping towards the same direction and opposite depending on location - Extension transferred southwards - Anticline geometry at the deepest structural levels
	Extensional Rollover Fault	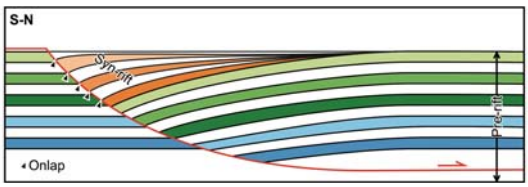	- Syn-rift southward thickening - Southward migrating onlaps against fault - Non planar syn-rift sediments - Pre- and syn-rift dipping towards the same direction - Anticline geometry at the deepest structural levels
Salt Tectonics	Salt migration triggered by extension	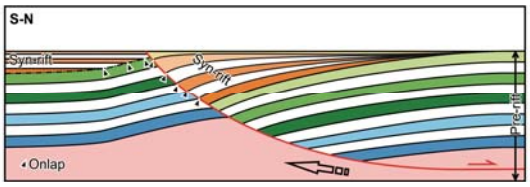	- Syn-rift southward thickening - Non planar syn-rift sediments - Hangingwall southward migrating onlaps against fault - Footwall northward migrating onlaps against the pre-rift - Pre- and syn-rift dipping towards the same direction
	Salt migration by sedimentary loading	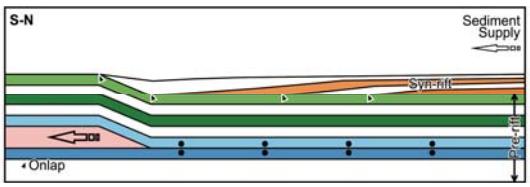	- Syn-rift southward thickening - Non planar syn-rift sediments - Southward migrating onlaps against pre-rift succession - Pre- and syn-rift dipping in opposite directions

Another possible theoretical model for the development of the onlaps described in the Hontomín area (Chapter 2) is by a pre-configuration of the area before the onset of extension instead of a layer-cake stratigraphy is presented below.

5.2.2 Forced folding

This theoretical model is characterised by a pre-configuration of the area at the cover level and with the presence of a ductile level (Fig. 5.19). This ductile level presents a thickened part towards the south and the geometry of the cover is defined with a north-dipping panel that more to the north it flattens where the ductile level is either absent or strongly reduced. The cover panel is onlapped by isopach and younger sediments with a migration towards the south (Fig. 5.19A). During the extension, the down-throw of the basement produces the folding of the cover thus resulting in a migration of salt towards the fault. The onlapping succession at the same time is folded resulting in an apparent downlap (Fig. 5.19B). Moreover, the amount of extension caused into the basement has to be balanced into the cover (represented by the red square in figure 5.19) either by transferring the extension towards the south in a more external fault of the basin affecting only the cover or, by thinning the cover with minor faults. The downlap geometries developed with this theoretical model could be similar to the ones described in the seismic lines of the Hontomín. In this area, the Jurassic seismic facies lie horizontal and are overlaid by the Lower Cretaceous syn-rift sediments with a downlap sedimentary relationship (Fig. 5A of Chapter 2). Although this model could partially explain the sedimentary geometries, it is difficult to develop the width of the onlaps shown in figure 5.10 invoking only this theoretical model. In addition, another mechanism should have acted before the extension in order to produce the pre-configuration of the area.

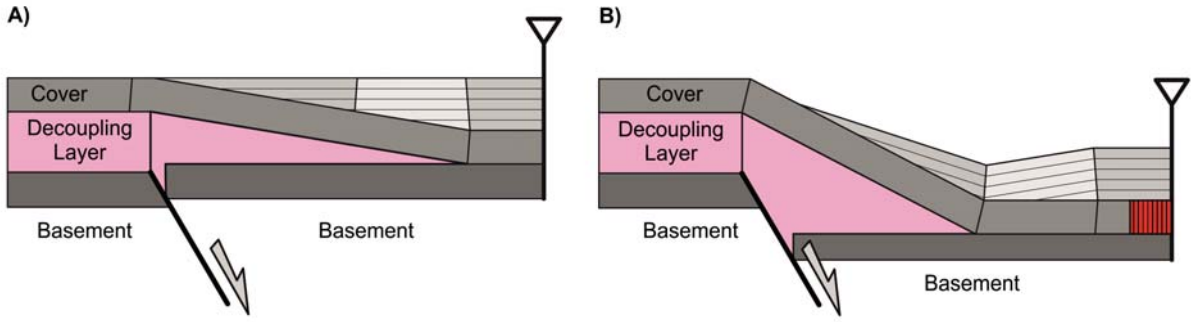

Fig. 5.19: Forced folding theoretical model. A) Pre-extension and salt mobilisation with a syn-rift succession southwards onlapping the pre-rift succession. B) Basement extension folds the cover and this triggers salt mobilisation towards the fault. Red square corresponds to the basement extension that must be balanced in the cover by minor faulting or transferring the extension southwards.

With the explained theoretical models, layer-cake or pre-configuration, it is not possible to fit all the constraints imposed by the sedimentary geometries, the relationship between the pre- and syn-rift and the mechanical stratigraphy. Therefore, a combined process would take place during the extensional event. A process that may explain all the constraints is the mix of extensional forced folding and detachment model. This model is characterised by a ductile layer between the basement and the cover that decouples the deformation. The faults affecting the basement result in the development of steps. The Upper Triassic salt layer decouples the deformation and the cover is only deformed showing a drape fold geometry above these steps. Similar forced folds are described in the literature in rifted areas such as the North Sea, the Dannemarie basin, the Gulf of Suez or the Grand Banks (Gawthorpe *et al.*, 1997; Gupta *et al.*, 1999; Sharp *et al.*, 2000; Davies *et al.*, 2000; Dawers and Underhill, 2000; Withjack and Callaway, 2000; Khalil and McClay, 2002; Jackson *et al.*, 2006; Ford *et al.*, 2007; Lewis *et al.*, 2013). In the study area, the Ubierna fault and related salt structure would be one of these basement steps and as a result of the northward translation of the cover above the step, syn-rift sediments onlapping onto the Jurassic were deposited. A northward displacement of more than 10 km above the extensional detachment is necessary in order to explain the width of the onlaps northwards of the Ubierna fault as shown in chapter 3 and in figures 5.10 and 5.12. Similar syn-rift geometries are described in the Kwanza Basin in Angola where the syn-extensional sediments onlap the cover when translated above a seaward ramp (Jackson and Hudec, 2005). This proposed model is in agreement with the mechanical stratigraphy of the study area and also with the development of contractional structures during the extensional event discussed in the next section.

5.3 The Huidobro north-directed thrust and the associated erosional truncation

In this section, the erosional truncation geometry and the differences in structural relief described in chapter 3 are expanded in order to better understand the implications of these characteristics.

The seismic sections of the northern boundary of the Burgalesa Platform show an isopach south-dipping panel made up of highly continuous and reflective seismic facies at the bottom and more discontinuous seismic facies above (Fig. 5.20). This panel attains a flat attitude towards the south as shown in chapter 3. These successions have been attributed to the Jurassic and Lower Cretaceous according to the well data thus constituting the pre-rift and early syn-rift successions. Above these successions, the base of the late syn-rift is poorly imaged and do not allow to determine the relationship with the previous succession. In contrast, the shallower part of the late syn-rift is characterised by an erosional truncation, which extends at least 3 km, resulting in an angularity between the syn-rift and post-rift that are constituted by the Albian Utrillas facies and the Upper Cretaceous successions. In the Huidobro structure, the Tejón Profundo-1 well testified the repetition of the Mesozoic succession. In addition, at the bottom of the well below the Jurassic succession, more than 1000 meters of Triassic salts were described without reaching the base of this unit. The well data together with the surface geology reflect differences in structural relief between the deepest and shallowest structural levels. The difference at the Jurassic level is more than 1200 meters according to the well data. In contrast, the difference for the Upper Cretaceous level is less than 600 meters as can be deduced from surface geology. The same features can be observed in the seismic sections of this area in which the differences are about 1.5 seconds in TWT for the Jurassic succession (Fig. 5.20) and less than 0.5 seconds in TWT for the Upper Cretaceous as shown in chapter 3. To the north, in the deepest part of the seismic line the pre-rift and syn-rift successions are truncated against a fault as reflected by the cutoffs imaged. The constraints provided by the well coupled with the seismic data allow to interpret the previously described structure as a north-directed thrust. The shallowest succession corresponds to the hangingwall of this thrust, being the southern sector of the seismic line the thrust flat-ramp transition. In contrast, the deepest part correspond to the footwall successions, which are imaged almost horizontal and the early syn-rift maintains its thickness as the one in the hangingwall. The post-rift succession is deformed at the north-east of the seismic section

whereas towards the south it is imaged horizontally (Fig. 5.20). This succession was not drilled by the Tejón Profundo-1 well.

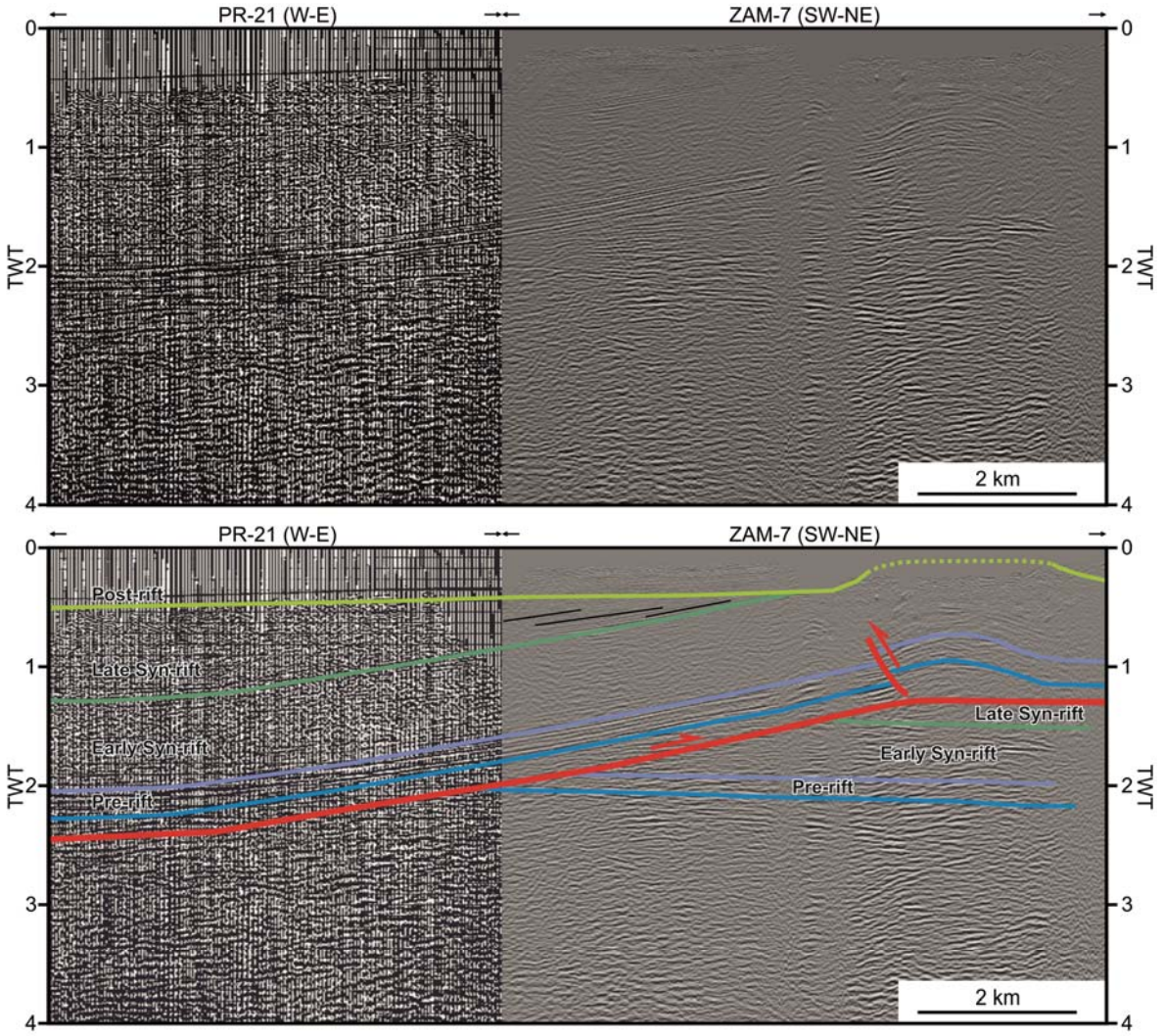

Fig. 5.20: Composite seismic section showing the deepest portions of the back-thrust and the geometric relationships between the Early and Late syn-rift and the Post-rift successions.

The almost horizontal post-rift succession in the southern part of the seismic section and the fact that it is only deformed to the north of the line contrasts with what is expected for a thrust fault bend fold model (Suppe, 1983). In the Burgalesa Platform, the Utrillas and the Upper Cretaceous are considered as post-extension and pre-contraction (Arnáiz *et al.*, 1991; Pujalte and Robles, 2008), and thus, a back-thrust developed during the contractional stage of the Pyrenean Orogeny should have a backlimb active axial surface pinned at the thrust flat-ramp transition that would deform the post-rift successions. In addition, the amount of shortening observed in the pre-rift Jurassic succession and in the post-rift Upper Cretaceous succession together with the differences in structural relief for both the deepest and shallowest structural levels mismatches the simple thrust theoretical model in which the amount of

shortening and structural relief for both levels must be equal (Fig. 5.21). The differences in shortening could be the result of the obliquity between the seismic section and the thrust transport direction. Nevertheless, this would not explain the observed differences in structural relief.

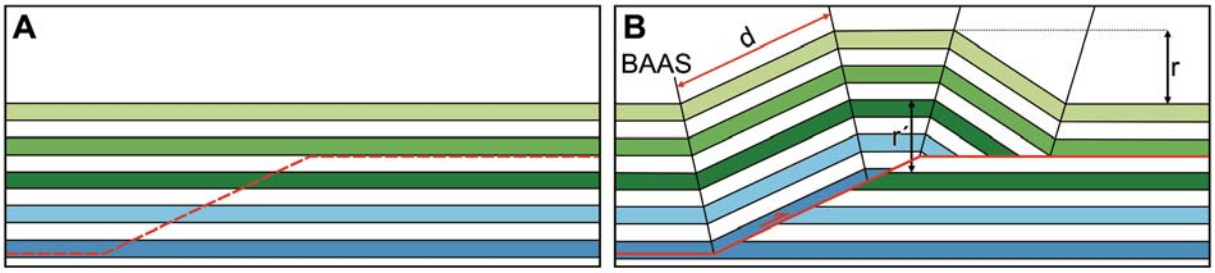

Fig. 5.21: Simple thrust theoretical model applying Suppe's fault bend fold model. A) Pre-contractive state and B) Development and displacement of the thrust a distance d. Structural relief for the deepest and shallowest structural levels is marked with r' and r, respectively. BAAS corresponds to Backlimb Active Axial Surface.

All the characteristics explained above: i) the almost horizontal Upper Cretaceous succession in the southern sector; ii) the angularity between the Upper Cretaceous and the Lower Cretaceous with the erosional truncation; iii) the horizontal succession in the footwall of the back-thrust; iv) the salt accumulation, with more than 1000 meters, below the Jurassic in the footwall of the north-directed thrust; v) the differences in the amount of shortening between the Jurassic and Upper Cretaceous; and, vi) the differences in structural relief between the deepest and shallowest structural levels, make difficult to explain this structure without a pre-contraction configuration departing from a simple layer-cake succession prior to the Pyrenean deformation. This pre-configuration requires the generation of a structural relief above the regional (Fig. 5.22A), which would be later eroded between the syn-rift and the post-rift in order to develop an erosional truncation (Fig. 5.22B) (Mitchum *et al.*, 1977; Emery & Myers, 1996). Therefore, the development of the north-directed thrust occurred during the Late Jurassic-Early Cretaceous extensional event. This contractional structure would be eroded and the Utrillas formation and the Upper Cretaceous successions unconformable deposited thus developing the erosional truncation observable in the seismic lines (Fig. 5.20).

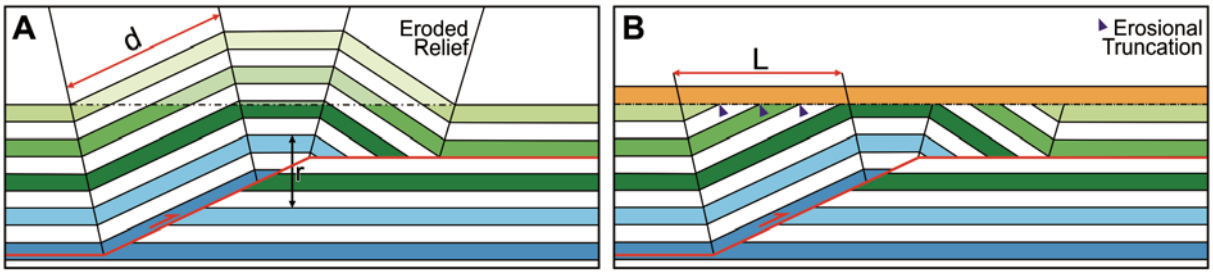

Fig. 5.22: A) Thrust displaced a distance d and generating a structural relief r. B) Erosion of the structural relief developing the truncation and later deposition of a post-contraction layer.

The pre-rift and the early syn-rift appear isopach in the seismic lines and therefore they can be considered as pre-contraction. This fact restricts the timing of this north-directed thrust during the Early Cretaceous. The late syn-rift succession cannot be constrained due to the absence of clear growth geometries against the early syn-rift and thus, it could be considered either pre-contraction or syn-contraction. The Utrillas and Upper Cretaceous of the Burgalesa Platform must be considered post-extensional deformation and pre-contraction with respect to the Pyrenean Orogeny. This is supported by the angularity between the syn-rift succession and the post-rift succession and by the fact that the Upper Cretaceous lies perfectly horizontal with the exception of the northern part of the section. This second point indicates that this north-directed thrust was not reactivated during the Pyrenean Orogeny along the footwall ramp, as a second stage of contraction would have deformed the Upper Cretaceous at the backlimb active axial surface (Fig. 5.20 and Fig. 5.23). This structure as revealed by the seismic line would correspond to a south-directed thrust detached from the upper flat of the previous north-directed thrust and located where the thickness of the Mesozoic successions was reduced at the northern sector. An upper detachment for the Pyrenean contractional structure with respect the older one would explain differences of structural relief between the Upper Cretaceous and the Jurassic beds. From all these observations, the mismatches between the structural relief and the amount of shortening are explained by the development of a north-directed thrust during the Late Jurassic-Early Cretaceous extensional event and by a south-directed thrust developed during the Pyrenean Orogeny.

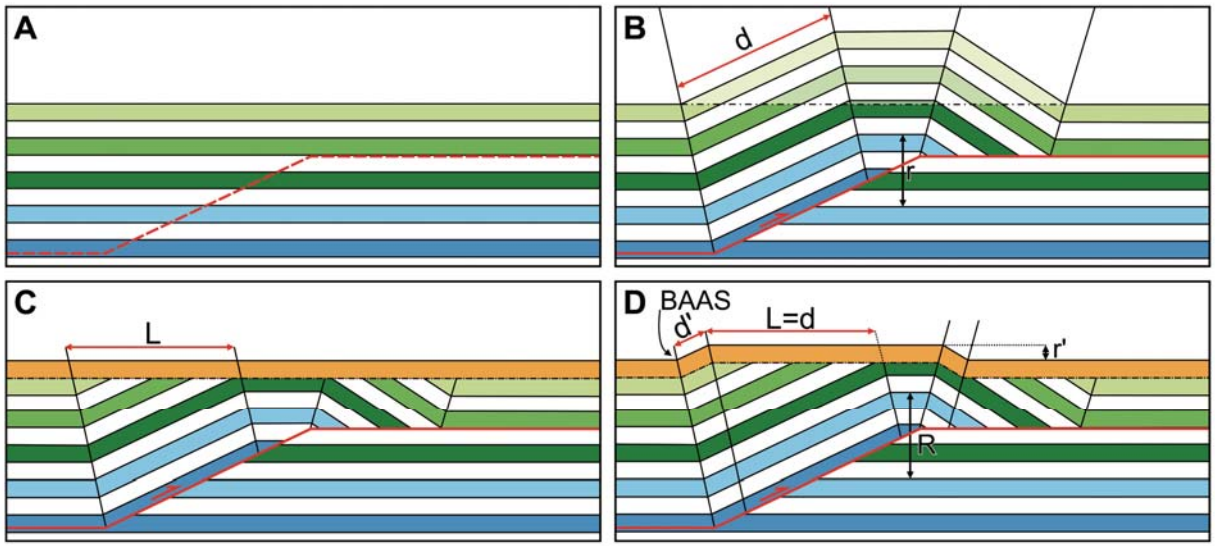

Fig. 5.23: Theoretical thrust fault bend fold model with two contractional stages. A) Pre-contraction stage. B) Thrust displaced a distance d generates a structural relief r. C) Erosional period and later sedimentation of a post-contraction layer. The length of the truncation corresponds to the displacement d occurred during the first stage. D) Second contractional stage deforming the whole succession generating a structural relief r' for the shallowest structural levels and a total structural relief R for the deepest structural levels. BAAS corresponds to Backlimb Active Axial Surface.

The question that arises at this point is to know the causes of the development of a contractional structure during the Late Jurassic-Early Cretaceous extensional event. Surprisingly, in the study area the contractional structure is not located in the deepest part of the basin where these structures are commonly developed (Peel *et al.*, 1995: Rowan *et al.*, 1999; Rowan *et al.*, 2004; Dooley *et al.*, 2004; Lacoste *et al.*, 2012; Cartwright *et al.*, 2012). Instead, it was developed in an intermediate position inside the basin and eroded and later fossilised by the Utrillas formation. As stated in section 5.2 the extensional model proposed for the southern area, is a combined model with forced folding and northward translation of the cover above a basement fault and the Upper Triassic salt layer acting as a decoupling level. In this setting, high-angle faults thinning the basement below the Triassic salts should be expected northwards of the basin margin. The translation of the cover above the developed basement steps resulted in the generation of drape folds at the cover and with the syn-rift sediments onlapping the Jurassic succession. More to the north of the Ubierna fault, the development of the contractional structure occurred. Integrating all these observations result in an extensional system that is characterised by extension and translation of the cover in the southern margin and more to the north by the development of a contractional structure (Fig. 5.24). This interpretation is in agreement with the more than 10 km of northward translation of the cover deduced from the sedimentary geometries in the southern margin. This amount of extension is in part are accommodated in this contractional structure as can be deduced in figure 5.18 where at least 8 km of northward displacement is observable. The location of this structure would be conditioned by the backstop produced by the salt wall and the thick Lower Cretaceous succession deposited northwards of this structure along the northern edge of the Burgalesa Platform (Fig. 5.24).

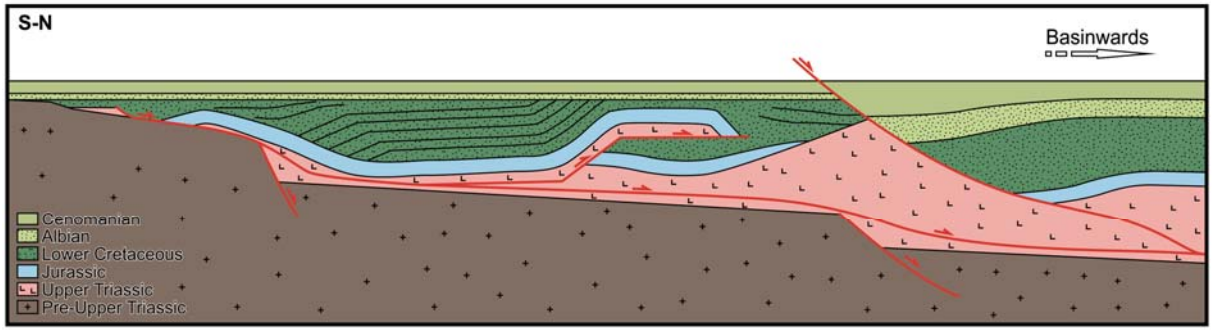

Fig. 5.24: Schematic representation of the extensional system at the end of the Cenomanian with detachment of the cover and development of the contractional structure in the middle of the Burgalesa Platform and thickening of the Utrillas and Cenomanian successions northwards.

The north-directed thrust deformed the cover, generating structural relief, and as the extension continued the deformation was transferred to the north explaining the basinwards thickening of the Utrillas and Cenomanian successions (Fig. 5.25). In contrast, in the Burgalesa Platform, the erosion of the structural relief of the contractional structure and the generation of the erosional truncation of the Lower Cretaceous successions described in the Huidobro area fossilised by the Utrillas that maintains its thickness allow to interpret this unit as post-extension. This kinematics explains the post-rift character of the Utrillas formation and the Cenomanian succession in the Burgalesa Platform and their syn-rift character more to the north, facts that are also in agreement with previous studies of the surface geology (García-Mondéjar, 1979; 1990; Arnáiz *et al.*, 1991; García-Mondéjar *et al.*, 1996; Hernáiz and Solé, 2000; Pujalte and Robles, 2008).

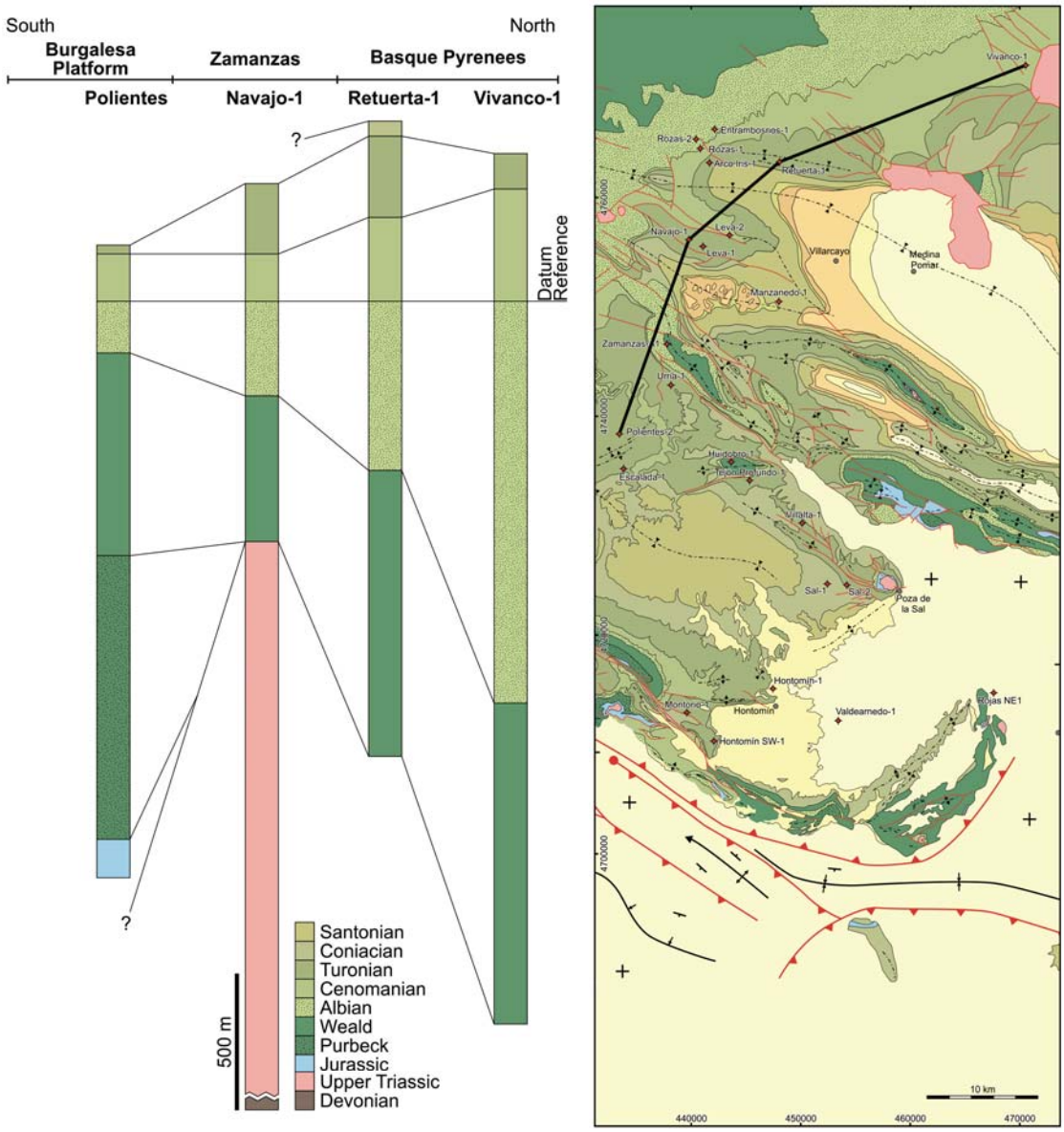

Fig. 5.25: Well correlation from the Burgalesa Platform to the Basque Pyrenees, flattened at the top of the Albian Utrillas Formation. Note that towards the north the Utrillas Formation and the Cenomanian successions thickens.

5.4 Reinterpretation of the surface geology in the Zamanzas area

The Zamanzas surface geology has been interpreted as a set of northeast-directed extensional faults affecting the Lower and Upper Cretaceous successions (Fig. 5.26) (Carreras Suárez *et al.*, 1978). However, the integration of surface geology and well data require a new reinterpretation of the structures. In broad strokes, this area can be simplified by two NW-SE faults delimiting three different blocks.

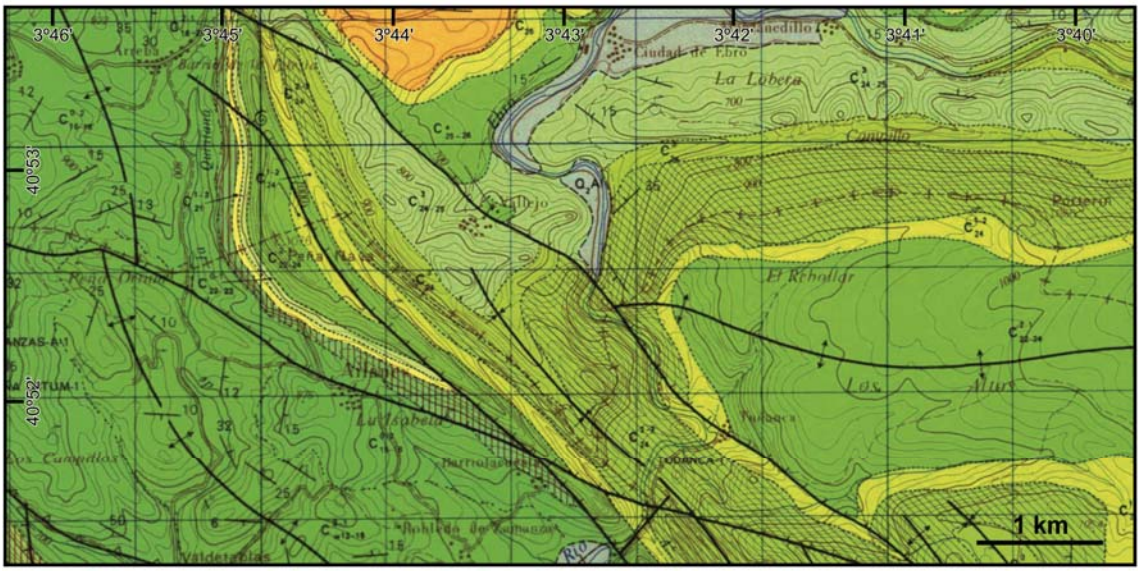

Fig. 5.26: Geological map of the Zamanzas sector (IGME, 1978).

The south-westernmost block is characterised by an anticline, cored with Lower Cretaceous, in which the northern limb, with Upper Cretaceous rocks, dips gently towards the north-east. In this southern block, several wells drilled the whole Mesozoic succession without encountering repetition as for example the Urria-1 well, that drilled from Santonian to Jurassic, reaching 1750 meters deep or the Zamanzas-A1 well that was drilled in the core of the anticline, testifying a succession from Lower Cretaceous to Jurassic. In this southern block the Cenomanian to Coniacian succession is almost horizontal and is topographically higher than the same succession in the middle block close to the southern fault, where the succession is almost vertical and parallel to the fault (Fig. 5.27). These facts together with the Upper Cretaceous cutoff that can be seen in the southern block allow to reinterpret the southern fault as a south-directed thrust instead of a north-directed extensional fault (Fig. 5.27). In addition, in the hangingwall the Turonian contact runs parallel to the trace of the southern fault (Fig. 5.26). This map pattern geometry is produced because the erosional level is between the trailing and the leading branch lines (Elliott and Johnson, 1980; Diegel, 1986). With such

interpretation, the southern block would constitute the footwall of the thrust, explaining the lack of Mesozoic repetition in the Zamanzas-A1 or Urria-1 wells as stated before.

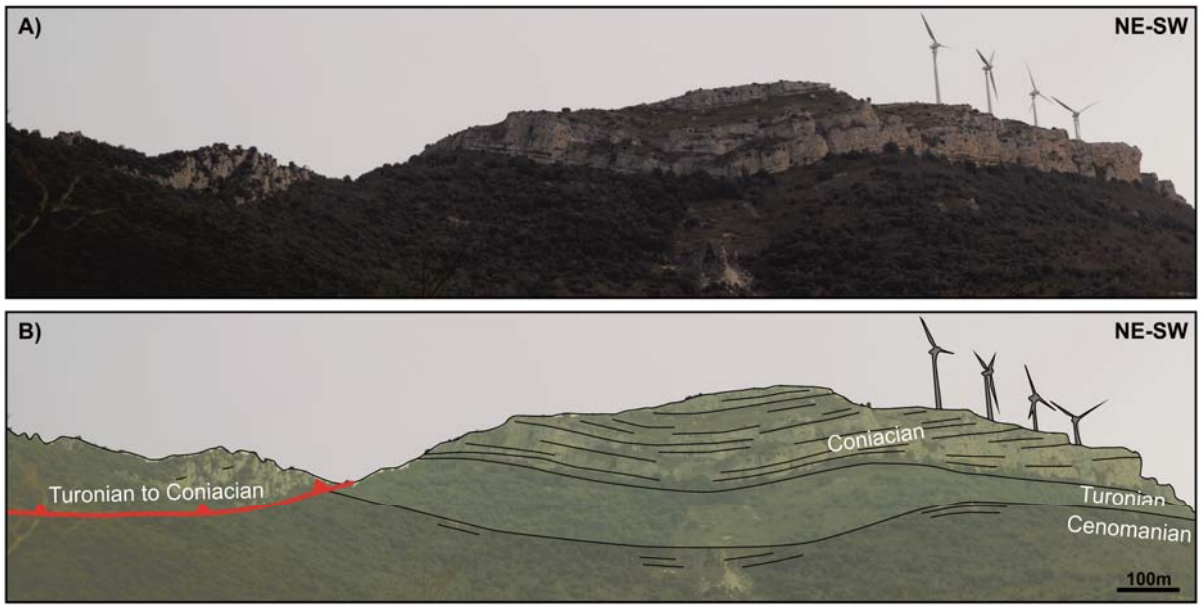

Fig. 5.27: A) Non interpreted and B) interpreted field photograph of the Zamanzas southern thrust footwall in which the Cenomanian to Coniacian successions dip few degrees whereas in the hangingwall these successions dip more than 70 degrees.

The middle block between the two faults presents more deformation, being a pair of NW-SE syncline-anticline the most important outcropping structure. The tight syncline has a southern limb that is almost vertical and the northern limb dips more than 60º passing to the adjacent anticline (Fig. 5.28). The core of the anticline is constituted by Turonian to Coniacian rocks. Below this succession, the Santonian succession of the northern block is truncated against the northern fault as denoted by the cutoff observable in the surface geology (Fig. 5.28). In addition, in the middle of this structure the Tudanca-1 well was drilled and testified a duplication of part of the Upper Cretaceous succession, drilling from the Turonian to Aptian succession from 0 to 230 meters below surface (m.b.s) and from Turonian to Albian from 230 to 450 m.b.s. The fact that the Tudanca-1 well encountered repetition of the Mesozoic makes difficult to interpret this fault as a northeast-directed extensional fault without invoking previously imposed geometries before the deformation. Thus, it is more plausible to reinterpret the northern fault as a northeast-directed thrust instead of a northeast-directed extensional fault. With such interpretation, the middle block constitutes the hangingwall of the north-directed thrust and the Santonian cutoff corresponds to the footwall of this thrust. This footwall is characterised by an E-W striking open anticline made up of Upper Cretaceous with Coniacian limestones in the core of the fold, which trace is truncated against the northern thrust (Fig. 5.27 and Fig. 5.28).

Fig. 5.28: A) Non interpreted and B) interpreted photograph of the Zamanzas area with the popup structure. The Turonian to Santonian rocks are deformed with a tight syncline and a gentle anticline inside the popup. More to the north, the succession only displays an anticline geometry.

The reinterpretation of the two faults results into a popup structure (Fig. 5.29). This structure was developed along the northern edge of the Burgalesa Platform during the Pyrenean Orogeny and accommodates part of the contractional deformation that occurred during this stage.

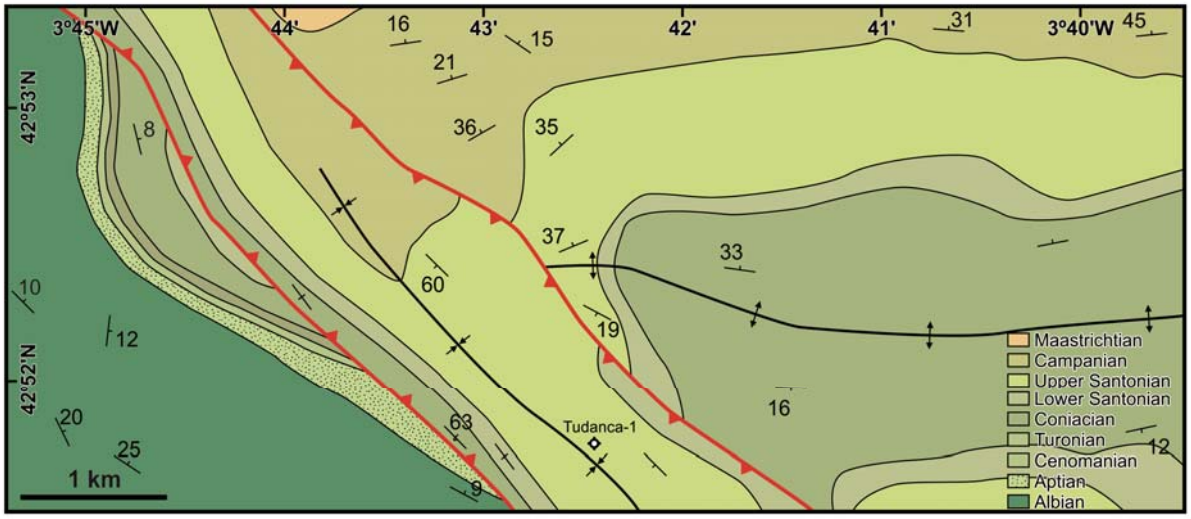

Fig. 5.29: Reinterpreted geological map of the Zamanzas area with the location of the Tudanca-1 well.

Chapter 6

Conclusions

In this chapter are summarised the conclusions that resulted from the research carried out in the Burgalesa Platform and vicinities during the accomplishment of the thesis. It has been divided into three sections:

- 6.1 Geometric and sedimentary relationship of the extensional system

- 6.2 The transition from thick-skin to thin-skin tectonics

-6.3 Vertical axis rotations pattern of the Burgalesa Platform and vicinities

6.1 Geometric and sedimentary relationship of the extensional system

The integration of surface geology with the interpretations of subsurface data (i.e. seismic sections and wells) allowed to determine the main geometric and kinematic features of the Late Jurassic-Early Cretaceous extensional system.

The initial stages of extension in the Burgalesa Platform were characterised by forced folding of the cover above a basement step triggering the mobilisation of salt. As the deformation continued, decoupling between the basement and the cover occurred, being the latter translated towards the north. The seismic interpretation has shown that during the Early Cretaceous a north-directed thrust was developed accommodating the extension produced at the southern margin of the basin. The onlap observed in the southern boundary has demonstrated that at least 10 km of northwards displacement of the cover occurred and that a similar amount of displacement was accommodated by the contractional structure. These onlaps were developed by the translation of the cover above the basement step, showing a forced folding geometry, allowed by the decoupling level corresponding to the Upper Triassic salt layer.

The Upper Triassic salt layer distribution resulted in two main trends in the Burgalesa Platform: a principal WNW-ESE orientation, related to the main extensional faults, at the southern and northern boundaries and a NE-SW second order orientation related to the transverse faults. The location of the contractional structure was controlled by the backstop produced by the northern WNW-ESE salt wall and the thick Lower Cretaceous succession deposited in the hangingwall of this structure. The erosional truncation geometry, observed along the northern edge of the Burgalesa Platform, between the syn-rift and the post-rift, is related to the erosion of the structural relief, developed by the north-directed thrust.

6.2 The transition from thick-skin to thin-skin tectonics

The results obtained during this thesis have demonstrated that the geometry of the extensional basin and the obliquity between the strike of the faults and the shortening direction strongly conditioned the inversion and the subsequent incorporation into the fold and thrust belt of the Burgalesa Platform during the Cenozoic.

A new evolution model that explains the deformational history of the studied area has been proposed. This new model is a combination of thick-skinned and thin-skinned modes of deformation during oblique tectonic inversion that was conditioned by the distribution of the Upper Triassic salts. The thick-skinned domain, located to the west, is characterised by the WNW-ESE to W-E basement-involved thrust structures of the Cantabrian Mountains and the Duero foreland basin. In contrast, the thin-skinned domain spans eastwards of the basement cutoff and decouples the Mesozoic succession of the entire Burgalesa Platform and also of the Basque-Pyrenees at the Upper Triassic salt layer.

The thick-skinned domain, characterised by high angle thrusts deforming the basement and the cover, is restricted not only in space, but also in time. The progressive eastwards thickening of the Upper Triassic salt layer in the Burgalesa Platform allowed to decouple the structures and to transfer the basement deformation of the Cantabrian Mountains into the cover towards the east in the Burgalesa Platform. In addition, the progression of deformation in time, southwards and involving deeper structural levels, produced the reactivation and inversion of inherited basement structures southwards and also below the detached Mesozoic Burgalesa Platform. The inversion of these south-directed basement structures during the Miocene resulted in an increase of structural relief and the regional eastwards plunge at the eastern termination of the Cantabrian Mountains and western sector of the Burgalesa Platform.

In the thin-skinned domain, the combined study of surface geology together with the data provided by the wells allowed to reinterpret the Zamanzas structure. Previously, this structure was considered as a set of northeast-directed extensional faults affecting the Lower and Upper Cretaceous successions. With this study it has been demonstrated that all the constraints fit with the reinterpretation of the Zamanzas as a pop-up structure instead of a set of extensional faults. With the proposed interpretation, the south-western and the north-eastern blocks constitute the footwalls of the pop-up and thus the hangingwall of the structure is the middle block. More to the southeast, the interpretation of the seismic data in the Bureba re-entrant, located between the Rojas structure of the Burgalesa Platform northern edge and the Basque Pyrenees frontal thrust, has shown the continuity of the seismic stratigraphy of the Bureba re-entrant with the Ebro and Duero basins. This geometry demonstrates the lack of continuity between the NE-SW trending Rojas structure and the Sierra de Cantabria frontal thrust. These facts demonstrate that the detachment and thrusting of the Mesozoic successions of the Burgalesa Platform above the Duero-Ebro basins occurred. Eastwards of the Rojas structure, the Ebro Foreland Basin does not present significant deformation. In contrast, towards the south-west of the Rojas structure, the Burgalesa Platform overrides the Duero Foreland Basin in which Oligocene deformation is caused by northeast-directed and basement-involved thrusts related to the San Pedro Structure.

The proposed model explaining the Cenozoic evolution of the Burgalesa Platform was conditioned by the confined location of this structural unit between the Cantabrian Mountains westward and the NW tip of the Iberian Range basement-involved structures southward. During the early stages of deformation (Oligocene times), the southwards displacement of the Burgalesa Platform and the north-eastward displacement of the San Pedro Structure where the

main active areas allowing the sedimentation between the two domains. As deformation continued, the two domains were oppositely displaced thus reducing the corridor between them until the Burgalesa Platform overrode the San Pedro structure. The backstop interference for the southward displacement of the Burgalesa Platform produced by the San Pedro structure forced the right-lateral reactivation of the Ubierna fault and, as a consequence, the lateral extrusion, with more than 15 km of displacement, of the Burgalesa Platform towards the SE overriding the Ebro Foreland. During the last stages of deformation (Miocene times) took place the reactivation of the Golobar fault thus preserving the tapper and also the oblique inversion of basement structures, located below the detached Burgalesa Platform, as the deformation progressed south-eastwards.

6.3 Vertical axis rotations pattern of the Burgalesa Platform and vicinities

The paleomagnetic study carried out in the Burgalesa Platform and vicinities revealed that the main remanence carrier of the Lower Cretaceous and Oligocene-Miocene fine grain sandstones and red clays is related to the hematite group mineralogy. In contrast, the main remanence carrier mineralogy of the Upper Cretaceous and Miocene limestones and grey clays is related to the (titano)magnetite group.

The positive local and regional fold tests revealed that magnetisation was acquired before the folding of the strata. This fact, makes suitable the application paleomagnetic vertical axis rotations studies in order to determine possible Cenozoic rotations in the study area.

The vertical axis rotation study is made up of 62 sampled sites where 26 of them allowed to calculate the mean site characteristic direction. This study points out that a counter-clockwise rotation of about 20º occurred at the eastern tip of the Burgalesa Platform and the clockwise rotation of about 25º took place at the western boundary of this structural unit. This vertical axis rotation pattern is completely in agreement with the theoretical model of a tightened arch developed previously to the rotations, in which rotations that occur at tips of the arch are clockwise and counter-clockwise pointing towards the inner parts of it whereas at the central parts of the arch a lack of rotation is expected.

Chapter 7

References

Aguilar, M.J. 1971. Correlaciones por ciclos de aporte en el Albense de la Cuenca Cantábrica. *Acta Geológica Hispánica*, **6**, 92-96.

Alcalde, J., Martí, D., Calahorrano, A., Marzan, I., Ayarza, P., Carbonell, R., Juhlin, C., Pérez-Estaún, A. 2013. Active seismic characterization experiments on the Hontomín research facility for geological storage of CO_2, Spain. *International Journal of Greenhouse Gas Control* **19**, 785-795.

Allerton, S. 1998. Geometry and kinematics of vertical-axis rotation in fold and thrust belts. *Tectonophysics*, **299**, 15-30. DOI: 10.1016/S0040-1951(98)00196-6.

Almar, Y., Garcés, M., Beamud, E., Muñoz, J.A. 2008. Timing and evolution of the frontal structure of the southwestern Pyrenees from paleomagnetic analysis on its foreland basin (Ebro basin). *Geotemas*, **10**, 1143-1146.

Alonso, J.L., Pulgar, F.J., García-Ramos, J.C., Barba, P., 1996. Tertiary Basins and Alpine Tectonics in the Cantabrian Mountains. In: Friend, P.F., Dabrio, C.J., (eds.). *Tertiary basins of Spain: The stratigraphic record of crustal kinematics*. Cambridge, Cambridge University Press, 214-227.

Alonso, J.L. 1987. Estructura y evolución tectonoestratigráfica de la región del Manto del Esla (Zona Cantábrica NW de España). Tesis Doctoral. Universidad de Oviedo. 276pp.

Alonso, J.L., Pulgar, J.A., Pedreira, D. 2007. Relieve de la Cordillera Cantábrica. *Enseñanza de las Ciencias de la Tierra*, **15.2**, 151-163.

Alonso, J.L., Marcos, A., Suárez, A. 2009. Paleogeographic inversion resulting from large out of sequence breaching thrusts: The León Fault (Cantabrian Zone, NW Iberia). A new picture of the external Variscan Thrust Belt in the Ibero-Armorican Arc. *Geologica acta*, **7**, 451-473.

Álvarez-Marrón, J., A. Pérez-Estaún, J.J. Danñobeitia, J.A. Pulgar, R. Martínez Catalán, A. Marcos, F. Bastida, P. Ayarza Arribas, J. Aller, A. Gallart, F. Gonzalez-Lodeiro, E. Banda, M.C. Comas and D. Córdoba. 1996. Seismic structure of the northern continental margin of Spain from ESCIN deep seismic profiles. *Tectonophysics*, **264**, 153-174.

Álvaro, M., Capote, R., Vegas, R. 1979. Un modelo de evolución geotectónica para la cadena Celtibérica. *Acta Geologica Hispanica*, **14**, 172-181.

Amilibia, A., McClay, K.R., Sàbat, F., Muñoz, J.A., Roca, E., 2005. Analogue modelling of inverted oblique rift systems. *Geologica Acta*, **3**, 251-271.

Arnáiz, I., Robles, S., Pujalte, V. 1991. Correlación entre registros de sondeos y series de superficie del Aptiense-Albiense continental del extremo SW de la Cuenca Vascocantábrica y su aplicación a la identificación de zonas lignitíferas. *Geogaceta*, **10**, 65-68.

Arthaud, F. & Matte P. 1977. Late Paleozoic strike-slip faulting in southern Europe and northern Africa: Result of a right-lateral shear zone between the Appalachians and the Urals. *Bulletin Geological Society of America*, **88**, 1305-1320.

Aurell, M., Robles, S., Bádenas, B., Rosales, I., Quesada, S., Meléndez, G., García-Ramos, J.C. 2003. Transgressive-regressive cycles and Jurassic paleogeography of northeast Iberia. *Sedimentary Geology,* **162**, 239-271. doi:10.1016/S0037-0738(03)00154-4.

Badley, M.E., Price, J-D., Backshall, L.C. 1989. Inversion, reactivated faults and related structures: seismic examples from the southern North Sea. In: Inversion tectonics Cooper, M.A. and Williams, G.D. (eds). *Geological Society Spececial Publications*, **44**, 201-219.

Bahroudi, A. and Koyi, H.A., 2003. Effect of spatial distribution of Hormuz salt on deformation style in the Zagros fold and thrust belt: an analogue modelling approach. *Journal of the Geological Society of London*, **160**, 719-733. doi: 10.1144/0016-764902-135.

Bally, A.W., Gordy, P.L., Stewart, G.A. 1966. Structure, seismic data, and orogenic evolution of the Southern Canadian Rocky Mountains. *Bulletin of Canadian Petroleum Geology*, **14**, 337-382.

Barnolas, A., Pujalte, V. 2004. La cordillera Pirenaica. *In:* Vera, J.A. (ed.) *Geología de España.* SGE-IGME, Madrid, 233-241.

Barrón, E., Gómez, J.J., Goy, A., Pieren, A.P. (2006) The Triassic-Jurassic boundary in Asturias (northern Spain): Palynological characterisation and facies. *Review of Palaeobotany & Palynology*, **138**, 187-208.

Bassi, G. 1995. Relative importance of strain rate and rheology for the mode of continental extension. *International Journal Geophysics*, **122**, 195-210.

Bates, M.P., 1989. Palaeomagnetic evidence for rotations and deformation in the Nogueras Zone, central southern Pyrenees, Spain. *Journal Geological Society London*, **146**, 459-476.

Beaumont, C., J. A. Muñoz, J. Hamilton, and P. Fullsack. 2000. Factors controlling the Alpine Evolution of the Central Pyrenees inferred from a comparison of observations and geodynamical models. *Journal of Geophysical Research,* **105**, 8121-8145. doi:10.1029/1999JB900390.

Beroiz, C. Permanyer, A. 2011. Hydrocarbon habitat of the Sedano Trough, Basque-Cantabrian Basin, Spain. *Journal of Petroleum Geology*, **34**, 387-410.

Bistacchi, A., Massironi, M., Dal Piaz, G., Monopoli, B., Schiavo, A., Toffolon, G. 2008. 3D fold and fault reconstruction with an uncertainty model: An example from an Alpine tunnel case study. *Computers & Geosciences*, **34**, 351-372.

Blanc, E.J.P., Allen, M.B., Inger, S., Hassani, H. 2003. Strctural styles in the Zagros Simple Folded Zone, Iran. *Journal of the Geological Society, London*, **160**, 401-412.

Boillot, G., & J. Malod. 1988. The North and North-West Spanish Continental Margin: A review, *Revista Sociedad Geologica España*, **1(3-4),** 295-316.

Bois, C.; Pinet, B. & Gariel, O. 1997. The sedimentary cover along the ECORS Bay of Biscay deep seismic reflection profile. A comparison between the Parentis basin and other European rifts and basins. *Mémoires de la Societé Géologique de France*, **171**, 143-165.

Boyer, S.E., Elliot,D. 1982. Thrust Systems. *American Association of Petroleum Geologists Bulletin*, **66**, 1196-1230.

Brown, R.N. 1980. History of exploration and discovery of Morgan, Ramadan, and July oilfields, Gulf of Suez, Egypt, *Canadian Society of Petroleum Geologists, Memoir,* in: A. D. Miall, Editor, *Facts and principles of world petroleum occurrence*, **6**, 733-764.

Brun, J.P., Maudit, T.P.O. 2008. Rollovers in salt tectonics: The inadequacy of the listric fault model. *Tectonophysics*, **457**, 1-11.

Buchanan, J.G., Buchanan, P.G., 1995. Basin inversion. Geological Society Spececial Publications, **88**, 596.

Butler, R.W.H. 1989. The influence of pre-existing basin structure on thrust system evolution in the Western Alps. In: Inversion tectonics Cooper, M.A. and Williams, G.D. (eds). *Geological Society Spececial Publications*, **44**, 105-122.

Bug, J.P., Greya, T.V. 2005. The role of viscous heating in Barrovian metamorphism of collisional orogens: thermomechanical models and application to the Lepontine Dome in the Central Alps. *Journal Metamorphic Geology*, **23**, 75-95.

Butler, R.F. 1992. *Paleomagnetism: Magnetic domains to geologic terranes.* 319pp. Boston: Blackwell Scientific Publications.

Butler, R.F., Richards, M.H., Sempere, T., Marshall, L.G. 1995. Paleomagnetic determinations of vertical-axis tectonic rotations from Late Cretaceous and Paleocene strata of Bolivia. *Geology*, **23**, 799-802.

Butler, R.W.H., Tavarnelli, E., Grasso, M. 2006. Structural inheritance in mountain belts: an Alpine-Apennine perspective, *Journal of Structural Geology*, **28**, 1893-1908. doi:10.1016/j.jsg.2006.09.006.

Calassou, S., Larroque, C., Malavielle, J. 1993. Transfer zones of deformation in thrust wedges: An experimental study. *Tectonophysics*, **221**, 325-344.

Cámara, P. 1997. The Basque-Cantabrian basin's Mesozoic tectono-sedimentary evolution**,** *Mém. Soc. géol. France,* **171**, 187-191.

Carey, W.S., 1958. The orocline concept in Geotectonics. *Proceedings of the Royal Society of Tasmania*, **89**, 255-288.

Carola, E.; Tavani, S.; Ferrer, O.; Granado, P.; Quintà, A.; Butillé, M.; Muñoz, J.A. 2013. Along-strike extrusion at the transition between thin- and thick-skinned domains in the Pyrenean Orogen (northern Spain). In *Thick-skin-dominated Orogens: From initial inversion to full accretion*. Nemcok,M.; Mora, A.R.; Cosgrove, J.W. (eds). *Geological Society of London Special Publications* **377**, 119-140. DOI:10.1144/SP377.3.

Carrera, N.; Muñoz, J. A. i Roca, E. 2009. 3D reconstruction of geological surfaces by the equivalent dip-domain method: An example from field data of the Cerro Bayo Anticline (Cordillera Oriental, NW Argentine Andes). *Journal of Structural Geology*, **31**, 1573-1585.

Carrera, N., Muñoz, J.A. 2013. Thick-skinned tectonic style resulting from the inversion of previous structures in the southern Cordillera Oriental (NW Argentine Andes). In: *Thick-Skin-Dominated Orogens: From Initial Inversion to Full Accretion* edited by Nemčok, M., Mora, A.R. and Cosgrove, J.W. Geological Society of London Special Publications, **377**, 77-100.

Carreras Suárez, F., del Olmo, P., Ramírez del Pozo, J. 1978. Mapa geológico 1:50.000, Hoja 109 (Villarcayo). IGME

Cartwrigth, J.A., Trudgill, B.D., Mansfield, C.S. 1995. Fault growth by segment linkage: an explanation for scatter in maximum displacement and trace length data from Canyonlands Grabens of SE Utah. *Journal of Structural Geology*, **17**, 1319-1326.

Cartwright, J., Jackson, M., Dooley, T., Higgins, S. 2012. Strain partitioning in gracity-driven shortening of a thick, multilayered evaporite sequence. In: *Salt Tectonics, Sediments and Prospectivity.* Alsop, G.I., Archer, S.G., Hartley, A.J., Grant, N.T., Hodgkinson, R. (eds). *Geological Society of London Special Publications*, **363**, 449-470.

Catañares, L. M., & S. Robles. 2004. El vulcanismo del Albiense-Santoniense en la Cuenca Vasco-Cantábrica, in *Geología de España*, edited by J. A. Vera, pp. 306-308, SGE-IGME, Madrid, Spain.

Chapman, T.J. 1989. The Permian to Cretaceous structural evolution of the Western Approaches Basin (Melville sub-basin), UK. In: Inversion tectonics Cooper, M.A. and Williams, G.D. (eds). *Geological Society Spececial Publications*, **44**, 177-200.

Choukroune P., and ECORS Team. 1989. The ECORS Pyrenean deep seismic profile reflection data and the overall structure of an orogenic belt. *Tectonics,* **8**, 23-39. doi:10.1029/TC008i001p00023.

Choukroune P., F. Roure, B. Pinet, Ecors Pyrenees Team. 1990. Main results of the ECORS Pyrenees profile. *Tectonophysics*, **173**, 411-423.

Choukroune, P. 1992. Tectonic Evolution of the Pyrenees. *Annual Review of Earth and Planetary Sciences*, **20**, 143-158.

Colleta, B., Le Quellec, P., Letouzey, J., Moretti, I. 1988. Longitudinal evolution of the Suez rift structure (Egypt). *Tectonophysics*, **153**, 221-233.

Cooper, M.A., Williams, G.D., 1989. Inversion tectonics. *Geological Society Spececial Publications*, **44**, 375 pp.

Corrado, S., Bucci, D., Naso, G., Faccenna, C. 1998. Influence of paleogeography on thrust system geometries: an analogue modelling approach from the Abruzzi-Molise (Italy) case history. *Tectonophysics*, **296**, 437-453.

Corretgé, L.G. & Suárez, O. 1991. Igneous rocks of the Cantabrian / Palentian Zone. In:Pre-Mesozoic Geology of Iberia. R.D. Dallmeyer & E. Martínez-García (Eds.).Springer-Verlag, Berlin: 72-79.

Cosgrove, J.W., Ameen, M.S. 1999. A comparison of the geometry, spatial organization and fracture patterns associated with forced folds and buckle folds, *Geological Society of London Special Publication*, in: J.W. Cosgrove, M.S. Ameen, Editors, *Folds and Fractures*, **169**, 7-21.

Coward, M.P., 1994. Inversion Tectonics. In: Hancock, P.L. (Ed.), Continental Deformation, Pergamon Oxford, 289-304.

Coward, M.P., Stewart, S. 1995. Salt-induced structures in the Mesozoic-Tertiary cover of the southern North Sea U.K. *In:* M.P.A. Jackson, D.G. Roberts, and S. Snelson (eds). Salt tectonics: a global perspective. *AAPG Memoir*, **65**, 229-250.

Cowie, P.A., Shipton, Z.K. 1998. Fault tip displacements gradients and process zone dimensions. *Journal of structural geology,* **20**, 983-997.

Cuevas, J., A. Aranguren, Badillo, J. M., J. M. Tubía. 1999. Estudio estructural del sector central del Arco Vasco (Cuenca Vasco-Cantábrica). *Bol. Geol. Min. España,* **110**, 3-18.

Dahlen, F.A. 1984. Noncohesive critical coulomb wedges: An exact solution. *Journal of Geophysical Research*, **89**, 10125-10133.

Dallmeyer, R.D. & Martínez-García, E. 1990. *Pre-Mesozoic Geology of Iberia* Springer-Verlag, Berlin.

Dallmeyer R.D., Martínez Catalán, J.R., Arenas, R., Gil Ibarguchi J.I., Gutiérrez Alonso G., Farias P., Bastida F., Aller J. 1997. Diachronous Variscan tectonothermal activity in the NW Iberian Massif: evidence from $^{40}Ar/^{39}Ar$ dating of regional fabrics. *Tectonophysics*, **227**, 307-337. doi:10.1016/S0040-1951(97)00035-8.

Davies, S.J., Dawers, N.H., McLeod, A.E., Underhill, J.R. 2000. The structural and sedimentological evolution of early synrift successions: the Middle Jurassic Tarbert Formation, North Sea. *Basin Research*, **12**, 343-365.

Davis, D.M., Engelder, T., 1985. The role of salt in fold-and-thrust belts. *Tectonophysics*, **119**, 67-88.

Davis, F.A., Suppe, J., D., Dahlen, 1983. Mechanics of fold-and-thrust belts and accretionary wedges. *Journal of Geophysical Research*, **88**, 1153-1172.

Davison, I. 1986. Listric normal fault profiles: calculation using bed-length balance and fault displacement. *Journal of Structural Geology*, **8,** 209-210.

Dawers, N.H., Underhill, J.R. 2000. The role of fault interaction and linkage in controlling synrift stratigraphic sequences: Late Jurassic, Statfjord east area, Northern North Sea. *American Association of Petroleum Geologists Bulletin*, **84**, 45-64.

de Kemp, E., 1998. Three-dimensional projection of curvilinear geological features through direction cosine interpolation of structural field observations. *Computers & Geosciences*, **24**(3), 269-284.

de Kemp, E., 2000. 3-D visualization of structural field data: examples from the Archean Caopatina Formation, Abitibi greenstone belt, Québec, Canada. *Computers & Geosciences*, **26**, 509-530.

De Sitter, L.U. 1962. The structure of the Southern slope of the Cantabrian Mountains. *Leidse Geol. Meded*, **26**, 255-264.

Dewey, J.F., Bird, J.M., 1970. Mountain belts and the new global tectonics. *Journal of Geophysical Research*, **75**, 2625-2647. doi:10.1029/JB075i014p02625.

Dinarès, J., McClelland, E., Santanach, P. 1992. Contrasting rotations within thrust sheets and kinematics of thrust tectonics as derived from palaeomagnetic data: an example from the Southern

Pyrenees. *In*: K.R. McClay (ed.), Thrust tectonics, 265-276, *Chapman and Hall Eds*., London, 447 pp.

Dooley, T.P., Jacosin, M.P.A., Hudec, M.R. 2007. Initiation and growth of salt-based thrust belts on passive margins: results from physical models. *Basin Research*, **19**, 165-177. DOI: 10.1111/j.1365-2117.2007.00317.x

Dula, W.F. 1991. Geometric models of listrc normal faults and rollover folds. *AAPG Bulletin*, **75**, 1609-1625.

Durand-Riard, P., Shaw, J.H., Plesch, A., Lufadeju, G. Enabling 3D geomechanical restoration of strike- and oblique-slip faults using geological constraints, with applications to the deep-water Niger Delta. *Journal of Structural Geology*, **48**, 33-44. DOI: 10.1016/j.jsg.2012.12.2009.

Elío, J., Ortega, M.F., Chacón, E., Mazadiego, L.F., Grandia, F. 2012. Sampling strategies using the "accumulation chamber" for monitoring geological storage of CO_2. *International Journal of Greenhouse Gas Control*, **9**, 303-311

Eldredge, S., Van der Voo, R. 1988. Paleomagnetic study of thrust sheet rotations in the Helena and Wyoming salients of the northern Rocky Mountains, *in* Scmidth, C.J. and Perry, W.J., Interaction of the Rocky Mountain Foreland and the Cordilleran Thrust Belt: *Geological Society of America Memoir*, **171**, 319-332.

Ellis, S., Beaumont, C., Jamieson, R.A., Quinlan, G. 1998. Continental collision including a weak zone: the vise model and its application to the Newfoundland Appalachians. *Canadian Journal of Earth Science*, **35**, 1323-1346.

Emery, D., Myers, K.J. 1996. Sequence Stratigraphy. Blackwell, Oxford. 297p.

Enkin, R.J. 2003. The direction-correction tilt test: an all-purpose tilt/fold test for paleomagnetic studies. *Earth and Planetary Science Letters*, **212 (1-2)**, 151-166.

Espina, R.G., Alonso, J.L., Pulgar, J.A. 1996a. Growth and propagation of buckle folds determined from syntectonic sediments (the Ubierna Fold Belt, Cantabrian Mountains, N Spain). *Journal of Structural Geology*, **18**, 431-441. doi:10.1016/0191-8141(95)00103-K.

Espina, R.G., De Vicente, G., Muñoz Martín, A. 1996b. Análisi poblacional de fallas alpinas en el borde occidenteal de la Cuenca Vasco-Cantábrica (Cordillera Cantábrica, NO de España). *Geogaceta*, **20**, 936-938.

Espina, R.G. 1997. La estructura y evolución tectonoestratigráfica del borde occidental de la Cuenca Vasco-Cantábrica (Cordillera Cantábrica, NO de España) Ph.D. Thesis, Univerity of Oviedo. 230pp.

Espina, R.G., Alonso, J.L., Pulgar, J.A., 2004. Extensión Triásica en la Cuenca Vasco-Cantábrica. In: Vera, J.A. (Ed.), Geología de España. Madrid, SGE-IGME, 338-339.

Ferrer, O., E. Roca, B. Benjumea, J. A. Muñoz, N. Ellouz, and MARCONI Team. 2008. The deep seismic reflection MARCONI-3 profile: role of extensional Mesozoic structure during the Pyrenean contractional deformation at the eastern part of the Bay of Biscay. *Marine and Petroleum Geology,* **25(8)**, 714-730. doi:10.1016/j.marpetgeo.2008.06.002.

Fernández, O.; Muñoz, J. A.; Arbués, P.; Falivene, O. i Marzo, M. 2004. 3D reconstruction of geological surfaces: an example of growth strata and turbidite systems from the Ainsa basin (Pyrenees, Spain). *AAPG Bulletin*, **88,** 1049-1068.

Fillon, C. 2012. Spatial and temporal variation in Cenozoic exhumation of the Pyrenean-Cantabrian mountain belt: coupling between tectonics and surface processes. PhD Thesis. Institut des Sciences de la Terre de Grenoble (ISTerre), Grenoble, France. 202p.

Fischer, M.P., Jackson, P.B., 1999. Stratigraphic controls on deformation patterns in fault-related folds: a detachment fold example from the Sierra Madre Oriental, northeast Mexico. *Journal of Structural Geology*, **21**, 613-633.

Floquet, M. 2004. El Cretácico Superior de la Cuenca Vasco-Cantábrica y áreas adyacentes, in *Geología de España*, edited by J. A. Vera, pp. 299-306, SGE-IGME, Madrid.

Ford, M., Le Carlier de Veslud, C., Bourgeois, O. 2007. Kinematic and geometric analysis of fault-related folds in a rift setting: The Dannemarie basin, Upper Rhine Graben, France. *Journal of Structural Geology*, **29**, 1811-1830.

Gallastegui, J. 2000. Estructura cortical de la Cordillera y Margen Continental Cantábricos: Perfiles ESCI-N. *Trabajos Geología,* **22**, 9-234.

Gallastegui, J., J. A. Pulgar, and J. Gallart. 2002. Initiation of an active margin at the North Iberian continent-ocean transition. *Tectonics,* **21(4)**, doi: 10.1029/2001TC901046.

García de Cortázar, A., Pujalte, V., 1982. Litoestratigrafía y facies del grupo Cabuérniga (Malm-Valanginiense Inferior?) al S deCantabria-NE de Palencia. *Cuadernos Geología Ibérica*, **8**, 5-21.

García-Mondéjar, J., Pujalte, V. & Robles, S. 1986. Características sedimentológicas secuenciales y tectoestratigráficas del Triásico de Cantabria y Norte de Palencia. *Cuadernos de Geología Ibérica,* **10**, 151-172.

García-Mondejar, J. 1979. El Complejo urgoniano del sur de Santander. Tesis Doctoral. Universidad Pais Vasco. 673pp.

García-Mondejar, J. 1987. Aptian-Albian carbonate episode of Basque-Cantabrian Basin, northern Spain, *AAPG Bulletin*, **71**, 558.

García-Mondejar, J. 1990. The Aptian Albian Carbonate Episode of the Basque Cantabrian Basin (Northern Sapin): General Characteristics, Controls and Evolution. *International Association of Sedimentologists Special Publication*, **9**, 257-290.

García-Mondéjar, J., Agirrezabala, L.M., Aranburu, A., Fernández-Mendiola, P.A., Gómez-Pérez, I. López-Horgue, M. Rosales, I. 1996. Aptian-Albian tectonic pattern of the Basque-Cantabrian Basin (Northern Spain). *Geological Journal*, **31**, 13-45.

García-Mondejar, J., P. A. Fernández-Mendiola, L. M. Agirrezabala, A. Aramburu, M. A. López-Horgue, E. Iriarte, S. Martínez de Rituerto. 2004. El Aptiense-Albiense de la Cuenca Vasco-Cantábrica, in *Geología de España*, edited by J. A. Vera, pp. 291-296, SGE-IGME, Madrid.

García Ramos, J.C., Colmenero J.R., Vargas, I., Manjón, M. Crespo, A., Matas, J. 1982. Mapa geológico 1:50.000, Hoja 132 (Guardo). IGME.

García-Ramos, J.C. & Gutiérrez-Claverol, M. 1995. La cobertera mesozoico-terciaria. In: Geología de Asturias (C. Aramubury y F. Bastida, eds.) Ed. Trea, 81-94.

Gawthorpe, R.L., Sharp, I., Underhill J.R., Gupta, S. 1997. Linked sequence stratigraphic and structural evolution of propagating normal faults. *Geology,* **25**, 795-798.

Ge, H., Jackson M.P.A., Vendeville, B.C. 1997. Kinematics and dynamics of salt tectonics driven by progradation. *AAPG Bulletin*, **81**, 398-423.

Gómez, M.; Vergés, J., Riaza, C. 2002. Inversion tectonics of the northern margin of the Basque Cantabrian Basin. *Bulletin de la Société Géologique de France*, **173 (5)**, 449-459.

Gray, M.B., Stamatakos, J. 1997. New model for evolution of fold and thrust belt curvature, based on integrated structural and paleomagnetic results from the Pennsylvania salient. *Geology*, **25**, 1067-1070.

Guimerà, J. 1984. Palaeogene evolution of deformation in the north-east Iberian Peninsula. *Geological Magazine*, **121**, 413-420.

Guimerà, J., Alonso, A., Mas, R. 1995. Inversion of an extensional-ramp basin by a newly formed thrust: The Cameros Basin (N Spain). *In:* Buchanan, J.G. and Buchanan, P.G. (eds). *Basin Inversion.* Geological Society of London Special Publications, **88**, 433-453.

Guimerà, J., Mas, R., Alonso, Á. 2004. Intraplate deformation in the NW Iberian Chain: Mesozoic extension and Tertiary contractional inversion. *Journal of the Geological Society of London*, **161**, 291-303.

Gupta, S., Underhill, J.R., Sharp, I.R., Gawthrope, R.L. 1999. Role of fault interactions in controlling synrift sediment dispersal patterns: Miocene, Abu Alaqa Group, Suez Rift, Sinai, Egypt. *Basin Research*, **11**, 167-189.

Gutiérrez-Alonso, G., Fernández-Suárez, J., Weil, A.B., Murphy, J.B., Nance, R.D., Corfú, F., Johnston S.T. 2008. Self-subduction of the Pangaean global plate, *Natutre Geoscience* **1**. 549-553. DOI:10.1038/ngeo250

Gutiérrez-Claverol, M., & Torres Alonso, M. 1995. *Geología de Oviedo. Descripción, recursos y aplicaciones. Ed. Paraíso, 276 pp.*

Harding, T.P., 1985. Seismic characteristics and identification of negative flower structures, positive flower structures and positive structural inversion. *American Association of Petroleum Geologists Bullet*in, **69**, 582-600.

Harry, D.L., Oldow J.S,. Sawyer, D.S. 1995. The growth of orogenic belts and the role of crustal heterogeneities in decollement tectonics. *Geological Society American Bulletin*, **107**, 1411-1426. doi: 10.1130/0016-7606(1995)107.

Hempel, P.M. 1967. Der diapir von Poza de la Sal (Nordspanien). *Beiheft Geologisches Jahrbuch*, **66**, 95-126.

Heredia, N. Alonso, J.L. Rodrígues Fernández, L.R. 1990. Mapa geológico 1:50.000, Hoja 105 (Riaño). IGME.

Heredia, N. 1998. Los Cabalgamientos del sector suroriental de las unidades del Ponga y de la Cuenca Carbonífera Central (Zona Cantábrica, NO de España). *Trabajos de Geología*, **20**, 53-127.

Hernáiz, P.P. 1994. La falla de Ubierna (margen SO de la cuenca Cantábrica). *Geogaceta.* **16**. 39-42.

Hernáiz, P.P., Serrano, A., Malagón, J., Rodríguez Cañas, C. 1994. Evolución estructural del margen SO de la cuenca Vasco Cantábrica. *Geogaceta*, **15**, 143-146.

Hernáiz, P.P. & Solé, J. 2000. Las estructuras del diapiro de Salinas del Rosío y del alto de San Pedro-Iglesias y sus implicaciones en la evolución tectónica de la transversal burgalesa de la Cordillera Vascocantábrica-Cuenca del Duero. *Revista Sociedad Geologica España*, **13**, 471-486.

Hernández, J.Mª., Pujalte, V., Robles, S., Martín-Closas, C. 1999. División estratigráfica genética del grupo Campóo (Malm-Cretácico Inferior, SW Cuenca Vascocantábrica). *Revista Sociedad Geologica España*, **12**, 377-396.

Hill, K.C., Kendrick, R.D., Crowhurst, P.V. and Gow, P., 2002. Predicting Cu-Au mineralisation in New Guinea: 1. Tectonics, lineaments, thermochronology and structure. *Australian Journal of Earth Sciences*, **49**, 737-752.

Hill, K.C., Bradey K., Iwanec J., Wilson N. & Lucas K. 2008. Structural exploration in the Papua New Guinea Fold Belt. *In;* Blevin, J.E., Bradshaw, B.E. and Uruski, C. (eds), *Eastern Australasian Basins Symposium III, Petroleum Exploration Society of Australia, Special Publication*, 225-238.

Holdsworth, R.E., 2004. Weak faults, rotten cores. *Science*, **303**, 181-182. doi: 10.1126/science.1092491.

Hudec, M.R., Jackson, M.P.A. 2007. Terra infima: Understanding salt tectonics. *Earth Science reviews*, **82**, 1-28. DOI: 10.1016/j.earscirev.2007.01.001.

IPCC-Intergovernmental Panel on Climate Change, 2005. IPCC Special Report on Carbon Dioxide Capture and Storage. Cambridge U. Press, Cambridge, UK, pp.195-276 (Chapter 5).

Jackson, C.A.L., Gawthorpe, R.L., Sharp, I. 2006. Style and sequence of deformation during extensional fault-propagation folding: examples from the Hammam Faraun and El-Qaa fault blocks, Suez Rift, Egypt. *Journal Structural Geology,* **28**, 519-535.

Jammes, S., G. Manatschal, L. Lavier, and E. Masini. 2009. Tectonosedimentary evolution related to extreme crustal thinning ahead of a propagating ocean: the example of the western Pyrenees, *Tectonics,* **28**, TC4012, doi:10.1029/2008TC002406.

James, S., Huismans, R.S. 2012. Structural styles of mountain building: controls of lithospheric rheologic stratification and extensional inheritance. *Journal of Geophysical Research*, **117**, 1978-2012.

Jammes, S., Huismans, R.S., Muñoz, J.A. 2014. Lateral variations in structural style of mountain guilding: controls of rheological and rift inheritance. *Terra Nova*, **26**, 201-207. DOI:10.1111/ter.12087.

Janecke, S.U., Vanderburg, C.J., Blankenau, J.J. 1998. Geometry, mechanisms and significance of extensional folds from examples in the Rocky Mountain Basin and Range province, U.S.A. *Journal of Structural Geology,* **20**, 841-856.

Jaumé, S. C., R. J. Lillie. 1988. Mechanics of the Salt Range-Potwar Plateau, Pakistan: A fold-and-thrust belt underlain by evaporites, *Tectonics*, **7**, 57- 71.

Julivert, M., Ramírez del Pozo, J., Truyols, J. 1971. Le réseau de failles et la couverture post-hercynienne dans les Asturies. *Historie structurale du Golfe de Gascogne.* ed Technip, París. V3.

Kane, K.E., Jackson, C.A.L., Larsen, E. 2010. Normal fault growth and fault-related folding in a salt-influenced rift basin: South Viking Graben, offshore Norway. *Journal of Structural Geology*, **32**, 490-506.

Keller, J.V.A. Lynch, G. 1999. Displacement transfer and forced folding in the Maritimes basin of Nova Scotia, Eastern Canada, *Geological Society of London Special Publication*, in: J.W. 549 Cosgrove, M.S. Ameen, Editors, *Folds and Fractures*, **169,** 87-101.

Khalil, S.M., McClay, K.R. 2002. Extensional fault-related folding, northwestern Red Sea, Egypt, *Journal of Structural Geology*, **24**, 743-762.

Kim, Y.-S., Sanderson, D.J. 2005. The relationship between displacement and length of faults: a review. *Earth-Science Reviews*, **68**, 317-334.

Kley, J., Monaldi, C.R., Salfity, J.A. 1999. Along-strike segmentation of the Andean foreland: causes and consequences. *Tectonophysics*, **301**, 75-94.

Koopman, A., Speksnijder, A., Horsfield, W.T. 1987. Sandbox model studies of inversion tectonics. *Tectonophysics*, **137**, 379-388.

Koyi, H., Jenyon, M.K., Peterson, K. 1993. The effect of basement faulting on diapirism. *Journal Petroleum Geology*, **16**, 285-312.

Lacombe, O., Mouthereau, F., Angelier, J., Deffontaines, B. 2001. Structural, geodetic and seismological evidence for tectonic escape in SW Taiwan, *Tectonophysics*, **333**, 323-345.

Lacoste, A., Vendeville, B.C., Mourgues, R., Loncke, L., Lebacq, M. 2012. Gravitational instabilities triggered by fluid overpressure and downslope incision - Insights from analytical and analogue modelling. *Journal of Structural Geology*, **42**, 151-162. DOI: 10.1016/j.jsg.2012.05.011.

Lamplugh, G.W., 1920. Structure of the Weald and analogous tracts. Quarterly Journal of the *Geological Society of London* 15, LXXIII-XCV.

Lanaja, J. M. 1987. *Contribución de la exploración petrolífera al conocimiento de la Geología de España.* IGME, Serv. Oubl. Min. Indust. Energ., Madrid. 465 pp.

Langereis, C.G., Krijgsman, W., Muttoni, G., Menning, M. 2010. Magnetostratigraphy concepts, definitions and applications. *Newsletter on Stratigraphy*, **43**, 207-233.

Larrasoaña, J. C., Parés J. M., Millán H., del Valle J., and Pueyo E. L.. 2003. Paleomagnetic, structural, and stratigraphic constraints on transverse fault kinematics during basin inversion: The Pamplona Fault (Pyrenees, north Spain), *Tectonics,* **22(6)**, 1071-1092, doi: 10.1029/2002TC001446.

Laubscher, H.P. 1982. Die Sudostecke des Rheingrabens-ein kinematisches und dynamisches problem. *Eclogae Geologicae Helvetiae*, **75**, 101-116.

Lemon, A.M., Jones, N.L., 2003. Building solid models from boreholes and user-defined cross-sections. *Computers & Geosciences*, **29**, 547-555.

Le Pichon, X., Sibuet, J.C., 1971. Western extension of boundary between European and Iberian plates during the Pyrenean orogeny. *Earth and Planetary Science Letters* **12**, 83-88. doi:10.1016/0012-821X(71)90058-6.

Le Pichon, X., Bonnin, J., Sibuet, J.-C., 1970. La faille nord-pyrénéenne: Faille transformante liée à l'ouverture du golfe de Gascogne. *Comptes Rendus de l'Académie des Sciences*, **271**, 1941-1944.

Lepvrier, C. & Martínez-García, E. 1990. Fault development and stress evolution of the post-Hercynian Asturian Basin (Asturias and Cantabria, northwestern Spain). *Tectonophysics*, **184**, 345-356. doi:10.1016/0040-1951(90)90447-G.

Lewis, M.M., Jackson, C.A.L., Gawthorpe, R.L. 2013. Salt-influenced normal fault growth and forced folding: The Stavanger Fault System, North Sea. *Journal of Structural Geology*, **54**, 156-173.

López-Fernández, C., Pulgar, J.A., González-Cortina, J.M., Gallart, J., Díaz, J. y Ruiz, M. 2004. Actividad sísmica en el Noroeste del a Península Ibérica observada por la red sísmica local del Proyecto GASPI (1999-2002). *Trabajos de Geología, Univ. de Oviedo*, **24**, 91-106.

Lowrie, W. 1990. Identification of ferromagnetic minerals in a rock by coercitivity and unblocking temperature properties. *Geophysical Research Letters*, **17**, 159-162. DOI: 10.1029/GL017i002p00159.

Luján, M., Storti, F., Balanyá, J.C., Crespo-Blanc, A. and Rossetti, F., 2003. Role of décollement material with different rheological properties in the structure of the Aljibe thrust imbricate (Flysch Trough, Gibraltar Arc): an analogue modelling approach. *Journal of Structural Geology*, **25**, 867-881. doi:10.1016/S0191-8141(02)00087-1.

Macedo, J., Marshak, S. 1999. Controls on the geometry of fold-thrust belt salients. *Geological Society of America Bulletin*, **111**, 1808-1822.

Malagón, J., Hernáiz, P.P., Rodríguez Cañas, C., Serrano. 1994. Notas sobre la inversión tectónica y aloctonia de la cuenca Vasco-Cantábrica. *Geogaceta*, **15**, 139-142.

Maerten, L., Pollard, D.D., and Maerten, F., 2001. Digital mapping of three-dimensional structures of the Chimney Rock fault system, central Utah. *Journal of Structural Geology*, **23**, 585-592.

Marshak, S., 2004. Salients, recesses, arcs, oroclines, and syntaxesda review of ideas concerning the formation of map-view curves in fold-thrust belts. In: McClay, K.R. (Ed.), Thrust tectonics and hydrocarbon systems. *Memoir of the American Association of Petroleum Geologists*, **82**, 131-156.

Martín-González, F. & Heredia, N. 2011a. Complex tectonic and tectonostratigraphic evolution of an Alpine foreland basin: The western Duero Basin and the related Tertiary depressions of the NW Iberian Peninsula. *Tectonophysics*, **502**, 75-89. doi:10.1016/j.tecto.2010.03.002.

Martín-González, F. & Heredia, N. 2011b. Geometry, structures and evolution of the western termination of the Alpine-Pyrenean Orogen reliefs (NW Iberian Peninsula). *Journal of Iberian Geology*, **37**, 103-120. doi: 10.5209/rev_JIGE.2011.v37.n2.1.

Martínez-Torres, L. M. 1993. Corte balanceado de la Sierra Cantabria (cabalgamiento de la Cuenca Vasco-Cantábrica sobre la Cuenca del Ebro), *Geogaceta,* **14**, 113-115.

Mathieu, C. 1986. Histoire géologique du sous-basin de Parentis. *Bulletin des Centres de Recherches Elf-Aquitaine (Production)*, **10**, 33-47.

Maurin, J.C. & Niviere, B. 2000. Extensional forced folding and décollement of the pre-rift series along the Rhine graben and their influence on the geometry of the syn-rift sequences. In: *Forced Folds and Fractures* (Ed. by J.W.Cosgrove & M.S.Ameen), *Geol. Soc. London, Spec. Publ.*, **169**, 73-86.

Mazzoli, S., D'Errico, M., Allega, L., Corrado, S., Invernizzi, C., Shiner, P., Zattin, M., 2008. Tectonic burial and 'young' (b10 Ma) exhumation in the southern Apennines fold and thrust belt (Italy). *Geology*, **36**, 243-246

McClay, K.R. 1989. Analogue models of inversion tectonics. In: Inversion tectonics Cooper, M.A. and Williams, G.D. (eds). *Geological Society Spececial Publications*. **44**, 41-59.

McClay, K.R. 1992. Glaossary of thrust tectonics terms. K.R. McClay, Editor. *Thrust Tectonics*. Chapman and Hall. pp. 419-433.

McClay, K.R., 1995. The geometries and kinematics of inverted fault systems: a review of analogue model studies. In: Buchanan, J.G., Buchanan, P.G. (Eds.), Basin Inversion. *Geological Society Special Publication*, **88**, 97-119.

McClelland, E., Courtillot, V., Tapponier, P. 1985. Introduction. *In E. McClelland, V. Courtillot, P. Tapponier (Eds.). Magnetotectonics. Tectonics*, **5**, 709-711.

McFadden, P.L. 1990. A new fold test for paleomagnetic studies. *Geophysical Journal International,* **103**, 163-169. DOI: 10.1111/j.1365-246X.1990.tb01761.x

McFadden, P.L. 1998. The fold test as an analytical tool. *Geophysical Journal International*, **135**, 329-338. DOI: 10.1046/j1365-246x.1998.00640.x.

Medwedeff, D. 1992. Geometry and kinematics of an active, laterally propagating wedge thrust, Wheeler Ridge, California. *In:* Structural geology of fold and thrust belts (S. Mitra i G. W. Fisher, eds.), Johns Hopkins University Press, Baltimore, 3-28.

Mencos, J., Muñoz, J.A., Hardy, S. 2011. Three-dimensional geometry and forward numerical modeling of hte Sant Corneli anticline (southern Pyrenees, Spain). *In:* McClay, K., Shaw, J.H., Suppe, J. eds. Thrust fault-related folding. *AAPG Memoir*, **94**, 283-300.

Menéndez-Casares, E., González-Ferréndez, B., Gutiérrez-Claverol, M., García-Ramos, J.C. (2004) Precisiones sobre los acuíferos de la cuenca jurásica asturiana (NO de España). *Trabajos de Geología*, **24**, 119-126.

Mitchum, R.M. Jr., Vail, P.R., Thompson, S. 1977. Seismic stratigraphy and global changes of sea level: Part 2. The depositional sequence as a basic unit for stratigraphic analysis. In Seismic stratigraphy - Applications to Hydrocarbon Exploration (Ed. by C.E. Payton). *American Association of Petroleum Geologists Memoir*, **26**, 53-62.

Mitra, G. 1997. Evolution of salients in a fold-and-thrust belt: the effects of sedimentary basin geometry, strain distribution and critical taper. In: Sengupta, S. (Ed.) Evolution of Geological Structures in Micro- to Macro-scales, Chapman and Hall, London. 59-90.

Montadert, L., Charpal, O., Roberts, D. G., Guennoc, P., Sibuet, J. C. 1979. Northeast Atlantic passive margins: rifting and subsidence processes. *American Geophysics Union, Revue*, **3**, 154-186.

Mouthereau, F., Lacombre, O. 2006. Inversion of the Paleogene Chinese continental margin and thick-skinned deformation in the Western Foreland of Taiwan. *Journal of Structural Geology*, **28**, 1977-1993.

Mouthereau, F., Tensi, J., Bellahsen, N., Lacombe, O. Boisgrollier, T., & Kargar, S. 2007. Tertiary sequence of deformation in a thin- skinned/thick- skinned collision belt: the Zagros Folded Belt (Fars, Iran). *Tectonics*, **26**, doi: 10.1029/2007TC002098.

Muñoz-Jiménez, A., Casas-Sainz, A.M. 1997. The Rioja Trough (N Spain): tectosedimentary evolution of a symmetric foreland basin. *Basin Research*, **9**, 65-85.

Muñoz, J. A. 1992. Evolution of a continental collision belt: ECORS-Pyrenees crustal balanced section, in *Thrust Tectonics*, edited by K. R. McClay, pp. 235-246, Chapman and Hall, London.

Muñoz, J.A. 2002. Alpine tectonics I: the Alpine system north of the Betic Cordillera: The Pyrenees, W. Gibbons, T. Moreno, Editors, *The Geology of Spain*, Geological Society, London, United Kingdom, 370-385.

Muñoz, J.A., Beamud, E., Fernández, O., Arbués, P., Cinarès-Turell, J., Poblet, J. 2013. The ainsa fold and thrust oblique zone of the central Pyrenees: Kinematics of a curved contractional system from paleomagnetic and structural data. *Tectonics*, **32**, 1142-1175. DOI: 10.1002/tect.20070.

Nielsen, S.B. & Hansen, D.L. 2000. Physical explanation of the formation and evolution of inversion zones and marginal troughs. Geology, **28**, 875-878.

Ogaya, X., Ledo, J., Queralt, P., Marcuello, Á., Quintà, A. 2013. First geoelectrical image of the subsurface of the Hontomín site (Spain) for CO_2 geological storage: A magnetotelluric 2D characterization. *International Journal of Greenhouse Gas Control*, **13**, 168-179.

Oliva-Urcia, B., Pueyo, E.L. 2007. Rotational basement kinematics deduced from remagnetized cover rocks (Internal Sierras, southwestern Pyrenees). *Tectonics*, **26**, DOI: 10.1029/2006TC001955

Olivet, J.L., Bonnin, J., Beuzart, P., Auzende, J.M. 1984. Cinématique de l'Atlantique Nord et Central. *Centr National Pour l'Exploitation des Océans (CNEXO) Rapport Scientifiques et Techniques.* **54**, 106pp.

Olivet, J.L. 1996. La cinématique de la plaque Ibérique*. Bulletin du Centre of Recherches Exploration-Production Elf-Aquitaine*, **20(1)**, 131-195.

Pedreira, D., J. A. Pulgar, J. Gallart, and J. Díaz. 2003. Seismic evidence of Alpine crustal thickening and wedging from the western Pyrenees to the Cantabrian Mountains (north Iberia). *Journal of Geophysical Research,* **108**(B4), doi: 10.1029/2001JB001667.

Pedreira, D., Pulgar, J. A., Gallart, J., Torné, M. 2007. Three-dimensional gravity and magnetic modeling of crustal indentation and wedging in the western Pyrenees- Cantabrian Mountains, *Journal of Geophysical Research,* **112**(B12405), doi: 10.1029/2007JB005021.

Peel, F.J., Travis, C.J., Hossack, J.R. 1995. Genetic structural provinces and salt tectonics of the Cenozoic offshore U.S. Gulf of Mexico: a preliminary analysis. *In:* M.P.A. Jackson, D.G. Roberts, and S. Snelson (eds). Salt tectonics: a global perspective. *AAPG Memoir*, **65**, 153-175.

Pérez-Estaún, A., Bastida, F., Alonso, J.L., Marquínez, J., Aller, J., Alvarez-Marrón, J., Marcos, A., Pulgar, J.A., 1988. A thin-skinned tectonics model for an arcuate fold and thrust belt: The Cantabrian Zone (Variscan Ibero-Armorican Arc). *Tectonics*, **7(3)**, 517-537. doi:10.1029/TC007i003p00517.

Pérez-Estaún, A., Martínez-Catalán, J.R., Bastida, F. 1991. Crustal thickening and deformation sequence in the footwall to the suture of the Variscan belt of northwest Spain. *Tectonophysics*, **191**, 243-253. doi:10.1016/0040-1951(91)90060-6.

Pérez-Estaún, A., Gómez, M., Carrera, J. 2009. El almacenamiento geologico de CO_2, una de las soluciones al efecto invernadero. Geological storage of CO_2, one of the solutions to the greenhouse effect. *Enseñanza de las Ciencias de la Tierra*, **17 (2)**, 179-189. ISSN: 1132-9157

Pfiffner, O.A., Hitz, L. 1997. Geological interpretation of the seismic profiles of the Eastern Traverse (lines E1-E3. E7-E9): eastern Swiss Alps. *in* Pfiffner, O.A., *et al.*, *Deep structure of the Swiss Alps: Results of NRP20: Basel*. Birkhäuser Verlag. pp.73-100.

Pfiffner, O. A. 2006. Thick-skined and thin-skined styles of continental contraction. In:Mazzoli, S. & Butler, R. W. H. (eds) *Styles of Continental Contraction. Geological Society of America Special Paper*, **414**, 153-177. doi: 10.1130/2006.2414(09).

Pinto, V., Casas, A., Rivero, L., Torné, M. 2005. 3D gravity modeling of the Triassic salt diapirs of the Cubeta Alavesa (northern Spain). Tectonophysics, **405**, 65-75.

Portero, J.M., Ramírez del Pozo, J., Aguilar, M. 1973. Mapa geológico 1:50.000, Hoja 170 (Haro). IGME.

Pueyo, E.L., Millán, H., Pocoví, A. 2002. Rotation velocity of a thrust: a paleomagnetic study in the External Sierras (Southern Pyrenees). *Sedimentary Geology*, **146**, 191-208.

Pueyo, E.L., Parés, J.M., Millán, H., Pocoví, A. 2003. Conical folds and apparent rotations in paleomagnetism (a case study in the Southern Pyrenees). *Tectonophysics*, **362**, 345-366.

Pueyo, E. L., López, M. A., Oliva, B., Sussman, A. J., Larrasoaña, J. C., Dinarés, J., Beamud, B., Soto, R., Garcés, M., Gil-Peña, I., Pérez-Rivarés, F.J., Rodríguez, A., Almar, Y., Fernández, O., Villalaín, J. J., Calvo, M., Bógalo, M. F., Costa, E., Mochales, T., Vidal, O., Pueyo-Anchuela, O., Gil-Imaz, A., Navas, J., and the *GeoKin3DPyr group.* 2006. The Pyrenean paleomagnetic database: state of the art and future tasks. *Proceedings MAGIBER IV*, 73-76.

Pujalte, V. 1979, Control tectónico de la sedimentación "purbeck-weald" en las provincias de Santander y N. de Burgos. *Acta geològica Hispànica,* **14**, 216-222.

Pujalte, V. 1981. Sedimentary succession and paleoenvironment within a fault-controled basin: the "Wealden" of the Santander area, northern Spain. *Sedimentary geology*, **28**, 293-325.

Pujalte, V. 1982. La evolución paleogeográfica de la cuenca "Wealdense" de Cantabria. *Cuadernos de Geología Ibérica*, **8**, 65-83.

Pujalte, V., Robles, S. & Hernández, J.Mª. 1996. La sedimentación continental del Grupo Campóo (Malm-Cretácico basal de Cantabria, Burgos y Palencia): testimonio de un reajuste hidrográfico al inicio de una fase rift. *Cuad. Geol. Ibérica*, **21**, 227-251.

Pujalte, V., Robles, S. & Valles, J.C. 1988. El Jurásico marino de las zonas de alto sedimentario relativo del borde SW de la Cuenca Vasco-Cantábrica (Rebolledo de la Torre, Palencia). *In: III Coloquio de Estratigrafía y Paleogeografía del Jurásico de España. Libro guía de las excursiones*. Ciencias de la Tierra (Instituto de Estudios Riojanos), **11**, 85-94.

Pujalte, V., Robles, S. & Hernández, J.Mª. 1996. La sedimentación continental del Grupo Campóo (Malm-Cretácico basal de Cantabria, Burgos y Palencia): testimonio de un reajuste hidrográfico al inicio de una fase rift. *Cuad. Geol. Ibérica*, **21** 227-251.

Pujalte, V., Robles, S., García-Ramos, J.C. & Hernández, J.M. 2004. El Malm-Barremiense no marinos de la Cordillera Cantábrica. *In:* Vera, J.A. (ed.) *Geología de España.* SGE-IGME, Madrid, 288-291.

Pujalte, V., Robles, S. 2008. Parasecuencias Transgresivo-Regresivas en un Cortejo Transgresivo: parte superior de la Fm Utrillas en Olleros de Pisuerga, Palencia. *Geogaceta*, **44**, 187-190.

Pulgar, J.A:, Gallart, J., Fernández-Viejo, G., Pérez-Estaún, A., Álvarez-Marrón, J., 1996. Seismic image of the Cantabrian Mountains in the western extension of the Pyrenees from integrated ESCIN reflection and refraction data. *Tectonophysics*, **264**, 1-19.

Pulgar, J. A., Alonso, J. L.,. Espina, R. G., Marín, J. A.. 1999. La deformación alpina en el basamento varisco de la Zona Cantábrica, *Trabajos de Geolología*, **21**, 283-294.

Quesada, S., Robles, S., Pujalte, V. 1991. Correlación secuencial y sedimentológica entre registros de sondeos y series de superficie del Jurásico Marino de la Cuenca de Santander (Cantabria, Palencia y Burgos). *Geogaceta*, **10**, 3-10.

Quesada, S., Robles, S., Pujalte, V., 1993. El Jurásico Marino del margen suroccidental de la Cuenca Vasco-Cantábrica y su relación con la exploración de hidrocarburos. *Geogaceta*, **13**, 92-96.

Quesada, S., Robles, S., Rosales, I., 2005. Depositional architecture and transgressive-regressive cycles within Liassic backstepping carbonate ramps in the Basque-Cantabrian basin, northern Spain. *Journal Geological Society of London*, **162**, 531-548.

Quintà, A., Tavani, S., Roca, E. 2012. Fracture pattern analysis as a tool for constraining the interaction between regional and diapir-related stress fields. The example of Poza de la Sal diapir (Basque

Pyrenees, Spain). In: *Salt Tectonics, Sediments and Prospectivity.* Alsop, G.I., Archer, S.G., Hartley, A.J., Grant, N.T., Hodgkinson, R., (ed) *Special Publication of the Geological Society of London*, **363**, 521-532.

Quintà, A. Tavani, S. 2012. The foreland deformation in the south-western Basque-Cantabrian Belt (Spain). *Tectonophysics,* **576-577**, 4-19.

Quintana, L., Alonso, J.L., Pulgar, J.A., Rodríguez-Fernández, L.R. 2006. Transpressional inversion in an extensional transfer zone (the Saltacaballos fault, northern Spain). *Journal of Structural Geology*, **28**, 2038-2048.

Ramírez del Pozo, J. 191. Bioestratigrafía y Microfacies del Jurássico y Cretácico del Norte de España (Región Cantábrica). *Memorias Instituto Geológico y Minero de España*, **78**, 1-357.

Ranalli, G. 2000. Rheology of the crust and its role in tectonic reactivation. *Journal Geodynamics*, **30** 3-15. doi:10.1016/S0264-3707(99)00024-1.

Rat, P., 1988. The Basque-Cantabrian basin between the Iberian and European plates; some facts but still many problems. *Revista de la Sociedad Geologica de España*, **1 (3-4)**, 327-348.

Ratschbacher, L., Frisch, W., Neubauer, F., Schmid, S.M., Neugebauer, J. 1989. Extension in compressional orogenic belts: the eastern Alps. *Geology*, **17**, 404-407.

Ratschbacher, L., Frisch, W., Linzer, H.G. Merle, O. 1991. Lateral extrusion in the Eastern Alps, Part 2. Structural analysis. *Tectonics*, **10**, 257-271.

Riba, O. and Juardo, M. J. 1992. Reflexiones sobre la geología de la parte occidental de la Depresión del Ebro. *Acta Geologica Hispanica*, **27**, 177-193.

Richardson, N.J., Underhill, J.R. Lewisw, G. 2005. The role of evaporite mobility in modifying subsidence patterns during normal fault growth and linkage, Halten Terrace, Mid-Norway. *Basin Research,* **17**, 203-223.

Robles, S., Pujalte, V., Valles, J.C. 1989. Sistemas sedimentarios del Jurásico de la parte occidental de la Cuenca Vasco-Cantatábrica. *Cuadernos Geología Ibérica*, **13**, 185-198.

Robles, S., Quesada, S., Rosales, I., Aurell, M. & García-Ramos, J.C. 2004. El Jurásico marino de la Cordillera Cantábrica. In: Vera, J.A. (ed.) Geología de España. SGE IGME, Madrid, 279-285.

Roca, E., Muñoz, J.A., Ferrer, O., Ellouz, N. 2011. The role of the Bay of Biscay Mesozoic extensional structure in the configuration of the Pyrenean orogen: Constraints from the MARCONI deep seismic reflection survey. *Tectonics*, **30**. TC2001. doi:10.1029/2010TC002735.

Rodríguez Cañas, C., Hernáiz, P.P., Malagón, J., Serrano, A. 1994. Notas sobre la estructura cabalgante de Rojas-Santa Casilda. *Geogaceta*, **15**, 135-138.

Roest, W.R. and Srivastava, S.P. 1991. Kinematics of the plate boundaries between Eurasia, Iberia and Africa in the North Atlantic from the Late Cretaceous to the Present. *Geology*, **19**, 613-616.

Rosenbaum, G., Lister, G.S. and Duboz, C. 2002. Relative motions of Africa, Iberia and Europe during Alpine orogeny. *Tectonophysics*, **359**, 117-129.

Roure, F., P. Choukroune, X. Berastegui, J. A. Munoz, A. Villien, P. Matheron, M. Bareyt, M. Seguret, P. Camara, and J. Deramond. 1989. Ecors deep seismic data and balanced cross sections: Geometric constraints on the evolution of the Pyrenees, *Tectonics*, **8(1)**, 41-50, doi:10.1029/TC008i001p00041.

Rowan, M.G., Jackson, M.P.A., Trudgill, B.D. 1999. Salt-Related fault families and fault welds in the Northern Gulf of Mexico. *AAPG Bulletin*, **83**, 1454-1484.

Rowan, M.G., Peel, F.J., Vendeville, B.C. 2004. Gravity-driven Fold Belts on passive Margins. *In:* McClay (eds). Thrust tectonics and hydrocarbon systems. *AAPG Memoir*, **82**, 157-182.

Rowan, M. 2014. Passive-margin salt basins: hyperextension, evaporite depositioon, and salt tectonics. *Basin Research*, **26**, 154-182. DOI: 10.1111/bre.12043.

Ruiz, M. 2007. Caracterització estructural i sismotectònica de la litosfera en el Domini Pirenaico-Cantàbric a partir de mètodes de sísmica activa i passiva, Ph.D. thesis, Univ. Barcelona, Barcelona, Spain.

Salas, R., Guimerà, J., Mas, R., Martín-Closas, C., Meléndez, A., Alonso, Á. 2001. Evolution of the Mesozoic Central Iberian Rift System and its Cainozoic inversion (Iberian Chain). *In:* Ziegler, P.A., Cavazza, W., Robertson, A.H.F., Crasquin-Soleau, S. (eds). *Peri-Tethys Memoir 6: Peri-Tethyan Rift/Wrench Basins and PAssive Margins. Mémories du Muséum National de l'Historie Naturelle,* **186**, 145-185.

Sánchez, F. 1991. *Evolución estructural post-kimmérica de la plataforma continental vasco-cantábrica*. PhD thesis, Escuela Técnica Superior de Ingenieros de Minas, Universidad Politécnica de Madrid, 174pp.

Sandiford, M. 1999. Mechanics of basin inversion. *Tectonophysics*, **305**, 109-120.

Savostin, L.A., Sibuet, J.C., Zonenshain, L.P., Le Pichon, X. and Roulet, M.J. 1986. Kinematic evolution of the Tethys belt from the Atlantic Ocean to the Pamirs since the Triassic. *Tectonophysics*, **123**, 1-35.

Schlische, R.W. 1992. Anatomy and evolution of the Jurassic continental rift system, Eastern North America. *Tectonics,* **12**, 1026-1042.

Schott, J.J. 1985. Paléomagnétisme des séries rouges du Permien, du Trias et du Crétacé inférieur dans les chaînes pyrénéo-cantabriques et nord-ouest ibérique. Implications géodynamiques. PhD Thesis, IPG, Strasbourg, 382 p.

Schott, J.J., Peres, A., 1987. Palaeomagnetism of Permo-Triassic red beds from the Asturias and Cantabric Chain (northern Spain): Evidence for strong lower Tertiary rernagnetizations, *Tectonophysics,* **6**, 499-519.

Schröder, B. 1987. Inversion tectonics along the western margin of the Bohemian Massif. *Tectonophysics*, **137**, 93-100.

Schwartz, S.Y., Van de Voo, R. 1984. Paleomagnetic study of thrust sheet rotation during foreland impingement in the Wyoming-Idaho Overthrust Belt. *Journal of Geophysical research.* **89**, 10077-10086. DOI: 10.1029/JB089iB12p10077.

Sepehr, M., Cosgrove, J., Moieni, M. 2006. The impact of cover rock rheology on the style of folding in the Zagros fold-thrust belt. *Tectonophysics*, **429**, 265-281. DOI: 10.1016/j.tecto.2006.05.021.

Sepher, M., Cosgrove, J.W. 2005. The role of the Kazerun fault zone in the formation and deformation of the Zagros fold-thrust belt, Iran. *Tectonics*, **28**, TC5005.

Serrano A., Martínez del Olmo, W. 1989. Diapirismo del Trías Salino en el Dominio Cántabro-Navarro, Libro homenaje a Rafael Soler, A.G.G.E.E.P. 115-121.

Serrano, A., Hernáiz, P.P., Magalón, J. Rodríguez-Cañas, C. 1994. Tectónica distensiva y halocinesis en el margen SO de la cuenca Vasco-Cantábrica. *Geogaceta*, **15**, 131-134.

Serrano, A., Martínez del Olmo, W. 2004. Estructuras diapíricas de la zona meridional de la Cuenca Vasco-Cantábrica. In: Vera, J.A. (Ed.), Geología de España. SGE-IGME Madrid, pp. 334-338.

Sharp, I., Gawthorpe, R.L., Underhill, J.R., Gupta, S. 2000. Fault-propagation folding in extensional settings: examples of structural style and synrift sedimentary response from the Suez rift, Sinai,Egypt. *Bulletin Geological Society of America,* **112**, 1877-1899.

Sibson, R.H., 1985. A note on fault reactivation. *Journal of Structural Geology*, **7**, 751-754.

Sibson, R.H., 1995. Selective fault reactivation during basin inversion: potential for fluid redistribution through fault-valve action. *Geological Society Spececial Publications*, **88**, 3-20.

Sibuet, J.C., Srivastava, S.P. and Spakman, W. 2004. Pyrenean orogeny and plate kinematics. *Journal of Geophysical Research*, **109**. B08104, 10.1029/2003JB00 2514.

Soto, R., Casas, A.M., Storti, F., Faccenna, C. 2002. Role of lateral thickness variations on the development of oblique structures at the Western end of the South Pyrenean Central Unit. *Tectonophysics*, **35**, 215-235.

Soto, R., Casas, A.M., Villalaín, J.J., Oliva-Urcia, B. 2007a. Mesozoic extension in the Basque-Cantabrian basin (N Spain): Contributions from AMS and brittle mesostructures. *Tectonophysics*, **445**, 373-394.

Soto, R., Casas-Sainz, A.M., Del Río, P. 2007. Geometry of half-grabens containing a mid-level viscous décollement. *Basin Research,* **19**, 437-450.

Soto, R., Casas-Sainz, A.M., Villalaín, J.J., Gil-Imaz, A., Fernández-González, G., Río, P., Calvo, M., Mochales, T. 2008. Charaterizing the Mesozoic extension direction in the northern Iberian Plate margin by anisotropy of magnetic susceptibility (AMS). *Journal of the Geological Society of London,* **165**, 1007-1018.

Soto, R., Casas-Sainz, A., Villalaín, J.J. 2011. Widespread Cretaceous inversion event in the northern Spain: evidence from subsurface and paleomagnetic data. *Journal of the Geological Society of London,* **168**, 899-912.

Sperner, B., Ratschbacher, L., Nemcok, M. 2002. Interplay between subduction retreat and lateral extrusion: Tectonics of the Western Carpathians, *Tectonics*, **21**. DOI:10.1029/2001TC901028.

Spratt, D.A., Dixon, J.M., Beattie, E.T. 2004. Changes in structural style controlled by lithofacies contrast across transverse carbonate bank margins - Canadian Rocky Mountains and scaled physical models. In: McClay, K.R. (Ed.), *Thrust tectonic and hydrocarbon systems: AAPG Memoir*, **82**, 259-275.

Srivastava, S.P., Roest, W.R., Kovacs, L.C., Oakey, G., Lévesque, S., Verhoef, J. and Macnab, R. 1990. Motion of Iberia since the Late Jurassic : Results from detailed aeromagnetic measurements in the Newfoundland Basin. *Tectonophysics*, **184**, 229-260.

Srivastava, S.P., Sibuet, J.C., Cande, S., Roest, W. R. and Reid, I.D. 2000. Magnetic evidence for slow seafloor spreading during the formation of the Newfoundland and Iberian margins. *Earth Planetary Science Letters*, **182**, 61-76.

Stauffer, K.W., Tarling, D.H. 1971. Age of the bay of Biscay: New paleomagnetic evidence. Histoire structurale du Golfe de Gascogne, Tome 1, *Editions Technip*, Paris p. II.2.1-18.

Steward, S.A., Argent, J.D. 2000. Relationship between polarity of extensional fault arrays and presence of detachments. *Journal of Structural Geology*, **22**, 693-711.

Stewart, S.A., Harvey, M.J., Otto, S.C. Weston, P.J. 1996 Influence of salt on salt geometry: examples from the UK salt basins, *Geological Society of London Special Publication,* **100**, in: G.I. Alsop, D.J. Blundell and I. Davison, Editors, *Salt Tectonics*, 175-202.

Stewart, S.A., Ruffell, A.H., Harvey, M.J. 1997. Relationship between basement-linked and gravity-driven fault systems in the UKCS salt basins. *Marine Petroleum Geology*, **14**, 581-604.

Stockmal, G.S., McMechan, M.E., Lebel, D., MacKay, P.A. 2001. Structural style and evolution of the triangle zone and external Foothills, southwestern Alberta: Implications for thin-skinned thrust-and-fold belt mechanics. *Bulletin of Canadian Petroleum Geology*, **49**, 472-496.

Storti, F., Soto-Marin, R., Rossetti, F., Casas-Sainz, A., 2007. Evolution of experimental thrust wedges accreted from along-strike tapered, silicone-floored multilayers. *Journal of the Geological Society of London*, **164**, 73-85.

Suppe, J. 1983. Geometry and kinematics of fault-bend folding. *American Journal of Science*, **283**, 684-721.

Sussman, A., Weil, A.B. 2004. *Orogenic Curvature: Integrating Paleomagnstic and Structural Analyses*. Geological Society of America Special Paper. **383**, 258pp.

Tapponnier, P., Peltzer, G., Le Dain, A.Y., Armijo, R. and Cobbold, P., 1982. Propagating extrusion tectonics in Asia: new insights from simple experiments with plasticine. *Geology*, **10**, 611-616.

Tavani, S. 2012. Plate-kinematics in the Cantabrian Domain of the Pyrenean Orogen. *Solid Earth*, **3**, 265-292.

Tavani, S. and Cifelli, F. (2010), Deformation pattern analysis and tectonic implications of a décollement level within the Central Apennines (Italy). *Geological Journal*, **45,** 582-596. doi: 10.1002/gj.1198

Tavani, S., Mencos, J., Bausà, J. and Muñoz, J.A., 2011a. The fracture pattern of the Sant Corneli-Bóixols oblique inversion anticline (Spanish Pyrenees). *Journal of Structural Geology*, **33**, 1662-1680. DOI:10.1016/j.jsg.2011.08.007.

Tavani, S., Quintà, A., Granado, P. 2011b. Cenozoic right-lateral wrench tectonics in the Western Pyrenees (Spain): The Ubierna Fault System. *Tectonophysics*, **509**, 238-253. DOI: 10.1016/j.tecto.2011.06.013.

Tavani, S.; Carola, E.; Granado, P.; Quintà, A.; Muñoz, J.A. 2013. Transpressive inversion of a Mesozoic extensional forced fold system with an intermediate décollement level in the Basque-Cantabrian Basin (Spain). *Tectonics*, **32**. DOI:10.1002/tect.20019.

Tavani, S. & Muñoz, J.A. 2012. Mesozoic rifting in the Basque-Cantabrian Basin (Spain): Inherited faults, transversal structures and stress perturbation. *Terranova*. **24**, 70-76. DOI: 10.1111/j.1365-3121.2011.01040.x.

Teixell, A., 1998. Crustal structure and orogenic material budget in the west central Pyrenees. *Tectonics*, **17**, 395-406.

Thinon, I., L. Matias, J. P. Réhault, A. Hirn, L. Fidalgo-González, and F. Avedik. 2003. Deep structure of the Armorican Basin (Bay of Biscay): a review of Norgasis seismic reflection and refraction data, *Journal Geological Society of London,* **160**, 99-116.

Turner, J.P. & Williams, G.A. 2004. Sedimentary basin inversion and intra-plate shortening. *Earth-Science Reviews*, **65**, 277-304.

van Wees, J.D. & Beekman, F. 2000. Lithosphere rheology during intraplate basin extension and inversion: inferences from automated modelling of four basins on western Europe. *Tectonophysics*, **320**, 219-242.

Vandenberg, J. 1980. New paleomagnetic data from the Iberian Peninsula. *Geologie en Mijnbouw*, **59**, 49-60.

Van der Voo, R., Channell, J.E.T. 1980. Paleomagnetism in orogenic belts: *Reviews of Geophysics and space physics*, **18**, 455-481. DOI: 10.1029-RG018i002p00455.

Veen, V. 1965. The tectonic and strarigraphic history of the Cardaño area, Cantabrian Mountains, northern Spain. *Leisde. Geol. Meded*, **35**, 45-104.

Vendeville, B.C., Jackson, M.P.A. 1992. The rise of diapirs during thin-skinned extension. *Marine and Petroleum Geology*, **9**, 331-353.

Vergés, J., García-Senz, J. 2001., Mesozoic evolution and Cainozoic inversión of the Pyrenean Rift, in *Peri-Tethys Memoir 6: Peri-Tethyan Rift/Wrench Basins and Passive Margins*, edited by P. A. Ziegler et al., *Mém. Mus. National Hist. Nat.,* **186**, 187-212.

Vergés, J., Fernàndez, M. and Martínez, A. 2002. The Pyrenean orogen: Pre-, syn-, and post-collisional evolution. In: Rosenbaum, G. and Lister, G.S. (eds.). *Reconstruction of the Evolution of the Alpine-Himalayan Orogen*. *Journal of the Virtual Explorer*, **8**, 57-76.

Vidal-Royo, O., Koyi, H.A., Muñoz, J.A. 2009. Formation of orogen-perpendicular thrusts due to mechanical contrasts in the basal décollement in the Central External Sierras (Southern Pyrenees, Spain). *Journal of Structural Geology*, **31**, 523-539.

Visseres, R.L., Meijer, P.T. 2012 Mesozoic rotation of Iberia: Subduction in the Pyrenees? *Earth-Science Review,* **110**, 93-110. doi:10.1016/j.earscirev.2011.11.001.

Walsh, J.J., Watterson, J. 1988. Analysis of the relationship between the displacements and dimensions of faults. *Journal of Structural Geology,* **10**, 239-247.

Wagner, R.H., Winkler Prins, C.F., Riding, R.E., Wagner-Gentis, C.H.T. 1971. Lithostratigraphic units of the lower part of the Carboniferous in northern León, Spain. *Trabajos de Geología*, **4**, 603-663.

Walsh, J.J., Bailey, W.R., Childs, C., Nichol, A., Bonson, C.G. 2003. Formation of segmented normal faults: a 3-D perspective. *Journal of Structural Geology*, **25**, 1251-1262.

Weil, A.B., Yonkee, A., Sussman, A. 2010. Reconstructing the kinematic evolution of curved mountain belts: A paleomagnetic study of Triassic red beds from the Wyoming salient, Sevier thrust belt U.S.A. *Geological Society of America Bulletin*, **122**, 3-23. DOI: 10.1130/B26483.1.

White, N.J., Jackson, J.A., McKenzie, D.P. 1986. The relationships between the geometry of normal faults and that of the sedimentary layers in their hangingwall. *Journal of Structural Geology*, **8**, 897-909.

Willemse, E.J.M., Pollard, D.D., Aydin, A. 1996. Three-dimensional analysis of slip distributions on normal fault arrays with consequences for fault scaling. *Journal of Structural Geology,* **18**, 295-309.

Williams, G.A., Turner, J.P., Holford, S.P. 2005. Inversion and exhumation of the St. George's Channel basin, offshore Wales, UK. *Journal Geological Society of London*, **162**, 97-110.

Withjack, M.O., Meisling, K., Russell, L. 1989. Forced folding and basement-detached normal faulting in the Haltenbanken area, offshore Norway. *American Association of Petroleum Geologists Memoir*,

in A.J. Tankard, H.R. Balkwill, Editors, *Extensional Tectonics and Stratigraphy of the North Atlantic Margins*, **46**, 567-575.

Withjack, M.O., Callaway, J.S. 2000. Active normal faulting beneath a salt layer - an experimental study of deformation in the cover sequence. *AAPG Bulletin*, **84**, 627-651.

Xiao, H., Suppe, J. 1992. Origin of rollover. *AAPG Bulletin*, **76** 509-529.

Ziegler, P.A. 1987. Compressional Intra-Plate Deformation in the Alpine Foreland. *Tectonophysics*, **137**, 420 pp.

Yamamoto, K., Nishiwaki, N., 1993. Automatic analysis of geolgical structure from dip-strike data. *Mathematic Geolology*, **25**(7), 819-832.

Ziegler, P.A. 1989. Evolution of the North Atlantic: An Overview. *American Association of Petroleum Geologists Memoir*, in A.J. Tankard, H.R. Balkwill, Editors, *Extensional Tectonics and* 645 *Stratigraphy of the North Atlantic Margins*, **46**, 111-129.

Chapter 8

Annexes

This chapter encloses the publication "Photograph of the month" published in 2012 in the Journal of Structural Geology volume 42.

In addition, in this chapter are attached the description of the paleomagnetic sites both, the sites without enough data to calculate the characteristic direction and, the sites with enough data to obtain a mean direction.

Journal of Structural Geology 42 (2012) 1

Contents lists available at SciVerse ScienceDirect

Journal of Structural Geology

journal homepage: www.elsevier.com/locate/jsg

Photograph of the month

In the footwall damage zone of the Mesozoic Golobar extensional fault (Ba sque Cantabrian Basin; Spain), at about 2 m from the principal displacement zone, a near vertical thin film of fibrous gypsum crystals strikes parallel to the fault and fills a fracture in the ground. Fibres plunge 60°–90° and have formed near the surface. Their coarse vertical alignment constraints the fluids paleocirculation direction and indicates that the footwall damage zone enhanced the vertical hydraulic connection between the surface and the Triassic evaporites, located at least 200 m below the surface. Photo location: 42° 52′ 51.94″ N, 4° 08′ 22.45″ W.

Submitted by Stefano Tavani (Università Federico II, Napoli) and Eloi Carola (Universitat de Barcelona).

17 December 2011
Available online 28 March 2012

0191-8141/$ – see front matter
doi:10.1016/j.jsg.2012.01.014

A.2 Paleomagnetic sampled sites

FC01 coords: 42.61476385 N, 2.84172052 W, 450 m									
Miocene: clays and sandstones									
HT component	**sample**	**Dg**	**Ig**	**Ds**	**Is**	**error**	**quality**	**Trange**	**dip strata**
	FC01-01a	333.567	-37.62807	331.9747	42.6909	6.205048	2	390-490	**175/84**
	FC01-03a	320.1581	-22.27552	311.4525	48.7472	9.295959	2	330-360	**162/76**
	FC01-10a	359.242	15.51108	20.41562	59.9216	6.592095	2	390-620	**161/50**
	FC01-11a	6.705827	10.14524	26.04246	51.44896	8.335952	2	300-580	**161/50**
	FC01-12a	351.5865	14.576	359.8311	33.32246	3.981521	2	360-570	**133/26**
	FC01-13a	342.7516	18.13917	351.2586	39.4066	20.11546	2	300-510	**133/26**
	FC01-14a	352.0398	25.33953	352.0398	25.33953	2.237538	2	390-530	**167/24**
	FC01-15b	359.2014	19.81892	359.2014	19.81892	5.257291	2	390-660	**159/26**
	FC01-16a	6.772068	30.93164	3.892314	16.30957	6.259993	2	240-530	**343/16**
	FC01-17a	337.4317	52.17372	338.3371	36.19967	13.02396	2	360-510	**343/16**
	FC01-18a	19.88799	48.43676	14.15074	28.63103	4.624578	2	330-530	**359/21**
	FC01-20a	283.7769	47.53623	308.9449	40.91206	2.797349	2	240-330	**014/26**
	FC01-21a	294.6602	80.02512	331.1009	51.73385	14.5095	2	300-420	**345/31**
	FC01-22a	348.2544	74.88132	345.0282	43.92286	6.112878	2	330-560	**345/31**
	FC01-23a	291.7602	76.49229	326.9245	49.32943	2.504325	2	270-530	**345/31**
	FC01-24a	22.78854	69.42088	11.60729	44.27967	4.611695	2	250-400	**003/26**
	FC01-25a	7.379884	41.39208	6.007593	15.50568	5.016076	2	250-400	**003/26**
	FC01-26a	28.26836	66.28976	8.655949	38.44532	4.238839	2	250-440	**353/31**
	FC01-27a	14.23731	45.41888	7.529059	16.28165	8.173167	2	280-530	**353/31**
	FC01-28a	20.5716	59.86557	7.465231	31.2143	3.536536	2	360-560	**353/31**
	mean direction in situ:		**352/41**			n/N=20/28	k=5,1	α_{95}= 8,7	site Q=1
	mean direction after total tectonic correction:						**354/38**	D error:	11.12

FC02 coords: 42.67426271 N, 2.84197235 W, 652 m									
Miocene: grey clays and limestones									
site strata dip: 005/56									
HT component	**sample**	**Dg**	**Ig**	**Ds**	**Is**	**error**	**quality**	**Trange**	
	FC02-02a	122.1423	70.055	26.34138	40.57302	4.443794	2	240-420	
	FC02-03a	124.3056	64.80807	32.89277	42.62986	9.533397	2	330-420	
	FC02-04a	1.258469	54.34016	2.067076	-2.643743	5.454105	2	270-330	
	FC02-08a	157.2692	73.9954	15.13387	48.82513	3.854001	1	330-470	
	FC02-09a	100.2502	76.54372	20.6725	35.30449	11.21783	2	330-510	
	mean direction in situ:		**126/72**			n/N=4/7	k=93,8	α_{95}= 8,9	site Q=1
	mean direction after total tectonic correction:						**024/42**	err Dec:	11.98

FC03 coords: 42.54458845 N, 3.41304784 W, 987 m								
Miocene: reddish to grey clays								
site strata dip: 290/05								
HT component	**sample**	**Dg**	**Ig**	**Ds**	**Is**	**error**	**quality**	**Trange**
	FC03-01a	56.49156	20.68427	54.87075	23.7283	2.724093	2	320-440
	FC03-04a	319.9395	68.20271	314.484	63.82451	7.256158	2	360-530
	FC03-05a	327.5703	28.57919	329.4763	32.39275	8.106125	2	240-510
	FC03-06a	55.18113	45.47105	50.78915	48.32687	8.454209	2	250-440
	FC03-07b	60.27035	66.67682	50.28263	69.70393	8.811411	2	280-440
	FC03-09a	36.88231	57.89263	28.97048	59.16744	7.383082	2	360-470
	mean direction in situ:		**027/56**			n/N=6/7	k=5,7	α_{95}= 28,6 site Q=3
	mean direction after total tectonic correction:						**021/57**	err Dec: 52.51

FC04 coords: 42.56620191 N, 3.41794166 W, 782 m								
Oligocene - Lower Miocene: red clays								
site strata dip: 272/45								
HT component	**sample**	**Dg**	**Ig**	**Ds**	**Is**	**error**	**quality**	**Trange**
	FC04-03a	224.186	0.305141	214.718	-29.16325	6.640721	2	440-530
	FC04-06a	177.959	-50.19348	138.9551	-31.70227	3.156916	3	280-360
	FC04-08a	252.5013	-26.55982	226.6825	-66.73935	5.771116	2	360-480
	FC04-09a	218.8893	8.659262	215.355	-19.2998	10.5681	2	440-500
	FC04-10a	219.406	-20.25651	193.6987	-41.61656	13.00161	2	330-390
	mean direction in situ:		**228/-10**			n/N=4/7	k=13	α_{95}= 26,5 site Q= 3
	mean direction after total tectonic correction:						**211/-40**	err Dec: 34.54

FC05 coords: 42.59382222 N, 3.40012432 W, 713 m								
Lower Miocene: red clays								
site strata dip: 115/10								
HT component	**sample**	**Dg**	**Ig**	**Ds**	**Is**	**error**	**quality**	**Trange**
	FC05-01a	130.362	-54.20015	136.0516	-63.611	3.431297	2	360-630
	FC05-02a	156.6689	-35.56411	162.5562	-42.47701	1.307707	2	390-540
	FC05-04b	217.4029	-44.07548	226.1129	-40.87633	3.785592	1	440-620
	FC05-05a	190.8092	-47.31232	201.8477	-48.51735	11.48291	2	360-680
	FC05-06a	159.2276	-26.65196	163.5413	-33.33344	2.536896	1	390-600
	FC05-07a	155.7937	-32.36515	160.9417	-39.43161	2.060267	1	320-680
	FC05-08a	155.7937	-34.65285	161.4077	-41.69176	5.982569	1	320-680
	mean direction in situ:		**158/-40**			n/N=6/7	k=23,1	α_{95}= 14,3 site Q= 2
	mean direction after total tectonic correction:						**165/-46**	err Dec: 20.62

FC06 coords: 42.56293578 N, 3.35574239 W, 748 m								
Miocene: grey clays and limestones								
site strata dip: 045/05								
HT component	**sample**	**Dg**	**Ig**	**Ds**	**Is**	**error**	**quality**	**Trange**
	FC06-02a	202.899	-43.55568	203.9266	-39.72586	6.055503	2	330-390
	FC06-03a	201.4808	-48.50324	202.793	-44.69998	5.183723	2	330-420
	FC06-04a	171.4815	-64.00603	177.0347	-61.22063	2.794625	2	270-390
	FC06-05b	182.3307	-45.36219	184.6221	-42.15496	2.328198	1	270-390
	FC06-06a	175.3302	-60.82113	179.9005	-57.87313	3.006574	2	270-390
	FC06-08a	196.296	-50.91579	199.5903	-45.67786	3.957098	2	270-420
	FC06-09a	196.4349	-53.80048	200.0485	-48.54691	2.668229	2	300-390
	mean direction in situ:		**191/-53**			n/N=7/7	k=57,6	α_{95}= 8.2 site Q= 1
	mean direction after total tectonic correction:						**194/-49**	err Dec: 12.50

FC07 coords: 42.57385214 N, 3.44075287 W, 774 m								
Lower Miocene: red clays								
site strata dip: 321/02								
HT component	**sample**	**Dg**	**Ig**	**Ds**	**Is**	**error**	**quality**	**Trange**
	FC07-01a	221.6045	-2.338878	221.5281	-2.073172	23.73978	2	300-600
	FC07-02a	254.0954	-30.15378	253.0192	-30.97873	13.95792	2	320-500
	FC07-04a	213.408	-45.8727	211.4533	-45.29551	9.169061	2	280-400
	FC07-05a	264.2509	-15.81187	263.768	-16.95365	1.00352	2	390-450
	FC07-07a	205.0504	-18.94118	204.4402	-18.11315	6.050432	2	300-510
	FC07-11a	197.0536	0.4177116	197.0817	1.481542	7.999657	2	420-480
	FC07-12a	193.932	-29.46066	193.0363	-28.29301	6.423312	2	330-510
	mean direction in situ:		**221/-22**			n/N=7/8	k=7,3	α_{95}= 24 site Q= 3
	mean direction after total tectonic correction:						**220/-22**	D error: 25.88

FC08 coords: 42.55945188 N, 3.45470887 W, 789 m								
Lower Miocene: red clays								
site strata dip: 320/02								
HT component	**sample**	**Dg**	**Ig**	**Ds**	**Is**	**error**	**quality**	**Trange**
	FC08-01a	345.2299	52.09471	344.1594	50.28935	5.394413	1	300-450
	FC08-03a	211.5528	-63.43332	207.8359	-62.7651	8.287055	2	470-530
	FC08-08a	352.3344	52.03745	350.9992	50.34987	4.794837	1	300-480
	FC08-09a	246.1068	38.6701	247.6157	38.06321	19.2337	3	500-590
	FC08-10a	343.8183	40.10233	343.1476	38.27921	3.784098	2	300-360
	FC08-11a	330.2586	34.87239	330.0038	32.90867	2.651552	2	250-360
	mean direction in situ:		**342/45**			n/N=4/7	k=55	α_{95}= 12,5 site Q= 2
	mean direction after total tectonic correction:						**341/43**	err Dec: 17.15

FC09 coords: 42.49578047 N, 3.57722768 W, 815 m								
Upper Cretaceous: limestones								
site strata dip: 017/39								
HT component	**sample**	**Dg**	**Ig**	**Ds**	**Is**	**error**	**quality**	**Trange**
	FC09-01b	303.0592	69.30347	348.6405	41.20717	6.592404	2	240-450
	FC09-02b	9.296436	65.32448	12.45192	26.41358	5.569027	2	270-420
	FC09-03a	4.600792	57.35943	9.187522	18.70941	11.93743	2	200-420
	FC09-04a	122.5169	-76.76691	177.0224	-45.53103	6.20293	2	330-450
	FC09-06b	354.2034	63.69318	5.03535	25.86661	3.139425	2	360-450
	FC09-07a	223.8819	-25.59004	221.2198	9.338823	4.642549	2	360-420
	mean direction in situ:		**346/69**			n/N=5/7	k=34,3	α_{95}= 13,2 site Q= 2
	mean direction after total tectonic correction:						**003/32**	err Dec: 15.53

FC10 coords: 42.47484373 N, 3.53425100 W, 921 m								
Miocene: red clays								
site strata dip: 202/11								
LT component	**sample**	**Dg**	**Ig**	**Ds**	**Is**	**error**	**quality**	**Trange**
	FC10-08a	204.0197	-10.86599	204.2416	-21.8403	29.37893	2	250-400
	FC10-12a	178.1115	-21.20307	175.9701	-31.3232	19.69895	2	280-400
	Not enough good quality samples to calculate the site mean direction							

	sample	**Dg**	**Ig**	**Ds**	**Is**	**error**	**quality**	**Trange**
HT component	FC10-04a	65.85709	47.33852	76.38405	54.31509	5.829499	2	440-530
	FC10-05a	186.844	-35.01324	184.4927	-45.66563	16.5968	2	280-470
	FC10-08a	24.96813	58.14699	27.26056	69.09097	10.30931	2	440-560
	FC10-09a	186.7372	-43.22192	183.4862	-53.84917	16.72398	2	280-470
	FC10-10a	199.1113	-45.83543	199.1113	-45.83543	4.532932	2	320-470
	FC10-12a	30.56931	28.77877	32.01046	39.57544	3.146918	2	400-470
	mean direction in situ:		**29/46**			n/N=5/7	k=19,2	α_{95}=17,9 site Q= 2
	mean direction after total tectonic correction:						**31/55**	err Dec: 31.21

FC11 coords: 42.56629277 N, 3.63689045 W, 928 m								
Lower Miocene: red clays								
site strata dip: 152/14								
HT component	**sample**	**Dg**	**Ig**	**Ds**	**Is**	**error**	**quality**	**Trange**
	FC11-01a	185.1121	-51.59164	199.6002	-62.07661	3.732744	2	250-480
	FC11-02a	186.4405	-33.79106	193.8051	-44.57194	2.846423	1	300-480
	FC11-04a	159.2375	-72.29873	188.3093	-85.56153	3.911962	2	350-510
	FC11-06a	185.6187	-41.44143	195.3193	-52.18415	5.027176	1	330-510
	FC11-07a	174.0905	-42.60107	181.5535	-55.04485	4.40374	2	300-510
	FC11-08a	194.129	-51.98257	210.898	-60.66048	2.592887	1	250-570
	mean direction in situ:		**185/-45**			n/N=5/7	k=78,7	α_{95}= 8,7 site Q= 1
	mean direction after total tectonic correction:						**196/-55**	err Dec: 15.28

FC12 coords: 42.62702872 N, 3.60807158 W, 963 m							
Lower Miocene: red clays							
site strata dip: 152/11							
LT component	**sample**	**Dg**	**Ig**	**Ds**	**Is**	**error**	**quality**	**Trange**
	FC12-05b	229.818	-48.02602	242.25	-48.83232	12.02614	2	280-440
	Not enough good quality samples to calculate the site mean direction							

HT component	**sample**	**Dg**	**Ig**	**Ds**	**Is**	**error**	**quality**	**Trange**	
	FC12-01b	355.5789	48.20145	2.672925	57.85447	3.820195	2	250-360	
	FC12-03a	206.0606	-36.12759	213.7581	-41.70113	12.17013	2	250-390	
	FC12-04a	194.1107	-57.80706	209.9719	-64.68184	9.083879	2	250-360	
	FC12-05b	319.4094	31.86594	317.7167	42.64236	8.345589	2	530-650	
	FC12-06a	172.2854	-60.34778	183.4066	-70.14424	5.127989	2	280-400	
	FC12-07b	203.2045	-42.566	212.7181	-48.46715	8.732308	2	280-400	
	mean direction in situ:		**016/47**			n/N=4/7	k=37,5	α_{95}= 15,2	site Q= 2
	mean direction after total tectonic correction:						**196/-55**	err Dec:	25.74

FC13 coords: 42.62947865 N, 3.58197365 W, 874 m							
Santonian: limestones							
site strata dip: 144/30							
HT component	**sample**	**Dg**	**Ig**	**Ds**	**Is**	**error**	**quality**	**Trange**
	FC13-02a	153.7282	-6.774429	156.411	-36.06126	4.629424	2	360-530
	Not enough good quality samples to calculate the site mean direction							

FC14 coords: 42.64092971 N, 3.54236600 W, 801 m								
Lower Miocene: red clays								
site strata dip: 155/21								
HT component	**sample**	**Dg**	**Ig**	**Ds**	**Is**	**error**	**quality**	**Trange**
	FC14-03a	46.25284	80.65792	354.5235	64.72128	2.616838	3	320-440
	FC14-05a	358.1087	18.57202	3.307959	37.2611	5.519188	2	440-560
	FC14-07a	13.73699	57.24515	13.73699	57.24515	5.840855	2	320-500
	FC14-08a	6.82E-03	34.24161	10.62528	52.1599	4.275996	1	320-560
	FC14-09a	331.2946	11.3858	330.9883	32.37262	4.37137	2	360-450
	FC14-10a	0.7661981	14.51553	5.402029	32.78848	7.614216	2	400-620
	FC14-12a	339.4176	29.93897	341.7347	50.77318	4.351836	2	390-450
	mean direction in situ:		**352/28**			n/N=6/7	k=14,4	α_{95}= 13,9	site Q= 2
	mean direction after total tectonic correction:						**357/45**	err Dec:	19.62

FC15 coords: 42.50227403 N, 3.64309215 W, 1009 m								
Upper Cretaceous: limestones								
site strata dip: 022/21								
HT component	**sample**	**Dg**	**Ig**	**Ds**	**Is**	**error**	**quality**	**Trange**
	FC15-04b	296.7578	52.9838	318.268	46.53518	5.177606	2	360-450
	FC15-05b	192.9558	33.97425	190.9869	52.86686	1.194924	3	490-510
	FC15-06a	329.9028	60.5281	346.4206	45.77484	6.79683	2	270-470
	FC15-07a	314.9597	65.32539	339.9928	52.93872	1.966789	2	330-450
	mean direction in situ:		**313/28**			n/N=3/7	k=57,9	α_{95}= 16,3 site Q= 2
	mean direction after total tectonic correction:						**335/49**	err Dec: 24.90

FC16 coords: 42.47960302 N, 3.65492849 W, 903 m								
Upper Cretaceous: limestones								
site strata dip: 009/71 (overturned)								
HT component	**sample**	**Dg**	**Ig**	**Ds**	**Is**	**error**	**quality**	**Trange**
	FC16-01a	243.0614	46.87947	232.2247	-36.894	11.77206	2	240-300
	FC16-02b	53.69033	80.15893	179.9169	-12.09404	10.24311	2	510-530
	FC16-03a	16.93744	-25.55676	59.3855	78.86358	8.022882	2	420-490
	FC16-06a	332.2174	-36.05933	313.5363	54.87524	16.58	2	330-490
	FC16-07a	32.63887	-24.38448	79.80207	65.79601	9.307719	3	420-470
	mean direction in situ:		**011/-56**			n/N=4/7	k=4,2	α_{95}= 51,1 site Q= 3
	mean direction after total tectonic correction:						**011/53**	err Dec: 83.94

FC17 coords: 42.92001160 N, 3.53194254 W, 608 m								
Oligocene: red clays								
site strata dip: 059/16								
HT component	**sample**	**Dg**	**Ig**	**Ds**	**Is**	**error**	**quality**	**Trange**
	FC17-01a	342.9873	25.42764	349.3936	20.18244	6.243848	2	250-500
	FC17-02a	355.4511	36.45858	343.1254	42.54401	6.203645	2	320-560
	FC17-04a	303.2924	27.5687	303.2924	27.5687	9.803722	2	400-530
	FC17-06b	339.8681	36.53739	350.245	31.58187	9.078247	2	360-530
	FC17-08a	304.9029	43.01463	320.57	47.07322	8.384504	2	420-600
	FC17-09a	333.4126	65.62075	2.819997	59.68194	3.714605	3	420-489
	mean direction in situ:		**337/37**			n/N=4/7	k=19,6	α_{95}=15.7 site Q= 2
	mean direction after total tectonic correction:						**342/36**	err Dec: 19.38

FC18 coords: 42.89114466 N, 3.50137210 W, 590 m								
Lower Miocene: limestones								
site strata dip: 063/26								
HT component	**sample**	**Dg**	**Ig**	**Ds**	**Is**	**error**	**quality**	**Trange**
	FC18-03a	217.153	5.797212	213.5041	29.27904	8.04029	3	450-470
	FC18-05a	35.73979	37.85382	40.73956	13.8293	3.021131	2	240-300
	FC18-06a	243.3284	-31.61786	243.0212	-5.632692	3.019904	2	300-330
	FC18-08a	278.3367	4.237305	282.631	24.51445	1.357605	3	270-300
	mean direction in situ:		**050/36**			n/N=2/7	k=24	α_{95}= 18,5 site Q=2
	mean direction after total tectonic correction:						**052/10**	err Dec: 18.78

FC19 coords: 42.88438164 N, 3.50143979 W, 596 m							
Oligocene - Lower Miocene: red clays							
site strata dip: 040/43							
HT component	**sample**	**Dg**	**Ig**	**Ds**	**Is**	**error**	**quality**	**Trange**
	FC19-01a	270.5354	22.09611	296.079	41.3935	6.338369	2	280-440
Not enough good quality samples to calculate the site mean direction							

FC20 coords: 42.86414832 N, 3.46495651 W, 627 m								
Oligocene: white clays								
site strata dip: 022/44								
HT component	**sample**	**Dg**	**Ig**	**Ds**	**Is**	**error**	**quality**	**Trange**
	FC20-02a	353.594	-77.27228	210.6327	-56.98244	14.51447	3	390-450
	FC20-03a	282.8256	70.07732	351.6702	44.96474	3.705439	2	240-300
	FC20-04a	352.5805	41.95527	2.71E-02	1.328703	30.16605	3	390-490
	FC20-05a	306.5348	41.30539	330.4608	19.15058	2.90041	3	360-420
	FC20-07a	292.1633	72.27594	355.7505	42.68368	5.293552	2	300-420
	mean direction in situ:		**287/71**			n/N=2/7	k=947,3	α_{95}= 8,1	site Q=1
	mean direction after total tectonic correction:						**354/44**	err Dec:	11.22

FC21 coords: 42.84410145 N, 3.60758961 W, 661 m								
Upper Cretaceous: dark shales								
site strata dip: 085/32								
HT component	**sample**	**Dg**	**Ig**	**Ds**	**Is**	**error**	**quality**	**Trange**
	FC21-02a	311.4422	12.34413	321.1334	30.69279	6.049188	2	200-330
	FC21-04b	319.528	49.48086	0.3821735	56.97709	4.457143	2	240-300
	FC21-05a	1.036627	33.01801	17.29349	24.50265	6.068331	2	300-360
	FC21-06b	359.5297	72.25698	52.26104	53.9041	3.557867	3	240-300
	mean direction in situ:		**330/34**			n/N=3/6	k=7,8	α_{95}= 47,6	site Q=3
	mean direction after total tectonic correction:						**353/40**	err Dec:	62.14

FC22 coords: 42.64228809 N, 3.13418579 W, 705 m								
Oligocene - Lower Miocene: red clays								
site strata dip: 217/73								
HT component	**sample**	**Dg**	**Ig**	**Ds**	**Is**	**error**	**quality**	**Trange**
	FC22-01b	11.33677	16.74648	11.33677	16.74648	5.004253	2	320-470
	FC22-02a	39.04996	-34.64787	39.17778	37.22499	4.877435	2	360-500
	FC22-03a	32.65687	-45.57611	33.21321	26.38195	5.546069	2	400-560
	FC22-04a	7.602329	-22.37547	0.3530157	41.43377	3.359256	2	400-500
	FC22-05a	80.30713	-42.28056	68.3924	16.78185	3.299346	3	360-500
	FC22-06a	71.15114	-54.55903	55.50855	11.22576	3.051219	2	320-590
	FC22-09b	71.2079	-67.54228	48.1785	0.4760662	4.238721	3	400-500
	mean direction in situ:		**028/-31**			n/N=5/7	k=5,8	α_{95}= 22,8	site Q=3
	mean direction after total tectonic correction:						**029/28**	err Dec:	25.82

FC24 coords: 42.67438584 N, 3.29236812 W, 740 m								
Lower Miocene: red clays								
site strata dip: 192/23								
HT component	**sample**	**Dg**	**Ig**	**Ds**	**Is**	**error**	**quality**	**Trange**
	FC24-01b	176.9959	-32.77614	170.6875	-54.90114	5.02001	2	250-630
	FC24-02b	223.1533	-9.167785	227.6823	-28.05641	9.479603	2	500-680
	FC24-03a	195.681	-60.61198	195.681	-60.61198	3.90854	2	360-590
	FC24-04a	192.8745	-41.98903	194.8979	-64.9462	3.247859	2	530-650
	FC24-05a	192.0633	-25.27064	192.7311	-48.25455	3.587459	2	470-620
	FC24-07a	157.9835	-36.77308	142.5976	-54.67166	4.892036	2	400-650
	FC24-08a	176.4536	-50.80343	160.4047	-72.40885	7.429403	2	400-530
	mean direction in situ:		**181/-42**			n/N=6/7	k=23,8	α_{95}= 11,8 site Q=2
	mean direction after total tectonic correction:						**177/-61**	err Dec: 24.26

FC25 coords: 42.72183576 N, 3.44109049 W, 634 m									
Lower Cretaceous: red sandstons with clays									
site strata dip: 029/39									
HT component	**sample**	**Dg**	**Ig**	**Ds**	**Is**	**error**	**quality**	**Trange**	**Obs**
	FC25-07b	117.9368	-15.47552	127.6394	-11.51147	6.157735	2	650-680	
	FC25-08a	127.7544	-27.10579	142.489	-14.56531	6.310901	2	650-680	
	FC25-09a	127.6953	-13.88427	134.0135	-4.312732	2.383743	2	650-680	
	FC25-01a	7.590964	-29.34574	345.6194	-63.84605	6.404963	9	360-680	GC
	FC25-04a	343.0406	-34.95963	306.7764	-54.61863	7.46443	9	280-590	GC
	FC25-05b	5.539693	-25.57702	345.9621	-59.66426	5.549693	9	400-680	GC
	FC25-07b	23.90459	-16.16244	21.66758	-55.06232	4.3586	9	320-680	GC
	FC25-08a	45.8819	-6.329847	52.8722	-42.70393	10.89856	9	400-680	GC
	FC25-09a	222.1978	-4.615197	45.09433	-32.91405	4.747647	9	280-680	GC
	FC25-10a	31.01042	-16.29305	33.61049	-55.1589	8.964902	9	360-680	GC
	mean direction in situ:		**124/-19**			n/N=10/10	k=81.3	α_{95}= 13,8	site Q=2
	mean direction after total tectonic correction:						**135/-10**	err Dec:	14.02

FC50 coords: 42.66437406 N, 2.95041141 W, 596 m								
Oligocene - Lower Miocene: red clays								
site strata dip: 063/29								
HT component	**sample**	**Dg**	**Ig**	**Ds**	**Is**	**error**	**quality**	**Trange**
	FC50-10a	209.2213	-21.26494	210.574	-14.44779	21.14512	2	6
	FC50-2b	199.3809	-16.40597	200.6462	-10.40843	10.95057	2	6
	FC50-3a	204.7073	-8.560815	205.1541	-2.131962	3.513307	2	4
	FC50-4b	191.5831	-17.89828	193.2371	-12.65388	18.71115	1	6
	FC50-5a	198.3906	2.610122	197.8587	8.429603	3.245534	1	6
	FC50-6a	180.2793	1.109604	179.9073	4.943135	3.206502	2	5
	FC50-7b	194.1279	-27.97431	196.8405	-22.4124	23.3059	2	4
	mean direction in situ:		**197/-13**			n/N=7/8	k=30.5	α_{95}= 11,1 site Q=2
	mean direction after total tectonic correction:						**198/-7**	err Dec: 11.18

FC51 coords: 42.68415404 N, 2.8822752 W, 530 m								
Oligocene - Lower Miocene: red clays								
site strata dip: 032/22								
HT component	**sample**	**Dg**	**Ig**	**Ds**	**Is**	**error**	**quality**	**Trange**
	FC51-10	38.37775	38.24583	38.37775	38.24583	5.919609	1	6
	FC51-1b	351.8255	67.85516	9.691793	48.46467	2.988998	2	4
	FC51-4a	2.262554	60.72731	12.82939	40.34682	6.795572	2	5
	FC51-6b	353.541	50.71699	3.865266	31.87997	3.581848	1	6
	FC51-7b	5.167892	46.23018	11.30604	25.80575	7.014441	2	6
	mean direction in situ:		**359/56**			n/N=4/8	k=60.9	α_{95}= 11,9 site Q=2
	mean direction after total tectonic correction:						**009/37**	err Dec: 14.84

FC52 coords: 42.71670159 N, 3.05463722 W, 534 m								
Oligocene - Lower Miocene: red clays								
site strata dip: 077/16								
HT component	**sample**	**Dg**	**Ig**	**Ds**	**Is**	**error**	**quality**	**Trange**
	FC52-10a	239.0105	-53.70472	243.1561	-38.19231	7.067171	2	4
	FC52-1a	139.7549	-25.05238	147.7283	-31.03137	3.999284	2	4
	FC52-2b	124.9648	-40.28376	138.2687	-49.30439	5.619752	2	5
	FC52-3b	138.5262	-29.90228	148.2048	-35.98626	4.769026	2	4
	FC52-4	353.8593	-83.81744	277.8635	-73.73702	6.079329	3	4
	FC52-5	139.5956	-50.29442	159.9122	-54.73224	7.250203	3	4
	FC52-6	130.8154	-24.93443	138.5063	-33.19452	3.786292	2	6
	FC52-8	139.0782	-12.30664	143.1827	-18.94862	9.886149	3	4
	Not enough good quality samples to calculate the site mean direction							

FC53 coords: 42.7067786 N, 3.09480013 W, 557 m								
Oligocene - Lower Miocene: red clays								
site strata dip: 127/24								
HT component	**sample**	**Dg**	**Ig**	**Ds**	**Is**	**error**	**quality**	**Trange**
	FC53-1a	73.26126	16.01986	76.042	0.7282378	9.846895	3	3
	FC53-2	69.11302	61.40035	91.86376	43.97132	3.294053	1	3
	FC53-3	132.5169	-59.13792	129.9008	-35.24747	10.74123	3	5
	FC53-4	319.9104	18.71685	323.9257	41.77874	21.30206	2	4
	FC53-5	39.25984	42.16523	58.72833	36.40343	7.544295	3	4
	FC53-6	125.609	2.04E-02	125.6193	-23.97958	8.478861	2	4
	FC53-7	200.4587	-21.98381	211.1843	-26.09495	7.520173	2	4
	Not enough good quality samples to calculate the site mean direction							

FC54 coords: 42.67994177 N, 3.084617 W, 616 m									
Oligocene - Lower Miocene: red clays									
site strata dip: 062/26									
HT component	**sample**	**Dg**	**Ig**	**Ds**	**Is**	**error**	**quality**	**Trange**	
	FC54-10	113.9905	41.09668	101.7313	23.21968	3.879163	2	4	
	FC54-10	343.9838	50.37527	7.733161	38.83627	9.49882	2	5	
	FC54-11	55.8205	52.85008	57.33289	26.90677	8.629043	3	5	
	FC54-2	222.6532	-25.31948	224.4164	-0.412029	18.21928	3	4	
	FC54-2	2.319504	56.17123	23.50971	38.16734	8.901773	3	5	
	FC54-3b	5.27354	7.462425	5.259371	-7.537138	4.715355	3	4	
	FC54-5	348.1238	40.24013	4.510412	28.63972	18.2454	3	3	
	FC54-9	15.77074	54.60747	31.22876	33.52658	17.96856	2	5	
	mean direction in situ:		**013/44**			n/N=6/8	k=23,8	α_{95}= 20.7	site Q=3
	mean direction after total tectonic correction:						**025/24**	err Dec:	22.69

FC55 coords: 42.7478274 N, 3.07913774 W, 587 m									
Lower Miocene: red clays									
site strata dip: 091/79									
HT component	**sample**	**Dg**	**Ig**	**Ds**	**Is**	**error**	**quality**	**Trange**	
	FC55-1	316.7514	32.26154	31.93419	40.88728	10.01788	2	4	
	FC55-2	308.3301	-33.71232	307.1299	31.41042	7.433873	2	4	
	FC55-3	121.1421	-17.54195	194.0038	-57.74236	8.280371	3	4	
	FC55-6a	298.5541	56.62547	67.79467	38.81031	8.946301	2	4	
	FC55-7b	335.4271	27.37362	23.72819	25.42679	2.041096	2	3	
	FC55-8b	328.7495	43.2876	42.20997	29.03907	11.25379	2	4	
	FC55-10a	336.0346	30.8693	27.57687	24.82627	5.306019	2	4	
	mean direction in situ:		**329/34**			n/N=5/8	k=63.1	α_{95}= 11,7	site Q=2
	mean direction after total tectonic correction:						**031/30**	err Dec:	13.54

FC56 coords: 42.81433173 N, 3.08969252 W, 587 m									
Cenomanian: marls									
site strata dip: 214/45									
HT component	**sample**	**Dg**	**Ig**	**Ds**	**Is**	**error**	**quality**	**Trange**	
	FC56-1	258.9707	9.346745	262.7316	-21.45045	12.1707	2	6	
	FC56-10	20.86591	2.408491	15.57823	46.19361	2.874205	1	5	
	FC56-10	288.9067	2.091502	291.3253	-8.063653	7.501964	2	6	
	FC56-2	10.65709	3.673337	1.158774	44.45077	5.977425	2	4	
	FC56-4	345.6436	21.61872	318.0702	45.23856	5.327009	1	5	
	FC56-7	2.516639	23.5417	333.8462	57.55732	2.696238	1	5	
	FC56-8	242.2585	-2.051014	252.6429	-39.70022	5.651474	2	4	
	FC56-9	254.9889	13.46185	256.8607	-20.02849	10.07968	2	5	
	Not enough good quality samples to calculate the site mean direction								

FC57 coords: 42.76876516 N, 3.07814993 W, 497 m								
Oligocene - Lower Miocene: red clays								
site strata dip: 082/81								
HT component	**sample**	**Dg**	**Ig**	**Ds**	**Is**	**error**	**quality**	**Trange**
	FC57-2	44.7295	52.75436	58.16159	-21.16772	17.59681	3	4
	FC57-3	43.95356	37.99219	46.89248	-31.99562	10.38215	3	3
	FC57-4	59.84605	-20.87052	317.1592	-66.9065	5.790133	2	4
	FC57-9	78.58121	54.03917	79.20203	-26.94205	13.96781	2	4
	FC57-10	36.59493	80.83272	74.06318	2.342488	8.917165	2	4
	FC57-11	235.6439	73.76604	87.74181	23.63694	10.99222	2	5
	FC57-12	84.32393	33.59576	85.2162	-47.24122	10.54966	2	4
	Not enough good quality samples to calculate the site mean direction							

FC58 coords: 42.7687838 N, 3.07722105 W, 481 m									
Oligocene - Lower Miocene: red clays									
site strata dip: 082/79									
HT component	**sample**	**Dg**	**Ig**	**Ds**	**Is**	**error**	**quality**	**Trange**	
	FC58-1	292.0899	27.92346	24.66642	55.83023	10.55745	2	4	
	FC58-2a	280.2737	38.62219	51.06036	57.17701	4.023149	3	3	
	FC58-3	88.98362	-60.90073	254.9867	-39.69991	3.576307	2	5	
	FC58-4	94.39047	-50.82814	247.0614	-48.55367	4.20E-03	3	3	
	FC58-5	84.08704	9.693261	90.58085	-68.98441	4.854595	2	3	
	FC58-6	80.5171	13.63724	80.67297	-65.3625	17.18729	2	4	
	FC58-7	84.55803	-72.31748	258.9622	-28.63127	18.48126	3	6	
	FC58-8	136.5506	33.24912	128.3218	-20.64954	12.76688	3	4	
	mean direction in situ:		**279/51**			n/N=6/7	k=23,8	α_{95}= 11,8	site Q=2
	mean direction after total tectonic correction:						**063/48**	err Dec:	17.50

FC59 coords: 42.78753644 N, 3.49009408 W, 701 m								
Oligocene - Lower Miocene: red clays								
site strata dip: 009/19								
HT component	**sample**	**Dg**	**Ig**	**Ds**	**Is**	**error**	**quality**	**Trange**
	FC59-2a	102.3519	53.05653	77.95716	50.61653	4.662627	3	3
	FC59-3b	103.5911	-13.25837	107.5824	-10.49345	6.910491	2	4
	FC59-4b	187.3808	-38.97949	187.3669	-19.9795	12.80426	2	4
	FC59-5a	216.675	-58.54966	207.1836	-41.19221	8.981757	3	3
	FC59-6	118.1148	-29.13092	126.267	-21.05283	12.44417	2	4
	FC59-8a	289.0009	25.89174	296.9571	20.7005	4.084196	3	3
	FC59-9b	137.3137	25.69626	127.8077	36.77015	16.97477	3	4
	Not enough good quality samples to calculate the site mean direction							

FC60 coords: 42.8124289 N, 3.50407485 W, 592 m

Lower Miocene: limestones

site strata dip: 031/33

HT component

sample	Dg	Ig	Ds	Is	error	quality	Trange
FC60-1	92.83348	56.30189	66.24165	34.269	8.870845	3	3
FC60-5a	260.7927	-26.59413	253.853	-4.141611	6.269366	3	3
FC60-8a	233.736	-48.58374	225.9759	-17.51287	4.698495	3	4
FC60-9b	156.2719	-88.10532	206.6043	-55.83076	18.91093	2	3

Not enough good quality samples to calculate the site mean direction

FC61 coords: 42.76314932 N, 3.29636597 W, 592 m

Upper Cretaceous: marls

site strata dip: 031/36

HT component

sample	Dg	Ig	Ds	Is	error	quality	Trange
FC61-8a	69.2	-82.59725	203.9578	-29.58911	23.23409	2	3
FC61-9a	336.5968	-6.90038	309.0425	-36.66634	10.37954	2	3

Not enough good quality samples to calculate the site mean direction

FC62 coords: 42.75149393 N, 3.27204354 W, 569 m

Oligocene - Lower Miocene: red clays

site strata dip: 134/43

HT component

sample	Dg	Ig	Ds	Is	error	quality	Trange
FC62-10a	44.56632	3.175302	46.14906	0.8462942	1.539977	2	4
FC62-1a	41.50337	43.55742	74.90227	30.77686	7.354335	3	4
FC62-2a	109.6699	36.58413	114.2798	-3.968765	8.527589	2	4
FC62-4a	131.1859	9.673254	130.9677	-33.31639	3.461372	2	3
FC62-6a	162.5657	30.88917	158.1821	-7.501047	2.223499	3	3
FC62-7a	166.7222	82.02031	138.2861	40.24676	7.447453	3	4
FC62-8a	159.9594	37.85481	153.8357	-1.637668	10.85797	2	4
FC62-9	158.49	7.885156	162.7435	-30.42312	8.068081	2	3
FC62-9	120.2702	-1.956353	115.5028	-43.73712	21.5956	2	5

Not enough good quality samples to calculate the site mean direction

FC63 coords: 42.68695037 N, 3.87743728 W, 787 m

Upper Cretaceous: limestones

site strata dip: 349/09

HT component

sample	Dg	Ig	Ds	Is	error	quality	Trange
FC63-2a	353.6924	53.11679	352.6286	44.16486	1.202719	3	2
FC63-4a	330.043	49.83095	332.5575	41.17186	20.00391	2	3
FC63-6a	41.09986	29.92821	37.44984	24.38664	21.87761	3	2

Not enough good quality samples to calculate the site mean direction

FC64 coords: 42.71355083 N, 3.97867821 W, 864 m								
Upper Cretaceous: limestones								
site strata dip: 148/45								
HT component	**sample**	**Dg**	**Ig**	**Ds**	**Is**	**error**	**quality**	**Trange**
	FC64-1a	196.3872	19.14991	193.9269	-11.28757	25.18196	3	2
	FC64-5a	225.9116	27.76441	209.329	12.57077	36.32027	3	3
	FC64-7a	222.8662	-5.047317	230.296	-12.9825	11.51509	3	2
	FC64-9	355.6641	50.53811	82.5186	69.58772	4.371237	3	2
	FC64-10b	358.8936	51.80301	85.53812	67.47106	3.030704	2	3
	Not enough good quality samples to calculate the site mean direction							

FC65 coords: 42.75947095 N, 4.07091922 W, 1104 m								
Upper Cretaceous: limestones								
site strata dip: 172/08								
HT component	**sample**	**Dg**	**Ig**	**Ds**	**Is**	**error**	**quality**	**Trange**
	FC65-1a	9.986959	52.01498	14.39085	59.44019	5.061935	3	2
	FC65-2b	340.026	59.28132	336.7831	67.11605	7.608358	3	3
	FC65-4b	163.5523	-22.21465	163.08	-30.15723	4.647804	3	2
	FC65-6a	28.92003	68.82372	46.7415	74.28557	5.537647	2	3
	Not enough good quality samples to calculate the site mean direction							

FC66 coords: 42.62883078 N, 4.05465273 W, 1033 m									
Upper Cretaceous: limestones									
HT component	**sample**	**Dg**	**Ig**	**Ds**	**Is**	**error**	**quality**	**Trange**	**dip strata**
	FC66-10a	194.3203	75.08375	206.5477	36.6404	4.904467	1	5	**224/35**
	FC66-11a	213.6411	33.08512	213.4139	-5.905272	12.61871	2	2	**241/23**
	FC66-12b	173.0373	62.65207	193.0573	27.78322	15.39109	2	4	**241/34**
	FC66-14a	323.5224	12.10212	311.206	22.74792	10.03414	3	3	**295/52**
	FC66-15a	329.3861	-52.55038	355.1126	-26.24009	9.410397	2	4	**278/64**
	FC66-15a	323.5881	36.99585	290.6231	40.61343	5.204353	2	4	**278/64**
	FC66-16	3.907476	55.40123	276.5119	72.62341	5.315167	3	3	**244/46**
	FC66-18a	160.5358	-4.415752	151.1244	-26.68107	12.76602	2	3	**341/51**
	FC66-19	196.7919	23.94414	197.7178	-13.83274	30.86153	2	2	**290/31**
	FC66-1a	34.99709	39.1212	24.97242	7.794467	7.46672	2	4	**252/33**
	FC66-2	46.31861	56.03247	23.65291	26.25224	9.100705	2	4	**197/40**
	FC66-23	320.1449	39.88883	301.3723	40.10892	6.967721	3	2	**237/35**
	Not enough good quality samples to calculate the site mean direction								

FC67 coords: 42.68649116 N, 4.07787934 W, 1103 m								
Upper Cretaceous: limestones								
site strata dip: 338/16								
HT component	**sample**	**Dg**	**Ig**	**Ds**	**Is**	**error**	**quality**	**Trange**
	FC67-10a	299.306	44.2129	306.1311	30.81796	3.755136	1	5
	FC67-1a	297.4745	49.39061	305.9198	36.1419	6.725628	2	5
	FC67-2a	293.9865	46.43844	302.3505	33.77112	11.45921	2	4
	FC67-3a	302.4245	48.59134	309.6286	34.70938	7.892948	2	5
	FC67-6a	297.3184	53.98659	307.0937	40.64604	3.918159	2	5
	FC67-7a	292.1143	64.57381	307.4905	51.54956	5.396749	2	5
	mean direction in situ:		**297/51**			n/N=6/7	k=112.4	α_{95}= 6.3 site Q=1
	mean direction after total tectonic correction:						**306/38**	err Dec: 7.98

FC68 coords: 42.77344279 N, 4.12211816 W, 1104 m								
Upper Cretaceous: limestones								
site strata dip: 178/06								
HT component	**sample**	**Dg**	**Ig**	**Ds**	**Is**	**error**	**quality**	**Trange**
	Not enough good quality samples to calculate the site mean direction							

FC69 coords: 42.81854702 N, 4.49769548 W, 1106 m								
Upper Cretaceous: limestones								
site strata dip: 130/28								
HT component	**sample**	**Dg**	**Ig**	**Ds**	**Is**	**error**	**quality**	**Trange**
	Not enough good quality samples to calculate the site mean direction							

FC70 coords: 42.68856799 N, 4.33392064 W, 967 m								
Eocene - Lower Miocene: red clays								
site strata dip: 228/35								
HT component	**sample**	**Dg**	**Ig**	**Ds**	**Is**	**error**	**quality**	**Trange**
	FC70-10b	199.7343	7.125524	197.2349	-24.10011	11.85935	1	4
	FC70-11b	202.6129	-39.52589	171.0003	-67.98664	16.39272	2	4
	FC70-12a	250.263	26.03484	247.82	-6.354467	1.74167	1	5
	FC70-1a	242.3203	38.08804	238.8338	4.11969	9.894295	3	3
	FC70-2a	13.99481	46.34338	326.0001	68.1337	7.661463	2	5
	FC70-3	2.748662	55.28494	297.4094	65.62502	5.651982	2	5
	FC70-6b	339.9189	46.02917	300.0175	48.62178	14.35532	2	5
	FC70-9a	219.3782	6.041054	218.4741	-28.70252	8.058953	2	4
	Not enough good quality samples to calculate the site mean direction							

FC71 coords: 42.70156275 N, 4.3794939 W, 926 m									
Oligocene - Lower Miocene: red clays									
site strata dip: 200/35									
HT component	**sample**	**Dg**	**Ig**	**Ds**	**Is**	**error**	**quality**	**Trange**	
	FC71-10a	225.8233	7.125513	228.3773	-23.71585	6.89144	1	5	
	FC71-1b	113.5743	-14.48107	104.0782	-14.94061	2.409231	2	6	
	FC71-2b	222.6421	12.09841	223.6699	-19.7844	7.816333	2	6	
	FC71-3b	192.7224	26.50568	193.2372	-8.363471	15.53901	3	5	
	FC71-4a	338.4687	-0.9710471	333.2237	25.32821	3.666062	2	4	
	FC71-6	202.6207	12.96582	202.8495	-21.92674	20.7029	2	5	
	FC71-8	200.6457	7.27502	200.952	-27.68864	13.45226	2	5	
	FC71-9	131.5029	31.43686	144.4745	13.46521	17.30061	3	5	
	mean direction in situ:		**209/14**			n/N=7/8	k=25.5	α_{95}= 15.5	site Q=2
	mean direction after total tectonic correction:						**209/-31**	err Dec:	16.59

FC72 coords: 42.72673711 N, 4.376815 W, 969 m								
Oligocene - Lower Miocene: red clays								
site strata dip: 014/37								
HT component	**sample**	**Dg**	**Ig**	**Ds**	**Is**	**error**	**quality**	**Trange**
	FC72-1a	61.1137	46.83109	42.80326	16.28436	11.98484	3	3
	FC72-2	86.07467	30.18781	69.24617	15.14995	2.419274	3	3
	FC72-5b	247.0339	59.1281	317.6741	55.2346	10.19914	3	4
	FC72-6b	47.9942	27.93226	42.78218	-5.231642	3.355812	3	4
	FC72-9b	106.0493	42.42438	71.53464	35.17771	12.58274	3	3
	Not enough good quality samples to calculate the site mean direction							

FC73 coords: 42.73276244 N, 4.36847106 W, 980 m								
Upper Cretaceous: limestones								
site strata dip: 061/90								
HT component	**sample**	**Dg**	**Ig**	**Ds**	**Is**	**error**	**quality**	**Trange**
	FC73-2b	84.0897	-50.95438	220.1857	-34.81765	8.639448	2	3
	FC73-5	48.60417	-62.90728	244.424	-26.60336	22.77522	3	2
	FC73-7a	121.2958	-62.21523	214.1113	-12.55855	6.19E-03	3	2
	Not enough good quality samples to calculate the site mean direction							

FC74 coords: 42.75478228 N, 4.42292839 W, 957 m								
Oligocene - Lower Miocene: red clays								
site strata dip: 015/28								
HT component	**sample**	**Dg**	**Ig**	**Ds**	**Is**	**error**	**quality**	**Trange**
	FC74-10a	53.14423	74.25132	28.46907	48.78605	2.5841	1	6
	FC74-11a	26.4247	64.75289	20.18327	37.13934	5.229255	1	6
	FC74-1a	250.9257	17.53114	262.2803	30.28795	1.884669	1	6
	FC74-3a	17.18204	78.70092	14.36237	50.72203	4.17028	2	5
	FC74-4b	47.05245	77.75777	24.01542	51.28741	3.334573	1	6
	FC74-6b	48.70803	38.79925	41.09394	14.81987	9.262928	2	5
	FC74-7	100.3647	64.97362	56.73262	52.23904	6.315718	2	5
	FC74-8b	48.52224	65.30886	31.51674	39.97183	4.022106	1	6
	mean direction in situ:		**051/68**			n/N=7/8	k=23,8	α_{95}= 12.6 site Q=2
	mean direction after total tectonic correction:						**031/43**	err Dec: 17.23

FC75 coords: 42.7930434 N, 4.3929808 W, 1064 m								
Upper Cretaceous: limestones								
site strata dip: 219/56								
HT component	**sample**	**Dg**	**Ig**	**Ds**	**Is**	**error**	**quality**	**Trange**
	FC75-1	113.8669	78.71934	203.5146	35.83924	8.006062	3	4
	FC75-3	211.5879	23.53408	211.1244	-32.22755	1.894239	3	2
	FC75-9a	139.3648	-31.97305	104.9035	-26.45529	25.75812	3	4
	Not enough good quality samples to calculate the site mean direction							

FC76 coords: 42.81450019 N, 4.47857849 W, 1105 m								
Oligocene - Lower Miocene: red clays								
site strata dip: 119/19								
HT component	**sample**	**Dg**	**Ig**	**Ds**	**Is**	**error**	**quality**	**Trange**
	FC76-1a	136.6232	16.60518	135.7837	-1.366508	6.608955	3	4
	FC76-2a	265.0462	12.17272	261.1253	27.97608	0.9076764	3	3
	FC76-3	67.31344	41.2892	76.67137	27.77295	9.624827	2	4
	FC76-6	132.2036	43.59364	129.1289	25.10794	9.061506	2	4
	FC76-7	334.474	30.50502	344.4284	44.65792	7.237694	2	5
	FC76-8	127.4226	-3.46979	128.2341	-22.14405	10.57009	2	4
	Not enough good quality samples to calculate the site mean direction							

FC77 coords: 42.63828529 N, 3.71130469 W, 1024 m								
Oligocene - Lower Miocene: red clays								
site strata dip: 070/10								
HT component	**sample**	**Dg**	**Ig**	**Ds**	**Is**	**error**	**quality**	**Trange**
	FC77-10a	223.8423	-42.38284	226.8714	-33.16715	7.144972	2	5
	FC77-2a	181.9613	-46.80526	190.6515	-42.0867	4.013573	1	5
	FC77-3b	187.426	-41.31468	194.1839	-35.92188	7.126198	2	5
	FC77-4	180.454	-64.92886	197.0207	-59.79988	4.103208	1	5
	FC77-5a	227.6725	-5.057313	227.6956	4.305246	14.1671	2	5
	FC77-8a	258.8466	-12.63299	258.6008	-2.797191	12.97685	2	5
	mean direction in situ:		**195/-50**			n/N=4/8	k=21.6	α_{95}= 20.2 site Q=3
	mean direction after total tectonic correction:						**031/43**	err Dec: 27.94

FC78 coords: 42.63572934 N, 3.73108227 W, 1007 m								
Upper Cretaceous: limestones								
site strata dip: 051/11								
HT component	**sample**	**Dg**	**Ig**	**Ds**	**Is**	**error**	**quality**	**Trange**
	FC78-1a	183.9491	-29.33807	187.5504	-21.35004	27.15152	2	4
	FC78-2	159.7566	-61.75123	175.9936	-56.42402	6.474102	2	5
	FC78-3	182.3638	-40.4592	188.0471	-32.53761	5.097372	2	3
	FC78-5a	172.6049	-61.86354	186.2862	-54.70794	5.692769	2	3
	FC78-6a	163.7058	-48.19246	173.5037	-42.77611	5.727464	2	4
	FC78-7a	139.8836	-76.09849	177.2889	-72.2524	14.94062	2	3
	FC78-8a	190.5322	-24.2607	192.966	-15.52785	13.37374	3	3
	FC78-9b	174.9705	-43.75949	182.2081	-36.76714	3.167455	2	3
	mean direction in situ:		**176/-49**			n/N=6/7	k=17.2	α_{95}= 13.7 site Q=2
	mean direction after total tectonic correction:						**184/-42**	err Dec: 18.35

FC79 coords: 42.97853897 N, 3.5151548 W, 627 m								
Miocene: white to grey clays								
site strata dip: 092/06								
HT component	**sample**	**Dg**	**Ig**	**Ds**	**Is**	**error**	**quality**	**Trange**
	FC79-10	212.832	3.358897	212.3911	6.559291	13.02176	3	3
	FC79-3b	39.48445	65.40936	48.17905	61.27054	6.333358	2	3
	FC79-5b	140.6954	-46.65183	146.1112	-50.26857	9.552375	2	3
	FC79-6	121.9919	-43.04123	125.351	-48.06124	15.56541	3	2
	FC79-8	107.6794	-68.05982	113.6867	-73.69612	1.795435	3	3
	Not enough good quality samples to calculate the site mean direction							

FC80 coords: 42.97042585 N, 3.39766416 W, 649 m								
Oligocene: grey clays								
site strata dip: 219/45								
HT component	**sample**	**Dg**	**Ig**	**Ds**	**Is**	**error**	**quality**	**Trange**
	FC80-2a	236.8371	-24.09666	260.9094	-63.81783	6.954084	3	2
	FC80-4a	162.6389	14.67511	163.3891	-12.44749	7.539585	3	2
	FC80-7a	149.871	-24.94531	123.7689	-32.90709	2.1252	3	2
	Not enough good quality samples to calculate the site mean direction							

FC81 coords: 42.97294598 N, 3.53692346 W, 606 m								
Oligocene: grey clays								
site strata dip: 116/14								
HT component	**sample**	**Dg**	**Ig**	**Ds**	**Is**	**error**	**quality**	**Trange**
	FC81-2b	170.9911	-26.73676	178.1141	-33.72284	14.06543	3	3
	FC81-3	148.7176	-55.59227	165.9479	-65.96591	8.118201	3	3
	FC81-6a	324.7508	25.88468	329.4762	37.67797	18.19908	3	3
	Not enough good quality samples to calculate the site mean direction							

FC82 coords: 42.9028659 N, 3.31549328 W, 600 m								
Oligocene: grey clays								
site strata dip: 255/52								
HT component	**sample**	**Dg**	**Ig**	**Ds**	**Is**	**error**	**quality**	**Trange**
	FC82-3a	211.1986	-5.423245	192.9782	-39.74137	2.932193	1	3
	FC82-4a	144.3275	59.56192	213.7378	41.39582	9.353224	2	3
	Not enough good quality samples to calculate the site mean direction							

FC83 coords: 42.85701659 N, 3.2640486 W, 718 m								
Lower Miocene: grey clays								
site strata dip: 217/31								
HT component	**sample**	**Dg**	**Ig**	**Ds**	**Is**	**error**	**quality**	**Trange**
	FC83-2a	254.3357	15.68053	253.1609	-8.861366	23.14344	3	2
	FC83-3a	344.0948	12.7198	333.6643	30.18672	13.5953	3	3
	FC83-5	319.612	30.14152	300.1771	32.6677	12.29184	2	3
	FC83-7a	247.7466	22.43358	245.1323	-4.306059	2.29222	2	3
	Not enough good quality samples to calculate the site mean direction							

FC84 coords: 42.85079275 N, 3.27231982 W, 702 m								
Lower Miocene: grey clays								
site strata dip: 234/47								
HT component	**sample**	**Dg**	**Ig**	**Ds**	**Is**	**error**	**quality**	**Trange**
	FC84-1a	9.179788	35.60403	320.1685	56.13699	5.206484	2	1
	FC84-2a	169.2963	-13.52115	150.8603	-28.75935	8.381662	2	3
	FC84-6a	244.0484	27.85633	243.2396	-18.33794	1.90181	2	1
	FC84-8b	158.3934	4.022618	156.381	-8.810592	6.94912	3	3
	Not enough good quality samples to calculate the site mean direction							

FC85 coords: 42.82736391 N, 3.41047233 W, 550 m									
Oligocene: red clays									
site strata dip: 119/19									
HT component	**sample**	**Dg**	**Ig**	**Ds**	**Is**	**error**	**quality**	**Trange**	
	FC85-1a	71.1717	47.03455	81.66586	32.57441	21.07068	2	3	
	FC85-2a	48.00063	77.35583	89.71336	63.8331	5.191113	2	4	
	FC85-3	355.984	67.39208	46.10669	69.73479	5.982624	2	5	
	FC85-4b	33.29615	46.31923	51.16751	41.35329	9.458716	2	4	
	FC85-5	319.4029	73.2495	56.09311	82.92941	6.732495	3	3	
	FC85-6c	44.73035	75.6401	85.82741	63.1162	3.475096	2	5	
	FC85-7b	41.87724	20.10246	47.5628	14.39128	6.329958	2	6	
	FC85-8a	303.688	59.42939	313.1373	78.14819	12.15778	2	5	
	mean direction in situ:		**027/65**			n/N=6/7	k=17.2	α_{95}= 20.5	site Q=3
	mean direction after total tectonic correction:						**062/59**	err Dec:	40.04

FC86 coords: 42.85874133 N, 3.59775748 W, 630 m								
Upper Cretaceous: marls								
site strata dip: 194/62								
HT component	**sample**	**Dg**	**Ig**	**Ds**	**Is**	**error**	**quality**	**Trange**
	FC86-10	118.5947	25.71501	131.9467	-0.86018	9.939809	3	2
	FC86-1b	245.1413	29.70189	236.9591	-11.30881	11.38688	2	3
	FC86-2	167.1601	47.46669	175.0189	-9.544279	19.6687	3	3
	FC86-5	212.4618	75.79582	196.6051	16.65095	7.585764	2	3
	FC86-6	220.6729	83.91061	194.5819	24.65295	6.401091	2	4
	FC86-8b	248.1907	12.29523	252.4277	-20.83823	2.693193	3	2
	Not enough good quality samples to calculate the site mean direction							